



Publicly Accessible Penn Dissertations

1-1-2012

Structural Studies of the SMN-Gemin2 Complex

Kathryn Lorenz Sarachan

University of Pennsylvania, klorenz@mail.med.upenn.edu

Follow this and additional works at: <http://repository.upenn.edu/edissertations>

 Part of the [Biochemistry Commons](#), and the [Biophysics Commons](#)

Recommended Citation

Sarachan, Kathryn Lorenz, "Structural Studies of the SMN-Gemin2 Complex" (2012). *Publicly Accessible Penn Dissertations*. 482.
<http://repository.upenn.edu/edissertations/482>

This paper is posted at ScholarlyCommons. <http://repository.upenn.edu/edissertations/482>
For more information, please contact libraryrepository@pobox.upenn.edu.

Structural Studies of the SMN-Gemin2 Complex

Abstract

The proteins SMN and Gemin2 form the conserved core of the larger eponymous SMN complex, which also contains Gemin3-8 and unrip in an unknown stoichiometry. The complex facilitates the ordered assembly of seven Sm proteins onto a conserved site of an snRNA to form spliceosomal snRNP cores. A deficit in functional SMN as a consequence of deletions or loss-of-function mutations in the gene *SMN1* underlies the disease spinal muscular atrophy (SMA), a severe neurodegenerative disorder and leading genetic cause of infant mortality. Here, the NMR solution structure of the interacting domains of human SMN and Gemin2 is reported. The Gemin2-SMN heterodimer forms a novel all α -helical fold, comprising a single SMN helix embedded in an elongated, hydrophobic cavity of Gemin2. The interface between SMN and Gemin2 is mediated through highly conserved residues on the hydrophobic face of the amphipathic SMN helix and on four Gemin2 helices far separated in primary sequence. Mutations of interfacial residues predicted by the structure to be essential, but not of known disease mutations, disrupted the SMN-Gemin2 interaction. A number of biophysical studies also showed that unbound Gemin2 undergoes a significant conformational change upon SMN binding to become more compact, but belied reports of a Gemin2 self-interaction. A related set of investigations conducted on the full-length orthologous *S. pombe* Gemin2-SMN proteins showed that the complex occupies small, discrete oligomers that self-associate to form larger assemblies; its apparently large molecular weight by analytical size-exclusion chromatography results from an elongated, partially unstructured state. Together, these NMR and biophysical studies of SMN and Gemin2 provide the first high-resolution glimpse of the SMN-Gemin2 heterodimer, establish a framework for future structure-function studies investigating snRNP biogenesis and SMA pathogenesis and provide new valuable insight into the overall oligomerization state of the SMN complex.

Degree Type

Dissertation

Degree Name

Doctor of Philosophy (PhD)

Graduate Group

Biochemistry & Molecular Biophysics

First Advisor

Gregory D. Van Duyne

Keywords

Gemin2, SMN, spinal muscular atrophy

Subject Categories

Biochemistry | Biophysics

STRUCTURAL STUDIES OF THE SMN-GEMIN2 COMPLEX

Kathryn Lorenz Sarachan

A DISSERTATION

in

Biochemistry and Molecular Biophysics

Presented to the Faculties of the University of Pennsylvania

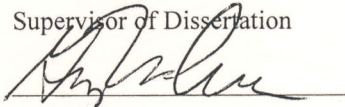
in

Partial Fulfillment of the Requirements for the

Degree of Doctor of Philosophy

2012

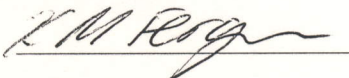
Supervisor of Dissertation



Gregory D. Van Duyne

Professor of Biochemistry and Biophysics

Graduate Group Chairperson



Kathryn M. Ferguson

Associate Professor of Physiology

Dissertation Committee

Mark A. Lemmon, Professor of Biochemistry and Biophysics

S. Walter Englander, Professor of Biochemistry and Biophysics

Mitchell Lewis, Professor of Biochemistry and Biophysics

Ronen Marmorstein, Professor of Chemistry

A. Joshua Wand, Professor of Biochemistry and Biophysics

Linda K. Nicholson, Professor of Molecular Biology and Genetics, Cornell University

STRUCTURAL STUDIES OF THE SMN-GEMIN2 COMPLEX

COPYRIGHT

Kathryn Lorenz Sarachan

2012

Dedicated with love to my parents, who, when I called sobbing from college that first day to declare that leaving home had been “a BIG mistake,” insisted that I stick it out

And to my husband, who made me very glad I did.

Acknowledgments

It takes nothing less than a proverbial village to raise up a young scientist, and I would be remiss if I failed to acknowledge the guidance and support I was privileged to receive from numerous friends and mentors at every stage of this work.

I owe a resounding debt of gratitude to Gregory Van Duyne, my thesis advisor, for the enthusiasm, intellectual rigor and collegiality that distinguishes our lab in my mind from any other I've worked in. I appreciated your trust in allowing me to work with autonomy when the project called for it as much as I did your assistance – of which I was sometimes only too eager to avail myself! I know that the scientific reasoning I learned under your aegis will always be one of my most valued assets.

I extend thanks in equal measure to A. Joshua Wand, my *de facto* co-advisor, who graciously extended the hospitality of his expertise and his laboratory during collaboration on a lengthy and challenging endeavor. Grappling that project into submission will remain indelibly engraved on my memory as one of my proudest achievements. I am grateful for the intellectual challenge, the unwavering support and the happy occasion of having been adopted, as it were, into a second laboratory family.

I also acknowledge with thanks the other members of my thesis committee, Mark Lemmon, Mitch Lewis, and Ronen Marmorstein, who shared their time and their words of encouragement and thought-provoking perspectives. Walter Englander kindly offered his services as a reader of this dissertation; Linda Nicholson of Cornell University, who has been getting me out of academic scrapes since I was eighteen, generously agreed to serve as external reviewer.

Members of the Van Duyne laboratory, past and present, have always provided a sure source of companionship and support. Kushol Gupta never hesitated to share his wizardry with the tools of biophysics; he and Kay Perry excellently filled the roles both of mentors and friends. Renee Martin and Nisha Ninan shared with me the dubious “Team SMN” moniker and all the commiseration and enthusiasm and occasional all-nighters involved therein. My friendships with Karen Rutherford, Bob Sharp, Bryan Gibb, Peng Yuan, Scott Pesiridis, Kaushik Ghosh and Megan Neary have been a fun, stimulating, irreplaceable part of the fabric of my life at Penn, and I thank you.

With generosity, the Wand laboratory adopted a stray collaborating graduate student into their family; I acknowledge with particular gratitude Vonni Moorman's abiding friendship and support, the endless hours Kathy Valentine spent helping me design and

run NMR experiments and John Gledhill's very patient help with the rudiments of data processing. Without Cecilia Tommos' help, CNS would likely have caught my computer on fire.

The Howard Hughes Medical Institute and a Structural Biology Training Grant from the National Institutes of Health supported my graduate training financially.

Outside the hallowed halls of academe, I acknowledge with love the support of my husband Tom Sarachan, patient throughout this long sojourn in Philadelphia, and of my parents, Stephen and Mary Anne Lorenz, my sister Jennifer and my grandparents, James Lorenz and Margaret Elliott, whose unshakable confidence in the success of this work guaranteed it in the end. I am as blessed in my spouse's family as in my own, and also offer warm thanks to my mother and father-in-law, Lisa Miller and Ron Sarachan, and to my sisters-in-law, Meg and Annie.

For laughter and music and inimitable friendship, my gratitude extends to the Orphans Company and the Acoustic Mayhem, including but certainly not limited to Liz, Drew, Joy and Charlie, Denise and Nate, Kitty, Katie Jr., Lexi, Terri, Aly, Rose and Johanna; so many of my happiest memories of the last seven years are memories of the lot of us. And I offer my deepest affection to Brionna and Alysia, Luci and Noël, Lisbeth and Liam, Hill and Danaan, Fiona, Chloe and Deven and the many fine scholars and musicians I've had the pleasure of teaching at the Penn Alexander School. I could ask no greater pleasure or privilege than that of walking beside each of you a little ways.

AMDG

December 2011

ABSTRACT

STRUCTURAL STUDIES OF THE SMN-GEMIN2 COMPLEX

Kathryn Lorenz Sarachan

Gregory D. Van Duyne

The proteins SMN and Gemin2 form the conserved core of the larger eponymous SMN complex, which also contains Gemins3-8 and unrip in an unknown stoichiometry. The complex facilitates the ordered assembly of seven Sm proteins onto a conserved site of an snRNA to form spliceosomal snRNP cores. A deficit in functional SMN as a consequence of deletions or loss-of-function mutations in the gene *SMN1* underlies the disease spinal muscular atrophy (SMA), a severe neurodegenerative disorder and leading genetic cause of infant mortality. Here, the NMR solution structure of the interacting domains of human SMN and Gemin2 is reported. The Gemin2-SMN heterodimer forms a novel all α -helical fold, comprising a single SMN helix embedded in an elongated, hydrophobic cavity of Gemin2. The interface between SMN and Gemin2 is mediated through highly conserved residues on the hydrophobic face of the amphipathic SMN helix and on four Gemin2 helices far separated in primary sequence. Mutations of interfacial residues predicted by the structure to be essential, but not of known disease mutations, disrupted the SMN-Gemin2 interaction. A number of biophysical studies also showed that unbound Gemin2 undergoes a significant conformational change upon SMN binding to become more compact, but belied reports

of a Gemin2 self-interaction. A related set of investigations conducted on the full-length orthologous *S. pombe* Gemin2-SMN proteins showed that the complex occupies small, discrete oligomers that self-associate to form larger assemblies; its apparently large molecular weight by analytical size-exclusion chromatography results from an elongated, partially unstructured state. Together, these NMR and biophysical studies of SMN and Gemin2 provide the first high-resolution glimpse of the SMN-Gemin2 heterodimer, establish a framework for future structure-function studies investigating snRNP biogenesis and SMA pathogenesis and provide new valuable insight into the overall oligomerization state of the SMN complex.

Table of Contents

Abstract	vi
Table of Contents	viii
List of Tables	xii
List of Illustrations	xii

Chapter I: Introduction

Pre-mRNA splicing I mediated by the catalytic activity of snRNPs in the context of the spliceosome	1
The biogenesis of spliceosomal snRNPs is mediated by the SMN complex	7
Both U-snRNAs and Sm proteins are escorted to the SMN complex by chaperone proteins	10
The SMN complex mediates snRNP assembly	15
Maturation of nascent assembled snRNP cores occurs in the nucleus	18
Spinal muscular atrophy is caused by a deficit in functional SMN	20
The <i>Schizosaccharomyces pombe</i> SMN and Gemin2 proteins form the simplest, most ancestral SMN complex	26
Thesis objectives	29

Chapter II: The NMR structure of the minimal binding domains of SMN and Gemin2

Introduction	34
Results	
Delineation of the minimal binding domains of human SMN and Gemin 2	35

SMN ²⁶⁻⁵¹ binds Gemin2 ⁹⁵⁻²⁸⁰ and full-length Gemin2 with similar high affinity	39
Phosphorylation of SMN serines 28 and 31 has no effect on Gemin2 binding	41
Purification and biophysical properties of the core SMN-Gemin2 complex	42
The solution structure of the core SMN-Gemin2 complex	48
The SMN-Gemin2 interface is mediated largely by hydrophobic residues	62
Mutation of key conserved interfacial residues confirms their importance in SMN-Gemin2 binding	65
Discussion	69
Materials and Methods	88
 Chapter III: The biophysical properties of Gemin2 in the presence and absence of SMN binding	
Introduction	112
Results	
Gemin2 ⁹⁵⁻²⁸⁰ , Gemin2 ¹²⁻²⁸⁰ and their SMN ²⁶⁻⁵¹ -bound complexes are monomeric species in solution	113
Gemin2 ⁹⁵⁻²⁸⁰ assumes an elongated structure in the absence of SMN binding	117
The Gemin2 ⁹⁵⁻²⁸⁰ structure adopted in the presence of SMN ²⁶⁻⁵¹ is destabilized in its absence	121
Shape reconstructions of Gemin2 ⁹⁵⁻²⁸⁰ and Gemin2 ¹²⁻²⁸⁰ -SMN ²⁶⁻⁵¹ demonstrate a conformational change in Gemin2 ⁹⁵⁻²⁸⁰ upon SMN binding	124
The solution conformation of Gemin2 ¹²⁻²⁸⁰ -SMN ²⁶⁻⁵¹ is extended, and the N-terminal region of Gemin2 ¹²⁻²⁸⁰ forms a rigid arm	126

Discussion	130
Materials and Methods	142
Chapter IV: Oligomerization properties of the <i>Schizosaccharomyces pombe</i> SMN-Gemin2 complex	
Introduction	147
Results	
The spSMN-Gemin2 heterodimer provides a model system for studying the oligomerization of human SMN	148
The spSMN-Gemin2 heterodimer occupies small, discrete oligomers that self-associate to form larger assemblies	150
The spSMN-Gemin2 complex possesses a partially disordered character	155
Discussion	161
Materials and Methods	169
Chapter V: Conclusions and Future Directions	177
Appendices	
Appendix A: Backbone and sidechain resonance assignments for SMN ²⁶⁻⁵¹ -Gemin2 ⁹⁵⁻²⁸⁰	
Table A1 Resonance assignments for SMN ²⁶⁻⁵¹	187
Table A2 Resonance assignments for Gemin2 ⁹⁵⁻²⁸⁰	191
Appendix B: Structural restraints	
Table B1 Nuclear Overhauser effect (NOE) distance restraints	212
Table B2 Backbone ϕ and ψ angles calculated from chemical shifts using the TALOS+	288
Table B3 Hydrogen bonding distance restraints	293
Table B4a Small-angle scattering data	295

Table B4b Sparsened small-angle scattering data	298
Table B5 $^1D_{NH}$ backbone amide and tryptophan $\epsilon 1$ residual dipolar couplings	300
Table B6 PRE distance restraints	303
Appendix C: Sample XPLOR-NIH Python refinement script	305
References	313

List of Tables

Table 2.1 Summary of structural ensemble statistics	58
Table 2.2 SMN ²⁶⁻⁵¹ -Gemin2 ⁹⁵⁻²⁸⁰ dissociation constants	68
Table 2.3 Human SMN and Gemin2 expression constructs used in this study	88
Table 2.4 Force constants employed at each stage of structural refinement in XPLOR-NIH	107
Table 3.1 Gemin2 structural parameters derived from small-angle x-ray scattering analysis	119
Table 4.1 Fit statistics for <i>S. pombe</i> SMN-Gemin2 sedimentation equilibrium analytical ultracentrifugation data to a variety of models	153

List of Illustrations

Figure 1.1	Pre-mRNA splicing by the U2-type spliceosome	3
Figure 1.2	Models of the U1 snRNP	5
Figure 1.3	Canonical cross-intron assembly pathway of the U2-type spliceosome	6
Figure 1.4	Schematic representation of the SMN complex	10
Figure 1.5	Overview of the survival motor neuron (SMN) functions in the assembly of mature spliceosome particles	14
Figure 1.6	The <i>Schizosaccharomyces pombe</i> SMN complex	28
Figure 2.1	Schematic of bacterial two-hybrid assay system	36
Figure 2.2	Domain boundaries of human SMN and Gemin2	38
Figure 2.3	Binding of SMN ²⁶⁻⁵¹ to Gemin2 or to Gemin2 ⁹⁵⁻²⁸⁰	41
Figure 2.4	Binding of SMN ²⁸⁻⁵¹ unphosphorylated and phosphorylated at Ser28 and Ser31 to Gemin2 ⁹⁵⁻²⁸⁰	42
Figure 2.5	Representative SEC-MALS analysis of the SMN ²⁶⁻⁵¹ - Gemin2 ⁹⁵⁻²⁸⁰ complex	44
Figure 2.6	Representative sedimentation equilibrium analytical ultracentrifugation experiment on the core SMN-Gemin2 complex	45
Figure 2.7	Sedimentation velocity analytical ultracentrifugation experiment On the SMN ²⁶⁻⁵¹ -Gemin2 ⁹⁵⁻²⁸⁰ complex	47
Figure 2.8	A two-dimensional ¹ H- ¹⁵ N HSQC of SMN ²⁶⁻⁵¹ -Gemin2 ⁹⁵⁻²⁸⁰	49
Figure 2.9	Triple-resonance backbone assignment of Gemin2 ⁹⁵⁻²⁸⁰	51
Figure 2.10	Triple-resonance sidechain assignment of SMN ²⁶⁻⁵¹ Ile33	53
Figure 2.11	Stereospecific assignment of SMN ²⁶⁻⁵¹ -Gemin2 ⁹⁵⁻²⁸⁰ valine and Leucine prochiral methyl groups	54

Figure 2.12 Residual dipolar couplings observed in partially aligned SMN ²⁶⁻⁵¹ -Gemin2 ⁹⁵⁻²⁸⁰ .	55
Figure 2.13 MTSSL-induced paramagnetic relaxation enhancement effects observed in the ¹ H- ¹⁵ N HSQC spectrum of SMN ²⁶⁻⁵¹ -Gemin2 ⁹⁵⁻²⁸⁰ .	56
Figure 2.14 Structure of SMN bound to Gemin2	60
Figure 2.15 Backbone amide ¹⁵ N T2 relaxation times of Gemin2 and the Bound SMN peptide	61
Figure 2.16 The conserved SMN-Gemin2 interface	62
Figure 2.17 Sequence alignments of SMN and Gemin2 from a diverse set of organisms	64
Figure 2.18 Binding of SMN ²⁶⁻⁵¹ mutants to Gemin2 ⁹⁵⁻²⁸⁰ using fluorescence anisotropy	66
Figure 2.19 Backbone order parameters (O ₂) of Gemin2 and the bound SMN peptide	73
Figure 2.20 Conserved surfaces in the core SMN-Gemin2 complex	81
Figure 2.21 Comparison of the NMR solution nstructure and x-ray crystal structure of SMN ²⁶⁻⁵¹ -Gemin2 ⁹⁵⁻²⁸⁰	83
Figure 2.22 An illustration of the Gemin2 residues comprising the HIV1 integrase-binding domain.	86
Figure 2.23. Peak volumes of NOEs used in distance calibration.	101
Figure 2.24 A histogram of ¹ D _{NH} RDCs for SMN ²⁶⁻⁵¹ -Gemin2 ⁹⁵⁻²⁸⁰	105
Figure 3.1 Representative SEC-MALS analyses of Gemin2 and Gemin2 ⁹⁵⁻²⁸⁰ complexes	116
Figure 3.2 Sedimentation velocity analysis of Gemin2 ⁹⁵⁻²⁸⁰ and Gemin2 ⁹⁵⁻²⁸⁰ -SMN ²⁶⁻⁵¹	118
Figure 3.3 The Gemin2 ⁹⁵⁻²⁸⁰ structure adopted in the presence of SMN ²⁶⁻⁵¹ is destabilized in its absences	121

Figure 3.4	Overlay of ^1H - ^{15}N HSQC spectra of Gemin2 ⁹⁵⁻²⁸⁰	122
Figure 3.5	Kratky plot of unbound Gemin2 ⁹⁵⁻²⁸⁰ and the SMN ²⁶⁻⁵¹ -Gemin2 ⁹⁵⁻²⁸⁰ complex	123
Figure 3.6	SAXS shape reconstructions of Gemin2 ⁹⁵⁻²⁸⁰ - SMN ²⁶⁻⁵¹	125
Figure 3.7	SAXS shape reconstructions of unbound Gemin2 ⁹⁵⁻²⁸⁰	126
Figure 3.8	SAXS shape reconstructions of Gemin2 ¹²⁻²⁸⁰ -SMN ²⁶⁻⁵¹	129
Figure 3.9	The $\alpha 1$ helix of Gemin2 primarily interacts with SMN	133
Figure 3.10	Alignment of Brr1 orthologues with human Gemin2	138
Figure 4.1	Analytical size exclusion chromatography profile of spSMN-Gemin2	150
Figure 4.2	Representative SEC-MALS analyses of spGemin2 over a concentration range	152
Figure 4.3	Representative sedimentation equilibrium analytical ultracentrifugation experiment on the <i>S. pombe</i> SMN-Gemin2 complex	154
Figure 4.4	Sedimentation velocity analytical ultracentrifugation experiment on the <i>S. pombe</i> SMN-Gemin2 complex	156
Figure 4.5	SAXS analysis of <i>S. pombe</i> SMN-Gemin2	157
Figure 4.6	Disorder predictions for spSMN and spGemin2	159
Figure 4.7	Kratky transformation of SAXS data from <i>S. pombe</i> SMN-Gemin2	160
Figure 4.8	Disorder prediction for human SMN	166

Chapter I: Introduction

1. Pre-mRNA splicing is mediated by the catalytic activity of snRNPs in the context of the spliceosome

Pre-mRNA splicing, the excision of non-coding intronic regions from nuclear mRNA precursors, is a multi-step process prerequisite to the expression of most eukaryotic genes (Burghes & Beattie, 2009). Prior to its discovery in 1977, the prevailing theory of “gene colinearity,” first articulated by Crick in 1958 and combining insights about the molecular nature of DNA and Beadle and Tatum’s 1941 “one gene-one enzyme” hypothesis, had described a gene as a sequence of nucleotides defining a sequence of amino acids (Beadle & Tatum, 1941; Crick, 1958). Although this notion accounts adequately for the nature of bacterial genes, Sharp and Roberts independently demonstrated by electron microscopy in 1977 that mRNA encoding a single adenoviral polypeptide hybridized to discontinuous segments of genomic DNA, suggesting compellingly that genetic material must “break apart and reform” (Berget *et al.*, 1977; Chow *et al.*, 1977). This paradigm, in which discontinuous genes consist of coding exons interleaved with noncoding introns and require splicing during pre-mRNA processing, was found to represent the norm in eukaryotes, although its prevalence and complexity varies. Only ten percent of *Saccharomyces cerevisiae* gene transcripts contain an intron, and never more than one; mammalian pre-mRNA transcripts, by contrast, contain an average of seven to eight introns and have been known to contain

more than fifty, with sizes ranging from eighty to 100,000 nucleotides (Burge *et al.*, 1999; Henry *et al.*, 1998).

Pre-mRNA splicing also serves as an important source of proteomic diversity. Shortly after Sharp and Roberts demonstrated the presence of discontinuous coding exons, researchers noted the existence of membrane-bound and secreted forms of an antibody that were encoded by the same gene (Early *et al.*, 1980); this differential exclusion and inclusion of exons, or “alternative splicing,” was found to serve as a mechanism for the generation of variable forms of mRNA from a single pre-mRNA transcript in a regulated manner (Nilsen & Graveley, 2010). Initially considered exceptional, estimates for the number of genes employing alternative splicing to generate more than one protein isoforms have risen over time, with recent studies suggesting that 94-96% of pre-mRNA sequences containing more than one exon are processed to generate more than one mRNA (and protein) isoform (Pan *et al.*, 2008).

The sequence data delineating an intron destined for removal consists of short consensus sequences at the 5' and 3' splice sites, as well as a “branch site” located 18-40 nucleotides upstream of the 3' splice site (Figure 1.1A). These splice site and branch site sequences vary between common U2-type introns and the much rarer U12-type introns, found only in a subset of eukaryotes. In U2-type introns, constant GU and AG dinucleotides nearly always demarcate the 5' and 3' boundaries of the intron, with additional nucleotide positions at each splice site showing a variable degree of

conservation. The branchpoint sequence contains a loose consensus sequence of eight nucleotides flanking a highly conserved branchpoint adenosine and frequently followed in higher eukaryotes by a polypyrimidine tract (Burge *et al.*, 1999).

The basic chemistry describing the removal of non-coding introns from coding sequences consists of two sequential transesterification reactions (Figure 1.1B). In the first step, the 2' hydroxyl of the conserved branchpoint adenosine executes a nucleophilic attack on the 5' splice site, releasing the 5' exon and forming a cyclic “lariat intermediate” characterized by a 2'-5' phosphodiester bond between the 5' end of the intron and the branchpoint adenosine. Subsequently, the 3' hydroxyl of the free 5' exon attacks the 3' splice site to ligate the exons and free the intron, still in its cyclic “branched lariat” form (Burge *et al.*, 1999; Staley & Guthrie, 1998).

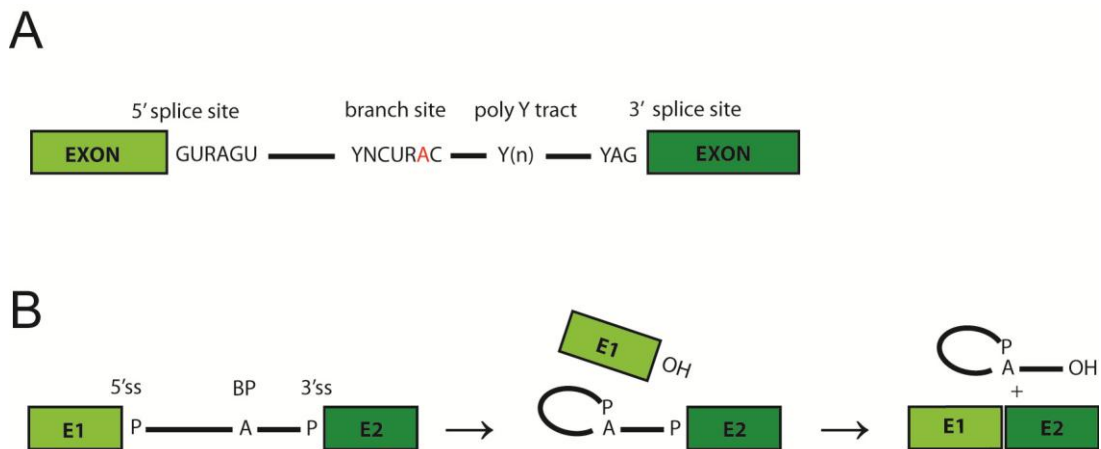


Figure 1.1 Pre-mRNA splicing by the U2-type spliceosome. A) Conserved sequences found at the 5' and 3' splice sites and branch site of U2-type pre-mRNA introns. Y depicts pyrimidines and R purines. The polypyrimidine tract is indicated. The branchpoint adenosine is colored red. B) Schematic representation of the two-step mechanism of pre-mRNA splicing. The branchpoint adenosine is indicated with an A.

Intronic excision from pre-mRNA is catalyzed by the spliceosome, a multi-megadalton ribonucleoprotein complex that acts to spatially orient the reactive groups of the pre-mRNA for the sequential steps in intron cleavage (Figure 1.3). A highly dynamic structure, the spliceosome varies constitutionally and conformationally over the course of the splicing reaction, involving perhaps as many as 300 total individual protein components (Ritchie *et al.*, 2009; Will & Lührmann, 2011). At its catalytic core lie five uridine-rich small nuclear ribonucleoprotein particles (U-snRNPs), each containing a unique, eponymous U-snRNA onto which seven Sm or Sm-like proteins assemble in a heptomeric ring, as well as several particle-specific accessory proteins (Raker *et al.*, 1996; Will & Lührmann, 2011). In an obvious parallel to the existence of distinct U2-type and U12-type introns, most eukaryotic cells contain two distinct spliceosomes; the U2-dependent (“major”) and much less abundant U12-dependent (“minor”) spliceosomes differ in their U-snRNP composition, the former including the U1, U2, and U5 snRNPs and the U4/U6 snRNP dimer and the latter sharing only U5 in addition to U11, U12 and U4atac/U6atac (Patel & Steitz, 2003; Will & Lührmann, 2005). In the case of the U1 snRNP, an analysis by mass spectrometry to determine the stoichiometry of all components indicated a single copy of each protein and RNA, and structures of the same particle based on single-particle electron microscopy and x-ray crystallography demonstrate that the U1 snRNA is threaded through a donut-shaped ring of Sm proteins (Figure 1.2) (Hochleitner *et al.*, 2004; Krummel *et al.*, 2010; Stark *et al.*, 2001).

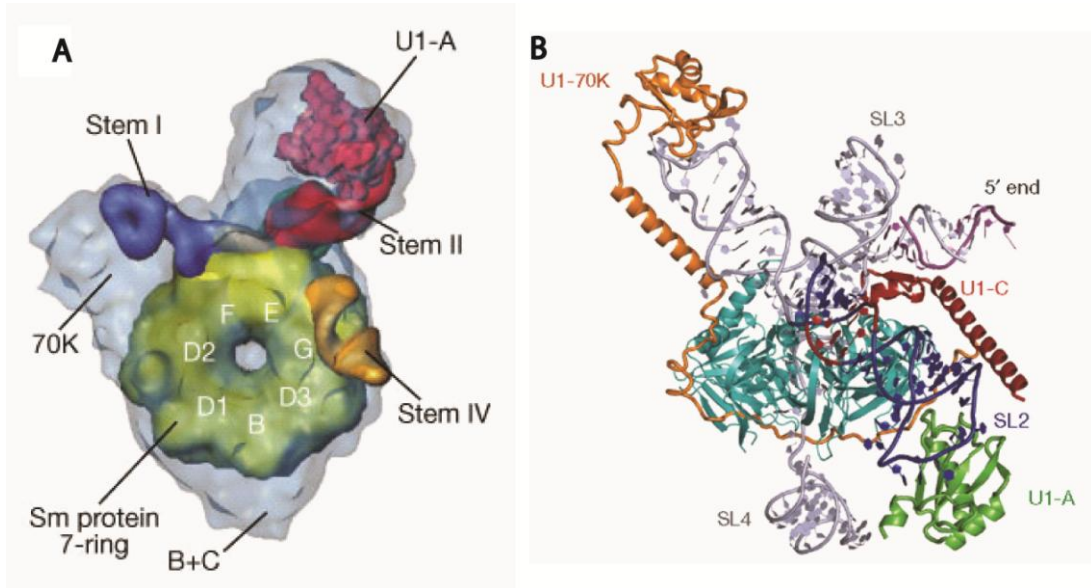


Figure 1.2. Models of the U1 snRNP. A) A cryoelectron microscopy model of the U1 snRNP. The Sm protein heptamer is colored yellow, U1-A red, and three stem loops of the U1 snRNA orange, red and blue. Positions of other snRNP components are indicated (Stark *et al.* 2001). B) 5.5Å x-ray crystallographic model (PDB: 3CW1) of the U1 snRNP. U1 small nuclear ribonucleic acid (snRNA) is colored in black, the seven Sm proteins in cyan, U1-70k in light brown, U1-A in green and U1-C in maroon. A 5' splice-site mimic RNA is colored blue (Krummel *et al.* 2010).

Spliceosome assembly for catalysis of pre-mRNA splicing occurs by the ordered binding and release of snRNPs and numerous other splicing factors (Figure 1.3). In cross-intron splicing, describing the splicing of an intron whose length does not exceed 200-250 nucleotides, the spliceosome recognizes splice sites and assembles across the intron (“intron definition”) in a series of discrete steps, all but the first of which are ATP dependent and require the action of DEAH-box RNA helicases (Fox-Walsh *et al.*, 2005; Ritchie *et al.*, 2009; Staley & Woolford, 2009). Following tight U1 snRNP association with the 5' splice site, non-snRNP protein factors including splicing factor 1 (SF1) and the heterodimer U2AF are recruited to the branch site and polypyrimidine tract and 3' splice site, respectively. The U2 snRNP then associates with the branch site, forming a

duplex between the U2 snRNA and the branch site and positioning the branchpoint adenosine, with an outward bulge, as the nucleophile for the first transesterification reaction (the “prespliceosome”). The pre-assembled U4/U6,U5 tri-snRNP is recruited to the complex, which undergoes a series of major rearrangements: the disruption of U1 snRNP binding at the 5' splice site by the U6 snRNP; the disruption of U4/U6 snRNA base-pairing; and the formation of a U2/U6 snRNA structure which is believed, after catalytic activation by the DEAH-box RNA helicase Prp2, to form the active site of the spliceosome. After splicing, the spliceosome dissociates and, after remodeling, the released snRNPs are competent for additional splicing reactions (Ritchie *et al.*, 2009; Will & Lührmann, 2011).

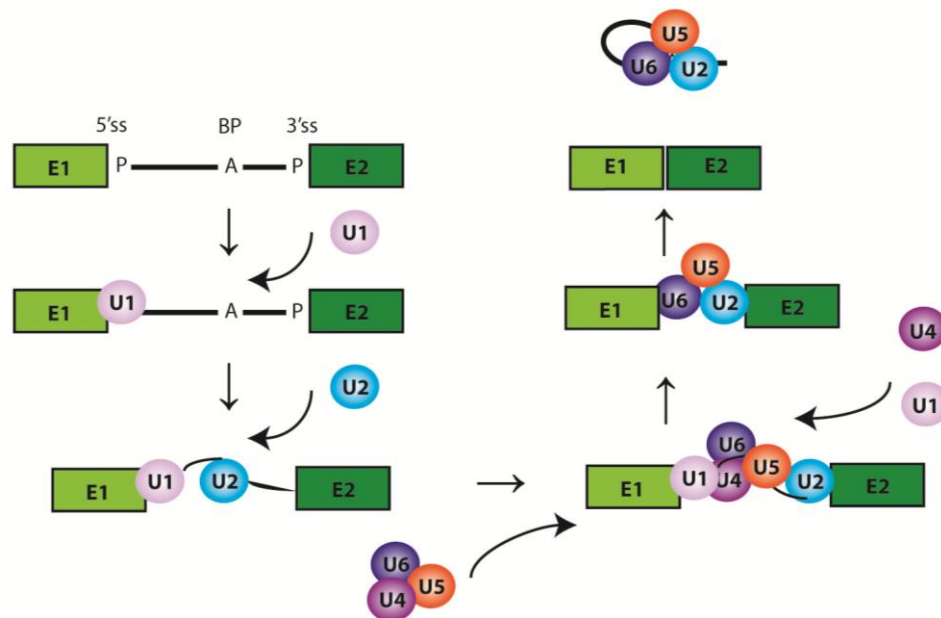


Figure 1.3 Canonical cross-intron assembly pathway of the U2-type spliceosome. The ordered interactions of the U-snRNPs (colored circles), but not of additional accessory proteins, are depicted interacting with exon (green boxes) and intron (black line) sequences.

Mammalian pre-mRNAs contain introns of lengths varying from a few hundred to several thousand nucleotides, while their exons maintain a roughly similar length of approximately 120 nucleotides (Ast, 2004; Deutsch & Long, 1999). Exons of increasing size are increasingly vulnerable to exon skipping unless their flanking introns are short; splice site definition is most efficient when either the exon or the intron is comparably short (Sternier *et al.*, 1996). In cases where intron lengths exceed 200-250 nucleotides, splice sites are recognized across the exon rather than across the intron, a process known as exon definition (Berget, 1995; Fox-Walsh *et al.*, 2005). The U1 snRNP binds to the 5' splice site downstream of the second exon, promoting the binding of U2AF with the polypyrimidine tract and 3' splice site of the upstream intron, thus promoting the recruitment of U2 snRNP to the branchpoint. The pairing of the defined 3' splice site with its upstream 5' counterpart is still poorly understood, but involves sequential disruption of the cross-exon complex and formation of a cross-intron prespliceosome (Reed, 2000; Will & Lührmann, 2011).

2. The biogenesis of spliceosomal snRNPs is mediated by the SMN complex

The assembly of the structural cores of the U1, U2, U4 and U5 snRNPs, as well as of the minor U11, U12 and U4atac snRNPs, involves the binding of a heteroheptameric ring of seven Sm proteins D1, D2, D3, B, E, F and G onto the conserved, uridine-rich “Sm site” of an snRNA (Burge *et al.*, 1999). This reaction proceeds spontaneously *in vitro*, in a hierarchical manner beginning with the formation of three Sm hetero-oligomers E/F/G, D1/D2 and D3/B, followed by the association of E/F/G and D1/D2

with the snRNA to form an intermediate structure to which the D3/B dimer binds to form the mature snRNP core (Raker *et al.*, 1996).

In vivo, however, U-snRNP biogenesis is an established function of the SMN complex (Figure 1.4) (Fischer *et al.*, 1997; Meister *et al.*, 2001a). This multi-component macromolecular machine counts as members at least nine proteins: the eponymous SMN; Gemins 2-8; and unrip-interacting protein (unrip) (Baccon *et al.*, 2002; Carissimi *et al.*, 2005; Carissimi *et al.*, 2006a; Carissimi *et al.*, 2006b; Charroux *et al.*, 1999; Charroux *et al.*, 2000; Gubitz *et al.*, 2002; Liu *et al.*, 1997; Pellizzoni *et al.*, 2002a). The assembly reaction is thought to be more stringently regulated *in vivo* to prevent the promiscuous and potentially deleterious assembly of Sm cores on random, inappropriate RNA molecules (Palfi *et al.*, 2009; Pellizzoni *et al.*, 2002b). In keeping with its role as cytoplasmic mediator of snRNP assembly, the SMN complex is diffusely distributed in the cytoplasm; it can also be found in the nucleus, in discrete, specifically enriched nuclear bodies described as gems (Liu & Dreyfuss, 1996; Liu *et al.*, 1997). The components of the SMN complex form a large stable species that sediments on sucrose gradients as a heterodisperse 30S-70S particle, suggesting a number of copies of one or more components (Gabanella *et al.*, 2005; Paushkin *et al.*, 2002). The SMN protein, as well as Gemin2 and Gemin8, have reported self-association activity, but the precise stoichiometry of those or any other components of the complex remains unknown (Lorson *et al.*, 1998; Ogawa *et al.*, 2007; Otter *et al.*, 2007; Young *et al.*, 2000). Protein-protein interaction studies, however, based on co-immunoprecipitations,

GST-pulldowns and yeast two-hybrid studies, suggest that the central part of the complex comprises SMN, Gemin7 and Gemin8, with Gemin2 and Gemin3 interacting with this backbone through direct contact with SMN, Gemin6 and unrip through Gemin7 and Gemin4 through Gemin8. A strong Gemin3-Gemin4 interaction has also been demonstrated, as well as a Gemin5 binding through Gemin2 (Otter *et al.*, 2007). Gemin2 also interacts directly with Gemin7 (Ogawa *et al.*, 2007). Alone among complex components, Gemin5's interaction with the SMN complex is substantially abrogated in the presence of high salt, and both Gemin5 and unrip co-immunoprecipitate weakly with epitope-tagged SMN (Otter *et al.*, 2007). Together with the observation that the two proteins exhibit compartment-specific localization, associating with the SMN complex in the cytoplasm but not in nuclear gems, a peripheral nature is usually ascribed to their interaction with the SMN complex (Battle *et al.*, 2007; Carissimi *et al.*, 2005; Grimmmler *et al.*, 2005a; Hao *et al.*, 2007). All components of the complex except for unrip, however, are required for the complete assembly reaction; knockdown of SMN and Gemins2-8 in HeLa cells is reported to disrupt efficient snRNP assembly (Carissimi *et al.*, 2006a; Feng *et al.*, 2005; Ogawa *et al.*, 2007).

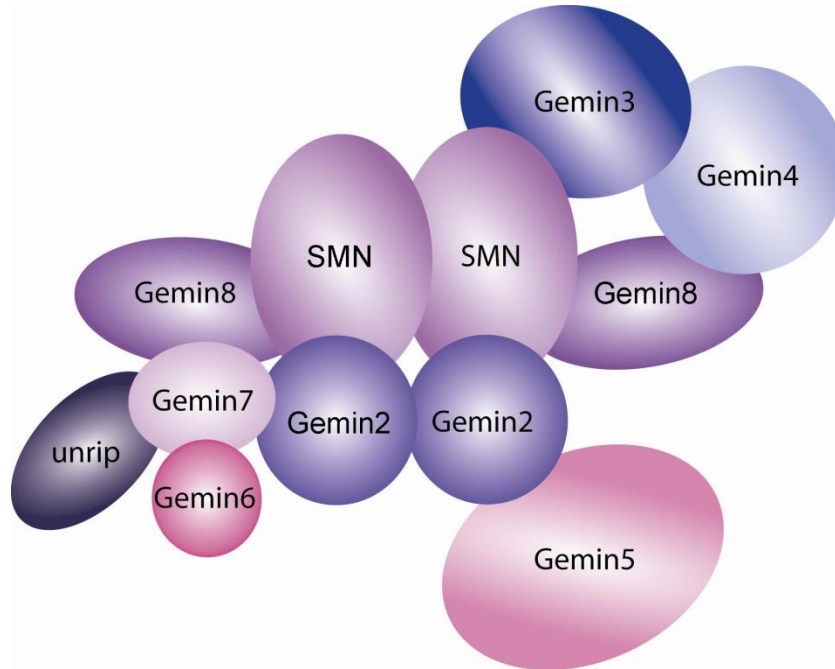


Figure 1.4 Schematic representation of the SMN complex. The central part of the complex comprises SMN, Gemin7 and Gemin8, with Gemin2 and Gemin3 interacting with this backbone through direct contact with SMN, Gemin6 and unrip through Gemin7 and Gemin4 through Gemin8. Gemin2 also binds Gemin5 and makes an interaction with Gemin7.

2.1 Both U-snRNAs and Sm proteins are escorted to the SMN complex by chaperone proteins

Before serving as substrates for SMN-chaperoned snRNP assembly, both nascent snRNAs and Sm proteins undergo upstream modifications before reaching their SMN complex destination under the aegis of specific protein escorts (Figure 1.5). After nuclear transcription by RNA polymerase II and co-transcriptional acquisition of a 7-methylguanosine cap (m^7G) cap (Will & Lührmann, 2001), nascent “pre”-snRNAs interact with cap-binding complex (CBC) and phosphorylated adaptor for RNA export (PHAX); the latter acts as an adaptor for the addition of RanGTP and additional

interactions with the export receptor exportin I (XPO1). XPO1 interaction with the nuclear pore complex ensures export of the nucleic acid to the cytoplasm, where accessory factors dissociate for recycling back to the nucleus (Matera *et al.*, 2007). Gemin5, a member of the SMN complex, specifically recognizes the conserved Sm sites of snRNAs and binds them through its characteristic WD repeat motif with high affinity (Battle *et al.*, 2006; Lau *et al.*, 2009). Consistent with its role as a U-snRNA chaperone, immunoprecipitation of Gemin5 from cell extracts indicated that a fraction of the protein exists free of other SMN complex components; a recent study of the effects on SMN complex activity of protein synthesis inhibition demonstrated the accumulation of an snRNA-Gemin5 dimer, consistent with an independent intermediate in which Gemin5 serves as a chaperone of the RNA species (Battle *et al.*, 2007). It is the highly specific interaction between U-snRNAs and Gemin5, and the subsequent interaction of that subcomplex with the SMN complex, that enables the equally specific SMN complex recognition of its RNA targets (Yong *et al.*, 2010).

The Sm protein substrates of the SMN complex comprise SmB, D1, D2, D3, E, F and G; SmB' is alternate splicing isoform of SmB and differs only in the absence of eleven amino acid residues at the C-terminus (Meister *et al.*, 2001a). A highly conserved family with orthologues from mammals to prokaryotes, all of the Sm proteins, as well as the related LSm proteins, are characterized by a common fold, the "Sm domain," consisting of an N-terminal helix followed by a highly bent five-stranded antiparallel β -sheet. The Sm and LSm proteins display a tendency to self-oligomerize or interact with each other,

forming a head-to-tail continuous β -sheet through interactions made between edge β -strands of interacting proteins (Kambach *et al.*, 1999). Both *in vitro* and *in vivo*, Sm proteins form preferential heteromeric subcomplexes: D1/D2; D3/B; and E/F/G (Camasses *et al.*, 1998; Lehmeier *et al.*, 1994; Raker *et al.*, 1996). Based on biochemical data and the geometric and physical properties of the Sm D3/B and D1/D2 crystal structures, Kambach *et al.* proposed a model in which the seven Sm proteins assemble into a hetero-heptameric ring around a central cationic aperture large enough to accommodate a single-stranded RNA (Kambach *et al.*, 1999). This view was subsequently confirmed in images generated by cryo-electron microscopy and x-ray crystallography (Figure 1.2) (Krummel *et al.*, 2010; Stark *et al.*, 2001).

Three Sm proteins, D1, D3 and B, contain “RG motifs,” arginine/glycine-rich regions C-terminal to their Sm domains that are symmetrically dimethylated prior to snRNP assembly; this modification is effected by the methylosome, a complex containing protein methyltransferase 5 (PRMT5), pICln and WD45/MEP50 (Brahms *et al.*, 2001; Friesen *et al.*, 2001a; Friesen *et al.*, 2001b). The conserved protein pICln competently binds all Sm protein monomers except SmE, as well as heterodimers D1/D2 and D3/B(B') in an otherwise unstable hetero-pentamer of D1/D2/E/F/G, and prevents their participation in snRNP assembly, presumably by averting their unregulated early self-association or interaction with RNA (Figure 1.5) (Chari *et al.*, 2008; Friesen *et al.*, 2001b; Meister *et al.*, 2001b; Pu *et al.*, 1999). It is suggested that pICln accompanies Sm D1, D3 and B to the methylosome, where its presence enhances PRMT5 methylation of

the Sm RG motifs, although it is unclear whether it recruits monomeric Sm proteins for this purpose or the dimers D1/D2 and D3/B (Pesiridis *et al.*, 2009; Pu *et al.*, 1999). Chari *et al.* showed that pICln also chaperones Sm proteins to the SMN complex when bound to the Sm dimer D3/B and the pentamer D1/D2/E/F/G; the latter is a long-lived species detectable by fractionation of HeLa extracts by gel filtration, while the former, although stable *in vitro* and necessary for snRNP assembly, is not detectable apart from the methylosome. Both biochemical studies and images based on electron microscopy indicate that pICln-Sm protein subcomplexes require, minimally, SMN and Gemin2 for efficient interaction and the dissociation of pICln after transfer of its Sm protein substrates, which is in turn necessary before the Sm protein-charged SMN complex becomes capable of proceeding in snRNP assembly (Chari *et al.*, 2008).

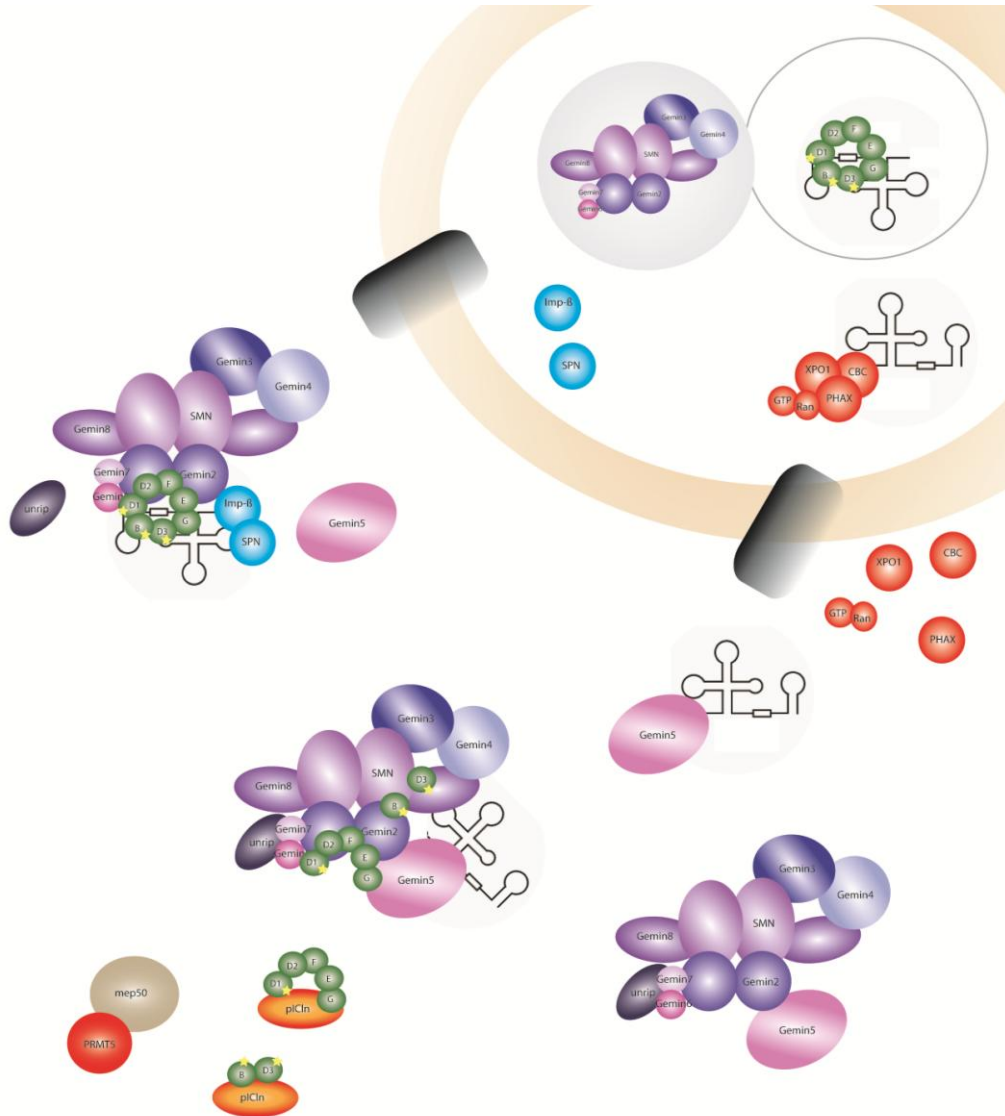


Figure 1.5. Overview of the survival motor neuron (SMN) functions in the assembly of mature spliceosome particles. Small nuclear RNAs (snRNAs) are transcribed by RNA polymerase II. After addition of a m^7G cap, binding is initiated by the nuclear export complex consisting of PHAX, XPO1/CRM1, RAN, and the cap-binding complex (CBC). Upon entering the cytoplasm, the nuclear export complex dissociates. Within the cytoplasm, pICln chaperones Sm proteins to the methylosome for PRMT5 methylation of the C-terminal tails of Smb, Smd1, and Smd3, then escorts the D1/D2/E/F/G and D3/B subcomplexes separately to the SMN complex. The SMN complex binds the chaperoned Sm protein pentamer, releasing pICln, then recruits the snRNA before completing the Sm protein ring with the D3/B dimer to achieve U-snRNP core assembly. The snRNA m^7G cap is hypermethylated, and the nuclear import complex consisting of snurportin and importin- β interacts with the m^3G cap and the SMN/snRNP complex and transports the entire complex into the nucleus. Upon entry, the SMN complex localizes to Gems and the snRNPs to Cajal bodies.

2.2 The SMN complex mediates snRNP assembly

The precise role played by each SMN complex component in the overall scheme of snRNP biogenesis remains unclear, although insights into the functions of certain members have begun to appear. Gemin5 is the established chaperone of U-snRNAs, responsible both for discriminately selecting its targets through high-affinity binding to their conserved Sm sites and for escorting those RNAs to the SMN complex and facilitating their binding there (Battle *et al.*, 2006; Lau *et al.*, 2009; Yong *et al.*, 2010). The crystal structure of the Gemin6-Gemin7 heterodimer demonstrates significant structural homology, for both proteins, to the conserved Sm fold of Sm proteins, suggesting a model in which Gemin6-Gemin7 substitutes for the SmD3/B heterodimer in the seven-membered Sm ring at some intermediate stage of snRNP assembly; a role for unrip in mediating this exchange has recently been imputed from pulldown assays showing disruption of a stable SMN-Gemin2-Gemin7 interaction in the presence of unrip (Ma *et al.*, 2005; Ogawa *et al.*, 2009). Sequence homology that indicates that Gemin3 is a DEAD-box helicase may ascribe to that protein a role in RNA unwinding activity (Charroux *et al.*, 1999).

The conserved catalytic core of the SMN complex, however, appears to consist of SMN and Gemin2. In *Schizosaccharomyces cerevisiae*, the perhaps simplest, most ancestral version of the SMN complex contains only those two proteins, and an SMN complex comprising only recombinant SMN and Gemin2 from *Drosophila melanogaster*, an

organism which does possess Gemin3 and Gemin5 orthologues, was fully competent to assemble snRNPs *in vitro* (Hannus *et al.*, 2000; Kroiss *et al.*, 2008).

SMN, a 294-residue, 32kDa protein (sometimes reported as 38kDa due to a tendency to run with an anomalously high apparent molecular weight in polyacrylimide gel electrophoresis experiments), is highly conserved evolutionarily among eukaryotes from humans to the fission yeast *S. pombe* (Liu *et al.*, 1997). SMN is essential for viability in all species tested to date: knockouts in yeast, worm, fly and mouse models result in lethality (Briese *et al.*, 2009; Chan *et al.*, 2003; Hannus *et al.*, 2000; Schrank *et al.*, 1997). Every SMN orthologue contains two regions of high sequence homology at its N- and C-termini, and metazoans share a third, central canonical Tudor domain (Liu *et al.*, 1997; Talbot *et al.*, 1998; Young *et al.*, 2000). The C-terminal region, including residues that map to exons 6 and 7, is characterized by an unusual YxxGYxxGYxxG motif and usually referred to as the “YG box” (Talbot *et al.*, 1998). A number of studies have pinpointed this region as necessary for SMN self-association that is, in turn, essential to its ability to assemble snRNPs (Liu *et al.*, 1997; Lorson *et al.*, 1998; Young *et al.*, 2000).

Two reports have also suggested an additional N-terminal region of SMN oligomerization (Ogawa *et al.*, 2007; Young *et al.*, 2000). The overall stoichiometry of SMN self-association, however, remains uncertain. Only the central Tudor domain is identifiable as a known structural motif based on sequence homology and has been

structurally characterized by both NMR spectroscopy and X-ray crystallography; like other Tudor domains, it forms a highly bent β -sheet consisting of five strands that form a barrel-like fold (Sprangers *et al.*, 2003; Talbot *et al.*, 1998). Several studies implicate it in Sm protein binding, highlighting in particular its preferential interactions with the symmetrically dimethylated arginine-rich C-terminal tails of Sm D1, D3 and B (Bühler *et al.*, 1999; Selenko *et al.*, 2001).

Gemin2 was identified early in the study of SMN as a core component of the SMN complex; its interaction with SMN remains intact even under stringent (high salt) conditions (Liu *et al.*, 1997). Coexpression of both proteins, but not expression of either protein alone, is required to reconstitute active SMN complex *in vitro*, and Gemin2 knockdown inhibits SMN complex-mediated snRNP assembly (Feng *et al.*, 2005; Kroiss *et al.*, 2008). The Gemin2-binding domain of SMN has been proposed to reside within the conserved N-terminal region of that protein (Liu *et al.*, 1997; Ogawa *et al.*, 2007; Young *et al.*, 2000).

Formerly referred to as SMN-interacting protein 1 (SIP1), Gemin2 itself is a 280-residue, 32 kDa protein even more highly conserved across evolutionary time than SMN; unlike that latter, an identifiable Gemin2 orthologue, Brr1, exists in the budding yeast *Saccharomyces cerevisiae* (Liu *et al.*, 1997; Noble & Guthrie, 1996a). Gemin2 is required for viability in mice, with homozygous knockout of the gene resulting in early embryonic lethality (Jablonka *et al.*, 2002). An analysis of Gemin2's primary sequence

reveals no immediately identifiable structural domains, although secondary structure predictions do propose an entirely α -helical fold. Isolating the SMN-binding domain of Gemin2 has proven challenging, although one report based on mammalian two-hybrid assays identified a Gemin2 fragment comprising the 180 C-terminal-most residues as the minimum necessary to bind SMN. Those researchers also reported a novel self-interaction for Gemin2, mapping to a slightly larger C-terminal fragment and purportedly acting to stabilize SMN's amino-terminal and carboxy-terminal self-association (Ogawa *et al.*, 2007).

Other protein interactions unrelated to Gemin2's role in snRNP assembly have also been imputed to the protein. In its SMN-bound form, Gemin2 is thought to play a key role in the repair of double-stranded DNA breaks by stimulating RAD51-mediated homologous pairing (Takaku *et al.*, 2011; Takizawa *et al.*, 2010). Gemin2 is also reported to interact with HIV-1 integrase, augmenting the assembly of reverse transcriptase onto viral RNA and facilitating HIV infection (Hamamoto *et al.*, 2006; Nishitsuji *et al.*, 2009).

2.3 Maturation of nascent assembled snRNP cores occurs in the nucleus

After SMN-mediated assembly, the snRNA component of the nascent snRNP cores undergoes two additional cytoplasmic processing steps (Figure 1.5). Hypermethylation under the auspices of trimethylguanosine synthase-1 (TGS1) converts the m⁷G cap to a 2,2,7-trimethylguanosine (TMG) cap, and the 3' end of the nucleic acid undergoes exonucleolytic removal of the 3' trailer sequences (so-called "3' trimming"); both

processes proceed only in the context of snRNAs bound to the Sm protein heptamer. The TMG cap and the assembled Sm protein core appear to act together as a nuclear localization signal, signaling nuclear import of the snRNP core via importin- β (Imp- β), during which course of events snuportin-1 (Snp1) serves as the adaptor specifically recognizing the TMG, while the still-bound SMN complex apparently fills that role for the Sm core (Matera *et al.*, 2007). Upon nuclear re-entry, the SMN complex and snRNP core dissociate, with the former enriching cellular bodies known as gems for eventual recycling by an uncertain mechanism to the cytoplasm. The latter temporarily inhabit Cajal bodies, where they are believed to undergo additional stages of maturation, including addition accessory proteins specific to the U-snRNP species, U-snRNP coupling to create the U4/U6 di-snRNP and U4/U6,U5 tri-snRNP and site-specific pseudouridylation and 2'-O-ribose-methylation, before participation in pre-mRNA splicing (Nizami *et al.*, 2010).

The U6 and U6atac snRNPs follow a different biogenesis pathway that remains confined to the nucleus. After transcription by RNA III polymerase, the U6 and U6atac snRNAs receive a γ -monomethyl cap. The snRNA lacks a canonical Sm site, but a heptameric ring of LSm ("Sm-like") proteins 2-8 assembles on a uridine-rich 3' sequence (the "U tract") of the snRNA. The LSm proteins share the same structural Sm fold with the Sm proteins, and U6 and U6atac snRNP assembly has been proposed as a nuclear function for the SMN complex, but conclusive evidence of that functionality is lacking. Given that the LSm2-LSm8 heteromer, unlike its Sm protein counterpart, can

be isolated as a stable seven-membered species in the absence of U6 snRNA, assembly of the U6 snRNP may follow a very different format (Will & Lührmann, 2001). LSM proteins also participate in a wider repertoire of cellular activities than the spliceosome-specific Sm proteins; a complex comprising LSM1-LSM7 (rather than LSM2-LSM8) has been documented to participate in mRNA degradation as part of an unrelated cytoplasmic complex, while another complex containing the LSM2-LSM7 proteins associates with snR5, a box H/ACA snoRNA that guides the site-specific pseudouridylation of rRNA (Bouveret *et al.*, 2000; Fernandez *et al.*, 2004; Spiller *et al.*, 2007; Tharun *et al.*, 2000).

3. Spinal muscular atrophy is caused by a deficit in functional SMN

Reduced levels of functional SMN lead to spinal muscular atrophy (SMA), an autosomal recessive neurodegenerative disorder characterized by degeneration of α -motor neurons in the anterior horn of the spinal cord, leading to progressive muscle weakness and wasting and, in severe cases, paralysis (Burghes & Beattie, 2009). The disease is typically subdivided into three types with onset during childhood and one type with adult onset; the most severe Type I SMN (Werdnig-Hoffmann disease) is typically diagnosed in the first months of life, and affected children are never able to sit or walk and have an average lifespan of eight months due to compromised breathing and airway protection. Types II and III SMA are less severe forms of the disease with later childhood onset; Type IV SMA is diagnosed in patients older than 30 (Zerres & Davies, 1999). SMA is the most common genetic cause of infant death, and affects 1 in 6000

live births with a carrier frequency of 1 in 35 for disease-causing mutations (D'Amico *et al.*, 2011).

The genetic underpinnings of SMA are well understood. The gene encoding the SMN protein was discovered in 1995 and exists in two copies mapped to chromosome 5q13 in the human genome, a telomeric copy (*SMN1*) and a centromeric copy (*SMN2*) present across a large inverted region of genomic duplication (Brzustowicz *et al.*, 1990; Brzustowicz *et al.*, 1992; Lefebvre *et al.*, 1995). The *SMN2* gene differs from its *SMN1* counterpart by a single base pair, a C → T transition at position +6 in exon 7 (Kashima & Manley, 2003). It is uncertain whether this base pair change, otherwise translationally silent, creates an exonic splicing silencer of exon 7 or disrupts an existing exonic splice enhancer; under either description, however, it ultimately prevents inclusion of exon 7 in the majority of transcripts (Cartegni & Krainer, 2002; Kashima & Manley, 2003). These transcripts, lacking exon 7, produce a truncated SMN protein (SMN Δ 7) that lacks the final sixteen amino acids. It is incompetent for self-association and thought to be highly unstable and rapidly degraded (Lorson & Androphy, 2000). The inclusion of four residues from exon 8 at the C-terminus of SMN Δ 7 transcripts, residues E-M-L-A, has been proposed to serve actively as a compelling degradation signal, or “degron”(Cho & Dreyfuss, 2010).

Most SMA cases are attributable to the homozygous loss of the *SMN1* gene or of exon 7 within it. The small percentage (estimated between 10-20%) of *SMN2* transcripts

containing exon 7 produces functional SMN protein, but at levels too low to fully compensate for the loss of *SMN1*. SMA is therefore the result of low levels of functional SMN protein, not its absence (Coover *et al.*, 1997; Lefebvre *et al.*, 1997). Homozygous loss of both *SMN1* and *SMN2* has never been reported, presumably as a result of lethality. Indeed, all SMA patients carry at least one copy of *SMN2*, and homozygous deletion of *SMN1* in mice, which carry no *SMN2*, is embryonic lethal (Hsieh-Li *et al.*, 2000; Schrank *et al.*, 1997). Copy number of *SMN2* correlates with disease severity; the additive effect of combining the functional SMN produced by several *SMN2* genes confers a protective effect (Yamashita *et al.*, 2004).

Although large deletion or conversion mutations in *SMN1* characterize the genetic basis of SMA in most patients, some 5% of patients instead display small deletions, splice mutations and missense point mutations (Alías *et al.*, 2009). Certain missense mutations localizing to exons 6 and 7 of SMN, the reported oligomerization domain, severely disrupt the ability of SMN to self-associate *in vitro* (Lorson *et al.*, 1998; Pellizzoni *et al.*, 1999). When accompanied by only one or two copies of *SMN2*, these patient mutations result in severe SMA phenotypes (Bühler *et al.*, 1999; Lorson *et al.*, 1998). Another set of severe SMA missense mutations appears in the SMN Tudor domain, where they may disrupt Sm protein-SMN interactions (Bühler *et al.*, 1999; Cuscó *et al.*, 2004; Sun *et al.*, 2005). A small number of milder mutations appear elsewhere in the protein, including D30N (Type II) and D44V (Type III) in the N-terminal Gemin2-binding domain (Sun *et al.*, 2005).

The molecular pathogenesis of spinal muscular atrophy, in particular the description of the link between deficiency in a ubiquitously expressed housekeeping protein and a motor neuron-specific disease phenotype, has proven a controversial field of inquiry. Hypotheses explaining the functional role of SMN in the mechanism of SMA fall broadly into two categories. The first, sometimes called the “nucleocentric dogma,” suggests that the disruption in snRNP biogenesis consequent to SMN deficiency causes deleterious effects in gene splicing, to which certain essential motor neuron proteins are particularly susceptible. In the second, it is proposed that SMN has a functional additional to its role in RNP assembly that is specific to motor neuron axons. Evidence exists to support both positions, and no clear consensus has yet emerged.

The first hypothesis predicts that an alteration in snRNP assembly will lead to a subsequent alteration in the amount or profile of snRNPs produced, then eliciting a change in splicing patterns (Eggert *et al.*, 2006; Gabanella *et al.*, 2007; Pellizzoni, 2007). Developed snRNP assembly assays have in fact demonstrated, in mice, a decrease in snRNP assembly activity concomitant with the severity of the SMA disease model (Gabanella *et al.*, 2007); in zebrafish, reintroduction of assembled snRNPs can rescue motor neuron defects caused by lower levels of SMN (Winkler *et al.*, 2005). Notably, in murine tissues from SMA-affected animals, reduced snRNP assembly also prompted uneven changes to snRNP profiles and a preferential reduction of snRNPs comprising the minor spliceosome, especially of U11 snRNP in the spinal cord,

although a target gene both spliced by the U12-spliceosome and possessing a functional implication in SMA has not been reported (Gabanella *et al.*, 2007; Zhang *et al.*, 2008). Although experiments using expression arrays and exon arrays have described hundreds of alterations in gene expression in SMA mice, these studies of tissues from older, terminally ill animals distinguish poorly between changes resulting from the disease state of the animal and those resulting from low SMN levels (Zhang *et al.*, 2008). While snRNP assembly does therefore appear to be altered in SMA, yielding reduced levels of certain snRNPs and perhaps altering splicing patterns across a number of genes, which target genes, if any, are specifically affected remains unknown.

An equally widespread counter-proposal holds that SMN exercises roles in axon outgrowth, guidance and/or the formation of neuromuscular junctions (NMJs) that are compromised in SMA (Briese *et al.*, 2005; Fan & Simard, 2002). Early immunohistochemical studies detected the presence of SMN in neural dendrites and axons (Béchade *et al.*, 1999; Jablonka *et al.*, 2002; Pagliardini *et al.*, 2000); GFP-SMN could also be visualized in granules that moved bidirectionally in neuronal processes, at speeds consistent with fast axonal transport (Hirokawa, 1998; Zhang *et al.*, 2003). SMN and Gemins, in the absence of Sm proteins, were later detected in both these mobile granules and larger, stationary counterparts, suggesting a role for SMN or the SMN complex outside of U-snRNP biogenesis (Zhang *et al.*, 2006). Another report demonstrated the presence of SMN in axons in the absence of Gemin2, strengthening

the claim for an SMN role in motor neurons separate from snRNP assembly (McWhorter *et al.*, 2008).

Additionally, SMN interacts and co-localizes in cultured cells with profilin IIa and hnRNP-R, both of which play important roles in neuronal axons and growth cones. Profilin IIa is involved in correct neurite outgrowth, while hnRNP-R binds β -actin mRNA, which in many neuron types must be transported to axon growth cones for local translation (Rossoll *et al.*, 2002; Rossoll *et al.*, 2003; Sharma *et al.*, 2005). Based on actin-specific anti-sense probes, both hnRNP-R, which contains both an SMN-interacting and an RNA-interacting domain, and SMN demonstrate involvement in β -actin mRNA translocation (Rossoll *et al.*, 2003). Impaired β -actin synthesis, perhaps the result of inhibited SMN function, is also suggested to underlie the reduced integration of voltage-gated Ca^{2+} channels observed in the growth cones of cultured model SMA cells (Jablonka *et al.*, 2007). An interaction with plastin 3, a stabilizer of β -actin, has also been proposed for SMN (Oprea *et al.*, 2008). A number of SMN mutations have been reported that fail to rescue motor axon outgrowth anomalies, but which retain SMN self-oligomerization and Sm binding capacity (Carrel *et al.*, 2006). (Perhaps more pertinently, however, snRNP assembly was unaddressed.) This body of data makes an axon-specific role for SMN underpins SMA a possibility, but conclusive evidence supporting that hypothesis, including a specific function for SMN and an explanation for the motor neuron specificity of the phenotype is still lacking.

A few reports also exist of a primary muscle effect. In *Drosophila* and mouse, SMN has been found at the actin-enriched I-band and actinin-enriched Z-disc of the sarcomere; in the latter organism, the entire SMN complex has been observed at the Z-disc (Rajendra *et al.*, 2007; Walker *et al.*, 2008). Expression of SMN in both neural and muscular tissues, but not muscles alone, dramatically improved the survival of severe SMA mice; in *smn*-knockout *Drosophila*, SMN expression in neural and mesodermal tissue evinced a similar decline in larval lethality (Chan *et al.*, 2003; Gavrilina *et al.*, 2008). Moreover, reduction of SMN in *Drosophila* mesodermal tissue had a much greater effect on adult viability than a similar reduction in neural tissue (Chang *et al.*, 2008). A possible muscle-specific role for SMN might include maintaining Z-disc integrity, signaling to the nucleus or localized transport of mRNPs at the sarcomeric Z-disc, and forms an intriguing additional field of study.

4. The *Schizosaccharomyces pombe* SMN and Gemin2 proteins form the simplest, most ancestral SMN complex

Schizosaccharomyces pombe is the most primitive organism with a recognizable SMN gene. After the discovery of human SMN as the disease gene for spinal muscular atrophy, bioinformatics searches in the late 1990s, Owen *et al.* identified a putative *S. pombe* orthologue demonstrating 25% sequence identity with its human counterpart (Lefebvre *et al.*, 1995; Owen *et al.*, 2000). Variously dubbed ySMN or yab8p and here described as spSMN, the 152 amino acid, 17.4 kDa protein is essential for *S. pombe* viability. It displays pronounced sequence conservation at its N- and C-termini,

recognizable as a Gemin2-binding domain and a YG box self-association domain (Owen *et al.*, 2000; Paushkin *et al.*, 2000). Its self-association can be demonstrated by GST-pulldowns and, in a remarkable example of structural conservation, extends to association with human SMN; it can also be disrupted by a deletion of the YG box, in analogy to similar deletions found in SMA disease mutants in its human counterpart (Owen *et al.*, 2000; Paushkin *et al.*, 2000). Unlike its counterparts in higher organisms, however, the *S. pombe* SMN lacks a signature Tudor domain.

S. pombe two-hybrid assays also identified a Gemin2 orthologue, the 235 amino acid, 27 kDa Yab8p-interacting protein (Yip1p; here spGemin2), which exhibits a sequence 20% identical and 45% similar to human Gemin2. Although lacking a region corresponding to human residues 152-179, it otherwise expresses homology throughout its primary sequence, with the most marked conservation at its N- and C-termini. spGemin2 displays robust affinity for spSMN in GST-pulldowns, but does not interact detectably with human SMN (Hannus *et al.*, 2000).

The *S. pombe* SMN complex functions, like its orthologues in higher organisms, as an assembly machine for spliceosomal snRNPs; using a strain of *S. pombe* containing an SMN temperature-degron allele and comparing with wild-type expression at the restrictive temperature, SMN disruption was demonstrably linked to a reduction in U-snRNA, Sm protein and U-snRNP levels (Campion *et al.*, 2010). The rudimentary

assembly of SMN and Gemin2 in *S. pombe* may represent the most evolutionarily basic SMN complex (Figure 1.6).

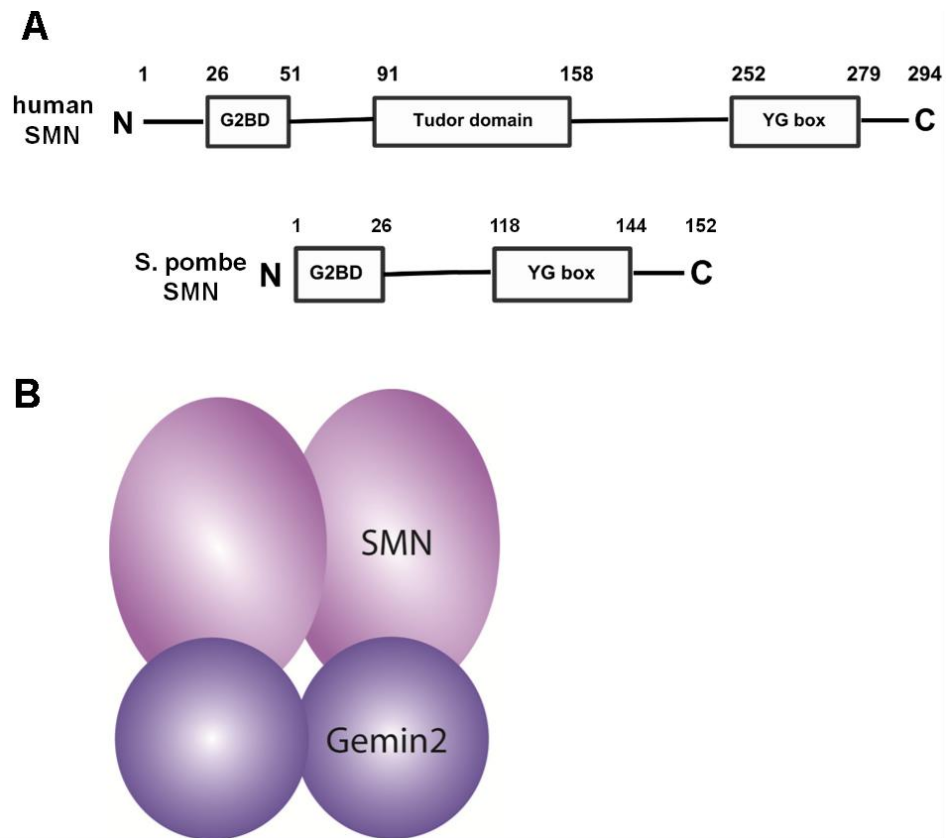


Figure 1.6. The *Schizosaccharomyces pombe* SMN complex A) The *S. pombe* SMN complex contains a Gemin2-binding domain and a YG box, but no Tudor domain. B) The *S. pombe* SMN complex contains only SMN and Gemin2.

5. Thesis objectives

The SMN complex contains at least nine protein members, among them Gemins2-8 and unrip and the eponymous SMN, the disease gene product in spinal muscular atrophy. An established function of the SMN complex lies in the assembly of seven Sm proteins onto an snRNA to form the structural core of a spliceosomal snRNP; the link between the role of SMN in that function or between another independent role of SMN and SMA remains uncertain.

A mounting body of evidence has begun to emerge detailing certain structural details and biochemical roles for members of the SMN complex, particularly relating to their roles in snRNP assembly. SMN demonstrates clear self-association, and failure of that oligomerization impedes SMN protein stability and catalysis of snRNP assembly and is linked to SMA pathogenesis. Gemin2 and Gemin8 are also thought to interact with themselves. One structural domain of SMN, its canonical Tudor domain, has been solved by both NMR and x-ray crystallography and is suggested to form a structural platform for the interaction of symmetrically dimethylated SmD1, D3 and B. Stable subunits of the SMN complex, comprising SMN-Gemin2-Gemin8, Gemin3-Gemin4-Gemin5, and Gemin6-Gemin7-unrip have been isolated *in vivo* and may represent assembly intermediates. Gemin5 has been pinpointed as a chaperone for newly transcribed nuclearly exported U-snRNAs, and Gemins 6 and 7 were demonstrated by protein x-ray crystallography to display an Sm-protein-like fold, bringing to mind a

hypothesis that they may act as an Sm dimer-surrogate in the construction of the Sm protein heteroheptamer.

This body of knowledge is still critically limited in several respects. Apart from the Tudor domain of SMN and the structure of the Gemin6-7 dimer, no atomic structures exist of any SMN complex components, severely handicapping efforts to understand the molecular basis of the complex's function in snRNP assembly and SMA pathogenesis. Functions have yet to be ascribed to several of the complex's proteins; despite the central, conserved role apparently played by SMN and Gemin2, the former remains largely undescribed and an absence of sequence homology or structural data for the latter has left its purpose wholly obscure. Without a structural knowledge of these two proteins, which form the catalytically competent core of the complex, a full understanding of the role of the SMN complex in biology and disease is unachievable.

With the goal of closing the gap in our knowledge of SMN and Gemin2, both in establishing a structural framework for those two proteins from which further studies probing their biological functions might be designed and in delineating the oligomeric state of SMN and Gemin2 and its relationship to disease, this dissertation undertakes three lines of experimental questioning. In the first, the NMR structure of the minimal binding domains of SMN and Gemin2 is presented, with accompanying mutational analysis of key SMN residues at the SMN-Gemin2 interface and a description of the role that two SMA patient mutations in that SMN construct play in that interaction. The

second describes a significant conformational change and stabilization of Gemin2 upon SMN binding and a low-resolution description of full-length, SMN-bound Gemin2. Finally, a third part characterizes the oligomerization state of the full-length SMN-Gemin2 hetero-oligomer from *Schizosaccharomyces pombe*.

The NMR structure of the minimal binding domains of SMN and Gemin2

In a previous, unpublished result, the Van Duyne laboratory at the University of Pennsylvania identified the minimal binding domains of Gemin2 and SMN using an in-house bacterial two-hybrid assay; these comprise a peptide of SMN containing residues 26-51 and a larger domain of Gemin2 including residues 95-280.

In the course of the investigations detailed in this dissertation, the SMN²⁶⁻⁵¹-Gemin2⁹⁵⁻²⁸⁰ interaction was confirmed using an *in vitro* fluorescence anisotropy binding assay and the minimal SMN-Gemin2 complex thus formed was probed biophysically by sedimentation velocity, sedimentation equilibrium and size-exclusion chromatography in-line with multi-angle light scattering. Its atomic structure was solved by triple-resonance multidimensional NMR spectroscopy based on backbone dihedral restraints, short-range NOE and long-range paramagnetic relaxation enhancement (PRE) distance restraints, small-angle scattering and residual dipolar coupling (RDC) orientational restraints. Gemin2 and SMN form a novel, all α -helical fold. The SMN-Gemin2 interface and two documented SMA patient mutations in that SMN construct were probed mutationally using fluorescent anisotropy binding assays, confirming the

essential nature of certain interfacial residues predicted by the NMR structure, while indicating no effect from either the D30N (Type II) or D44V (Type III) SMA on SMN-Gemin2.

The biophysical properties of Gemin2 in the presence and absence of SMN binding

To describe changes to Gemin2⁹⁵⁻²⁸⁰ upon SMN binding, the structure of unbound Gemin2⁹⁵⁻²⁸⁰ was compared to that of SMN²⁶⁻⁵¹-Gemin2⁹⁵⁻²⁸⁰. Sedimentation equilibrium and SEC-MALS indicated that both species exist as monomers in solution, but the radius of gyration, maximum dimension and stable shape reconstructions of unbound Gemin⁹⁵⁻²⁸⁰ in SAXS studies pointed to a much more extended shape. A ¹H-¹⁵N HSQC of ¹⁵N-labeled unbound Gemin2⁹⁵⁻²⁸⁰ showed line broadening and a collapse of peak dispersion, indicating incomplete folding. SMN may therefore play a role in stabilizing the structure of Gemin2.

The structure of the SMN²⁶⁻⁵¹-Gemin2⁹⁵⁻²⁸⁰ minimal complex and the SMN²⁶⁻⁵¹-Gemin2¹²⁻²⁸⁰ (full-length) complex were also characterized biophysically for comparison. Contrary to reports of Gemin2 self-interaction, both of the Gemin2-SMN complexes, as well as unbound Gemin2⁹⁵⁻²⁸⁰ and Gemin2¹²⁻²⁸⁰, are monomeric at all concentrations tested. The SMN²⁶⁻⁵¹-Gemin2¹²⁻²⁸⁰ complex demonstrated a more elongated character than the globular minimal complex, attributable to its N-terminal region, which forms a rigid arm-like structure in SAXS shape reconstructions and suggests a number of functional hypotheses.

Determination of the stoichiometry of SMN and Gemin2 in the full-length *S. pombe* complex

An array of biophysical techniques was employed to determine the oligomeric state of the complex formed by the full-length *Schizosaccharomyces pombe* SMN and Gemin2 orthologues. Analytical size-exclusion chromatography suggested a high molecular weight species, but sedimentation equilibrium analytical ultracentrifugation studies provided, surprisingly, a superior description of the spSMN-Gemin2 complex as a dimer-tetramer equilibrium. SEC-MALS analysis over a range of protein concentrations also indicated that a dimer of the spSMN-Gemin2 heterodimer is actually the smallest discrete oligomer of the complex sampled at low concentrations. Small-angle x-ray scattering (SAXS) and sedimentation velocity experiments confirmed the extended nature of the particle, indicating a large radius of gyration and maximum dimension, and sequence analysis and the characteristic shape of a Kratky plot derived from SAXS data suggested that spSMN may possess a region of disorder. This model of SMN self-oligomerization yields the startling insight that, contrary its apparent behavior in self-exclusion chromatography and sucrose gradient fractionation experiments, the SMN complex forms small, discrete oligomers with unusual hydrodynamic properties.

Chapter II: The NMR structure of the minimal binding domains of SMN and Gemin2

Introduction

The SMN and Gemin2 proteins comprise the minimal catalytic machinery necessary to perform the critical function of spliceosomal U-snRNP assembly; the *S. pombe* SMN complex contains only those two members, and the more complex *D. melanogaster* SMN complex, reduced to SMN and Gemin2, is still competent for U-snRNP assembly *in vitro* (Campion *et al.*, 2010; Kroiss *et al.*, 2008). Gemin2, a 32 kDa, 269 residue protein, binds tightly and directly to SMN. Unlike SMN, however, with its known Tudor domain platform for Sm protein interaction and a tyrosine-glycine-rich oligomerization domain that plays a role in spinal muscular atrophy, the structure and function of Gemin2 remain nearly opaque.

A structural understanding of SMN and Gemin2 will provide insight into the role played by Gemin2, answers to mechanistic questions about the molecular details of SMN complex-mediated U-snRNP biogenesis and a structural framework off of which to build future structure-function studies. Here the structure of the complex formed by the minimal binding domains of Gemin2 and SMN is solved by heteronuclear multidimensional nuclear magnetic resonance spectroscopy. The hydrophobic interface between the two protein components is described, and the roles played by key conserved interfacial residues in binding are probed by mutagenesis. The two SMA patient

mutations within the SMN Gemin2-binding domain are shown, despite mixed reports in the literature, to have no effect on SMN-Gemin2 binding.

Results

Delineation of the minimal binding domains of human SMN and Gemin2

Despite a keen interest in SMN and Gemin2, owing to their evident importance in both cellular housekeeping and human disease, the considerable difficulty encountered expressing and purifying full-length human SMN and Gemin2 for biochemical studies limited the variety of experimental pathways open to pursuit, particularly structural studies for which stable monodisperse protein preparations are requisite. In an attempt to circumvent the difficulties inherent to full-length SMN and Gemin2, the minimal binding domains of the two proteins were sought instead; it was hoped that a minimal SMN-Gemin2 complex containing only the protein domains necessary and sufficient for binding might possess more tractable solution properties and permit structural studies to proceed.

An in-house bacterial two-hybrid assay based on the methods of Dmitrova *et al.* was employed for this purpose (Dmitrova *et al.*, 1998). Briefly, the *lexA* DNA-binding domain fusions were expressed from a *lac* promoter on compatible plasmids and the reporter construct was present on an F'-episome in strain CSH142, such that a positive interaction resulted in repression of *lacZ* transcription and white colonies on plates

containing X-gal or white-pink colonies on MacConkey agar (Figure 2.1; reviewed in more detail in Materials and Methods.).

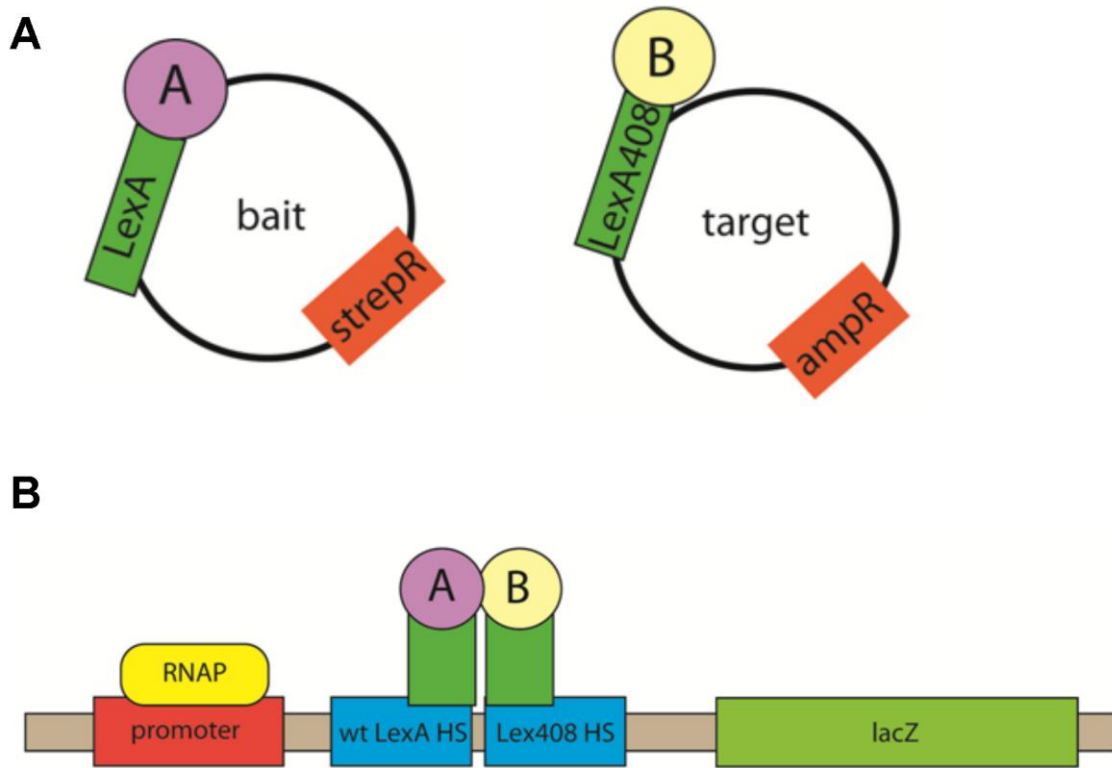


Figure 2.1 Schematic of bacterial two-hybrid assay system. A) Proteins of interest (A and B) are cloned in-frame with wildtype LexA (bait) and *lexA408* (target) in a modified pETDuet in which the T7 promoter has been replaced by a *lac* promoter. B) After co-transformation into a reporter strain, a positive interaction between A and B results in repression of *lacZ* transcription and white colonies on plates containing X-gal.

Matthew Bernens, a technician in the Van Duyne laboratory at the University of Pennsylvania, performed the initial bacterial two-hybrid analyses and showed that an SMN fragment corresponding to exons 1-2b (residues 16-60) interacts robustly with Gemin2, as does a fragment corresponding to exons 1-3 (residues 16-156), consistent with reports that localized the Gemin2-binding domain to the N-terminus of SMN (Liu *et al.*, 1997; Ogawa *et al.*, 2007). No independent binding was observed, however, for

an SMN fragment containing exons 2b-3 (residues 52-156), contrary to one report that exon 2b mediates the SMN-Gemin2 interaction (Young *et al.*, 2000). Further truncations of the fragment containing residues 16-60 generated a minimal SMN fragment still capable of high-affinity binding to Gemin2 consisting of residues 31-51, approximately corresponding to exon 2a (Figure 2.2A,B).

The minimal SMN-binding domain of Gemin2 was identified at the same time as a region containing residues 95-280, corresponding roughly to the C-terminal two-thirds to the protein. No additional C-terminal truncations were supported. These results are in agreement with previous findings based on a mammalian two-hybrid assay that suggested a minimal Gemin2 binding domain of residues 101-280 (Figure 2.2A, B) (Ogawa *et al.*, 2007).

A

	G2 25-280	G2 47-280	G2 95-280	G2 165-280	G2 95-253
SMN 14-60	+	+	+	-	ND
SMN 14-156	+	+	+	-	-
SMN 31-156	ND	ND	+	ND	ND
SMN 31-51	+	ND	+	ND	ND
SMN 88-156	-	-	-	-	ND

	G2 100-280	G2 105-280	G2 110-280	G2 115-280	G2 120-280	G2 125-280
SMN 31-51	+	+	+	-	-	-

+: positive interaction; -: no interaction or weak interaction; ND: not determined

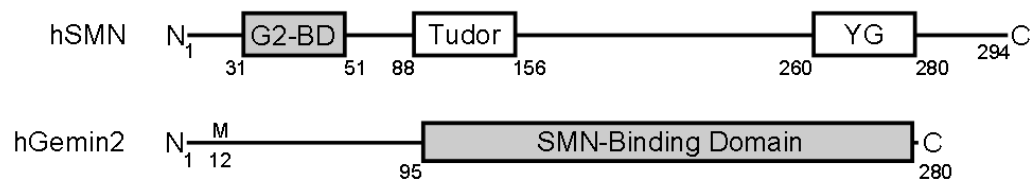
B

Figure 2.2 Domain boundaries of human SMN and Gemin2 A) Bacterial two-hybrid interactions between regions of hSMN and regions of hGemin2. B) Domain structures of SMN and Gemin2. The conserved Gemin2-binding domain, Tudor domain, and YG-box are shown for SMN. Minimal interaction domains are shaded. Gemin2 is assumed to initiate translation at M12, but numbering in this work follows that used elsewhere in the literature.

Under the auspices of this dissertation, the boundaries of the SMN Gemin2-binding peptide were expanded slightly to include residues 26-51. Serine residues 28 and 31 are reported to be phosphorylated in SMN *in vivo* and are suggested to modulate the efficiency of snRNP core assembly (Grimmler *et al.*, 2005b); since the affect of this post-translational modification on the interaction of SMN with Gemin2 was unknown, the residues were also included. Using the same bacterial two-hybrid system, the N-

terminal boundary of the Gemin2 SMN-binding domain was progressively truncated, and additional deletions of up to 15 residues from the N-terminus were tolerated. However, secondary structure predictions indicated these involved truncations of a long α -helix beginning at residue 100, and the Gemin2 boundaries of residues 95-280 were retained. Both SMN²⁶⁻⁵¹ and Gemin2⁹⁵⁻²⁸⁰ could be expressed bacterially and purified, and both were soluble to the micromolar concentration range.

SMN²⁶⁻⁵¹ binds Gemin2⁹⁵⁻²⁸⁰ and full-length Gemin2 with similar high affinity

Although SMN and Gemin2 have been reported qualitatively to interact with high-affinity, based on the resistance of their interaction to disruption in high salt (Liu *et al.*, 1997), a rigorous quantitative evaluation of their binding affinity has been lacking, due likely to the difficulty employing the full-length proteins in any experimental context. The minimal SMN²⁶⁻⁵¹ and Gemin2⁹⁵⁻²⁸⁰ constructs, however, could be purified separately and demonstrated reasonable solution behavior, opening the door to a more thorough determination of the binding affinity with which the two proteins interact.

To quantify the affinity of the interaction between SMN²⁶⁻⁵¹ and Gemin2⁹⁵⁻²⁸⁰, and to compare it to the interaction between SMN²⁶⁻⁵¹ and full-length Gemin2, the fluorescence anisotropy of fluorescein-labeled SMN was measured against increasing concentrations of Gemin2.

For this and all experiments described, full-length Gemin2 refers to the Gemin2 construct comprising residues 12-280. The primary sequence for human Gemin2 contains two possible initiator methionines, Met1 and Met12. The first eleven amino acids, however, are not present in so closely related an organism as the mouse, nor does the upstream methionine Met1 have a strong Kozak consensus sequence, the mRNA sequence three codons prior to the initiator methionine that signals the translational start site to the ribosome. Gemin2¹²⁻²⁸⁰ is therefore considered to be “full-length”.

The anisotropy binding curves were fit with a two-state binding isotherm corrected for receptor depletion, due to the comparatively high concentration of SMN (15 nM) with respect to the dissociation constant (Kenakin, 1993). Both Gemin2⁹⁵⁻²⁸⁰ and Gemin2¹²⁻²⁸⁰ bound the SMN peptide tightly, with similar affinities (3.3 ± 1.8 nM and 7.0 ± 2.5 nM, respectively; Figure 2.3), suggesting that the Gemin2⁹⁵⁻²⁸⁰ construct captures all the features of Gemin2 necessary to mediate its interaction with SMN.

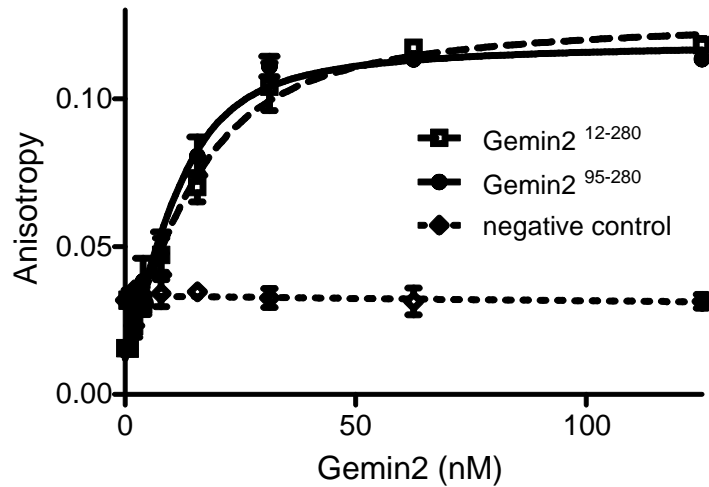


Figure 2.3 Binding of SMN²⁶⁻⁵¹ to Gemin2 or to Gemin2⁹⁵⁻²⁸⁰. Binding was based on fluorescence anisotropy of SMN N-terminally labeled with fluorescein isothiocyanate. The K_D values fit to the binding curves are 7.0 ± 2.5 nM and 3.3 ± 1.8 nM for Gemin2¹²⁻²⁸⁰ and Gemin2⁹⁵⁻²⁸⁰, respectively. No binding was observed to a labeled, unrelated peptide (NC). Error bars represent one standard deviation from the mean, based on three replicate experiments.

Phosphorylation of SMN serines 28 and 31 has no effect on Gemin2 binding

A report by Grimmer *et al.* found that SMN serine residues 28 and 31 are phosphorylated *in vivo*, at levels measurably higher in the cytoplasm than in the nucleus. Their phosphorylation appeared to correlate with the ability of the SMN complex to efficiently assemble spliceosomal U-snRNPs (Grimmer *et al.*, 2005b). These residues fall within the boundaries of the minimal SMN Gemin2-binding domain used in this study, and it seemed within the realm of speculation that their phosphorylation state might influence the interaction between SMN and Gemin2.

The effect of the phosphorylation of SMN serine residues 28 and 31 on SMN-Gemin2 binding was tested using synthetic phosphorylated (pSer28,pSer31) and

dephosphorylated SMN peptides in the same fluorescence anisotropy binding assay described above. The anisotropy of fluorescein-labeled SMN peptide was measured against increasing concentrations of Gemin2⁹⁵⁻²⁸⁰, and the anisotropy binding curves were fit with a two-state binding isotherm corrected for receptor depletion. SMN²⁸⁻⁵¹ and SMN²⁸⁻⁵¹(pSer28,pSer31) bound Gemin2⁹⁵⁻²⁸⁰ tightly, with substantially similar affinities (9.0 ± 1.6 nM and 4.1 ± 0.7 nM, respectively; Figure 2.4 and Table 2.2). The phosphorylation state of SMN serines 28 and 31 appears to have very minor influence on Gemin2 binding.

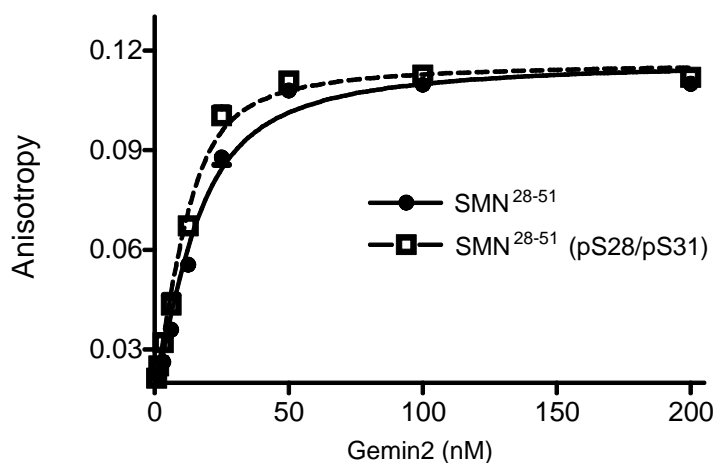


Figure 2.4 Binding of SMN²⁸⁻⁵¹ unphosphorylated and phosphorylated at Ser28 and Ser31 to Gemin2⁹⁵⁻²⁸⁰. The experiment employed the fluorescence anisotropy assay described in Figure 2.3. The K_D values fit to the binding curves are 9.0 ± 1.6 nM and 4.1 ± 0.7 nM for SMN²⁸⁻⁵¹ and SMN²⁸⁻⁵¹ (pSer28,pSer31), respectively. Error bars represent one standard deviation from the mean, based on three replicate experiments.

Purification and biophysical properties of the core SMN-Gemin2 complex

In an encouraging advance over the behavior of their full-length counterparts, both SMN²⁶⁻⁵¹ and Gemin2⁹⁵⁻²⁸⁰ as C-terminal Mxe intein-chitin binding domain-His6x

constructs were readily purified over sequential nickel NTA and chitin columns, followed by cleavage of the affinity tag, anion exchange chromatography, complex formation at room temperature in a molar excess of SMN²⁶⁻⁵¹ and gel filtration.

A number of biophysical properties of the unexpectedly tractable core SMN-Gemin2 complex were described during preparation for a planned series of crystallization attempts. Both size-exclusion chromatography in-line with multi-angle light scattering (SEC-MALS) and sedimentation equilibrium analytical ultracentrifugation indicated that the complex formed a 1:1 heterodimer of SMN²⁶⁻⁵¹ (3 kDa) and Gemin2⁹⁵⁻²⁸⁰ (21 kDa) in solution. SEC-MALS showed that the SMN²⁶⁻⁵¹-Gemin2⁹⁵⁻²⁸⁰ complex eluted as a single peak with an apparent molecular weight of 25 kDa with respect to globular molecular weight standards, while possessing a stable mass profile across the eluted peak with a weight-averaged molecular weight of 23.7 ± 0.1 kDa. Both values are highly consistent with the expected 24 kDa molar mass of a 1:1 SMN²⁶⁻⁵¹-Gemin2⁹⁵⁻²⁸⁰ complex (Figure 2.5).

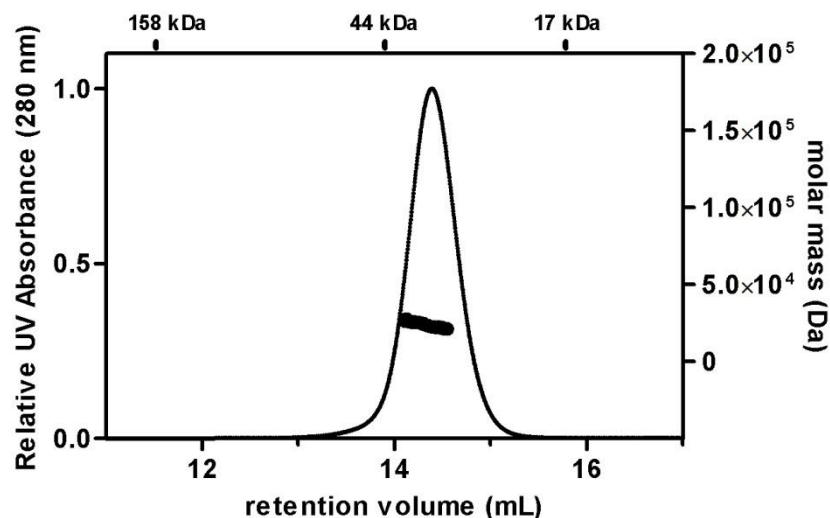


Figure 2.5. Representative SEC-MALS analysis of the Gemin2⁹⁵⁻²⁸⁰-SMN²⁶⁻⁵¹ complex. The elution volumes of globular protein standards are shown above the panel.

Sedimentation equilibrium analytical ultracentrifugation data on SMN²⁶⁻⁵¹-Gemin2⁹⁵⁻²⁸⁰ were collected at three speeds and three concentrations at 20°C and best fit to a non-interacting single species model that produced an estimate of a molecular weight of 30 kDa (Figure 2.6). While slightly higher than the predicted molecular weight of a core SMN-Gemin2 heterodimer, it generally corroborated the SEC-MALS estimate of the molecular weight and certainly failed to suggest oligomerization; instead, the three-day room-temperature experiment, performed before trial and error had fully defined the requirements for SMN²⁶⁻⁵¹-Gemin2⁹⁵⁻²⁸⁰ stability, contained no reducing agent and likely experienced protein aggregation.

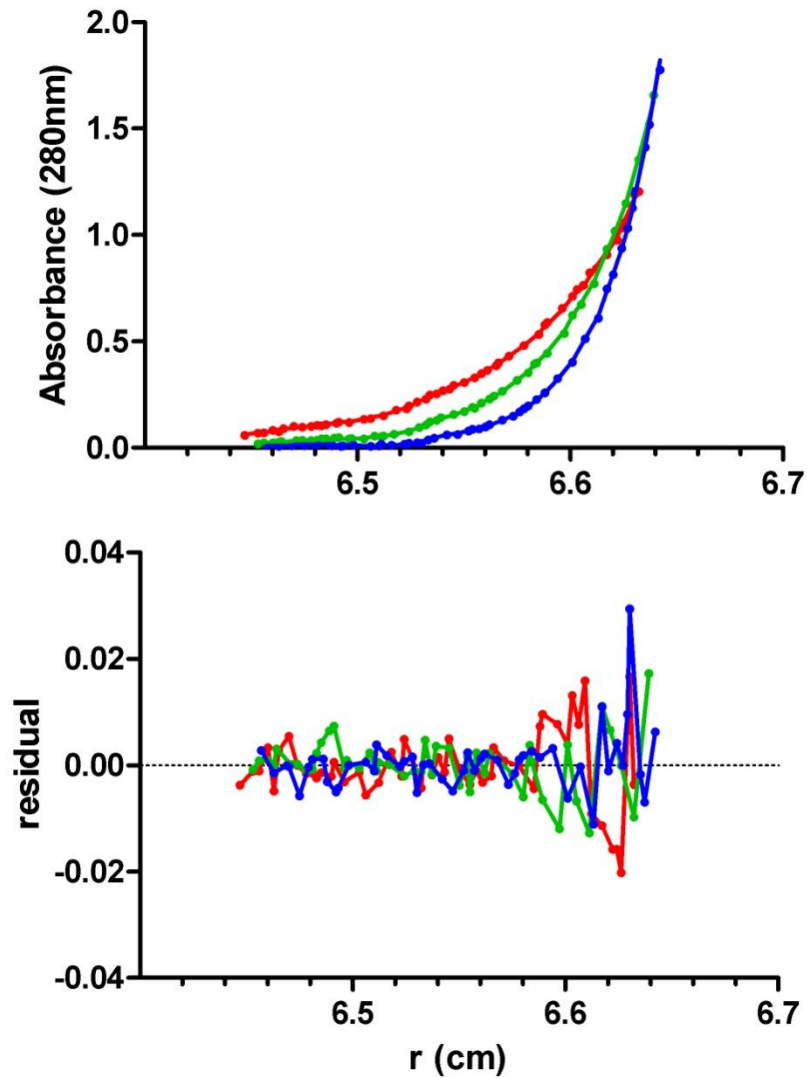


Figure 2.6 Representative sedimentation equilibrium analytical ultracentrifugation experiment on the core SMN-Gemin2 complex. Conducted at 4°C at 18 μ M, 11 μ M and 5 μ M. Here the curves are fit to non-interacting single species model.

Sedimentation velocity analytical ultracentrifugation provided an evaluation of the sedimentation coefficient and frictional ratio f/f_0 of the core SMN-Gemin2 complex. The frictional ratio is the ratio of the frictional coefficient f experienced by the molecule

when sedimenting to the theoretical frictional coefficient f_o for an ideal sphere of identical molecular weight and serves as a measure of particle elongation. It is related to the sedimentation coefficient through the Svedberg equation, where

$$f_o = 6\pi\eta r$$

for a perfect sphere of radius r in solution of viscosity η , and

$$f = \frac{M(1 - \bar{v}\rho)}{N_a S}$$

where M is the molar mass of the particle, N_a Avogadro's number, S the sedimentation coefficient, \bar{v} the partial specific volume and ρ the solvent density (Lebowitz *et al.*, 2002).

Sedimentation velocity data for SMN²⁶⁻⁵¹-Gemin2⁹⁵⁻²⁸⁰ at 25 μ M was collected at 20°C and fit well to a continuous $c(s)$ distribution yielding a single species with a sedimentation coefficient of 2.4S (Figure 2.7). From the sedimentation coefficient, the frictional ratio was calculated to be 1.27, very near the value of 1.2 cited for globular proteins and in accord with the observation that the complex evinced behavior in size-exclusion chromatography similar to that of globular molecular weight standards.

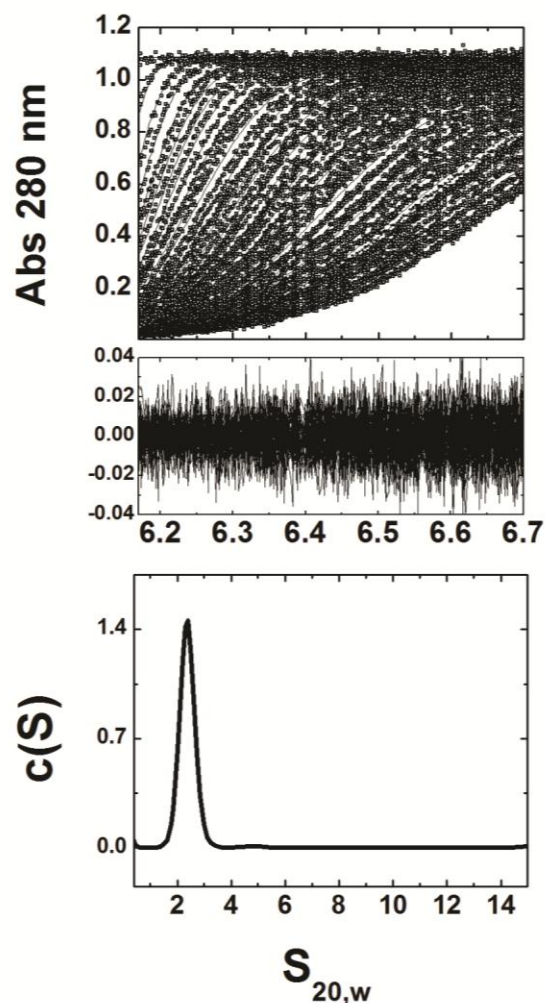


Figure 2.7 Sedimentation velocity analytical ultracentrifugation experiment on the SMN²⁶⁻⁵¹-Gemin2⁹⁵⁻²⁸⁰ complex at 20°C. Sedimentation velocity absorbance traces of SMN²⁶⁻⁵¹-Gemin2⁹⁵⁻²⁸⁰ at 280 nm occupy the top panel, with residuals of the experimental fits in the middle panel and a continuous sedimentation coefficient distribution ($c(S)$) of the protein in the bottom panel.

The SMN²⁶⁻⁵¹-Gemin2⁹⁵⁻²⁸⁰ complex formed a well-behaved, compact 1:1 heterodimer of the two proteins and appeared, and both SEC-MALS and sedimentation velocity experiments suggested monodisperse purified preparations. Protein crystallization experiments with the protein were undertaken, with an eye toward solving an elusive atomic structure, but neither the SMN²⁶⁻⁵¹-Gemin2⁹⁵⁻²⁸⁰ complex nor Gemin2⁹⁵⁻²⁸⁰ alone,

nor the complex formed by SMN²⁶⁻⁵¹ with any of the additional Gemin2 N-terminal truncations tolerated by the bacterial two-hybrid interaction screen, nor orthologous protein constructs from *D. melanogaster* or *S. pombe* yielded crystal hits.

The solution structure of the core SMN-Gemin2 complex

After the core SMN²⁶⁻⁵¹-Gemin2⁹⁵⁻²⁸⁰ complex proved refractory to crystallization, an initial ¹H-¹⁵N-HSQC of ¹⁵N-labeled protein showed dispersed peaks with sharp linewidths (Figure 2.8), suggesting a possibility of success for structural studies by NMR spectroscopy, and heteronuclear multidimensional nuclear magnetic resonance spectroscopy using both ¹⁵N- and ¹⁵N/¹³C-enriched SMN²⁶⁻⁵¹ and Gemin2⁹⁵⁻²⁸⁰ was employed to determine the solution structure of the core SMN-Gemin2 complex.

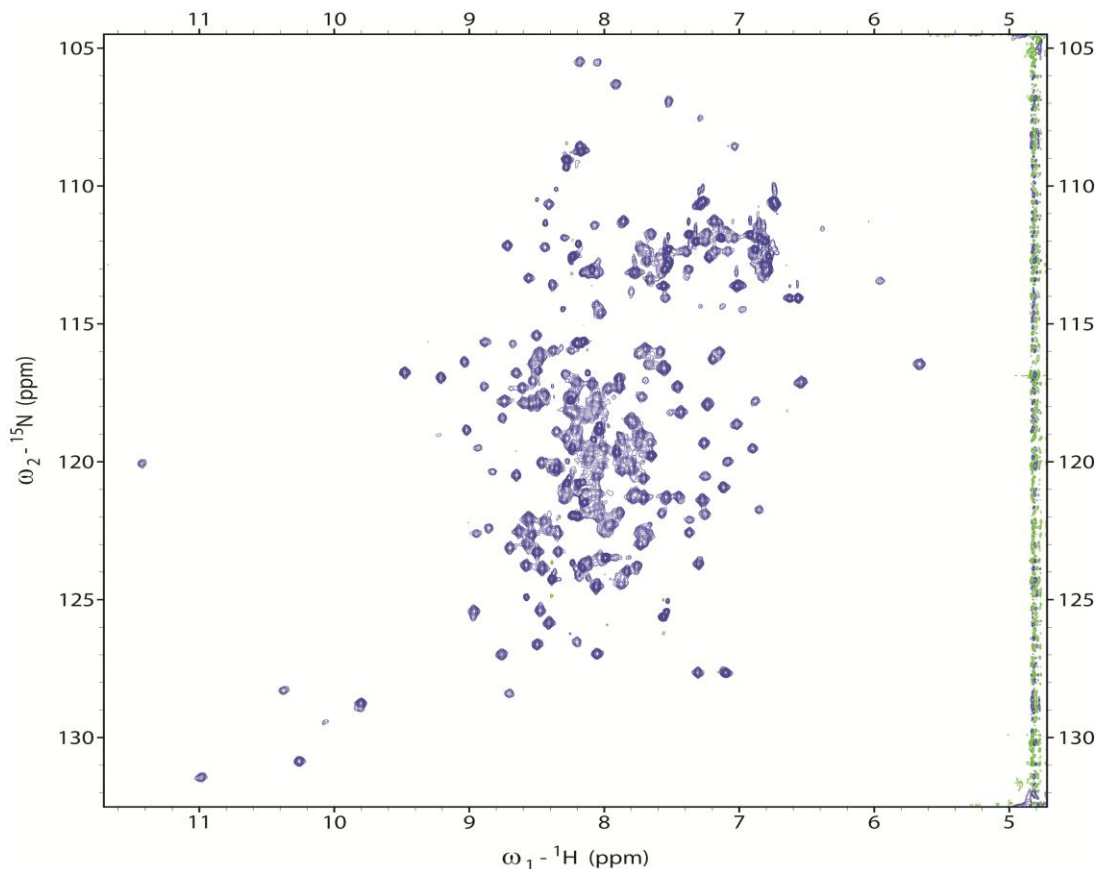


Figure 2.8 A two-dimensional ^1H - ^{15}N HSQC of SMN^{26-51} - Gemin2^{95-280}

NMR structural studies proved non-trivial with respect to SMN^{26-51} - Gemin2^{95-280} ; the complex's susceptibility to proteolysis hampered its stability for multi-day experiments at 25°C, as did a proclivity for oxidative precipitation only surmountable at very high concentrations of reducing agent, exchanged often for fresh buffer. At 24 kDa, the complex experienced many of the challenges to which solution NMR is heir with respect to large systems; weak signal due to line broadening made interpretation of some data challenging, and spectral overlap was sufficiently severe at times to require creative strategies for making backbone and sidechain peak assignments, and an unusual recourse was made to 4-dimensional through-space NOESY experiments to supplement the more typical 3D NOESY-HSQC and to resolve uninterpretable areas of peak

degeneracy. The SMN²⁶⁻⁵¹-Gemin2⁹⁵⁻²⁸⁰ complex also experienced a broad dynamic range, and the wide range of peak intensities from different regions of the protein provided another complicating factor in data collection and analysis.

Comprehensive resonance assignments were obtained using triple resonance, total correlation spectroscopy and NOE-based strategies. Backbone assignments were obtained first from a standard suite of through-space experiments, HNCA, HN(CO)CA, HNCACB, CBCA(CO)NH, HNCO and HN(CA)CO. Representative strip plots from the HNCA and HNCOCA, forming a “C α walk” for Gemin2 residues K137-E142, are depicted in Figure 2.9 and make clear, if some strips, the difficulty imposed by spectral crowding.

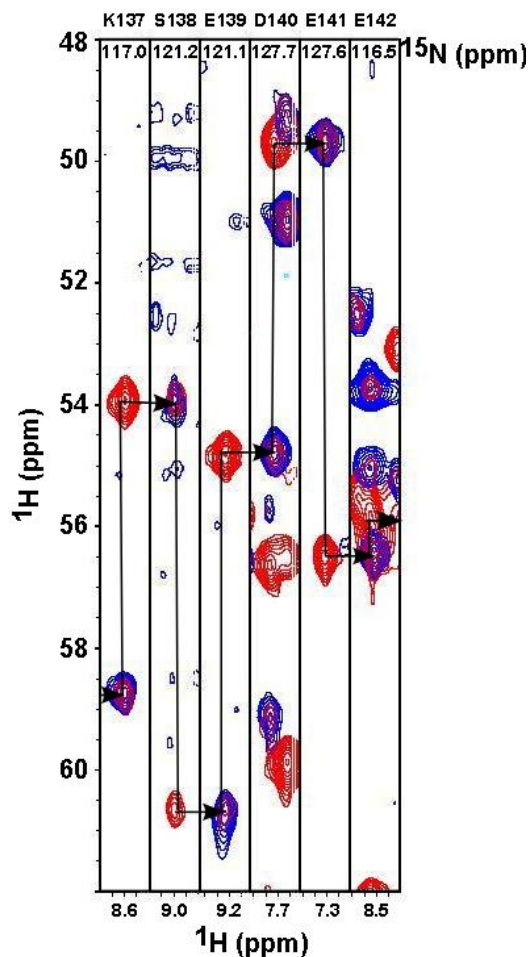


Figure 2.9 Triple resonance backbone assignment of Gemin2⁹⁵⁻²⁸⁰. Slices of the overlaid HNCA (red) and HNCOCA (blue) spectra of SMN²⁶⁻⁵¹-Gemin2⁹⁵⁻²⁸⁰ showing the connectivities for Gemin2 from K137-E142. The C_α connectivity is shown by a dotted black line.

Later experiments supplemented those listed above to facilitate assignments in areas of weak signal or spectral degeneracy. An ¹⁵N HSQC of a sample in which only Gemin2 was labeled with ¹⁵N-leucine enabled the assignment of most leucine backbone resonances, and a sample in which only SMN²⁶⁻⁵¹ was labeled resulted in complete

assignment of the SMN peptide backbone. Backbone assignments were complete to 97.3% of HN and N resonances and 94.4% of carbonyl carbon resonances.

Side chain assignments were obtained from H(CC)(CO)NH, (H)CC(CO)NH, HCCH-TOCSY and HCCH-COSY experiments. Assignment of all aliphatic sidechain proton and carbon resonances for SMN²⁶⁻⁵¹ Ile33 is illustrated in Figure 10. While neither the HCCH-TOCSY nor the HCCH-COSY (Figure 10A,B) evince complexity due to spectral degeneracy, the substantial overlap of resonances characteristic of many regions of the SMN²⁶⁻⁵¹-Gemin2⁹⁵⁻²⁸⁰ spectra are in evidence in the HCCH-TOCSY and HCCH-COSY spectra, especially in the HCCH-TOCSY slices at the H γ 1 and H γ 2 H-C frequencies.

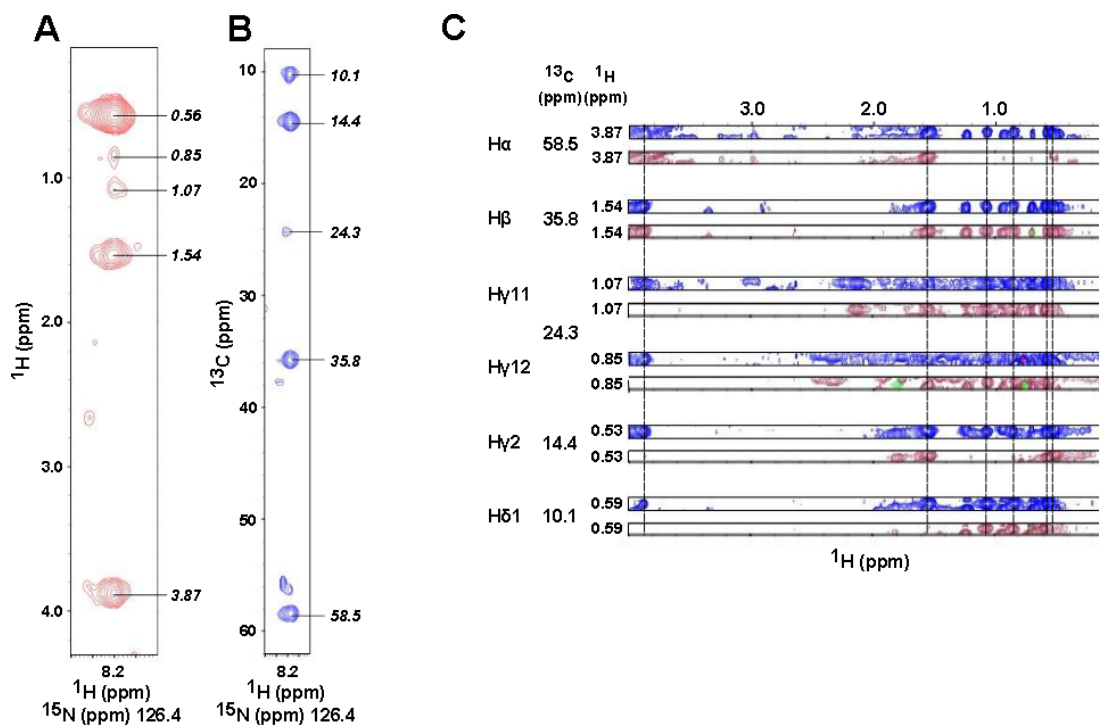


Figure 2.10 Triple resonance sidechain assignment of SMN²⁶⁻⁵¹ Ile33. A) H(CC)(CO)NH and B) (H)CC(CO)NH slices at the Trp34 backbone amide frequencies showing all Ile33 sidechain proton and carbon resonances, respectively. C) HCCH-TOCSY and HCCH-COSY slices showing all and immediately adjacent sidechain proton resonances, respectively, at each sidechain carbon frequency. The frequencies of each sidechain proton are depicted as dotted black lines.

Due to difficulty in making some sidechain assignments due to spectral degeneracy in some cases and to weak signal in others, some assignments were facilitated by three-dimensional ¹⁵N and ¹³C-edited NOESY-HSQC spectra. Stereo-specific side chain assignments of valine and leucine were determined from the ¹³C-coupled carbon HSQC of trace-labeled protein sample, in which only the *pro-S* (Val H γ 2, Leu H δ 2) methyl resonances appear as singlets (Neri *et al.*, 1989); a representative expansion of overlaid HSQCs from fully labeled and trace-labeled samples appears as Figure 2.11. Aromatic side-chain assignments were made using three-dimensional aromatic-optimized ¹³C NOESY-HSQC and HCCH-TOCSY experiments.

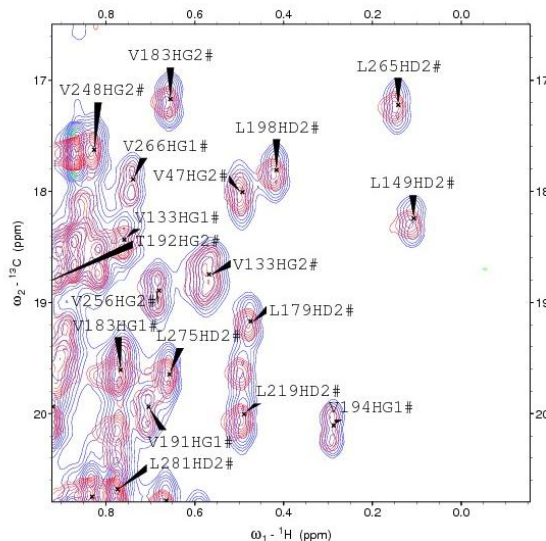


Figure 2.11 Stereospecific assignment of SMN²⁶⁻⁵¹-Gemin2⁹⁵⁻²⁸⁰ valine and leucine prochiral methyl groups. An overlay of the ¹H-decoupled ¹H-¹³C HSQC spectra of fully ¹³C isotopically labeled (blue) and trace-labeled (red) SMN²⁶⁻⁵¹-Gemin2⁹⁵⁻²⁸⁰. The *pro-S* methyl groups (H γ 2 and H δ 2) are singlets in the spectrum from the trace-labeled sample.

Appendix A provides a table of all SMN²⁶⁻⁵¹-Gemin2⁹⁵⁻²⁸⁰ resonance assignments.

Structural restraints primarily consisted of the traditional combination of nuclear Overhauser effect (NOE) inter-proton distances derived from three and four-dimensional ¹⁵N- and ¹³C-edited NOE spectra and backbone dihedral restraints calculated based on chemical shifts, but the number of available NOE and dihedral restraints alone was too few compared to the size of the protein to obtain a structural ensemble of the desired precision. Several other sources of structural restraint, with an emphasis on those providing longer-distance restraints than the short-range 5 Å NOE, were introduced to improve ensemble precision. A constraint on overall molecular shape was imposed from small-angle X-ray scattering data. Residual dipolar couplings measured in a bacteriophage Pf1 liquid crystalline medium provided long-distance

orientational restraints. To create a visual example, both unaligned (both blue) and partially aligned (both red) SMN²⁶⁻⁵¹-Gemin2⁹⁵⁻²⁸⁰, in-phase and anti-phase ¹H-¹⁵N HSQC-IPAP spectra were added and subtracted, and the resulting spectra superimposed. The two resulting combined spectra were then overlaid on each other to illustrate changes in splitting obtained in Pf1 (Figure 2.12). The blue and red arrows indicate the aligned and unaligned splitting observed for SMN T37 and Gemin2 G203 and G212.

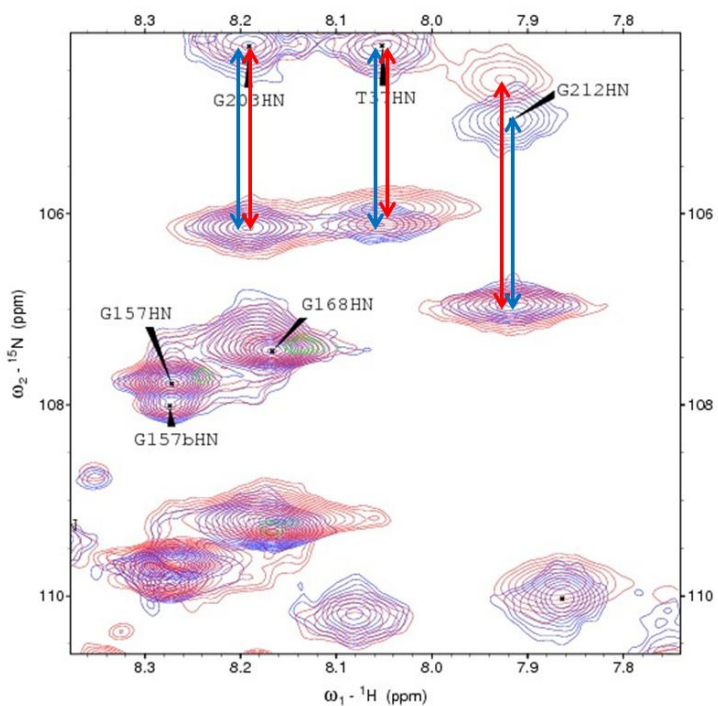


Figure 2.12 Residual dipolar couplings observed in partially aligned SMN²⁶⁻⁵¹-Gemin2⁹⁵⁻²⁸⁰. Spectra obtained by adding and subtracting in-phase and anti-phase ¹H-¹⁵N HSQC-IPAP spectra were first overlaid for both unaligned (both red) and partially aligned (both blue) SMN²⁶⁻⁵¹-Gemin2⁹⁵⁻²⁸⁰. The two resulting combined spectra were then overlaid to illustrate differences in splitting. The red and blue arrows indicate the aligned and unaligned splitting observed for SMN T37 and Gemin2 G203 and G212.

Tables of all structural restraints appear as Appendix B.

Long-range distance restraints were also obtained from paramagnetic relaxation enhancements (PREs) in which Cys241 of Gemin2(C154S/C221S/C264S) was coupled to the paramagnetic nitroxide spin label MTSSL (S-(2,2,5,5-tetramethyl-2,5-dihydro-¹H-pyrrol-3-yl)methyl methanesulfonothioate). Distance restraints from PREs are calculated based on attenuation of signal intensity in HSQC of resonances in proximity to the spin label, an effect reversed when the spin label is reduced; Figure 2.13 shows an example of the attenuation and recovery of the intensity of the R205 H-N resonance, based on its proximity to the MTSSL moiety, in of an overlay of ¹H-¹⁵N HSQC spectra of oxidized and reduced Cys241-MTSSL-conjugated SMN²⁶⁻⁵¹-Gemin2⁹⁵⁻²⁸⁰ (C154S/C221S/C264S).

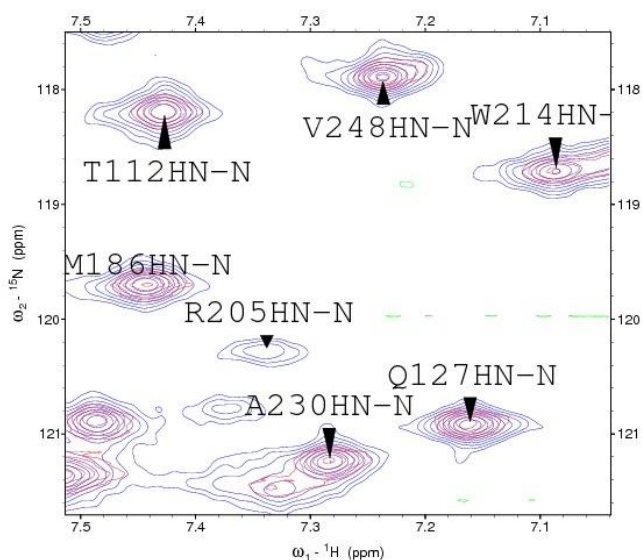


Figure 2.13 MTSSL-induced paramagnetic relaxation enhancement effects observed in the ¹H-¹⁵N HSQC spectrum of SMN²⁶⁻⁵¹-Gemin2⁹⁵⁻²⁸⁰. Expansion of the ¹H-¹⁵N HSQC spectra of oxidized (red) and reduced (blue) C241-MTSSL-conjugated SMN²⁶⁻⁵¹-Gemin2⁹⁵⁻²⁸⁰ (C154S/C221S/C264S). The cross-peak corresponding to R205 H-N decreases noticeably in intensity in the oxidized sample.

Design of the (C154S/C221S/C264S) mutant aimed to leave one conserved cysteine unmutated and accessible for spin labeling. Although C148 also remains unchanged in

this construct, NMR data from an $^{15}\text{N}/^1\text{H}$ -edited HSQC of the paramagnetic labeled species displayed no attenuation of signal intensity of amide resonances of residues in near three-dimensional proximity to C148, suggesting that that buried residue remains unmodified.

The ensemble of structures was calculated using the XPLOR-NIH software program by simulated annealing molecular dynamics employing both torsion angle and Cartesian coordinate dynamics (Schwieters *et al.*, 2003; Schwieters *et al.*, 2006). Out of 400 trial structures calculated, the 32 with lowest energy comprise an ensemble that represents the structure of the SMN²⁶⁻⁵¹-Gemin2⁹⁵⁻²⁸⁰ heterodimer and possess a backbone RMSD of 0.59 Å. (Figure 2.14A) NMR structural and refinement statistics are summarized in Table 2.1.

Table 2.1. Summary of structural ensemble statistics

Experimental restraints	
NOE distance restraints	
All	1849
Intraresidue	616
Sequential ($ i - j = 1$)	541
Medium-range ($1 < i - j < 5$)	453
Long-range ($ i - j > 5$)	239
Inter-protein	50
PRE distance restraints	31
Hydrogen bond restraints	55
Dihedral angle restraints	
Φ	139
Ψ	134
^{15}N - ^1H RDCs	84
RMSD from idealized covalent geometry	
Bonds (Å)	0.0040 ± 0.0001
Angles (°)	0.589 ± 0.006
Improper (°)	0.441 ± 0.011
RMSD from solution NMR restraints	
NOE distance restraints (Å)	0.0210 ± 0.001
PRE distance restraints (Å)	0.0423 ± 0.009
Dihedral restraints (°)	0.787 ± 0.069
RDC restraints (Hz)	0.116 ± 0.014
SAXS data fit (χ)†	0.761 ± 0.292
RDC quality factor	0.311 ± 0.012
Precision of atomic coordinates	
Secondary structure ‡	
Backbone (N, Ca, C', O) (Å)	0.596 ± 0.096
Heavy atoms (Å)	1.056 ± 0.081
Ramachandran statistics	
Favored (%)	98.0
Allowed (%)	1.8
Disallowed (%)	0.2

† χ is the square root of the normalized χ^2 difference between observed and predicted scattering data

‡ The secondary elements used were as follows: Gemin2 residues 107-124,142-148, 180-185, 188-201, 210-220,229-246 and 259-269; SMN residues 38-48.

Gemin2⁹⁵⁻²⁸⁰ folds into a helical bundle containing seven α -helices, the locations of which correspond well to those predicted by secondary structure prediction algorithms. The Gemin2-binding domain of SMN also forms an α -helix that interacts with Gemin2 in an extended hydrophobic cleft formed by four helices of Gemin2 (Figure 2.14B: labeled 1, 3, 5 and 7) far separated in primary sequence.

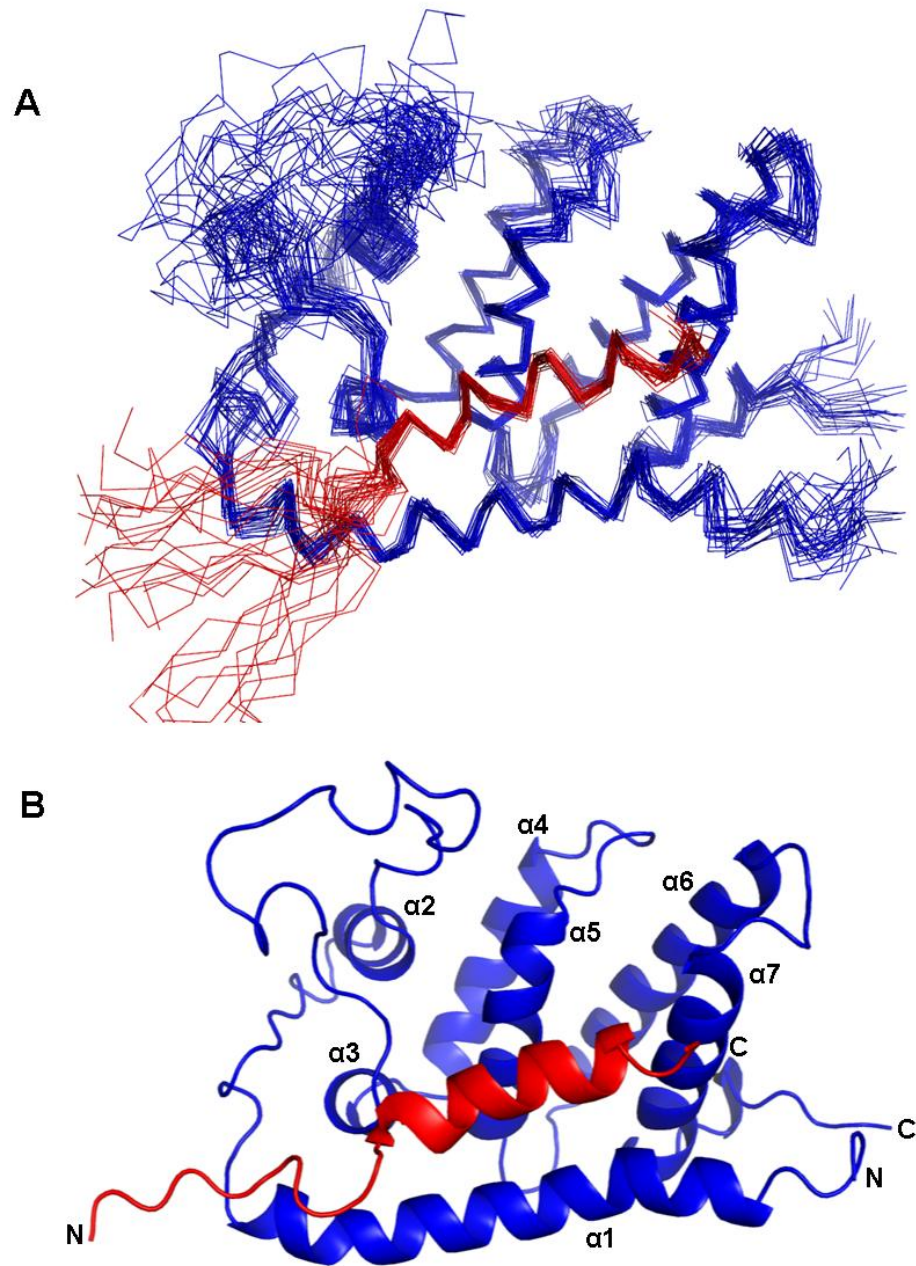


Figure 2.14 Structure of SMN bound to Gemin2. A) Overlay of C α -traces for the 32 lowest energy structures. B) Cartoon drawing of the lowest energy structure. SMN²⁶⁻⁵¹ is in red, Gemin2⁹⁵⁻²⁸⁰ is in blue. In B, the Gemin2 helices are numbered.

The structure is largely well-defined, with the notable exception of a large, poorly conserved loop in Gemin2 (residues 150-175) that is disordered and which demonstrates no long-range NOEs. This region of the protein is highly mobile in solution, as indicated by the relatively long ^{15}N T_2 relaxation time constants calculated for it by Veronica Moorman, a graduate student in the Wand laboratory at the University of Pennsylvania (Figure 2.15). In addition, the first seven residues in the SMN peptide (residues 26-32) exhibit significant disorder, which is consistent with their lack of importance for Gemin2-binding in the bacterial two-hybrid assays described above.

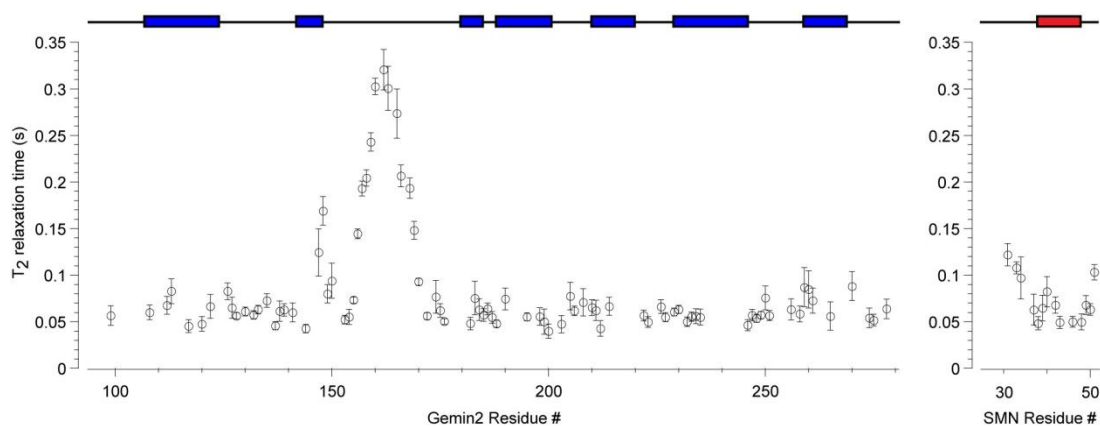


Figure 2.15 Backbone amide ^{15}N T_2 relaxation times of Gemin2 and the bound SMN peptide. Obtained by Veronica Moorman in the Wand laboratory at the University of Pennsylvania at 750MHz (^1H). Helices are depicted above the graph as rectangles for reference. High T_2 times are indicative of increased backbone flexibility.

Neither the seven α -helices of Gemin2 $^{95-280}$ alone nor the eight that make up the SMN $^{26-51}$ -Gemin2 $^{95-280}$ complex display any significant structural homology to known protein structures. Using the lowest-energy NMR structure as a query structure, searches of the Dali database yielded no persuasive matches (Holm & Sander, 1995; Sun *et al.*,

2005). Of those structures with scores indicating the highest degree of similarity, all had root-mean-squared deviations greater than 3 Å and typically treated as the region of structural homology the four-helix bundle formed by helices 4-7 of Gemin2, which is similar to that found in a number of helical sub-domains. Given this apparent lack of structural resemblance, the spatial arrangement of helices in Gemin2 and in the SMN-Gemin2 complex may be considered to comprise a unique protein fold.

The SMN-Gemin2 interface is mediated largely by hydrophobic interactions

Within the SMN²⁶⁻⁵¹ peptide, residues 37-50 form an α -helix with a strongly amphipathic character. Its hydrophobic face interacts with Gemin2 in a shallow, hydrophobic cavity formed by Gemin2 helices $\alpha 1$, $\alpha 3$, $\alpha 5$, and $\alpha 7$ (Figure 2.16).

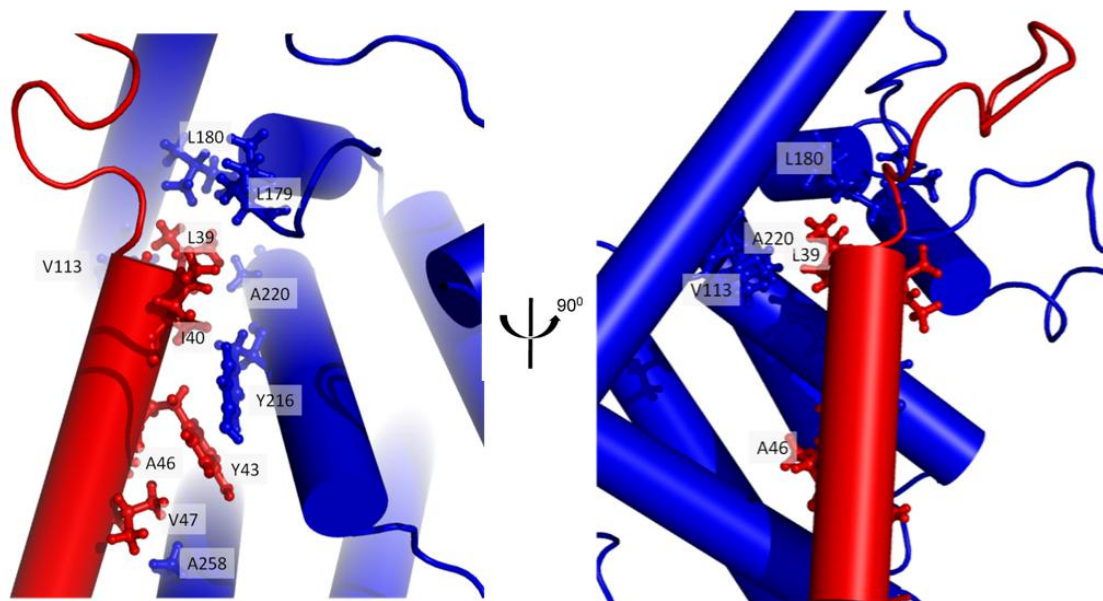


Figure 2.16 The conserved SMN-Gemin2 interface. A) Closeup of the interface. Gemin2 is depicted in blue and SMN in red. Key interfacial sidechains are labeled and represented as stick models. B) A 90° rotation of the view shown in panel A.

Fifty short-range proton-proton NOE distance restraints define the interface between SMN and Gemin2. Eleven of the 18 SMN residues from Ile33 through Phe50 are positioned close to the Gemin2 core domain, and SMN sequence alignments reveal that most of these residues involved in the interface with Gemin2 are conserved (Figure 2.17A) Leu39, Ala42, Tyr43, Ala46, and Val47 seem to play key roles mediating the hydrophobic interface; they are largely buried, with little solvent-accessible surface in members of the low energy structural ensemble. NOEs between Ile33, Asp36, Thr37, Ala38, Ile40 and Phe50 and Gemin2 are also observable. In the lowest-energy structure, the SMN-Gemin2 interface buries a total of 1800 \AA^2 of solvent-accessible surface area, which is consistent with a high-affinity interaction. The Gemin2 residues involved in binding to SMN, many also highly conserved, are located throughout the sequence, explaining why a smaller SMN-binding domain has not been previously reported (Figure 2.17B).

A. SMN

<i>H.s.</i>	1	MAMSSGGSGG	GVPEQEDSVL	FRRGT	EQSDD	SDI	WDDTALI	KAYDKAVASF	K	HALKNGDIC	ETSGKPKTTP	KRKPAKK...	77
<i>M.m.</i>	1	MAMGSGG	AGSEQEDTVL	FRRGT	EQSDD	SDI	WDDTALI	KAYDKAVASF	K	HALKNGDIC	ETPDKPKGTA	RRKPAKK...	74
<i>X.l.</i>	1	M	AGLEDGGEVL	FRRG	AGQSDD	SDI	WDDTALI	KAYDKAVSSF	K	KRALKNEDCT	IGAETEENP	RTKRKNN...	68
<i>D.m.</i>	1			MSDET	N	AA	WDDSLLV	KTYDES	VGLA	REALARRLAD	STNKREEENA	AAAEAAA...	53
<i>C.e.</i>	1			MEV	DD	WDDTELI	KMYDES	LQEI	S---	KNETSA	KITSRK----	FKGEDG...	42
<i>S.p.</i>	1			MDQSQ	KE	WDDSELR	NAFETAL	HEF	KKYHSIEAKG	GVSDPD----	--SRLDG...	46	

B. Gemin2

<i>H.s.</i>	95	...	GYSPTL	QWQQQ	QVAHF	STV	RQNVNKH	RSHWKS	QQLD	SNVTMPKSED	EEG	WKKFCLG	EKLCADGAVG	PATN-ESPGI	169	
<i>M.m.</i>	84	...	GYSPTL	QWQQQ	QVAHF	STV	RQSVHKK	RNHWKS	QQLD	SNVAMPKSED	EEG	WKKFCLG	ERLCAEGATG	PSTE-ESPGI	158	
<i>X.l.</i>	71	...	GYSPTL	QWQQQ	QVAHF	SAV	RQSLHKK	RGHWRS	QQPLD	SNVTMPSTED	EEG	WKKFCLG	ERLYSDLAAA	LNSESQHPGI	146	
<i>D.m.</i>	80	...	CLLPTP	EWRE	QVKSF	QAARS	QVLVL	RKELANN	NYD	QS	GEPLTSD	QEKWKE	FCRN	-----	134	
<i>C.e.</i>	82	...	PLIPSE	EWRE	QVKSF	EET	RAKMALK	IEKFS	PMRID	RLNS	PPEEEM	HEILLEK	CLP	EFQDIAGNPL	N-----	148
<i>S.p.</i>	85	...	TEAGKK	SFDPF	RYL	NID	KEGERL	EQYMES	SSLD	ASILPKN	---	LQWRV	YIEH	-----	137	

<i>H.s.</i>	170	DYVQIG	PPL	LSIV	SRMQA	TVTSV	LEYLS	NWFG	ERDFTP	-----	ELGR	WY	YALLACLE	KPLL	PEAHS	IRQL	ARRCSE	243						
<i>M.m.</i>	159	DYVQVG	PPL	LSIV	SRMQA	TVTSV	LEYLS	NWFG	ERDFTP	-----	ELGR	WY	YALLACLE	KPLL	PEAHS	IRQL	ARRCSE	232						
<i>X.l.</i>	147	DYIKVG	PPL	LSIV	SRMQA	TVTSV	LEYLV	NWFE	ERNFTP	-----	ELGR	WY	YALLACLE	KPLL	PEAHS	IRQL	ARRCSE	220						
<i>D.m.</i>	135	-----	QPL	LSTL	LHLTQ	DLELL	LEM	L	KWLQ	PNTTV	DL	LHDV	W	W	YATL	W	CLH	LPL	PHV	FST	LRY	ART	CIH	209
<i>C.e.</i>	149	---HTGT	PPA	LRM	VFSIPKR	HLSQL	IEYLV	DWSI	EEGLNR	-----	PIRE	WY	SLL	AVID	LPLV	QDVV	SA	LRRL	VKE	CRS	219			
<i>S.p.</i>	138	-----	KAPC	WAI	AVVDLA	TVLEI	LESLS	SWLEK	DAID	-----	LQSQ	WIF	FCY	KLP	ELL	NGED	IST	LR	SVL	KSLRS	204			

<i>H.s.</i>	244	VRL	LVDSKDD	ERV	PA	NLE	LI	CLV	SRY	FDQR	DLAD	--EPS	280
<i>M.m.</i>	233	VRL	LVGSKED	ERV	PA	NLE	LI	CLV	SRY	FDQR	DLAD	--EPS	269
<i>X.l.</i>	221	IRAG	VEHKED	DRV	SP	NLE	FI	CLV	GRY	FEQR	DLAD	CGDPS	259
<i>D.m.</i>	210	LRN	QLKEDEV	QRAA	PN	LL	TL	TV	QV	FAQN	DF	KDYI	245
<i>C.e.</i>	220	LRSE	LSIDRK	SEAN	FS	LE	FI	TI	TI	FFGQK	DLAD	I	254
<i>S.p.</i>	205	THTS	FPALQM	---	SASA	LQ	AVL	VY	RY	GQK	DL	FQT	235

Figure 2.17 Sequence alignments of SMN and Gemin2 from a diverse set of organisms.

A) SMN alignment in the N-terminal region. B) Gemin2 alignment, with helices numbered as in Figure 2.14. Residues that are identical in four out of the six sequences are in bold font. Residues involved in the SMN-Gemin2 interface are shaded yellow. The sequences shown are human (*H.s.*), mouse (*M.m.*), frog (*X.l.*), fly (*D.m.*), worm (*C.e.*), and fission yeast (*S.p.*)

At the N-terminus of the SMN helix, residues from the $\alpha 3$ helix of Gemin2 (Pro177, Pro178, Leu179, Leu180, Val183) and from helix $\alpha 5$ (Ala217, Ala220) contribute to a dense network of proton-proton NOEs with SMN Thr37, Ala38, Leu39 and Ile40. Helices $\alpha 5$ and $\alpha 7$ contribute interactions (Gly212, Leu215, Tyr216, Leu265) to SMN mid-helix residues (Tyr43, Ala46, Val47), and $\alpha 7$ (Pro257, Ala 258, Leu262, Leu265) caps the C-terminus. The $\alpha 1$ helix, running almost antiparallel to SMN, contributes interactions along its length (His120, Val117 and Val113 to Ala38 and Leu39; Val113, Gln109 and Gln106 to Ala42; Gln109 and Gln106 to Ala46) (Figure 2.16).

In addition, Gemin2's His120 interacts with Asp36 and Ile33 of SMN, beyond the N-terminal boundary of the SMN α -helix. Asp36, along with Trp34 and Asp35, is one of three invariably conserved residues that serve no immediately discernible role in mediating the SMN-Gemin2 interaction. Asp36, however, is directed towards the Gemin2 interface, where it could interact with His120 and/or Trp124. Another highly conserved SMN residue, Asp44, is oriented away from the hydrophobic interface but might be positioned to form a polar interaction with the sidechain of Arg213.

Mutation of key conserved interfacial residues confirms their importance in SMN-Gemin2 binding

Several highly conserved SMN residues appear to play key roles in mediating the hydrophobic SMN-Gemin2 interface, while other equally conserved residues serve no apparent role in protein-protein binding. To assess the effect of the most conserved SMN residues on Gemin2 binding, a series of SMN²⁶⁻⁵¹ mutants were constructed and tested for binding to Gemin2⁹⁵⁻²⁸⁰ using the fluorescence anisotropy binding assay. Of those tested, binding affinity was reduced over 100-fold for Y43A, 20-fold for L39A, and 10-fold for A46N, all in accord with their apparent roles in Gemin2-binding. Other conserved residues, however, showed no effect on binding: W34A, D35A, D36A and K41A had dissociation constants similar to that of WT SMN²⁶⁻⁵¹ (Figure 2.18; Table 2.2).

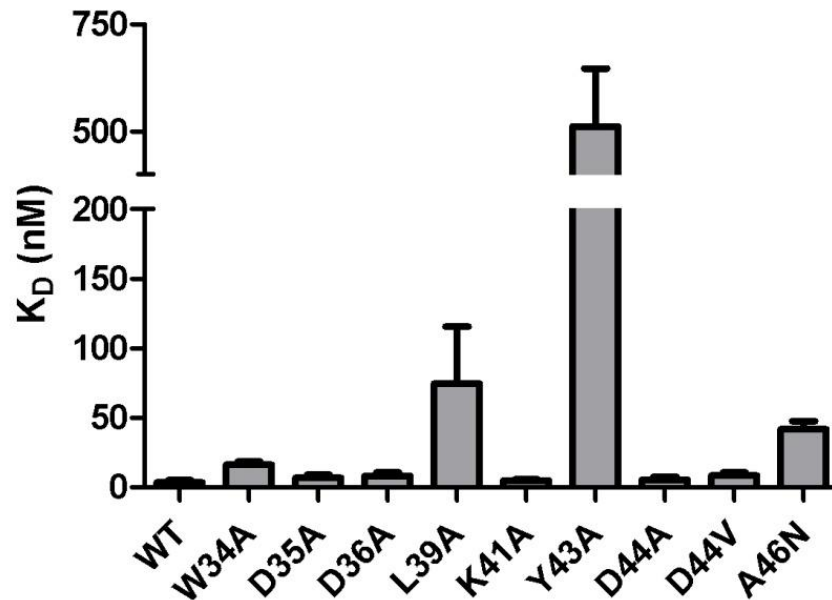


Figure 2.18 Binding of SMN²⁶⁻⁵¹ mutants to Gemin2⁹⁵⁻²⁸⁰. Using the fluorescence anisotropy assay described in Figure 2.3, each binding titration was repeated three times and the average dissociation constant is shown. Error bars represent one standard deviation from the mean.

Asp44, another highly conserved SMN residue, is the site of an SMA patient mutation in which valine is substituted at this position. An electrostatic interaction between Asp44 and Arg213 of Gemin2 seemed geometrically possible, but the likelihood of a significant energetic contribution from this interaction to binding was unclear. The mutants D44A and D44V were therefore probed for interaction with Gemin2. Both bound as well as wild-type SMN, suggesting that the functional defect in patients with the D44V mutation is unlikely to be an abrogation of SMN-Gemin2 binding.

Previous reports on the effect of the D44V SMN patient mutation on Gemin2 binding have been mixed; the original report of the mutation found no effect on binding, but later mammalian two-hybrid and GST pulldown studies of an SMN(exons1-5) construct

found D44V binding reduced compared to wildtype SMN (Ogawa *et al.*, 2007; Sun *et al.*, 2005; Zhang *et al.*, 2011).

Given the hydrophobic nature of the SMN-Gemin2 interface and the typical addition of detergents to reduce non-specific binding in buffers used in GST pull-down assays, it seemed possible that the discrepancy in results reported for the effect of D44V on Gemin2 binding might be the result of sensitivity to the presence of detergents, to temperature, or to both. To address this possibility, the same fluorescence anisotropy peptide binding experiments were repeated for SMN²⁶⁻⁵¹ wildtype and D44V in the presence and absence of 0.05% Nonidet P40, both at 25°C and at 4°C.

Neither 4° conditions nor the presence of detergent at 25°C had any observable effect on wildtype SMN²⁶⁻⁵¹ binding to Gemin2; a combination of the two effects, however, showed a mild reduction in binding affinity by about a factor of 25. Binding of SMN²⁶⁻⁵¹ D44V to Gemin2 was also unaffected at 4°C ($K_D = 1.5 \pm 0.47$ nM), but was reduced by a factor of ~500 at 25°C in the presence of detergent ($K_D = 1.8 \pm 0.24$ μM). When the two effects were combined, binding of D44V was nearly undetectable over the range of titrations, indicating a dissociation constant greater than 4 μM. The combined effects of low temperature and detergent observed for wild-type SMN²⁶⁻⁵¹ are greatly amplified for the D44V mutant, and suggest that the abrogation of D44V binding reported in some studies may be a result seen only under the artefactual conditions of detergent and low

temperature and do not provide a realistic representation of the effect of the mutant on binding under physiological conditions. (Summarized in Table 2.2)

Table 2.2 SMN²⁶⁻⁵¹-Gemin2⁹⁵⁻²⁸⁰ dissociation constants

SMN (26-51)	Gemin2	Buffer ¹	Temperature (°C)	K _D (nM) ²
Wild-type	12-280	PBS	25	7.0 ± 2.5
Wild-type	95-280	PBS	25	3.3 ± 1.8
Wild-type	95-280	PBS, 300 mM NaCl	25	5.2 ± 1.8
Wild-type	95-280	PBS, 600 mM NaCl	25	2.4 ± 1.5
Wild-type	95-280	PBS	4	2.3 ± 0.92
Wild-type	95-280	PBS + NP40	25	2.2 ± 1.7
Wild-type	95-280	PBS + NP40	4	180 ± 27
W34A	95-280	PBS	25	16 ± 2.2
D35A	95-280	PBS	25	6.8 ± 2.1
D36A	95-280	PBS	25	8.3 ± 2.5
L39A	95-280	PBS	25	74 ± 41
K41A	95-280	PBS	25	4.8 ± 1.0
Y43A	95-280	PBS	25	510 ± 130
D44A	95-280	PBS	25	5.3 ± 2.4
D44V	95-280	PBS	25	8.4 ± 2.4
D44V	95-280	PBS	4	1.5 ± 0.47
D44V	95-280	PBS + NP40	25	1800 ± 240
D44V	95-280	PBS + NP40	4	> 4000
A46N	95-280	PBS	25	42 ± 5.9
p28, p31	95-280	PBS	25	4.2 ± 1.3

¹PBS = 10 mM Na₂HPO₄, 2 mM KH₂PO₄, 137 mM NaCl, 2.7 mM KCl, pH 7.4, 2 mM DTT; NaCl concentration is modified where indicated. NP40 = Nonidet P40.

²The K_d values reported are based on 3-6 individual binding titrations. The K_D for SMN D44V in NP40-containing buffer at 4°C could not be fit, but a lower limit of 4 μM could be established.

The effect of ionic strength on the affinity of the SMN-Gemin2 interaction was also examined. Consistent with the hydrophobic nature of the interface, the binding affinity of SMN²⁶⁻⁵¹ for Gemin2⁹⁵⁻²⁸⁰ in 300 mM or 600 mM NaCl (K_D = 5.2±1.8 nM and

2.4±1.5 nM, respectively) remains essentially unchanged from that observed in PBS buffer at 137 mM salt ($K_D = 3.3\pm 1.8$ nM) (Table 2.2).

Discussion

Despite occupying the focal point of considerable research interest – due to the central role they play in spliceosomal U-snRNP biogenesis, but even more urgently to their vital urgent role in SMA pathogenesis – SMN and Gemin2 have eluded structural analysis at the atomic level for fifteen years after their discovery. Full-length SMN and Gemin2, expressed either bacterially or in Sf9 cells, proved largely intractable in solution: the former protein tends to aggregate; the latter expresses poorly, is minimally soluble and degrades readily (its tendency to bind all nitrocellulose membranes irreversibly also fails to recommend it). The coexpressed complex of the two full-length proteins elutes as a broad peak near the void volume of a Superdex 200 size exclusion chromatography column, suggesting that it forms a oligomer too large, and possibly too heterogeneous, for ready characterization.

The desire for an SMN-Gemin2 complex less refractory to all attempts at analysis stimulated the design of a minimal SMN-Gemin2 complex. The boundaries determined from bacterial two-hybrid experiments using SMN and Gemin2 truncations largely confirmed the locations of the binding domains reported in earlier studies. The minimal

binding domain of Gemin2, comprising residues 95-280, is closely consistent with results from a mammalian two-hybrid assay reported by Ogawa *et al* that pinpointed that domain as residues 101-280 (Ogawa *et al.*, 2007). This region includes nearly two-thirds of the polypeptide, suggesting a reason why a shorter functional Gemin2 construct has never been reported.

The 21-residue minimal Gemin2 binding domain of SMN, S31-K51, also corresponds broadly to previous reports: Liu *et al.* demonstrated that a peptide comprising SMN¹³⁻⁴⁴ successfully competed with full-length SMN for Gemin2 binding, and Ogawa *et al.* positioned SMN's Gemin2 binding domain in exons 1-2b (residues 1-62) (Liu *et al.*, 1997; Otter *et al.*, 2007). By contrast, however, Young *et al.* (2000) used surface plasmon resonance experiments to identify exon 2b (residues 52-62) as the site of independent Gemin2 binding, a conclusion not supported by the results described in this dissertation (Young *et al.*, 2000).

The SMN²⁶⁻⁵¹ and Gemin2⁹⁵⁻²⁸⁰ proteins both proved tractable to heterologous expression in *E. coli*; the protein heterodimer they formed could be purified to homogeneity and was amenable to biochemical and biophysical characterization. Although disappointingly refractory to the formation of diffraction-quality (or, indeed, any) protein crystals, a ¹H-¹⁵N HSQC of the SMN²⁶⁻⁵¹-Gemin2⁹⁵⁻²⁸⁰ complex showed peak dispersion and sharp linewidths, the hallmarks of a folded protein potentially amenable to structure determination by NMR spectroscopy (Figure 2.8). That possibility

proved predictive in this case, and heteronuclear multi-dimensional NMR was employed to solve the atomic-level structure of the SMN²⁶⁻⁵¹-Gemin2⁹⁵⁻²⁸⁰ heterodimer.

The NMR structure of SMN²⁶⁻⁵¹-Gemin2⁹⁵⁻²⁸⁰ reported in this work marks a substantial advance over the preceding fifteen years' research, representing the first view of the structure of Gemin2 and its binding interaction with the Gemin2-binding domain of SMN. Forming a helical bundle comprising seven α -helices, Gemin2 interacts with the single α -helix of SMN²⁶⁻⁵¹ in an extended hydrophobic cavity formed by four helices, $\alpha 1$, $\alpha 3$, $\alpha 5$ and $\alpha 7$, far separated in primary sequence. The SMN helix displays a markedly amphipathic character, with a solvent-exposed polar face and a buried interfacial hydrophobic face (Figure 2.16).

Both Gemin2⁹⁵⁻²⁸⁰ in complex with SMN²⁶⁻⁵¹ and taken alone appear to bear no significant structural homology to any other known protein structures. Using the lowest-energy member of the NMR ensemble as a representative structure, a search of the Dali structural database yielded no strong matches with or without the inclusion of the SMN peptide. The highest-scoring hits boasted fairly significant r.m.s. deviations ($>3\text{\AA}$) and typically pinpointed the four-helix bundle comprising helices $\alpha 4$ - $\alpha 7$, a motif encountered in a variety of helical protein folds, as the center of structural conservation. The spatial arrangement of helices in the structure of Gemin2 bound to SMN, then, appears to comprise a novel protein fold. Although the discovery of structural novelty in the study of heretofore uncharacterized Gemin2 failed to suggest immediately a

functional role for the protein as analogy to an obvious structural homologue might have done, the availability of a structural model for SMN-Gemin2 serves as a platform for design of the next generation of experiments, logical structure-function studies to probe the role of Gemin2 in U-snRNP assembly and in other reported protein-protein interactions.

Although the prediction of protein constructs that will crystallize resembles an art more than a science, certain characteristics of the SMN²⁶⁻⁵¹-Gemin2⁹⁵⁻²⁸⁰ heterodimer that became apparent from the NMR structure likely prejudiced early crystallization attempts. While most of the structure is fairly well-defined, it also contains two significant regions of disorder. A large, poorly conserved loop in Gemin2 (residues 150-175, a region entirely absent as recently evolutionarily as *Drosophila*) is entirely disordered, with no long-range NOEs observed. This region of the protein is highly mobile, as indicated from ¹⁵N relaxation experiments performed and analyzed on SMN-Gemin2 by the Wand laboratory at the University of Pennsylvania, which yielded indicative long ¹⁵N T₂ relaxation time constants for that region (Farrow *et al.*, 1994; Lipari & Szabo, 1982) (Figure 2.15)

In addition, the first seven residues in the SMN peptide (residues 26-32) are disordered, which is consistent with their lack of importance for Gemin2-binding as indicated by our interaction assays. An overall low order parameter O₂ (0.6-0.8) was also found for

backbone amides in areas of helical structure, indicating a degree of backbone mobility that may have hampered crystallization (Figure 2.19).

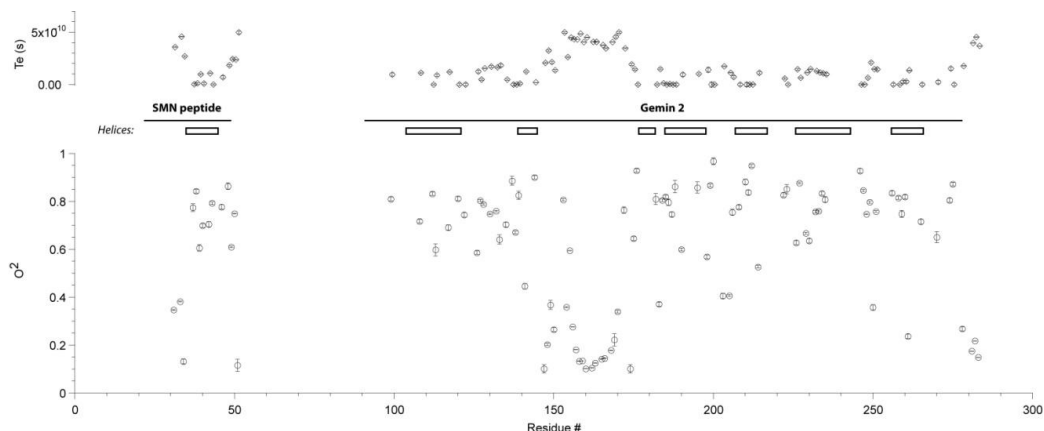


Figure 2.19 Backbone order parameters (O_2) of Gemin2 and the bound SMN peptide. Obtained by Veronica Moorman in the Wand laboratory at the University of Pennsylvania from T_1 and T_2 relaxation times at 750 MHz and 600 MHz (^1H). Helices are depicted above the graph as rectangles for reference. Order parameters near one imply rigidity; those near zero indicate a wide range of possible motion.

The importance of key conserved SMN residues at the hydrophobic interface with Gemin2 was confirmed in mutagenesis binding studies. Eleven SMN residues on the hydrophobic face of the amphipathic SMN helix mediate the interaction with Gemin2 in the cavity formed by the four α -helices α_1 , α_3 , α_5 and α_7 ; Leu39, Tyr43 and Ala46 exhibit strong evolutionary conservation and are essential for high affinity SMN-Gemin2 binding. The highly conserved Asp36 occupies a flanking position N-terminal to the beginning of the SMN helix and is possibly positioned to contribute a polar interaction with His120 or His124; its alanine mutation shows a mild effect on Gemin2 binding.

The position of helix $\alpha 1$ relative to SMN explains the observation made during delineation of domain boundaries that additional N-terminal deletions of Gemin2 beyond Gly95 to Phe110 still resulted in an SMN-Gemin2 interaction. Helix $\alpha 1$, comprising residues 100-124, runs roughly antiparallel to the SMN helix and contributes hydrophobic interactions with SMN along its length; it is apparent that the minor N-terminal truncations, including the loss of the contributions of Q106 and Q109 to the hydrophobic protein-peptide interface, still results in a detectable interaction between the two components, but that the cumulative loss of those residues plus the more centrally positioned and arguably more significant V113, V117 and H120 proves inimical to sustaining the SMN-Gemin2 interaction.

A number of conserved residues in the Gemin2-binding domain of SMN, however, serve no apparent role in Gemin2 binding. Conspicuous among them, Trp34 and Asp35 are invariantly conserved through evolutionary time, and Lys41 and Asp44 are invariant from humans to worms. No NOEs providing distance restraints were observed between the protons in these atoms and Gemin2, nor did alanine substitutions at any of their positions have an effect on the affinity of the SMN-Gemin2 interaction. These residues may form part of another binding surface or surfaces for other components of the SMN complex or its substrates. In considering other possible roles, the degree of evolutionary conservation evinced may provide certain clues. Trp34 and Asp35, for example, are conserved from mammals to *S. pombe*, an organism whose functional SMN complex consists only of SMN and Gemin2; those residues are therefore unlikely to play a role in

recruiting other Gemin components to the complex but may instead serve as part of an interaction platform for Sm protein substrates or for SMN or Gemin2 as part of the formation of higher-order oligomers.

Of the highly conserved SMN residues with no apparent role in binding, Asp44 has been singled out for examination as the site of a Type III (mild; adult onset) SMA missense mutation, in which valine is substituted at its position. Conclusions from a number of reports have been mixed with respect to the functional defect introduced by the D44V substitution. The original report of the mutation indicated no effect on Gemin2 binding based on *in vitro* GST pulldowns; the fluorescence anisotropy peptide binding studies employed in this work mirror that conclusion (Sun *et al.*, 2005). Ogawa *et al.*, however, reported that the interaction between Gemin2 and a truncated SMN (exons1-5) D44V construct was diminished with respect to wildtype binding in both GST pulldown experiments and mammalian two-hybrid assays (Sun *et al.*, 2005)(Sun *et al.*, 2005){Sun2005}(Ogawa *et al.*, 2007). More recently, Zhang *et al.* also used *in vitro* pulldown assays of SMN produced by *in vitro* translation to demonstrate elimination of SMN D44V binding to Gemin2, a result considered attributable to disruption of a salt bridge formed at the SMN-Gemin2 interface between Asp44 and Gemin2 Arg213 (Zhang *et al.*, 2011).

The flat discrepancy between one set of conclusions recounting no effect of D44V on Gemin2 binding, including the peptide binding results reported here, and another

reporting an abrogation of that same interaction bore careful consideration. One pronounced difference between experiments relates to the conditions under which they were performed: in both studies reporting diminution of D44V binding to Gemin2 as the result of *in vitro* pulldowns, the binding experiments were performed at 4°C in the presence of non-denaturing detergent, standard experimental procedures used to minimize non-specific interactions and promote the stability of proteins. Given the categorically hydrophobic nature of the SMN-Gemin2 interface, it seemed possible that temperature and detergent might have an effect on the affinity of the interaction.

The same fluorescence anisotropy SMN peptide binding assays used to quantitate the affinity of wildtype and D44V SMN²⁶⁻⁵¹ for Gemin2⁹⁵⁻²⁸⁰ in physiological buffer at room temperature were repeated at lower temperature, in the presence of detergents and under a combination of the two conditions, with startling results. Wildtype SMN²⁶⁻⁵¹ binding to Gemin2 remains unaffected at 4°C and in 0.05% Nonidet P-40 at 25°C, but is reduced by a factor of ~25 when both conditions are present. The SMN D44V mutation also bound with wildtype affinity at 4°C, but was strikingly more sensitive to detergent: at 25°C with detergent present, Gemin2 binding was reduced by a factor of ~500, and at 4°C was so abrogated that no binding activity was observed over the range of Gemin2 concentrations titrated. It seems clear that the SMN D44V patient mutation only disturbs Gemin2 binding under the conditions of low temperature and high detergent concentration present in many standard *in vitro* binding assays. As neither condition seems likely to be operative *in vivo*, it seems a likely conclusion that the functional

deficiency introduced by the substitution of a valine at the Asp44 position in SMN is not a disruption of the SMN-Gemin2 binding interface.

The possibility of a role for Asp44 in promoting higher-order SMN complex interactions cannot be ruled out, however. SMN is known to form higher order oligomers, an effect primarily attributed to its tyrosine-glycine rich exon6/exon7 “YG box” oligomerization domain (Lorson *et al.*, 1998; Pellizzoni *et al.*, 1999). Young *et al.* first proposed the possibility of an additional N-terminal exon 2 SMN self-interaction based on surface plasmon resonance binding experiments, and suggested an interaction of that region with SMN exon 4 (Young *et al.*, 2000). More trenchantly, Ogawa *et al.* (2007) also observed using mammalian two-hybrid assays the presence of an N-terminal SMN self-interaction that they reported required Gemin2 for stability and was significantly weakened in the SMN D44V mutant (Ogawa *et al.*, 2007). An *in vitro* dissociation assay showed a substantial impairment of SMN self-association in SMN D44V compared to wildtype; they also found SMN D44V mutants deficient in snRNP assembly in *in vitro* assembly assays. The authors conclude that an impairment in N-terminal SMN self-association underpins SMN in D44V patients.

SMN has also been shown to be a target for *in vivo* cleavage by calpain at a site that is located in exon4, in the C-terminal half of the protein. The functional significance of this observation is still unclear, but it is speculated to pertain to a specific role of SMN in the sarcomeric Z-discs of skeletal and cardiac muscle. The SMN D44V mutant

drastically decreases the efficiency of calpain cleavage, however, and this effect is dependent on SMN oligomerization (Walker *et al.*, 2008). Asp44, as well as other conserved residues in the Gemin2-binding region of SMN that play no role in binding, may be involved in higher order interactions within the oligomeric SMN complex. As mentioned above, the idea that the region encoded by exon 4 may interact with the Gemin2-binding domain has already been proposed by Young *et al.* The possibility that an N-terminal association of SMN plays a functional role and can be interrupted in the case of D44V seems an avenue of inquiry worthy of pursuit.

Another SMA patient missense mutation (Type II; intermediate) localizes to the region of SMN contained within residues 26-51 (Sun *et al.*, 2005), where an asparagine residue substitutes for Asp30. Unlike its D44V neighbor, however, the functional defect introduced by this patient mutation remains unclear. No binding assay to date has recorded any effect of the mutant on Gemin2 binding (Ogawa *et al.*, 2007; Sun *et al.*, 2005). Given that the NMR structure of the SMN-Gemin2 heterodimer indicates that the residue lies within an unstructured region of the SMN peptide, this result is unsurprising. Neither, however, did Ogawa *et al.* observe any effect of the mutation on SMN N-terminal self-interaction or SMN oligomerization stability in a dissociation assay. When introduced into an *in vitro* snRNP assembly assay, however, the D30N mutation exhibited an impairment of snRNP assembly at a level similar to that exhibited by D44V (Ogawa *et al.*, 2007).

Of the highly conserved residues in Gemin2, many play obvious roles in inter-helical packing and the formation of the SMN binding pocket. A number of others, however, are located on the protein's surface without close proximity to SMN and perhaps forming other functional interaction surfaces (Figure 2.20). These platforms for protein-protein interaction stand to play important roles in the structural organization of the SMN complex or in the molecular mechanics of snRNP assembly. Self-association has been imputed to the region of Gemin2 comprising the construct used in these studies (Ogawa *et al.*, 2007). It is also highly probable that Gemin2 interacts with one or several of the substrates of snRNP biogenesis. Chari *et al.* illustrated the composition of two snRNP assembly intermediates involving Gemin2 and SMN (Chari *et al.*, 2008). In the first, Gemin2 and SMN interact with a complex containing Sm proteins D1, D2, E, F, and G and the chaperone pICln. In the second, pICln dissociates, leaving a complex comprising SMN, Gemin2, and the D1/D2/E/F/G pentamer; the Sm D3/B dimer will later complete the heptameric Sm ring. The precise location of Gemin2 relative to the Sm proteins is unclear in the low-resolution electron microscopy images provided in the Chari *et al.* study; from that data, it seemed likely that conserved surface residues of Gemin2 might interact with one or several of them.

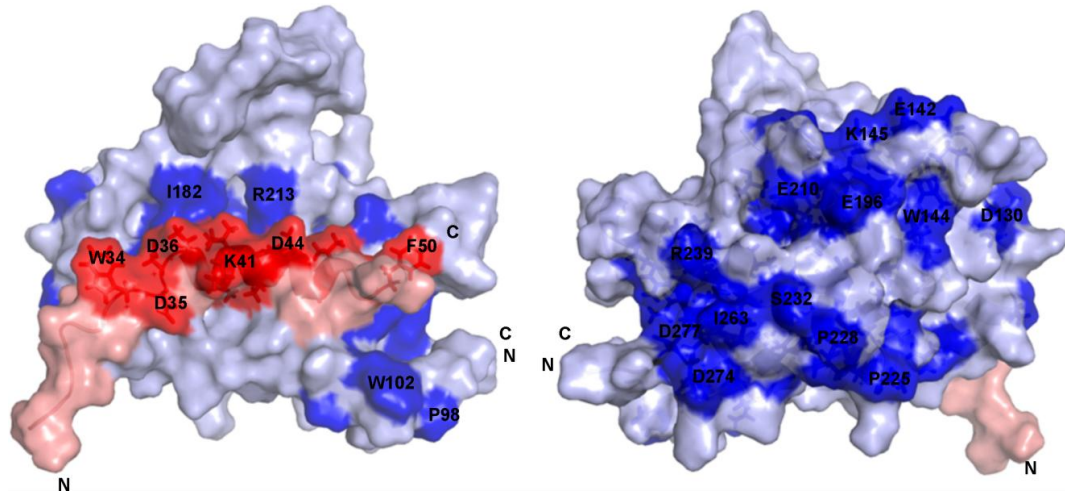


Figure 2.20 Conserved surfaces in the SMN-Gemin2 complex. A) View of the SMN-Gemin2 surface in the same orientation as that shown in Figure 2.9. B) View of the opposite side of the complex. Conserved residues (boldface type in Figure 2.12) are drawn in red for SMN and dark blue for Gemin2. Other residues are in pale red for SMN and pale blue for Gemin2. Selected conserved residues are labeled.

Indeed, during the preparation of this written dissertation, a 2.5Å crystal structure was published of the second snRNP assembly intermediate described above, consisting of Gemin2 bound to the Gemin2-binding domain of SMN and to the Sm D1/D2/E/F/G pentamer. As expected, a series of Gemin2-Sm protein interactions does appear in this structure; Gemin2 clearly coordinates direct interactions with several Sm proteins. Sm D1 and D2 appear to interact directly with the domain that corresponds to Gemin2⁹⁵⁻²⁸⁰ on the face opposite SMN binding, while E/F/G binds its extended N-terminal arm (Zhang *et al.*, 2011).

A superposition, based on backbone atoms in the eight α -helices of the NMR and crystal structures of Gemin2⁹⁵⁻²⁸⁰, illustrates regions of both significant similarity and noticeable dissimilarity (Figure 2.21A,B). Interestingly, the face of the protein that

appears to comprise the Sm D1/D2 binding surface shows the least difference between the two structures, with only slight orientational differences in the surface accessible regions of helices $\alpha 4$ and $\alpha 7$, and near perfect overlap of $\alpha 5$ and $\alpha 6$. This suggests that Gemin2 may undergo little structural change upon Sm protein binding, as the binding surface for the two Sm proteins appears to adopt the same configuration in the solution structure of the apo protein.

Other regions of the structures, however, evinced comparative differences that may result from crystal packing artifacts, the misinterpretation of crystallographic data or simple dissimilarity between the crystal and solution structures (Figure 2.21B). The latter is certainly a reasonable possibility given the comparatively low backbone amide order parameters evinced by the SMN-Gemin2 heterodimer in this study, indicating an unusual degree of backbone mobility. The position of the short $\alpha 2$ helix flanking the large unstructured G150-G175 loop is substantially translated between the two structures, and the crystal structure's $\alpha 2$ helix falls $\sim 120^\circ$ out of register based on its violation of a large number of observed long-range NOEs. This helix forms lies at the surface of the protein and contains several conserved residues whose surface accessibility varies drastically between the two models, complicating attempts to assess their relative importance in helix-helix packing versus forming a solvent-accessible binding surface. The $\alpha 3$ and $\alpha 7$ helices also suffer a displacement in the crystal structure relative to their positions in the solution structure, which complicates interpretation of the Gemin2 SMN binding pocket. Indeed, Zhang *et al.* fail to mention the important

contribution either the $\alpha 3$ or the $\alpha 7$ helix makes to the SMN-Gemin2 interface (Zhang *et al.*, 2011). Some discrepancy is also visible between the two structures in the conformation of the $\alpha 1$ helix, which adopts a more bent, less ideal form in the NMR structure in response to RDC orientational restraints and to NOEs between its residues and those of SMN and helix $\alpha 3$. A systematic consideration of the differences between the crystal and NMR structures of SMN-Gemin2 will prove important in defining the structural model that best represents the two proteins and from which basis future experiments, especially structure-function studies probing the role of the complex in Sm protein binding and snRNP assembly, can most accurately be designed.

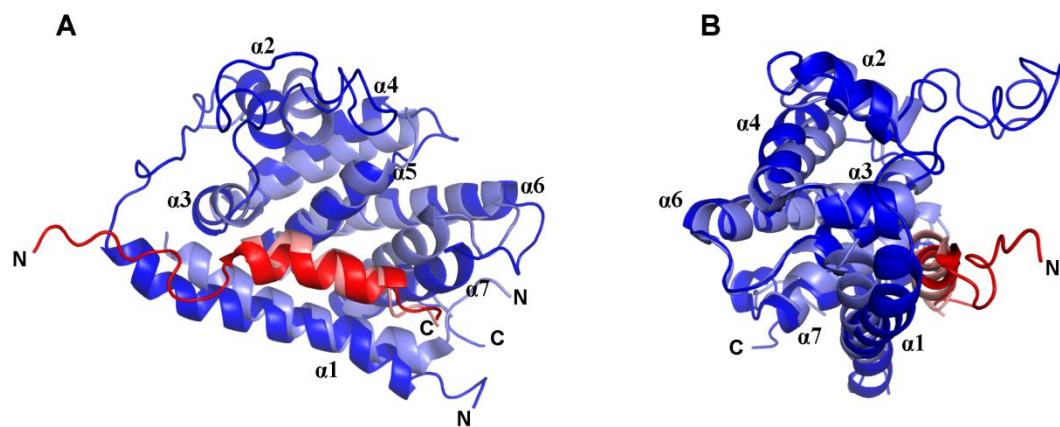


Figure 2.21 Comparison of the the NMR solution structure and x-ray crystal structure of SMN²⁶⁻⁵¹-Gemin2⁹⁵⁻²⁸⁰. A) Overlay of the NMR and x-ray crystal structures of SMN²⁶⁻⁵¹-Gemin2⁹⁵⁻²⁸⁰. SMN²⁶⁻⁵¹ is depicted in dark red for the NMR structure and in pink for the x-ray structure. The NMR structure of Gemin2⁹⁵⁻²⁸⁰ is in blue and the x-ray structure in light blue. B) A 90° rotation of the view in the first panel.

Gemin2 is also the established point of interaction at least two other Gemin components of the SMN complex. A direct interaction between Gemin2 and Gemin5, the snRNA chaperone, was established through co-immunoprecipitation and yeast two-hybrid assays and likely explains the early finding that Gemin2 mediates snRNA binding; the binding interface between Gemin2 and Gemin5 has yet to be defined (Lorson & Androphy, 1998; Otter *et al.*, 2007). Gemin2 has also been shown to bind Gemin7, perhaps in the context of the Gemin7-Gemin6 heterodimer that is thought to serve as a surrogate for the SmD3/B dimer in the nascent Sm D1/D2/E/F/G pentamer (Ma *et al.*, 2005). The Gemin2 Gemin7-binding domain appears to comprise residues 56-280, with a significant decrease in binding occurring after truncation to residues 101-280; this strongly implies that at least part of the binding surface crucial to Gemin2's interaction with Gemin7 lies along its N-terminal Sm protein-binding arm. The presence of SMN strongly enhances the stability of the Gemin2-Gemin7 interaction, suggesting that that interaction occurs in the context of the SMN-bound Gemin2 fold observed in the NMR and crystal structures (Ogawa *et al.*, 2009).

Apart from its well-documented role in snRNP assembly, Gemin2 has also been implicated in other biological processes, including HIV infection and homologous recombination (Hamamoto *et al.*, 2006; Takizawa *et al.*, 2010). In HIV-infected cells, following the reverse transcription of the viral genome by reverse transcriptase, HIV-1 integrase (HIV-1 IN) integrates the newly made cDNA copy into the host chromosome. HIV-1 IN is also reported to influence reverse transcription and thereby stimulate viral

cDNA synthesis, possibly by facilitating the loading of reverse transcriptase onto viral RNA. This activity appears to be influenced by a direct interaction of Gemin2 with HIV-1 IN; interruption of the Gemin2-IN interaction, either by introducing mutations in HIV-1 IN, by competing for integrase binding with a peptide corresponding to Gemin2's IN binding domain or by siRNA depletion of Gemin2 abrogates reverse transcription activity. The possibility of SMN involvement in this process remains unclear, although other Gemins appear to be uninvolved (Hamamoto *et al.*, 2006; Nishitsuji *et al.*, 2009). The authors identify residues 137-238 of Gemin2 as its integrase binding domain, which, assuming a fold in this context similar to that assumed by the SMN²⁶⁻⁵¹Gemin2⁹⁵⁻²⁸⁰ complex, allows a partial visualization of the integrase binding surface (Figure 2.22). The integrase binding domain comprises Gemin2 helices $\alpha 2$, $\alpha 3$, $\alpha 4$, $\alpha 5$ and a portion of $\alpha 6$, as well as the large unstructured loop containing residues 150-175. If Gemin2 adopts the same fold in the context of HIV-1 IN binding that it does when binding SMN, this suggests that HIV-1 integrase, like the Sm D1-D2 dimer, interacts with Gemin2 on the face of the protein opposite its SMN binding site.

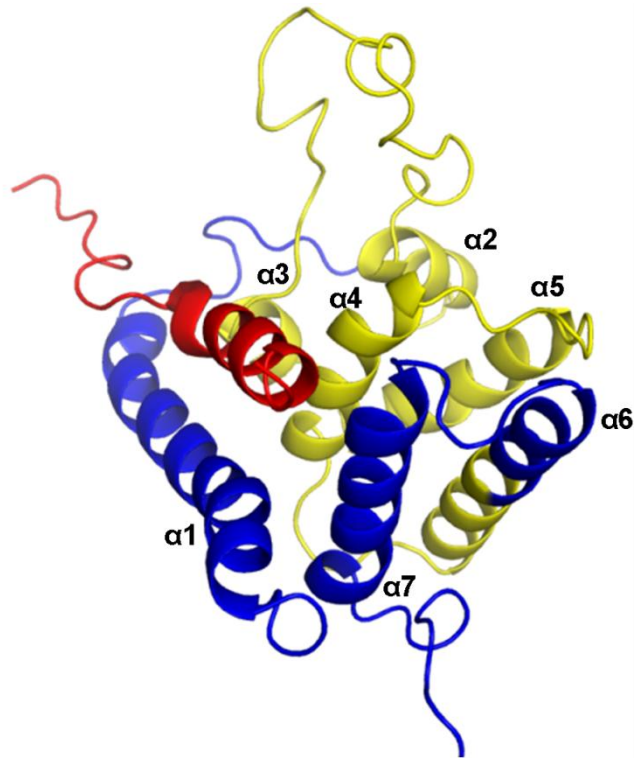


Figure 2.22 An illustration of the Gemin2 residues comprising the HIV-1 integrase binding domain. SMN is depicted in red, the INBD in yellow and Gemin2 residues not involved in HIV-1 integrase binding in blue. Gemin2 helices are labeled.

Another body of research has reported an interaction between Gemin2 and Rad51 (Takaku *et al.*, 2011; Takizawa *et al.*, 2010). Rad51, a eukaryotic recombinase, catalyzes the homologous pairing and strand exchanges reactions that make up part of the homologous recombination repair of double-stranded breaks in DNA. Gemin2 was demonstrated to enhance Rad51 activity in homologous pairing both *in vitro* and *in vivo*. The same results, as well as the appearance of DNA-binding activity and a significant increase in secondary duplex DNA capture by the RAD51-single-stranded DNA complex during homologous pairing, were reported for a fusion protein comprising full-length SMN joined at its C-terminus to Gemin2 at its N-terminus; the physiological

relevance of such a chimera has yet to be ascertained. The mode of Rad51 binding to Gemin2 in this case and the mechanics of its function in homologous recombination are uncertain, but it should now be straightforward to identify the regions of interest using the structural framework for Gemin2 reported in this work.

The SMN-Gemin2 structure reported here represents the achievement of a goal toward which effort has been applied for more than a decade. The protein fold of Gemin2 demonstrated obvious novelty, which failed to suggest function through structural homology but which established a vital framework for designing the next generation of structure-function experiments to probe the functional role of SMN-Gemin2 in snRNP assembly and SMA pathogenesis, as well as other biological roles for Gemin2.

Materials and Methods

DNA constructs

The DNA constructs employed in the experiments described in this chapter are listed in

Table 2.3.

Table 2.3 Human SMN and Gemin2 expression constructs used in this study

expression construct	mutation	expression vector	ID#
SMN 26-51	WT	MxeDuet/-LEY**	1449
	W34A	MxeDuet/-LEY**	2256
	D35A	MxeDuet/-LEY**	2257
	D36A	MxeDuet/-LEY**	2258
	L39A	MxeDuet/-LEY**	2417
	K41A	MxeDuet/-LEY**	2259
	Y43A	MxeDuet/-LEY**	2418
	D44A	MxeDuet/-LEY**	2260
	D44V	MxeDuet/-LEY**	2261
	A46N	MxeDuet/-LEY**	2419
Gemin2 95-280	WT	MxeDuet*	987
	C154S/C221S/C264S	MxeDuet*	1525
Gemin2 12-280	WT	MxeDuet*	371

* MxeDuet denotes a modified pETDuet vector in which in-frame Mxe intein, chitin binding domain and hexahistidine tags have been added C-terminal to MCS II. Cloning into XhoI leaves a C-terminal L-E-Y

** MxeDuet/-LEY denotes an MxeDuet vector in which the C-terminal L-E-Y cloning tag has been removed by inverse PCR mutagenesis.

Human Gemin2¹²⁻²⁸⁰ and Gemin2⁹⁵⁻²⁸⁰ were amplified by PCR and cloned into the NdeI and XhoI sites of pet21a (EMD Biosciences) and subsequently subcloned as an

NdeI/XhoI fragment into MCS II of a pETDuet (Novagen) expression vector modified to contain an in-frame C-terminal Mxe intein domain, chitin binding domain (New England Biosystems) and hexahistidine affinity tag. For this and all experiments described, full-length Gemin2 refers to the Gemin2 construct comprising residues 12-280.

Human SMN²⁶⁻⁵¹ was originally amplified by PCR and cloned into MCS I of a petDUET expression vector; it was subsequently subcloned as an NdeI/XhoI fragment into MCS II of the same modified Mxe intein-chitin binding domain-His6x pETDuet vector described above. Cloning into the XhoI site of MCSII of this vector results in the inclusion of residues Leu-Glu-Tyr at the C-terminus of the protein just prior to the intein's thiol-reactive catalytic cysteine; all Gemin2 constructs described here retain the C-terminal LEY, while for the SMN²⁶⁻⁵¹ peptide, inverse PCR mutagenesis was used to delete those residues. SMN K51 occupies the amino acid position immediately preceding the catalytic cysteine, rather than a well-tolerated tyrosine, but appears to have no effect on the efficiency of catalytic cleavage of the Mxe intein-CBD-His6x affinity tag from the SMN peptide.

Point mutations in SMN²⁶⁻⁵¹ were generated by inverse PCR mutagenesis (New England BioLabs). To create the Gemin2⁹⁵⁻²⁸⁰ (C154S/C221S/C264S) mutant, the expression plasmid encoding wildtype Gemin2⁹⁵⁻²⁸⁰ in frame with C-terminal Mxe intein, chitin

binding domain and hexahistidine tags was used as a template for multiple simultaneous site-directed mutagenesis (Seyfang & Jin, 2004).

Bacterial Two-Hybrid Screens.

A modified version of the *lexA*-based bacterial two-hybrid assay based on the methods of Dmitrova *et al.* was used to test the interaction of Gemin2 and SMN truncations (Dmitrova *et al.*, 1998). The bait vector consisted of wildtype LexA (1-87) cloned upstream of the MCS in a modified pETDuet in which the T7 promoter has been replaced by a *lac* promoter and in which the standard MCS II has been deleted. The target vector contained the *lexA408* (1-87) mutant in a similarly modified pCDFDuet vector. Human SMN and Gemin2 truncations (Table 2.2) were PCR amplified from existing expression constructs and cloned into BamHI/HindIII sites of the target and bait vectors. Both target and bait vectors were co-transformed into a reporter strain based on CSH142 in which the reporter construct was present on an F'-episome (Whipple, 1998). Positive transformants, as identified by growth on Luria-Bertani (LB) media containing ampicillin, kanamycin and streptomycin, were selected and transferred to either of two reporter media: LB/Amp/Kan/Strep containing X-gal and IPTG or MacConkey Base/Amp/Kan/Strep containing 1% lactose and IPTG and incubated overnight at 37°C. A positive interaction resulted in repression of *lacZ* transcription and, in the first case, white colonies on plates containing X-gal and in the second, white-pink colonies on MacConkey agar. A schematic of the bacterial two-hybrid system is depicted in Figure 2.18.

Expression and purification of human Gemin2 and SMN protein constructs

DNA expression constructs were co-transformed into *E. coli* BL21(DE3) cells; a culture grown from one positive transformant, identified by growth on Luria-Bertani media containing ampicillin and streptomycin, was used to create a 10% glycerol stock stored at -80°C. SMN²⁶⁻⁵¹ and either Gemin2¹²⁻²⁸⁰ or Gemin2⁹⁵⁻²⁸⁰ were expressed separately in Luria-Bertain (LB) cell cultures grown at 15°C for 20 hours after the addition of IPTG (isopropyl-β-D-thio-galactoside) to a final concentration of 0.65 mM.

For ¹⁵N and ¹⁵N/¹³C-enriched samples for NMR analysis, cultures grown in MOPS minimal medium with ¹⁵NH₄Cl as the main nitrogen source and U-[¹²C/¹H] or U-[¹³C/¹H] glucose (Cambridge Isotope Laboratories) as the main carbon source were induced with IPTG and incubated at 15°C for 24 hours. For leucine-selective ¹⁵N labeling, in which Gemin2 was uniformly enriched with ¹⁵N-leucine, the Neidhardt *et al.* protocol for amino acid-supplemented MOPS was followed, substituting ¹⁵N leucine (Cambridge Isotope Laboratories) for ¹⁴N leucine (Neidhardt *et al.*, 1974). To create a fractionally ¹³C labeled SMN-Gemin2 for stereo-specific methyl assignments, a mixture of 10% U-[¹³C/¹H] glucose and 90% U-[¹²C/¹H] glucose added to the MOPS minimal medium provided the main carbon source.

Cells were harvested by centrifugation at 4000 x g for 30 minutes at 4°C. Each liter of cells was resuspended in approximately 20ml of 50mM Na/K phosphate, pH 8.0,

300mM NaCl, 10mM imidazole, 0.5mM ethylenediaminetetraacetic acid (EDTA), 0.5mM 4-(2-Aminoethyl) benzenesulfonyl fluoride hydrochloride (AEBSF; Fisher Scientific), 10 μ M proteinase inhibitor E-64 (Sigma) and 2mM benzamidine (Fisher Scientific). Cells were lysed in two sequential passes through an Avestin Emulsiflex C-3 homogenizer at approximately 18,000 psi, and the crude lysate thereby obtained was cleared by centrifugation at 30590 x g at 4°C for 30 minutes.

Cleared lysate was filtered through grade 802 fluted filter paper (Whatman) and loaded onto 4ml (per 6 liters of cell culture) nickel nitriloacetic acid (Ni-NTA; Qiagen) in a 5.3 cm x 10cm Kontes column equilibrated with 50mM Na/K phosphate pH 8.0, 300mM NaCl, 10mM imidazole. The preparation was nutated at room temperature for 60 minutes; the resin and bound protein were then washed with ten column volumes of buffer containing 50mM Na/K phosphate, 300mM NaCl, 20mM imidazole and eluted in 50mM Na/K phosphate, 300mM NaCl, 250mM imidazole. The Ni-NTA eluant was loaded onto chitin resin equilibrated in a 2.5 cm x 10 cm Kontes column with 50mM Na/K phosphate, 300mM NaCl, 250mM imidazole and nutated for 90 minutes at room temperature. The resin and bound protein were washed with ten column volumes of 20mM Hepes pH 8.0, 300mM NaCl, 0.1mM EDTA.

Human Gemin2 and SMN²⁶⁻⁵¹ proteins were cleaved from the C-terminal Mxe intein-chitin binding domain-hexahistidine tag by addition of 20mM Hepes pH 8.0, 300mM NaCl, 0.1mM EDTA, plus 50mM 2-mercaptoethanol (β ME) acting as the cleavage-

inducing thiol reagent, to the protein-bound chitin resin followed by overnight (~16 hours) incubation at room temperature (18°C – 22°C). The preparation was then added to 4ml of fresh chitin resin equilibrated with 20mM Hepes pH 8.0, 300mM NaCl, 0.1mM EDTA, and the cleaved protein complex was collected in the flow-through.

Human Gemin2 and SMN²⁶⁻⁵¹ proteins were then diluted three-fold in 20mM Tris pH 8.0, 10mM βME and were immediately loaded on a MonoQ HR 10/10 column (Pharmacia) equilibrated in 20mM Tris pH 8.0, 50mM NaCl, 2mM βME for purification by anion exchange chromatography. Proteins were eluted in a linear gradient of 50-450mM NaCl over 7 column volumes at 4ml/min. Gemin2 preparations eluted in a single peak well-separated from excess cleaved affinity tag; SMN²⁶⁻⁵¹ and its cleaved affinity tag co-eluted.

When necessary, purified Gemin2¹²⁻²⁸⁰ was stored after this purification step at -80°C after the addition of 40% glycerol. Final protein concentration was assessed using the absorbance at 280 nm (A_{280}), assuming an extinction coefficient of $42440 \text{ M}^{-1} \text{ cm}^{-1}$ based on amino acid compositional analysis by the ProtParam software tool on the ExPASy Proteomics Server (Swiss Institute of Bioinformatics) (Gasteiger *et al.*, 2003). Gemin2¹²⁻²⁸⁰ was stored at concentrations $\leq 200 \mu\text{M}$. This preparation typically yielded $3 \text{ mg Gemin2 L}^{-1}$ LB media.

SMN²⁶⁻⁵¹ peak fractions collected after purification on MonoQ resin were then concentrated at 5000 x g at 4°C in 15ml Amicon Ultra 10,000 MWCO Centrifugal Filters (Millipore) to one milliliter for further purification by size exclusion chromatography at room temperature on a Superdex 75 HiLoad 16/60 column (Pharmacia) in 10mM Tris pH 8.0, 50mM NaCl, 2mM dithiothreitol (DTT) for biophysical studies, in 0.1M sodium bicarbonate, pH 9.0 for labeling with fluorescein-5-isothiocyanate (FITC) for binding studies or in 50mM Na/K phosphate, 50mM NaCl, 2mM DTT for NMR studies. Excess Mxe affinity tag was easily separated from SMN²⁶⁻⁵¹. Gemin2⁹⁵⁻²⁸⁰ intended for characterization as a single protein species rather than in complex with SMN²⁶⁻⁵¹ was similarly purified by size exclusion chromatography after MonoQ elution. To form the human SMN²⁶⁻⁵¹-Gemin2 complexes, however, SMN²⁶⁻⁵¹ purified by size exclusion chromatography was combined in molar excess with MonoQ-purified Gemin2⁹⁵⁻²⁸⁰ or Gemin2¹²⁻²⁸⁰, and the resulting complex purified in a second step on Superdex-75.

When necessary, homogeneous purified SMN²⁶⁻⁵¹, Gemin2⁹⁵⁻²⁸⁰ or their complex was stored in its sizing buffer plus 10% glycerol at -80°C. Final protein concentration was assessed using the absorbance at 280 nm (A_{280}), assuming extinction coefficients of 36690 M⁻¹ cm⁻¹ (human Gemin2⁹⁵⁻²⁸⁰) and 6990 M⁻¹ cm⁻¹ (human SMN²⁶⁻⁵¹) based on amino acid compositional analysis by the ProtParam software tool on the ExPASy Proteomics Server (Swiss Institute of Bioinformatics) (Gasteiger *et al.*, 2003). SMN²⁶⁻⁵¹ proved highly soluble and was stored at concentrations ≥ 1 mM. Gemin2⁹⁵⁻²⁸⁰ was stored

at concentrations $\leq 200 \mu\text{M}$. These preparations typically yielded 3mg Gemin2⁹⁵⁻²⁸⁰ and 1mg SMN²⁶⁻⁵¹ L⁻¹ LB media, and 1.5mg Gemin2 and 0.5mg SMN²⁶⁻⁵¹ L⁻¹ in MOPS minimal media.

Purification of synthetic SMN²⁸⁻⁵¹ and SMN²⁸⁻⁵¹(pSer28,pSer31) peptides

Synthetic SMN²⁸⁻⁵¹ and SMN²⁸⁻⁵¹ phosphorylated at positions Ser28 and Ser31 (SMN²⁸⁻⁵¹(pSer28,pSer31)) were obtained from the W. M. Keck Foundation Biotechnology Resource Laboratory (Yale University, New Haven, CT, USA). Both peptides were solubilized in 0.1% trifluoroacetic acid (TFA) and purified by reverse-phase HPLC on a Vydac 218TP1010 (10 x 250 mm) protein and peptide C18 column (Grace Division Discovery Sciences, Deerfield Park, IL) at 1ml/min over a linear gradient of 20%-42% acetonitrile (MeCN) for 30 minutes. All solvents contained 0.1% TFA. Mass analysis of peak fractions by matrix-assisted laser desorption/ionization time-of-flight (MALDI-TOF) mass spectrometry confirmed the presence and identities of the desired peptides.

SMN²⁶⁻⁵¹-Gemin2⁹⁵⁻²⁸⁰ (C154S/C221S/C264S) Spin Labeling with MTSSL

A 3-fold molar excess of MTSSL ((1-oxyl-2,2,5,5-tetramethyl-3-pyrroline-3-methyl)-methanethiosulfonate, Toronto Research Chemicals, North York, ON) was added from a concentrated stock in acetonitrile to ¹⁵N-labeled SMN²⁶⁻⁵¹-Gemin2⁹⁵⁻²⁸⁰ (C154S/C221S/C264S) at 0.3mM in 50mM Na/K phosphate, pH 6.5, 50mM NaCl, 2mM DTT, 50 μM EDTA, 0.2mM sodium azide buffer and incubated overnight in the

dark at 4°C with constant stirring. The unreacted spin label was removed by extensive buffer exchange into 50mM Na/K phosphate, pH 6.5, 50mM NaCl, 50mM DTT, 50 μM EDTA, 0.2mM sodium azide and 10% D2O.

Fluorescence Anisotropy Binding Assays

Purified SMN²⁶⁻⁵¹ peptides and an unrelated 32-mer control peptide in 0.1M sodium bicarbonate, pH 9.0 were concentrated in Amicon Ultra 0.5ml 3000 MWCO centrifugal filters at 14,000 rpm at 4°C to ≥ 5 mg/ml. The relatively high pH favors labeling of the amino terminus. Amine-reactive fluorescein-5-isothiocyanate (FITC; Invitrogen) was dissolved to 10mg/ml in dimethylsulfoxide (DMSO) and a volume equal to 1/10 the volume of each concentrated SMN²⁶⁻⁵¹ peptide solution was added to that solution in an amber Eppendorf tube for light protection. The labeling reaction was further protected from light with aluminum foil and nutated for one hour at room temperature. The reaction was quenched by addition of a volume of 1.5M hydroxylamine, pH 8.5 equal to 1/10 the volume of the original concentrated SMN²⁶⁻⁵¹ peptide solution and nutated as before for one hour.

Unreacted FITC label was removed by buffer exchange into 1x PBS (10 mM Na₂HPO₄, 2 mM KH₂PO₄, 137 mM NaCl, 2.7 mM KCl, pH 7.4) at 2ml/min over a 5ml HiTrap desalting column. Protein and free FITC peak elution was monitored using UV absorbance at 280 nm (A_{280}) and 495 nm (A_{495}), and final FITC-labeled peptide concentration was assessed using A_{280} and A_{495} values following the formula

$$A_{protein} = A_{280} - A_{495} (CF)$$

where the correction factor CF is defined as (A_{280} free dye / A_{max} free dye) and is equivalent to 0.3 for fluorescein-5-isothiocyanate.

For binding studies, FITC-SMN peptides were diluted into PBS to which 2mM DTT was added, and Gemin2 was dialyzed into the same buffer in D-Tube Dialyzers, Midi 6-8kDa MWCO (Novagen). Binding reactions (100 μ l) containing 20 μ l 75nM FITC-labeled SMN (15nM final) and 80 μ l of increasing concentrations of Gemin2 (for a final concentration range of 0–1 or 0–4 μ M) were analyzed using a Beacon 2000 fluorescence polarization instrument (Panvera) to record millipolarization values, a ratio of light intensities providing a measure of the extent of molecular rotation during the period between excitation and emission. Millipolarization values were converted to polarization by a factor of 1000 and then converted to anisotropy using the following equation:

$$Anisotropy = \frac{2 * polarization}{(3 - polarization)}$$

Data were fit to a simple binding isotherm corrected for receptor depletion (Kenakin, 1993). Typically, the equation for a simple binding isotherm assumes that the total titrated concentration of receptor (here Gemin2) approximates the concentration of free receptor.

$$B = \frac{R_T B_T}{(K_D + R_T)}$$

where B = [total concentration complex], R_T = total concentration of receptor (Gemin2) and L_T = total concentration of ligand (SMN).

Because the concentration of FITC-peptide (15nM) so nearly approximates the dissociation constant of complex, the total receptor (Gemin2) concentration is depleted at concentrations near K_D and cannot be used as a good approximation of the free receptor concentration across the range of concentrations tested.

An explicit correction for receptor depletion was made according to the formula

$$A = A_f + (A_b - A_f) \times (L_T + K_D + R_T) - \frac{[(L_T - K_D - R_T)^2 - 4L_T R_T]^{0.5}}{2L_T}$$

where A = the experimental anisotropy, A_f = the anisotropy for the free ligand (here FITC-SMN), A_b = the anisotropy for the fully bound ligand, R_T = the total receptor (Gemin2) concentration and L_T = the total added concentration of the ligand and where B was converted to anisotropy according to

$$[\textit{ligand bound}] = \frac{L_T (A - A_f)}{(A_b - A_f)} = B$$

To determine K_D , non-linear least squares regression was performed using GraphPad Prism version 5.04 for Windows (GraphPad Software, San Diego California USA, www.graphpad.com) with L_T fixed at 15.0nM.

NMR Spectroscopy and Analysis

All NMR samples were prepared in Shigemi NMR tubes (Shigemi, Inc.) in buffer containing 50mM Na/K phosphate, pH 6.5, 50 mM NaCl, 50 mM DTT, 50 μ M EDTA, 0.2mM sodium azide and either 90% H₂O/10% D₂O or 99.99% D₂O. Spectra were collected at 25°C at either 750MHz or 500MHz (¹H) on Bruker AVANCE III NMR spectrometers equipped with triple resonance (H/N/C) cryo-probes. Proton chemical shifts were referenced to DSS in the buffer, while ¹³C and ¹⁵N chemical shifts were indirectly referenced. Data were processed using FELIX (Molecular Simulations, San Diego, CA, USA) and analyzed in SPARKY (Goddard & Kneller, 2008).

Backbone amide ¹H and ¹⁵N, C α , C=O, and side-chain C β resonances were obtained using the HNCA, HN(CO)CA, HNCACB, CBCA(CO)NH, HNCO and HN(CA)CO experiments; 97.3% of HN and N resonances were assigned and 94.4% of carbonyl carbon resonances. Side chain assignments were obtained from H(CCCO)NNH, (H)CC(CO)NNH and HCCH-TOCSY experiments, facilitated by three-dimensional ¹⁵N and ¹³C-edited NOESY-HSQC spectra, ¹⁵N and ¹³C HSQC spectra of a sample in which only SMN was labeled assisted in the assignment of SMN peptide resonances. These experiments are described in a review by Sattler *et al.*, and references therein (Sattler *et al.*, 1999). To aid in the assignment of aliphatic sidechains, an ¹⁵N HSQC of a sample in which only Gemin2 was labeled with ¹⁵N-leucine, and stereo-specific side chain assignments of valine and leucine were determined from the ¹³C HSQC of trace-labeled protein sample (Neidhardt *et al.*, 1974; Neri *et al.*, 1989). Of aliphatic residues,

7/7 isoleucine, 19/24 leucine and 14/14 valine side-chains were completely assigned. Aromatic side-chain assignments were made using three-dimensional aromatic-optimized ^{13}C NOESY-HSQC and HCCH-TOCSY experiments; 4/6 tryptophan, 6/6 tyrosine and 4/6 phenylalanine side-chains were fully assigned. All resonance assignments may be found listed in Appendix A.

NOE distance restraints were derived, in H_2O , from 3D ^{13}C -edited NOESY-HSQC (Diercks *et al.*, 1999) and from 4D HNCH-NOESY-HSQC experiments and, in D_2O , from a 4D HCCH-NOESY-HMQC (Ross *et al.*, 1993; Vuister *et al.*, 1993). All mixing times were 110 ms.

NOE-derived inter-proton distances in each NOESY spectrum were sorted into classes, corresponding to approximate distance ranges based on the volumes of “calibration NOEs” representing known short-range distances in secondary structure elements. The volumes of peaks in each NOESY spectrum representing a certain short-range interaction ($\text{HN}_i \rightarrow \text{HA}_i$, $\text{HN}_i \rightarrow \text{HA}_{i-1}$ and $\text{HA}_i \rightarrow \text{HB}_{i+3}$ as appropriate) were represented as histograms, as in Figure 2.23.

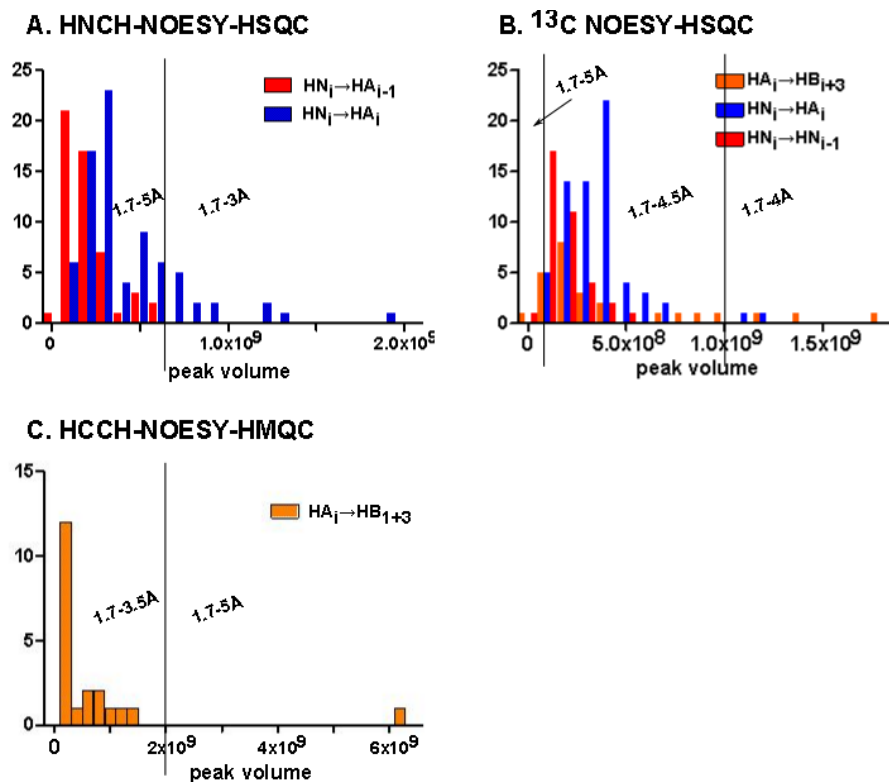


Figure 2.23. Peak volumes of NOEs used in distance calibration. Histograms of NOEs used to calibrate distance restraint limits for observed NOEs in the HNCH-NOESY-HSQC, ^{13}C NOESY-HSQC and HCCH-NOESY-HMQC experiments. Cutoff volumes are indicated with black arrows and the respective distance ranges are depicted in slanted text.

Based on the known $\text{HN}_i \rightarrow \text{HA}_i$ (2.7 Å), $\text{HN}_i \rightarrow \text{HA}_{i-1}$ (3.5Å) and $\text{HA}_i \rightarrow \text{HB}_{i+3}$ (3.6Å) distances in alpha helices (Wüthrich, 1986) and considering the volumes of various NOESY peaks corresponding to those interactions, bins were established at 1.8-3.0 Å (strong), 1.8-3.5Å (medium-strong), 1.8-4.0Å (medium), 1.8-4.5 Å (medium-weak) and 1.8-5.0Å (weak). All inter-proton restraints derived from the aromatic-optimized ^{13}C NOESY-HSQC were classified into the 1.8-5.0 Å distance range. A distance restraint involving one or two methyl groups was afforded an empirical correction of 0.5 Å per methyl group added to its upper distance boundary (Clare *et al.*, 1987).

Backbone torsion angle restraints were derived from chemical shifts using the TALOS+ program (Shen *et al.*, 2009). Hydrogen bonds were entered on the basis of secondary structure as indicated by calculated backbone torsion angles. For residual dipolar couplings, ^{15}N -labeled protein was aligned in bacteriophage Pf1 (ASLA Biotech) to a final concentration of 12 mg/ml. $^1\text{D}_{\text{HN}}$ couplings were obtained from a 2D ^1H - ^{15}N HSQC IPAP (Ottiger *et al.*, 1998). SAXS data were collected at APS BioCAT beamline 18-ID and PRE distance restraints were derived from the attenuation of signal intensity of amide resonances in $^1\text{H}/^{15}\text{N}$ HSQCs collected under identical conditions in the presence of (paramagnetic) SMN²⁶⁻⁵¹-Gemin2⁹⁵⁻²⁸⁰ (C154S/C221S/C264S) labeled with MTSL at Cys241 and, after reduction with a 3-fold molar excess of ascorbic acid, its diamagnetic analogue (Battiste & Wagner, 2000).

NMR Structure Calculations

Generation of a “first stage” model comprised a standard Cartesian simulated annealing protocol performed using the Crystallography and NMR System (CNS) software, beginning from an extended structure and including active energy terms for bonds, angles, impropers, repulsive-only non-bonded interactions, NOEs from the ^{13}C NOESY-HSQC and backbone dihedral angles (Brünger *et al.*, 1998).

Structures were then calculated using the torsion angle/Cartesian space simulated annealing molecular dynamics refinement protocol within the python interface of the program XPLOR-NIH 2.26 (Schwieters *et al.*, 2003; Schwieters *et al.*, 2006). The first

ensemble used the lowest-energy “first stage” CNS model as a starting structure and was calculated using all NOEs, backbone dihedral angles and hydrogen bonds. These restraints may be found listed in Appendix B, Tables 1-3.

In every structure calculation, the trajectory was started at 3000K for 25ps and cooled down linearly in 10K temperature steps to 0K, first with the variable time step internal variable dynamics module (IVM) and then by Cartesian minimization. Each temperature step was propagated for 1000 simulation steps or 2ps, whichever was less. A quartic van der Waals repulsion term for the non-bonded contacts was used, in which the atomic radii were scaled from the van der Waals values multiplicatively, from 0.90 to 0.80. In the first round, the distance restraint force constants derived from NOEs and inferred hydrogen bonds were ramped multiplicatively from 2 to 30 kcal/Å² using a hard-square potential. Backbone dihedral angle (ϕ and ψ) restraints derived from chemical shifts using the software program TALOS+ operated under a force constant at 10 kcal mol⁻¹ rad⁻² at high temperature and were enforced during cooling by a strong force constant unramped at 200 kcal mol⁻¹ rad⁻².

Subsequent rounds added a small-angle x-ray scattering (SAXS) term, residual dipolar couplings (RDCs) and distance restraints derived from paramagnetic relaxation enhancements (PREs). After each new class of restraint was added, eight structures were calculated, of which the lowest energy structure served as the starting structure for the

next round of refinement. The complete and sparsened SAXS data appear in Appendix B, Table 4.

The experimental SAXS data extended from 0.007 to 0.17Å⁻¹ and were sparsened to 50 data points prior to input for the refinement calculations, in which a force constant of 40 kcal/ Å⁻² was employed. Residual dipolar coupling (RDC) restraints describe the orientation of a given bond relative to an overall alignment tensor, described as D^{AB}

$$D^{AB}(\theta, \varphi) = D_a^{AB} \left\{ (3 \cos^2 \theta - 1) + \frac{3}{2} R (\sin^2 \theta \cos 2\varphi) \right\}$$

where the axial (D_a^{AB}) and rhombic (D_r^{AB}) components of the traceless second rank diagonal tensor are given as

$$D_a^{AB} = \frac{1}{3} \left[D_{zz}^{AB} - \frac{(D_{xx}^{AB} + D_{yy}^{AB})}{2} \right]$$

$$D_r^{AB} = \frac{1}{3} [D_{xx}^{AB} - D_{yy}^{AB}]$$

with

$$|D_{zz}^{AB}| > |D_{yy}^{AB}| \geq |D_{xx}^{AB}|$$

and rhombicity (R) defined as

$$R = \frac{D_r^{AB}}{D_a^{AB}} > 0$$

A histogram of measured RDCs from a sample provides an estimate of D_{yy} and D_{zz} (the extremes of the plotted data) and D_{xx} (the highest probability dipolar coupling value), as in Figure 2.24 (Clare *et al.*, 1998).

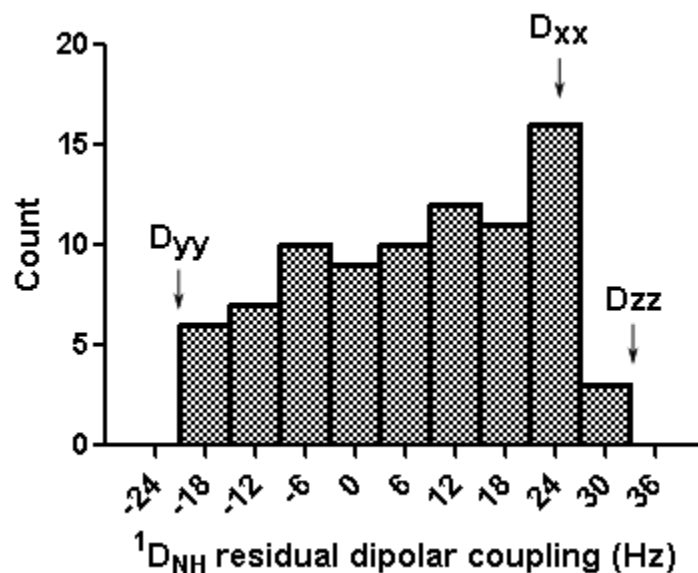


Figure 2.24 A histogram of $^1D_{NH}$ RDCs for SMN²⁶⁻⁵¹-Gemin2⁹⁵⁻²⁸⁰. The values of D_{xx} , D_{yy} and D_{zz} are indicated by black arrows.

Based on the values of D_{xx} , D_{yy} and D_{zz} (24 Hz, -21 Hz and 34 Hz, respectively) obtained from the histogram of RDCs, the calculated values for D_a and R were calculated as -10.6 and 1.23.

After addition of the SAXS term, an ensemble of eight structures was generated by XPLOR-NIH incorporating the RDC restraints. When the value of the alignment tensor was permitted to float, becoming optimized over the course of each calculation, the values obtained for D_a and R were calculated to be -10.56 and 0.35. While the estimate of the axial component from the histogram closely mirrored that calculated by XPLOR-NIH, the estimate of rhombicity varied rather more. RDC distance restraints were implemented using a hard-square potential with a force constant ramped multiplicatively from 0.03 to 3.0 kcal/Hz² for $^1D_{NH}$ couplings during the 3000 → 0 K cool down. The

components of the alignment tensor were first allowed to vary; the alignment tensor common to the lowest-energy structures in that round was fixed in the subsequent round. RDC restraints are listed in Appendix B, Table 5.

Paramagnetic relaxation enhancements based on observed attenuation of peak intensities in an 1H-15N HSQC were added last. The ratio of the intensities of each resonance is given by

$$\frac{I_{ox}}{I_{red}} = \frac{R2 \exp(-R2^{sp} t)}{R2 + R2^{sp}}$$

where R2 is the experimentally determined transverse relaxation rate of the reduced sample and R2^{sp} is the relaxation rate enhancement.

Solving for R2^{sp} for each resonance allows the calculation of its distance from the spin label as

$$r = \left[\frac{K}{R2^{sp}} \left(4\tau_c + \frac{3\tau_c}{1 + \omega_h^2 \tau_c^2} \right) \right]^{1/6}$$

where τ_c is the correlation time for the electron-nuclear interaction, ω_h is the Larmor frequency and K is $1.23 \times 10^{-32} \text{ cm}^6 \text{ s}^{-2}$ (Battiste & Wagner, 2000) .

Only two classes of PRE distance restraints were used for structure calculations; peaks with an intensity ratio >0.5 were restrained as the calculated distance $\pm 3.0 \text{ \AA}$, while those with intensity ratios <0.5 were assigned a distance of 15 \AA , with a 3.0 \AA upper

bound and no lower bound. In XPLOR-NIH, the PRE distance restraint force was ramped multiplicatively from 2 to 50 kcal/Å² using a hard-square potential.

The evolution of all force constants over the sequential rounds of ensemble calculation as classes of restraints were added is summarized in Table 2.4.

Table 2.4. Force constants employed at each stage of structural refinement in XPLOR-NIH.

	<u>stage of refinement</u>				
	NOE/dihedrals	SAXS	RDCs (variable)	RDCs(fixed)	PREs
NOE	2→30	2→50	2→50	2→50	2→50
hbond	2→30	2→50	2→50	2→50	2→50
backbone dihedrals	200	200	200	200	200
SAXS		40	40	40	40
RDCs			0.3→3	0.3→3	0.3→3
PREs					2→50
Rama database potential	0.002→1	0.002→1	0.002→1	0.002→1	0.002→1
angles	0.4→1	0.4→1	0.4→1	0.4→1	0.4→1
impropers	0.1→1	0.1→1	0.1→1	0.1→1	0.1→1

In the final stage of model refinement, four hundred structures were generated, of which the 32 lowest energy structures form the ensemble. The final XPLOR-NIH python script employed can be found in Appendix C. Structure figures were generated using PyMOL (Delano, 2002).

There were no persistent NOE violations above 0.5 Å, dihedral angle violations above 5° or RDC violations above 0.5 Hz.

Small-angle x-ray scattering

Samples were dialyzed against 100% D₂O buffer (20mM Na/K PO₄, 50 mM NaCl, 2mM DTT) and were centrifuged at 10,000 x g for ten minutes at 4°C immediately before data collection. X-ray radiation at 12 keV was used to collect 10-15 individual one second exposures while the sample was oscillated in a quartz capillary to minimize radiation damage. Data were corrected for the intensity of the incident radiation and reduced to provide one-dimensional intensity profiles as a function of Q (which is equal to $4\pi\sin\theta/\lambda$, where 2θ is the scattering angle) using the data software Igor Pro. Accessible scattering was recorded in the range of $0.006 < Q < 0.35 \text{ \AA}^{-1}$. Exposures were examined for radiation damage before averaging and subsequent subtraction of buffer scatter.

Averaged scattering curves from the SAXS and WAXS detectors were scaled and merged in PRIMUS; scattering from a matching buffer solution was subtracted from the data and corrected for the incident intensity of x-rays. Replicate exposures were examined carefully for evidence of radiation damage by Guinier analysis and Kratky plot analysis. Silver behenate powder was used to locate the beam center and to calibrate the sample-to-detector distance.

Evidence of the monodispersity of the preparation was gained by analysis of linearity in the Guinier region of the scattering data and agreement of the $I(0)$ and R_g values

determined with inverse Fourier transform analysis by the programs GNOM and AUTOGNOM (Semenyuk & Svergun D, 1991). Molecular mass was derived from $I(0)$ measurements, using the forward scatter from bovine serum albumin as a control, and was consistent with the molecular masses determined by centrifugation and SEC-MALS. When fitting manually, the maximum diameter of the particle (D_{max}) was adjusted in 10-Å increments in GNOM to maximize the goodness-of-fit parameter. This analysis also yielded determinations of R_g and $I(0)$.

Sedimentation velocity

Sedimentation velocity ultracentrifugation experiments were performed at 20 °C with an XL-A analytical ultracentrifuge (Beckman Coulter) and a TiAn60 rotor with two-channel charcoal-filled Epon centerpieces and quartz windows. Complete sedimentation velocity profiles of SMN²⁶⁻⁵¹-Gemin2⁹⁵⁻²⁸⁰ (25 μM, optical density of 0.6 at A_{280}) in 1x PBS pH 7.4 were collected every 60 seconds at 42,000 rpm for 200 scans, followed by data analysis using the continuous size-distribution ($c(s)$) analysis of the Lamm equation in SEDFIT (Schuck & Rossmanith, 2000). After optimizing meniscus position and fitting limits, the sedimentation coefficient (s) and best-fit frictional ratio (f/f_0) were determined by iterative least squares analysis.

Sedimentation equilibrium

Sedimentation equilibrium ultracentrifugation (SE) experiments were performed at 4°C with an XL-A analytical ultracentrifuge (Beckman Coulter) and a TiAn60 rotor with

six-channel charcoal-filled Epon centerpieces and quartz windows. Radial absorption scan data at 280 nm for three protein concentrations were measured (18.0 μM , 11 μM , 5 μM ; 0.8OD, 0.5OD, 0.2OD) at 20 and 22 h for each of three different rotor speeds (22,000, 28,000 and 32,000 rpm). Comparison of radial absorption scans verified that equilibrium had been reached. Data were analyzed using the programs SEDFIT and SEDPHAT and fit variously to a single species model and to several models of self-association, with the best solutions exhibiting small goodness of fit and low and randomly distributed residual errors (Schuck & Rossmanith, 2000; Vistica *et al.*, 2004).

Size exclusion chromatography in-line with multi-angle light scattering

The absolute molecular weight of the SMN²⁶⁻⁵¹-Gemin2⁹⁵⁻²⁸⁰ oligomer was determined using multi-angle light scattering (MALS) in-line with a Superdex 75 10/300 column (GE Healthcare). The column was calibrated using the following proteins (Bio-Rad): thyroglobulin (670,000 Da), bovine gamma globulin (158,000 Da), chicken ovalbumin (44,000 Da), equine myoglobin (17,000 Da) and vitamin B-12 (1350 Da). Blue dextran (Sigma) was used to define the void volume of the column.

SMN²⁶⁻⁵¹-Gemin2⁹⁵⁻²⁸⁰, 20 μl at 10 mg/ml was injected onto the column at 0.5 ml/min in buffer containing 1x PBS, pH 7.0 and 2mM dithiothreitol at room temperature. The scattered light intensity of the column eluant was recorded at 16 different angles using a DAWN-HELEOS MALS detector (Wyatt Technology Corp.) operating at 658 nm after calibration with 20 μl of 20mg/ml lysozyme (Sigma). Protein concentration of the eluant

was determined using an in-line Optilab DSP interferometric refractometer (Wyatt Technology Corp.). The weight-averaged molecular weight of species within defined chromatographic peaks was calculated using the ASTRA software version 5.2 (Wyatt Technology Corp.), by construction of Debye plots ($KC/R \Theta$ versus $\sin^2[\Theta/2]$) at one-second data intervals. The weight-averaged molecular weight was then calculated at each point of the chromatographic trace from the Debye plot intercept, and an overall average molecular weight was calculated by averaging across the peak.

Chapter III: The biophysical properties of Gemin2 in the presence and absence of SMN binding

Introduction

Gemin2 plays a key role in SMN complex-mediated assembly of spliceosomal snRNPs. Gemin2's structure and function eluded description until recently, when NMR and x-ray crystal structures permitted development of a model in which a single α -helix of SMN binds the globular domain of residues 95-280 of Gemin2 on one face, while all five components of the Sm D1/D2/E/F/G pentamer bind the opposite face and along Gemin2's extended N-terminal arm.

Here, solution properties of Gemin2⁹⁵⁻²⁸⁰-SMN²⁶⁻⁵¹ are compared to those of unbound Gemin2⁹⁵⁻²⁸⁰ to illustrate changes in the structure of the latter adopted upon SMN binding. Addressing the recent report of a functionally significant Gemin2-Gemin2 interaction (Ogawa *et al.*, 2007), the oligomerization states of Gemin2⁹⁵⁻²⁸⁰-SMN²⁶⁻⁵¹ and Gemin2⁹⁵⁻²⁸⁰, as well as those of full-length Gemin2¹²⁻²⁸⁰ both unbound and bound to SMN²⁶⁻⁵¹, are described. A comparison is also offered between low-resolution solution structures of the minimal Gemin2⁹⁵⁻²⁸⁰-SMN²⁶⁻⁵¹ and full-length Gemin2¹²⁻²⁸⁰-SMN²⁶⁻⁵¹ complexes.

Results

Gemin2⁹⁵⁻²⁸⁰, Gemin2¹²⁻²⁸⁰ and their SMN²⁶⁻⁵¹-bound complexes are monomeric species in solution

In a recent report, Ogawa *et al.* proposed a Gemin2 self-interaction, which they attributed to residues 56-280 and suggested is necessary for the stabilization of SMN self-association at its N-terminal oligomerization domain (Ogawa *et al.*, 2007). In the current x-ray crystallographic model of full-length Gemin2 in complex with SMN²⁶⁻⁶², the reported Gemin2 self-association domain obliges a joint contribution from the globular SMN-binding domain of residues 95-280 and from the N-terminal Sm-protein binding arm to the creation or stabilization of the putative Gemin2 self-interaction surface (Zhang *et al.*, 2011). No evidence of Gemin2 dimerization, however, was apparent in the NMR studies of its minimal complex with SMN or in the crystal structure of Gemin2 bound both to a minimal SMN construct and its Sm protein substrates, leaving unclear the circumstances under which a Gemin2-Gemin2 interaction occurs.

In an effort to establish the oligomeric state and protein stoichiometry of several Gemin2 and Gemin2-SMN²⁶⁻⁵¹ species in solution, analytical size-exclusion chromatography in-line with multi-angle light scattering (SEC-MALS) was used to determine the absolute molecular weights of Gemin2⁹⁵⁻²⁸⁰, Gemin2¹²⁻²⁸⁰ and those

species bound to SMN²⁶⁻⁵¹. For this and all experiments described, full-length Gemin2 refers to the Gemin2 construct comprising residues 12-280.

A simple interpretation of the analytical size exclusion chromatography elution profiles of each species in comparison with those of globular molecular weight standards and apparent molecular weight. As mentioned in Chapter II, Gemin2⁹⁵⁻²⁸⁰-SMN²⁶⁻⁵¹, injected at 10 mg/ml (410 μ M), elutes as a single peak with an approximate molecular weight of 25 kDa, consistent with a 1:1 heterodimer of one Gemin2⁹⁵⁻²⁸⁰ molecule (21 kDa) and one SMN²⁶⁻⁵¹ molecule (3 kDa). This is entirely consistent with observations about the complex made from its NMR solution structure and from its analysis by sedimentation equilibrium (also presented in Chapter II). Unbound Gemin2⁹⁵⁻²⁸⁰ at 1.7 mg/ml (79 μ M), however, elutes as a single peak with an apparent molecular weight of 60 kDa, consistent with a trimer of globular 21 kDa monomers (Figure 3.1).

Proteins with non-standard hydrodynamic properties due to an elongated shape or conformational flexibility can elute in size-exclusion chromatography experiments at the abbreviated retention times characteristic of larger globular particles. To discriminate between oligomerization and non-globular shape as the basis of elution from a size exclusion chromatography column at a large apparent molecular weight, a measure of the absolute molecular weights for the same Gemin2 species were determined considering multi-angle light scattering data coupled to size exclusion chromatography (SEC-MALS) on a Superdex 75 10/300 column. The weight-averaged molecular weight

of the Gemin2⁹⁵⁻²⁸⁰-SMN²⁶⁻⁵¹ complex was calculated to be 23.7 ± 0.1 kDa, again confirming its established nature as a single 1:1 heterodimer in solution. Despite the suggestion from its elution profile that it forms an oligomer in solution, Gemin2⁹⁵⁻²⁸⁰ showed a weight-averaged molecular weight of 22.9 ± 0.1 kDa, indicating that its solution state is also monomeric (Figure 3.1).

Full-length Gemin2¹²⁻²⁸⁰ bound to SMN²⁶⁻⁵¹ contains all the residues of Gemin2 reported involved in Gemin2 self-interaction. Injected at 1.4 mg/ml (41 μ M), it elutes as a single peak from a Superdex 75 10/300 size exclusion chromatography column, with an apparent molecular weight of 94 kDa, suggesting a trimer of 1:1 heterodimers consisting of one Gemin2¹²⁻²⁸⁰ molecule (32 kDa) and one SMN²⁶⁻⁵¹ molecule (3 kDa). Its weight-averaged molecular weight based SEC-MALS analysis, however, was calculated to be 33.7 ± 0.4 kDa, again consistent with a 1:1 heterodimer of 35 kDa and displaying no evidence of oligomerization (Figure 3.1).

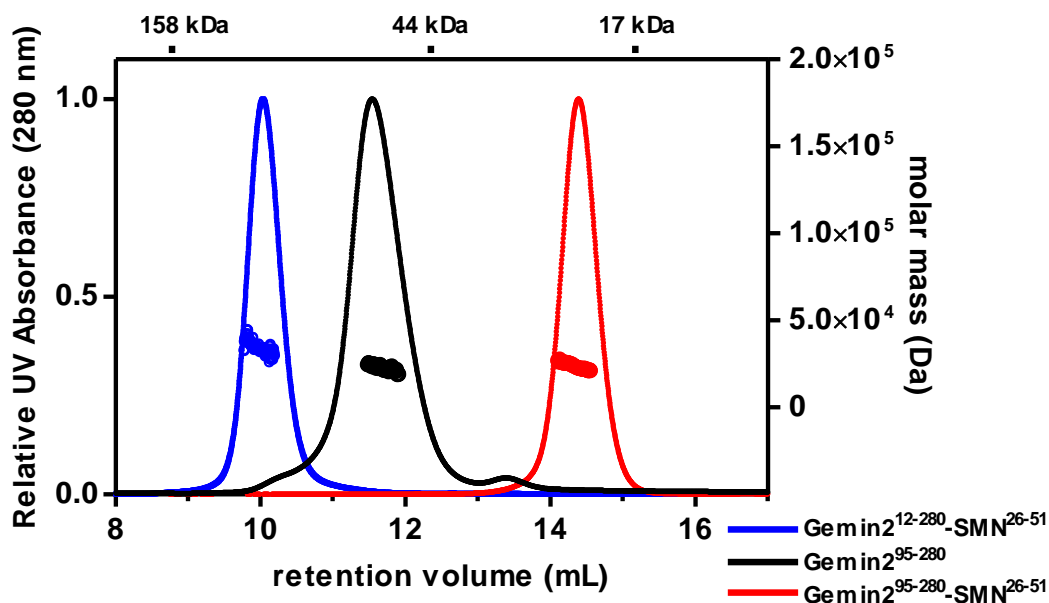


Figure 3.1 Representative SEC-MALS analyses of Gemin2 and Gemin2-SMN²⁶⁻⁵¹ complexes. The elution profiles depict Gemin2¹²⁻²⁸⁰-SMN²⁶⁻⁵¹ (blue), Gemin2⁹⁵⁻²⁸⁰ (black) and Gemin2⁹⁵⁻²⁸⁰-SMN²⁶⁻⁵¹ (red) from a Superdex 75 10/300 column. The elution volumes of globular protein standards are shown above the panel. None of the three proteins show evidence of higher order oligomers.

In all previous attempts at its study, unbound full-length Gemin2¹²⁻²⁸⁰ evinced resoundingly poor solution properties, including poor solubility, a tendency toward aggregation, susceptibility to proteolysis and a severe disposition toward promiscuous and irreversible binding to a number of chemical substrates, including all nitrocellulose membranes and dextran agarose sizing resin. Attempts to manipulate it experimentally remained very limited. Nisha Ninan, however, a graduate student in the Gregory Van Duyne laboratory at the University of Pennsylvania, recently succeeded in performing SEC-MALS analysis on the protein in buffer containing 5% glycerol. Gemin2¹²⁻²⁸⁰ too elutes as a single peak with a weight-averaged molecular weight calculated to be 29.2 ± 0.3 kDa, in good agreement with its calculated molecular weight of 32 kDa. In evident

disagreement with the study by Ogawa *et al.*, Gemin2 dimerization was not apparent at the relatively high protein concentrations tested in these analyses for either Gemin2⁹⁵⁻²⁸⁰ or Gemin2¹²⁻²⁸⁰, either unbound or bound to a minimal SMN peptide.

Gemin2⁹⁵⁻²⁸⁰ assumes an elongated structure in the absence of SMN binding

The disparity in the apparent and absolute molecular weights of Gemin2⁹⁵⁻²⁸⁰ species studied by SEC-MALS could be the result of unusual hydrodynamic properties, such as an elongated shape or conformational heterogeneity. To better understand the conformation adopted by Gemin2⁹⁵⁻²⁸⁰ in the presence and absence of SMN²⁶⁻⁵¹, sedimentation velocity analysis and small-angle x-ray scattering were employed to evaluate structural parameters such as the frictional ratio (f/f_o), radius of gyration (R_g) (a description of the mass distribution of the macromolecule around its center of gravity) and maximum dimension (D_{max}), all indicators of the extent of a particle's elongation.

Sedimentation velocity analytical ultracentrifugation data was collected for Gemin2⁹⁵⁻²⁸⁰ and Gemin2⁹⁵⁻²⁸⁰-SMN²⁶⁻⁵¹ at 20°C and 8.2 μM and 18.3 μM, respectively, and fit to a continuous $c(s)$ distribution yielding estimates for their sedimentation coefficients ($S_{20,w}$) of 3.0 and 2.4. It becomes possible to calculate the frictional ratio f/f_o , the ratio of the frictional coefficient from the sedimentation coefficient, as discussed in Chapter II; the frictional ratio of a protein also correlates with its shape, with f/f_o values ~1.25 typically indicating a globular protein (Janson, 2011). Here, comparison of f/f_o values determined for Gemin2⁹⁵⁻²⁸⁰ and Gemin2⁹⁵⁻²⁸⁰-SMN²⁶⁻⁵¹ is illustrative. Compared to the f/f_o of 1.25

calculated for the Gemin2⁹⁵⁻²⁸⁰-SMN²⁶⁻⁵¹ complex, Gemin2⁹⁵⁻²⁸⁰ has a value of 1.5, suggesting a relative elongation of that species (Figure 3.2).

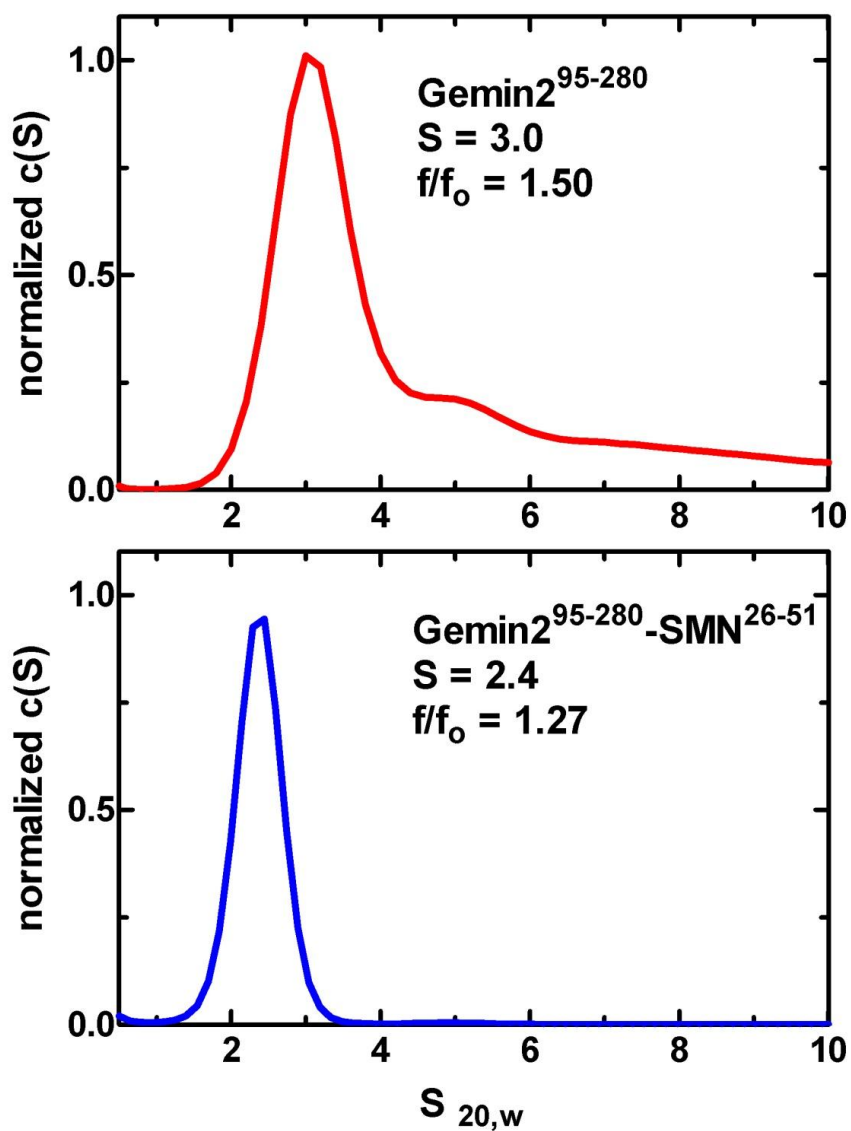


Figure 3.2 Sedimentation velocity analysis of Gemin2⁹⁵⁻²⁸⁰ and Gemin2⁹⁵⁻²⁸⁰-SMN²⁶⁻⁵¹. Representative c(S) analyses of Gemin2⁹⁵⁻²⁸⁰ (top; red) and Gemin2⁹⁵⁻²⁸⁰-SMN²⁶⁻⁵¹ (bottom; blue) from sedimentation velocity data.

A number of useful structural parameters related to the overall shape of a scattering particle can be derived from small-angle scattering experiments, including small-angle x-ray scattering. Radii of gyration for Gemin2⁹⁵⁻²⁸⁰ and Gemin2⁹⁵⁻²⁸⁰-SMN²⁶⁻⁵¹ were calculated by Guinier analysis of the SAXS scattering curve at very low scattering angles (Figure 3.3A), with values calculated as $25.6 \pm 0.38 \text{ \AA}$ and $19.4 \pm 0.13 \text{ \AA}$, respectively, indicating that unbound Gemin2⁹⁵⁻²⁸⁰ occupies more extended conformation in solution than it does when bound to SMN²⁶⁻⁵¹. A summary of results for Gemin2⁹⁵⁻²⁸⁰-SMN²⁶⁻⁵¹ and unbound Gemin2⁹⁵⁻²⁸⁰ is presented in Table 3.1.

Table 3.1 Gemin2 structural parameters derived from small-angle x-ray scattering analyses

Sample	Conc. (mg/mL)	Rg (Å)	I(0)	Q	D_{max} (Å)
Gemin2 ⁹⁵⁻²⁸⁰	0.5	25.6 ± 0.38	31.8 ± 0.41	0.017 - 0.35	75
Gemin2 ⁹⁵⁻²⁸⁰ - SMN ²⁶⁻⁵¹	3.6	19.4 ± 0.13	267.1 ± 1.40	0.025-0.35	54
Gemin2 ¹²⁻²⁸⁰ - SMN ²⁶⁻⁵¹	8.5	29.1 ± 0.10	286.1 ± 0.56	0.011-0.32	134

P(r) curves, distance distribution functions that describe the probability of an interatomic vector of length r and that reach zero at the particle's maximum dimension

(D_{\max}), were calculated from the collected intensity using an inverse Fourier transform (Figure 3.3B).

One measure of the elongation of a given protein is to compare its D_{\max} to that of an ideal sphere of the same molar mass. The volume of protein of molecular mass M (Da), assuming an average partial specific volume for most proteins of $v = 0.73 \text{ cm}^3/\text{g}$, can be calculated as:

$$V(\text{nm}^3) = \frac{(0.73 \frac{\text{cm}^3}{\text{g}})(10^{21} \frac{\text{nm}^3}{\text{cm}^3})}{6.023 \times 10^{23} \frac{\text{Da}}{\text{g}}} \times M(\text{Da})$$

Treating this volume as the most compact possible globular model, a sphere, one can calculate an approximate D_{\max} as twice the sphere's radius. For Gemin2⁹⁵⁻²⁸⁰-SMN²⁶⁻⁵¹ and unbound Gemin2⁹⁵⁻²⁸⁰, these values are 61 Å and 57 Å, respectively (Erickson, 2009).

Based on $P(r)$ curves generated from SAXS intensity data, the experimental D_{\max} values for the two species were determined to be 54 Å and 75 Å for Gemin2⁹⁵⁻²⁸⁰-SMN²⁶⁻⁵¹ and Gemin2⁹⁵⁻²⁸⁰. The D_{\max} value obtained for Gemin2⁹⁵⁻²⁸⁰-SMN²⁶⁻⁵¹ is consistent with its known globular character; unbound Gemin2⁹⁵⁻²⁸⁰ has a much longer maximum dimension than its peptide-bound counterpart, further supporting the notion that the Gemin2-SMN heterodimer occupies a compact shape and confirming a much elongated character, comparatively, for the unbound Gemin2⁹⁵⁻²⁸⁰ (Figure 3.3B).

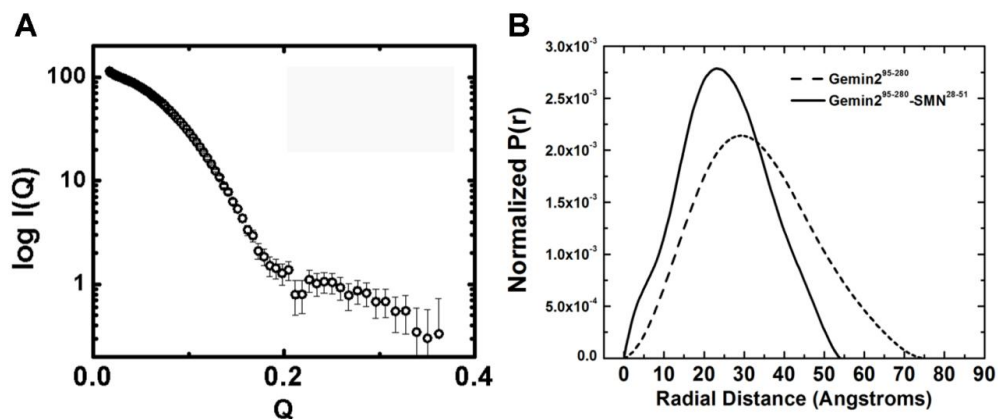


Figure 3.3 SAXS analysis of Gemin2⁹⁵⁻²⁸⁰ and Gemin2⁹⁵⁻²⁸⁰-SMN²⁶⁻⁵¹. A) Small-angle scattering data from Gemin2⁹⁵⁻²⁸⁰-SMN²⁶⁻⁵¹. Shown in black circles is the recorded intensity as a function of Q. B) P(r) shape functions for Gemin2⁹⁵⁻²⁸⁰ (dotted line) and Gemin2⁹⁵⁻²⁸⁰-SMN²⁶⁻⁵¹ (solid line).

The Gemin2⁹⁵⁻²⁸⁰ structure adopted in the presence of SMN²⁶⁻⁵¹ is destabilized in its absence

The apparent elongation of Gemin2⁹⁵⁻²⁸⁰ in the absence of SMN might be visualized either as an ordered rearrangement of secondary structure elements into another, more extended stable protein fold or as the destabilization and partial unfolding of a portion of that protein. Certain characteristics of the ¹H-¹⁵N HSQC spectrum of a protein or the Kratky analysis of its small-angle scattering data are consistently indicative of protein unfolding and were considered here. Two-dimensional ¹H-¹⁵N HSQC spectra of Gemin2⁹⁵⁻²⁸⁰ and Gemin2⁹⁵⁻²⁸⁰-SMN²⁶⁻⁵¹ were recorded at 25°C at 750 MHz (¹H) and overlain to illustrate the differences between them (Figure 3.4). The HSQC spectrum of Gemin2⁹⁵⁻²⁸⁰ shows substantial spectral changes relative to that of the Gemin2⁹⁵⁻²⁸⁰-SMN²⁶⁻⁵¹ complex, including line broadening and a loss of peak dispersion. The number of discrete peaks (51) is far fewer than expected for the molecule (271 including sidechains); they largely correspond to known assignments in the unstructured loop

comprising residues 150-175. These spectral characteristics are highly suggestive of at least partial protein unfolding and conformational flexibility, suggesting that the structure of Gemin2⁹⁵⁻²⁸⁰ is poorly defined when SMN is not bound.

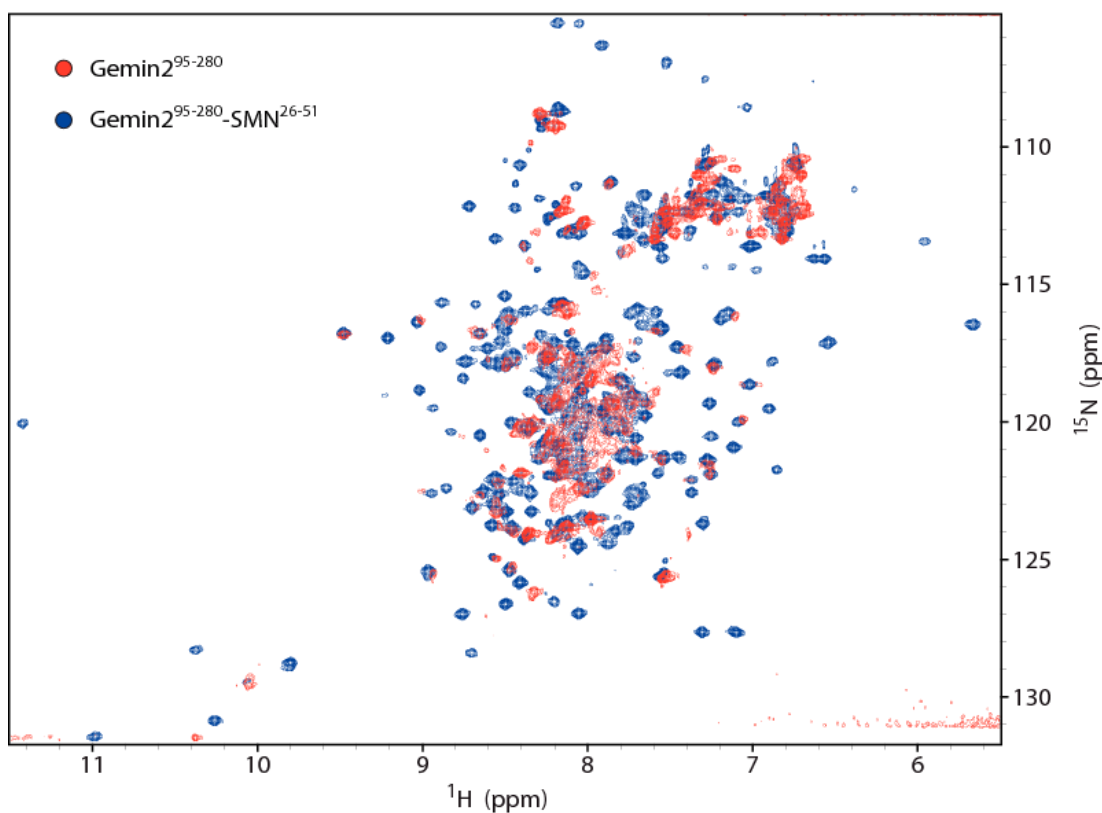


Figure 3.4 Overlay of ¹H/¹⁵N HSQC spectra of Gemin2⁹⁵⁻²⁸⁰. Overlay of ¹H/¹⁵N HSQC spectra of Gemin2⁹⁵⁻²⁸⁰ (red) and Gemin2⁹⁵⁻²⁸⁰ bound to SMN²⁶⁻⁵¹ (blue).

A Kratky analysis of small angle scattering data plots the intensity of the signal times

the square of the scattering vector Q versus Q (where $Q = \frac{4\pi \sin \theta}{\lambda}$; 2θ is the scattering

angle and λ is the wavelength) and serves as a diagnostic measure of protein unfolding.

The Kratky curve of a folded protein displays a symmetric peak at low values of Q ,

approaching zero with increasing Q . In the case of a disordered polypeptide, the Kratky curve instead increases linearly as Q increases (Doniach, 2001). Here, while the Kratky plot of the scattering data from the Gemin2⁹⁵⁻²⁸⁰-SMN²⁶⁻⁵¹ complex conforms to the curve typical of a folded protein, the curve of the Kratky plot from the scattering data measured for unbound Gemin2⁹⁵⁻²⁸⁰ shows clear characteristics of both the folded and unfolded theoretical curves and supports evidence from the ¹H-¹⁵N HSQC spectrum that Gemin2⁹⁵⁻²⁸⁰ is partially unfolded (Figure 3.5).

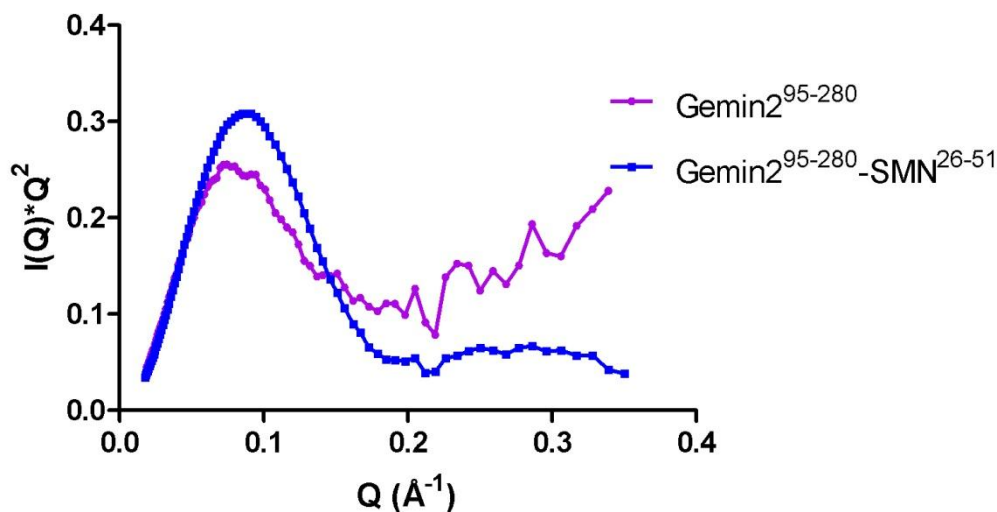


Figure 3.5 Kratky plot of unbound Gemin2⁹⁵⁻²⁸⁰ and the Gemin2⁹⁵⁻²⁸⁰-SMN²⁶⁻⁵¹ complex

Although the results of SEC-MALS analysis, the HSQC overlay and D_{\max} values from SAXS and Kratky analysis clearly indicate that unbound Gemin2⁹⁵⁻²⁸⁰ adopts a partially disordered and comparatively elongated conformation relative to the Gemin2-SMN heterodimer, shape reconstructions based on SAXS scattering data were calculated to visualize the differences between the low-resolution solution structures of the two macromolecular species.

Shape reconstructions of Gemin2⁹⁵⁻²⁸⁰ and Gemin2⁹⁵⁻²⁸⁰-SMN²⁶⁻⁵¹ demonstrate a conformational change in Gemin2⁹⁵⁻²⁸⁰ upon SMN binding

To extend the comparison of the conformations adopted by Gemin2⁹⁵⁻²⁸⁰-SMN²⁶⁻⁵¹ and Gemin2⁹⁵⁻²⁸⁰, low-resolution shape reconstructions from an ensemble of dummy residues were generated from their small-angle x-ray scattering data using GASBOR (Svergun *et al.*, 2001). For Gemin2⁹⁵⁻²⁸⁰-SMN²⁶⁻⁵¹, this approach reproducibly yielded envelopes with good correlations between experimental and calculated scattering data ($\sqrt{\chi} \sim 1.3$) (Figure 3.6A). The ensemble of envelopes generated from multiple iterations of the reconstruction process also agreed well with one another; normalized spatial discrepancy (NSD) values between the simulated shapes were calculated to establish the reliability of the solution and here ranged from 0.89 to 0.97 (where a value of unity corresponds to identity between two structures, and values below 1 indicate a high degree of overlap). The averaged molecular envelope of the Gemin2⁹⁵⁻²⁸⁰-SMN²⁶⁻⁵¹ heterodimer is a fairly compact prolate ellipsoid, entirely consistent with the NMR solution structure of the model (which, indeed, used this scattering data as a restraint) (Figure 3.6B).

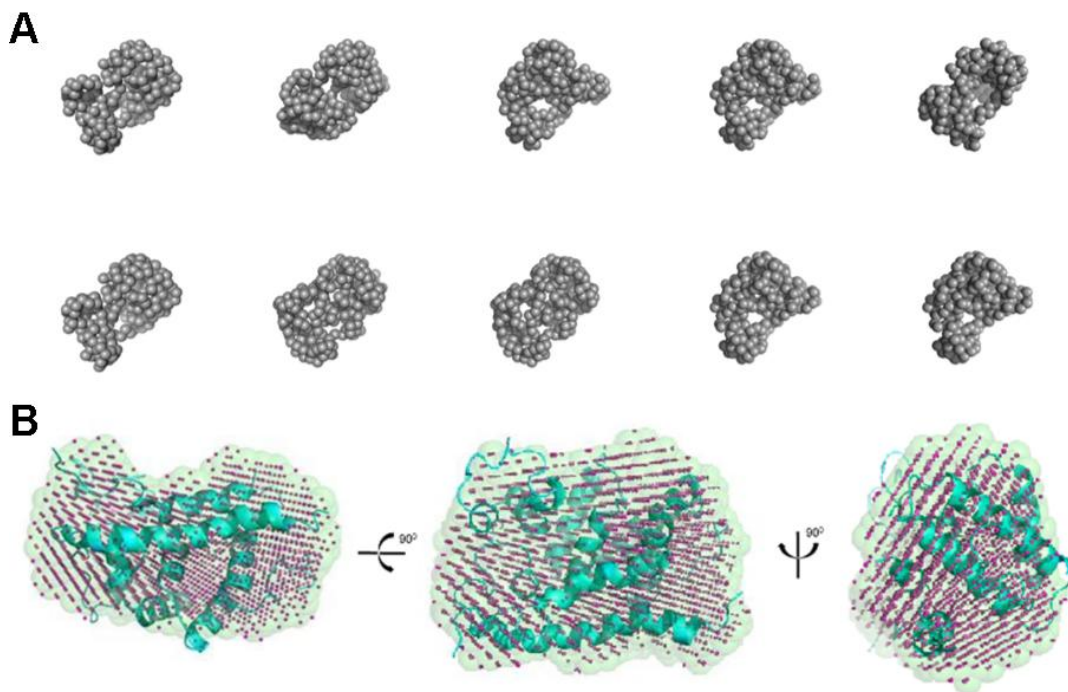


Figure 3.6 SAXS shape reconstructions of Gemin2⁹⁵⁻²⁸⁰-SMN²⁶⁻⁵¹. A) Ten independent *ab initio* envelopes generated from SAXS data using GASBOR. B) Orthogonal views of the NMR structure of Gemin2⁹⁵⁻²⁸⁰-SMN²⁶⁻⁵¹ (cyan) docked into an *ab initio* averaged molecular envelope calculated by DAMAVER (purple spheres) and filtered by DAMFILT (light blue spheres).

A similar GASBOR analysis of the unbound Gemin2⁹⁵⁻²⁸⁰ scattering data yielded shape envelopes with ($\sqrt{\chi} \sim 0.4$) and NSD values ranging from 1.25 – 1.47, the latter value suggesting the envelopes comprising the ensemble varied more with respect to each other than did those calculated for Gemin2⁹⁵⁻²⁸⁰-SMN²⁶⁻⁵¹ (Figure 3.7A). The filtered averaged molecular envelope adopted the appearance of an elongated prolate ellipsoid (Figure 3.7B). An important caveat in the interpretation of the averaged envelope of a biological macromolecule that exhibits some intrinsic disorder, however, is that the averaging and filtering step of shape reconstruction often removes relevant features of these systems sampled in only some shape reconstructions, establishing a misleading single shape.

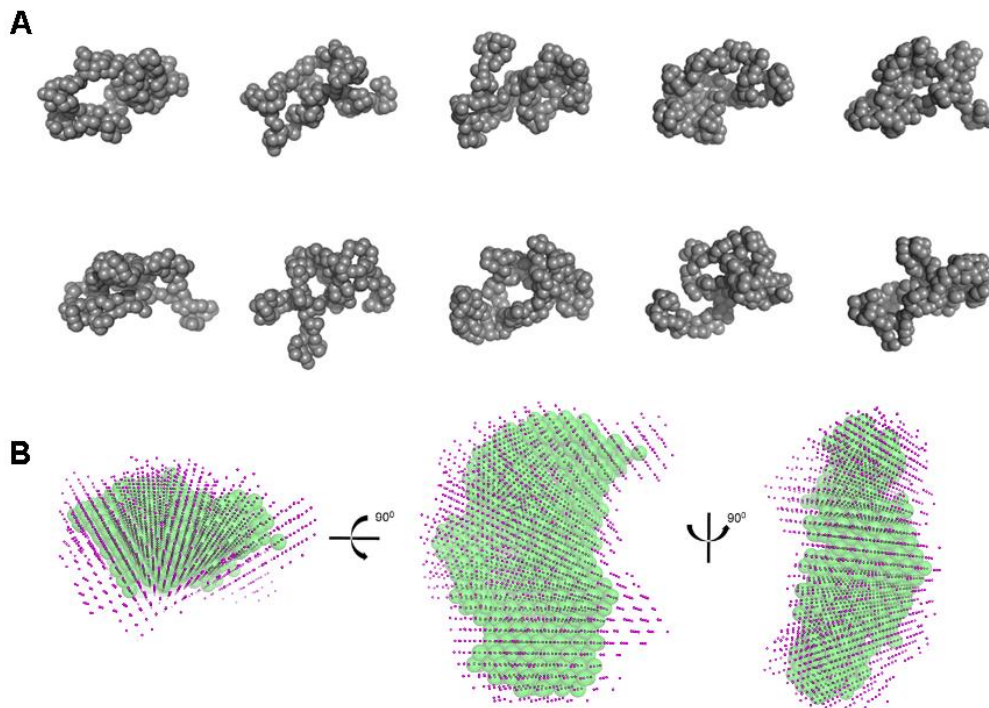


Figure 3.7 SAXS shape reconstructions of unbound Gemin2⁹⁵⁻²⁸⁰. A) Ten independent *ab initio* envelopes generated from SAXS using GASBOR data. B) Orthogonal views of the *ab initio* averaged molecular envelope calculated by DAMAVER (purple spheres) and filtered by DAMFILT (green spheres).

The solution conformation Gemin¹²⁻²⁸⁰-SMN²⁶⁻⁵¹ is extended, and the N-terminal region of Gemin¹²⁻²⁸⁰ forms a rigid arm

A recent crystal structure of Gemin2 bound to an SMN peptide and the Sm D1/D2/E/F/G pentamer represented a step forward in understanding the molecular function of Gemin2 in the context of the SMN complex; after escort to SMN and Gemin2 by the chaperone pICln, it appears that Gemin2 coordinates the pentamer before snRNA binding and addition of the Sm D3/B dimer to complete the Sm protein heptamer, forming the spliceosomal U-snRNP core. In particular, it is noteworthy that

Sm protein interactions with Gemin2 take place on its globular SMN-binding domain on the face opposite SMN binding, as well as along an extended region corresponding to the N-terminal 83 residues of the protein (Zhang *et al.*, 2011). Although that N-terminal binding arm appears to possess some helical character when bound to its Sm protein substrates, the conformation Gemin2 adopts in the absence of its substrates has yet to be explored.

Small-angle x-ray scattering analysis was applied to a description of the structural parameters of Gemin2¹²⁻²⁸⁰-SMN²⁶⁻⁵¹ and to the *ab initio* calculation of a low-resolution molecular envelope. Although a comparable analysis of data from unbound Gemin2¹²⁻²⁸⁰ might have served as an additional source of insight, the poor solubility and stability of that protein precluded its inclusion in SAXS analysis. Guinier analysis of Gemin2¹²⁻²⁸⁰-SMN²⁶⁻⁵¹ demonstrated an R_g of 29.1 ± 0.10 Å; from a P(r) distance distribution function, D_{max} was calculated to be 134 Å (Table 3.1). Given the theoretical D_{max} of 69 Å for a perfect 35 kDa sphere of specific density $\nu = 0.73$ cm³/g, it is obvious that Gemin2¹²⁻²⁸⁰, even bound to SMN, adopts an extended conformation. Given previous SEC-MALS analysis showing that Gemin2¹²⁻²⁸⁰-SMN²⁶⁻⁵¹ forms a 1:1 heterodimer in solution but elutes with a smaller retention volume than predicted for a globular monomer, the confirmation of its elongated character is unsurprising.

GASBOR was employed to generate shape reconstructions from the Gemin2¹²⁻²⁸⁰-SMN²⁶⁻⁵¹ scattering data (Svergun *et al.*, 2001). Independent shape reconstructions

showed good agreement, with $\sqrt{\chi}$ values near 1.3 and NSD values ranging from 0.98-1.05, indicating a very stable structural solution (Figure 3.8A). The averaged molecular envelope of the Gemin2¹²⁻²⁸⁰-SMN²⁶⁻⁵¹ heterodimer displayed a globular domain consistent with the region of the protein (residues 95-280) bound to SMN²⁶⁻⁵¹ that was solved by NMR spectroscopy. Surprisingly, however, the N-terminal region forms a rigid arm-like protrusion reproduced stably in each shape reconstruction and their averaged structure (Figure 3.8B). It appears that residues 12-94 of Gemin2 do indeed extend away from the globular SMN binding domain to interact with the Sm proteins; indeed, the NMR structure of the Gemin2 SMN-binding domain bound to SMN²⁶⁻⁵¹ docks readily by rigid body modeling into the globular domain of the Gemin2¹²⁻²⁸⁰-SMN²⁶⁻⁵¹ molecular envelope, with its N-terminal-most helix positioned to extend into region of the envelope likely representing the N-terminal Sm protein-binding arm (Figure 3.8C). The shape reconstruction invites speculation that the N-terminal region of Gemin2 serves as a preformed binding surface, rather than adopting upon Sm protein binding what modest structure is evidenced in the crystal structure.

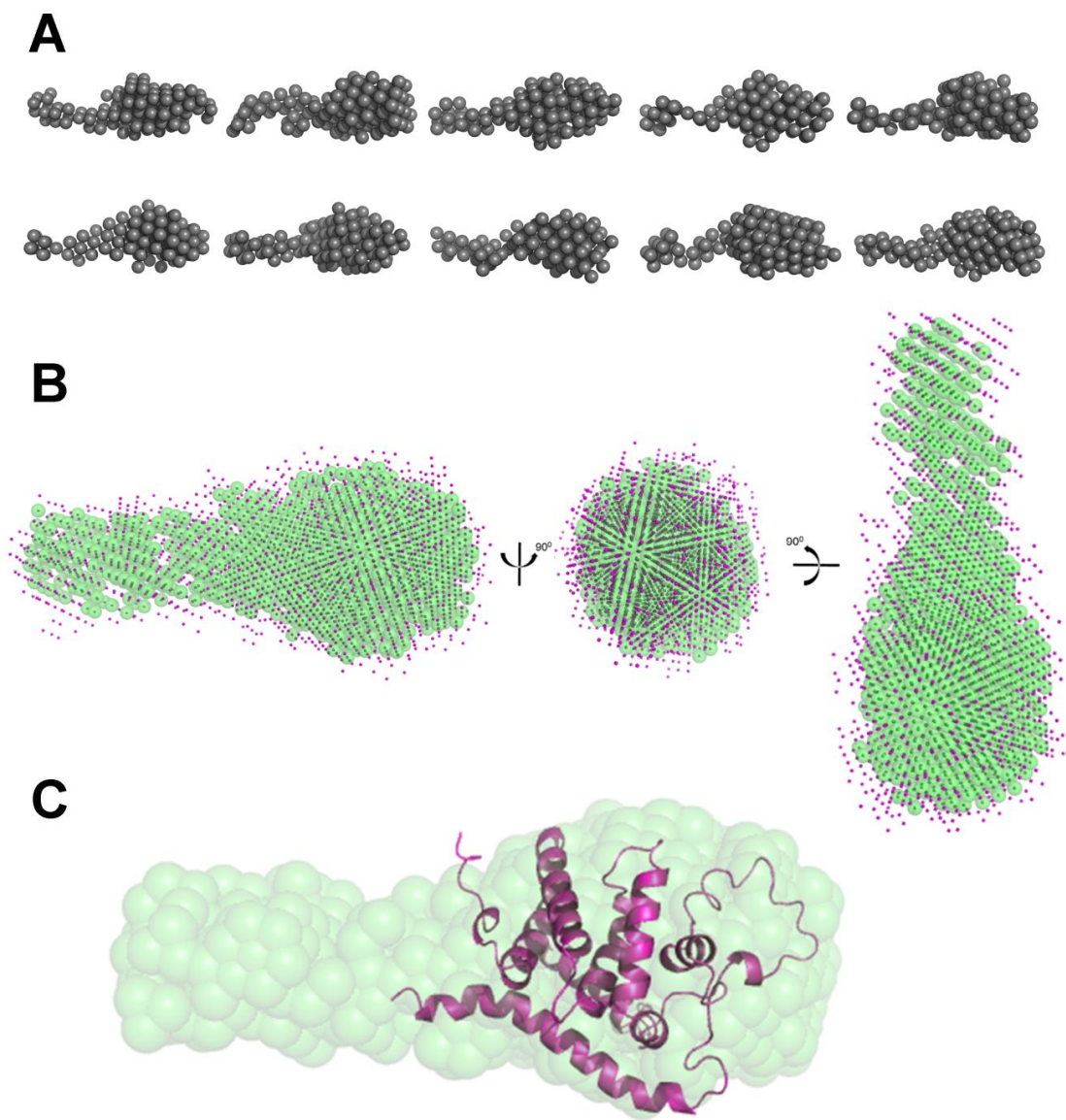


Figure 3.8 SAXS shape reconstructions of Gemin2¹²⁻²⁸⁰-SMN²⁶⁻⁵¹. A) Ten independent *ab initio* envelopes generated from SAXS using GASBOR data. B) Orthogonal views of the *ab initio* averaged molecular envelope calculated by DAMAVER (purple spheres) and filtered by DAMFILT (green spheres). C) View of the NMR structure of Gemin2⁹⁵⁻²⁸⁰-SMN²⁶⁻⁵¹ (purple) docked into an *ab initio* averaged molecular envelope calculated by DAMAVER and filtered by DAMFILT (green spheres).

Discussion

Gemin2 appears to play its crucial role in binding a subset of Sm proteins during snRNP biogenesis in the context of a tight binding interaction with the protein SMN. Based on the NMR solution structure of the minimal Gemin2⁹⁵⁻²⁸⁰-SMN²⁶⁻⁵¹ heterodimer, it is apparent that the seven α -helices of Gemin2⁹⁵⁻²⁸⁰ adopt a fold unlikely to remain stable in the absence of the SMN helix. Here the stoichiometry and conformational states of Gemin2⁹⁵⁻²⁸⁰ and Gemin2¹²⁻²⁸⁰ were examined as a source of insight into the likely requirement that Gemin2 must “fold on” to SMN to gain both stability and its functionally relevant structural fold, and to consider the implications of this constraint on Gemin2’s involvement in processes and in organisms apart from SMN.

Ogawa *et al.* recently proposed a self-interaction for Gemin2 attributed to residues 56-280, which they suggest acts to stabilize the established SMN oligomer (Lorson *et al.*, 1998; Ogawa *et al.*, 2007). In the x-ray crystallographic model of Zhang *et al.*, the reported self-association domain implies the joint contribution of the globular SMN-binding domain of residues 95-280 and the N-terminal Sm-protein binding arm to the creation or stabilization of a Gemin2 self-interaction surface (Zhang *et al.*, 2011). A number of experiments in the Ogawa *et al.* study were cited as evidence in support of Gemin2 dimerization, including size-exclusion chromatography, a mammalian two-hybrid assay and *in vitro* pulldowns (Ogawa *et al.*, 2007). Results gained here over the course of this dissertation, however, especially those obtained from absolute molecular

weight calculations based on SEC-MALS experiments, cast doubt on some of the interpretations offered by Ogawa *et al.*

Among the evidence advanced in support of the dimerization of full-length 32 kDa Gemin2 included the 66 kDa apparent molecular weight with which it elutes from an analytical size-exclusion chromatography column (Ogawa *et al.*, 2007). Indeed, analytical size exclusion chromatography experiments conducted here demonstrated that Gemin2⁹⁵⁻²⁸⁰, Gemin2¹²⁻²⁸⁰-SMN²⁶⁻⁵¹ and Gemin2¹²⁻²⁸⁰ all elute with apparent molecular weights in excess of those expected for monomers. However, both molecular oligomerization and non-standard hydrodynamic properties readily explain the elution of a peak in a size-exclusion chromatography experiment with an unusually abbreviated retention time. Here, the addition of multi-angle light scattering to the size-exclusion chromatography analysis allows the calculation of absolute molecular weights for the protein species comprising each elution peak; this SEC-MALS analysis neatly confirms that both Gemin2⁹⁵⁻²⁸⁰ and Gemin2¹²⁻²⁸⁰, alone or in complex with SMN²⁶⁻⁵¹, exist as exclusive monomers in solution at micromolar concentrations, suggesting a misinterpretation of the sizing profile of full-length Gemin2 in the Ogawa *et al.* study.

Positive results obtained using mammalian two-hybrid assays and interaction assays involving both *in vitro* synthesized Gemin2 from rabbit reticulocyte lysate and bacterially expressed GST and His-tagged protein are also cited in support of a Gemin2 self-interaction, a conclusion that runs contrary to the observation of Gemin2's

monomeric solution state made here. An indirect association through the established self-interaction of endogenous SMN readily explains an apparent Gemin2-Gemin2 interaction in the context of mammalian two-hybrid experiments or pulldowns involving protein synthesized from rabbit reticulocyte lysate (Lorson *et al.*, 1998; Young *et al.*, 2000).

A note of caution must also be struck when considering any experiment employing purified full-length Gemin2 in solution, such as the *in vitro* pulldowns using GST-Gemin2 and His-tagged Gemin2 furnished as evidence of a direct and specific Gemin2 self-association. Full-length Gemin2 was observed over the course of this dissertation work to exhibit exceptionally poor behavior in solution either as an N-terminal GST-fusion or in its wildtype state; it is poorly soluble, inclined to proteolysis and aggregation and, perhaps germane to this discussion, extremely prone to promiscuous and irreversible binding to a large number of targets (including dextran-agarose size-exclusion resin and all nitrocellulose-based membranes). Indeed, within the context of these studies, only at low protein concentrations in high ionic strength buffer containing glycerol could full-length Gemin2 be stabilized for SEC-MALS analysis. It seems necessary to consider that the interaction described as a relevant direct Gemin2-Gemin2 binding event may actually result, in the physiological ionic-strength buffer conditions described, from a non-specific interaction of full-length His-tagged Gemin2 with GST-Gemin2, the GST tag of its protein target or with the glutathione agarose itself.

In the NMR structure of Gemin2⁹⁵⁻²⁸⁰-SMN²⁶⁻⁵¹, careful consideration of the arrangement of the seven α -helices of Gemin2 with respect to the bound SMN helix draws the attention of the observer to the long $\alpha 1$ helix, which runs antiparallel to SMN and makes numerous hydrophobic contacts with it along its length, but very few contacts with any other regions of Gemin2 (Figure 3.9). The likelihood that that helix would maintain its position in the absence of SMN and any other intermolecular anchors seems remote, and a model suggests itself in which Gemin2 adopts a less restrained conformation when unbound, before “folding on” to SMN.

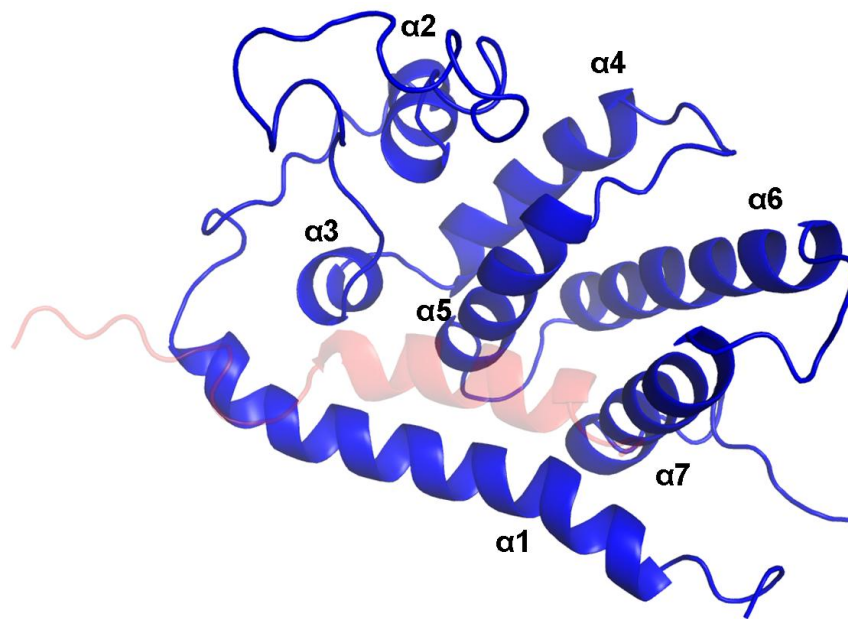


Figure 3.9 The $\alpha 1$ helix of Gemin2 primarily interacts with SMN. A view of the Gemin2⁹⁵⁻²⁸⁰-SMN²⁶⁻⁵¹ complex in which SMN (faded red) is de-emphasized to draw attention to the position of the $\alpha 1$ helix, forming very few interactions with other regions of Gemin2 despite an extensive interface with SMN.

The experiments detailed in this chapter describing both the Gemin2⁹⁵⁻²⁸⁰-SMN²⁶⁻⁵¹ complex and unbound Gemin2⁹⁵⁻²⁸⁰ support a model in which the latter is stabilized upon SMN binding. Both analytical ultracentrifugation and small-angle x-ray scattering studies allowed the calculation of basic structural parameters that indicate an elongation of Gemin2⁹⁵⁻²⁸⁰ relative to the fairly compact structure adopted by Gemin2⁹⁵⁻²⁸⁰-SMN²⁶⁻⁵¹, with the former evincing a significantly larger frictional ratio and radius of gyration than its SMN-bound counterpart. Calculation of the molecular envelopes of the two species based on small-angle x-ray scattering add to the body of evidence supporting a substantial conformational change in Gemin2 upon SMN binding, showing more extended shape reconstructions comprising a much more variable ensemble from the Gemin2⁹⁵⁻²⁸⁰ scattering data than those determined for Gemin2⁹⁵⁻²⁸⁰-SMN²⁶⁻⁵¹.

The apparent elongation of unbound Gemin2⁹⁵⁻²⁸⁰ could be interpreted as a destabilization and partial unfolding of the N-terminal 30-40 residues of the construct, as examination of the α 1 helix comprising those residues in the context of SMN binding might suggest. Alternatively, an ordered rearrangement of Gemin2's helices into a different, more extended but similarly stable protein fold could elicit a similar modification of its structural parameters. Evidence from both the ¹H-¹⁵N HSQC of unbound Gemin2⁹⁵⁻²⁸⁰ and the Kratky analysis of its scattering data argue for the acquisition of disorder in the absence of SMN. Compared to the broad peak dispersion and sharp linewidths characteristic of a folded, soluble protein and present in the ¹H-¹⁵N HSQC of Gemin⁹⁵⁻²⁸⁰ bound to SMN²⁶⁻⁵¹, the same spectrum of Gemin2⁹⁵⁻²⁸⁰ alone

shows considerable line broadening and a loss of peak dispersion, typically hallmarks of protein unfolding (Figure 3.4). Although peak broadening might also have resulted from Gemin2 self-association, SEC-MALS analysis demonstrating that Gemin2⁹⁵⁻²⁸⁰ exists as a monomer in solution establishes that that hypothesis is not operative in this case; the alterations in the characteristics of the HSQC spectrum of Gemin2 in the absence of bound SMN are more likely the result of a gain in conformational flexibility relative to the folded heterodimer.

Kratky analysis of the two sets of scattering data corroborates the notion that Gemin2 acquires a partially unfolded character in the absence of SMN. The Kratky curve ($I(Q) \cdot Q^2$ v. Q , where Q is the scattering vector) characteristically increases monotonically for random coil, while peaking and tapering to zero for a folded protein; while the Kratky plot of Gemin2⁹⁵⁻²⁸⁰-SMN²⁶⁻⁵¹ complex scattering data conforms to the second set of criteria, confirming its folded, globular nature, Gemin2⁹⁵⁻²⁸⁰ alone demonstrates features of both theoretical curves, suggesting that it is partially but not entirely folded when unbound (Figure 3.5).

The biological relevance of partially unfolded Gemin2 in the absence of SMN is uncertain; indeed, it may not exist in appreciable quantities in the cell in the absence of its stabilizing binding partner. Destabilization of its fold in the absence of SMN could explain the repeated observation that a decrease in cellular SMN levels yields a concomitant decrease in Gemin2 (Jablonka *et al.*, 2002; Shpargel & Matera, 2005).

Other cellular functions have been attributed to Gemin2, however, and the mutual involvement of SMN in those cases is uncertain, inviting speculation about additional binding partners that could bind in place of SMN to stabilize the Gemin2 fold or the possibility of Gemin2 operating outside of the fold observed in its SMN-defined structure in some circumstances. In the reported interaction of Gemin2 with HIV-1 integrase (IN), for example, by which it facilitates the assembly of reverse transcriptase on viral RNA, the direct interaction between Gemin2 and IN is mapped to residues that would comprise the face of Gemin2 opposite SMN binding in the current NMR and crystallographic models. The involvement of SMN in the process is uncertain; SMN knockdown depletes cellular Gemin2 so efficiently that it became difficult to distinguish between a direct and an indirect effect of SMN on HIV infection (Hamamoto *et al.*, 2006; Nishitsuji *et al.*, 2009). Without SMN, it seems unlikely that the five α -helices ($\alpha 2$ - $\alpha 6$) contained in the IN-binding domain of Gemin2 could adopt their SMN-bound conformation, predicting the presence of a non-SMN binding partner to stabilize Gemin2.

Gemin2 is also reported to bind Rad51 directly *in vivo* and to contribute to the ability of that latter to repair double-stranded DNA breaks through homologous recombination. Although the presence of an SMN-Gemin2 chimera (in which the C-terminus of the former was fused to the N-terminus of the latter) was reported to further enhance Rad51-mediated homologous pairing, the structural improbability of the engineered molecule makes a true evaluation of the role of SMN in the process difficult. In its

contribution to homologous recombination as in HIV-1 infection, however, Gemin2 is also likely to require an unidentified binding partner to stabilize its fold if SMN is indeed absent.

Returning to the discussion of the role of Gemin2 in snRNP biogenesis, another question of Gemin2 function in the absence of SMN invites speculation. Both SMN and Gemin2 are highly conserved proteins, consistent with the key functional role they play in cellular housekeeping, and sequence alignments reveal clear orthologues of both proteins from mammals to the fission yeast *S. pombe*. Gemin2, however, also possesses a yet more primitive orthologue named Brr1 in the family of budding yeasts related to and including *Saccharomyces cerevisiae*, even though these organisms lack a recognizable SMN (Liu *et al.*, 1997; Noble & Guthrie, 1996a). Brr1 is demonstrably involved in snRNP biogenesis, fortifying its claim as a functional relative of Gemin2 (Noble & Guthrie, 1996b). An alignment of Brr1 sequences from several species of budding yeast to human Gemin2 demonstrates the strongest conservation in regions corresponding to α -helices in human Gemin2 (Figure 3.10).

<i>S. cerevisiae</i>	1	MKRGESQAP-	DAIFGQSRFAF	ALSDSSVNP	VIEYLKSVRQ	EALRTNAISI	KNHMNLQKRT	59
<i>C. glabrata</i>	13	KEALSSAI-	DPVFGQAKAF	NINDEPVNPL	VKSYLESEVRN	EALHTNAIS-	-HQIQGVSKN	68
<i>K. lactis</i>	7	NQGPL	DPVFGQHSFAF	ALNDEGVSPN	VIRYLLDVRN	EALSNSPLYS	TSRTEQNSHN	61
<i>A. gossypii</i>	2	GHTSGPV	DPVFGQCQVF	DCSAAEVNPE	VVKYLAHVDR	EALHTVGV-V	PSASNLRRKR	57
<i>P. pastoris</i>	4							3
hGemin2								
<i>S. cerevisiae</i>	60	RHKSSMYDDE	DEGAL---KR	HAISPSLIRL	QRNVEIW---	-VRWFNSVKA	TV--LTNAYE	110
<i>C. glabrata</i>	69	TFDANIYDDE	DDSTSIPSDT	KVKSDQITEY	LYSIENW---	-YKWFENISD	II--WHGCVV	122
<i>K. lactis</i>	62	VVETGLVADT	SDLLN---AR	SILEDSE---	-----EAI---	-NEWINEIRK	EMEPLEESPS	106
<i>A. gossypii</i>	58	IEIS----YD	DEEVV---KR	PSEGEKAIEL	PFDMDEV---	-ISWFDQVKE	DA--LSEREA	104
<i>P. pastoris</i>	4	QNQPVEL	LTLKK---QK	AEQPESIEH	THGPVDLQFG	QRKAFPVDLD	ID--PSRLPQ	55
hGemin2								
<i>S. cerevisiae</i>	111	FTGYEDELTD	LLLLFLKNYL	E---DMPSKC	TTVEKIISVL	NQHSFPEK--	A---EEKEEN	162
<i>C. glabrata</i>	123	FEGYDDESIS	HLTQLLRFYL	QKKIDENRAS	SFDRHLVNIF	RDQLKCSDD-	P---DPVNGT	177
<i>K. lactis</i>	107	DSIYTDMDLD	LLVSEIKKYL	D---QHPEE-	-----INDP	VRVTRSV--	L---PIANPE	151
<i>A. gossypii</i>	105	FEGYDEETLN	TLLVGIRDYI	S---RMSSRD	ESTNNLIKLL	EGV----Q--	P---VVTNEA	152
<i>P. pastoris</i>	56	NEGSLPQDVM	TYLAMVRMEA	E---G-NARY	NIDEDENFYL	HETVKTKE--	NIALDPVDNE	109
hGemin2	110			L QWQQQVAQF	STVRQNVNKH	RSHWKSQQLD	S---NVTMPK	137
<i>S. cerevisiae</i>	163	LQIDEEWAKN	ILVRLEKTKI	DSVEDVKKVI	TEGDK-HELV	GYNQWFQYLI	NNEPQHTTFH	221
<i>C. glabrata</i>	178	LEIDEDWAEN	LLKTRNSKI	KDLNTVKYCI	RTDYK-RAPH	GLKFWAKYVT	SNQPTHTAFI	236
<i>K. lactis</i>	152	YDISTETVQS	MVAKLRNKR	SDVSFLKRYI	NRPMP-I-PT	NFRQWFGHIK	HNEPTR-QFM	208
<i>A. gossypii</i>	153	LELDEKWAAK	LVARLGRKRF	TTLDNLKLR	NTQLP-IPTR	A-KAWKIHIP	INEPSHEFFH	210
<i>P. pastoris</i>	110	HQVHITWHHD	YTEYF-KARQ	EKLSILGKEI	EGDEKFIEPS	SAQLWKKYVF	ETTPD-DRLI	167
hGemin2	138	SEDEEGWKKF	CLGE-----	-----KLC	ADGAV-GPAT	NESPGIDYVQ	IGFPPLLSIV	183
<i>S. cerevisiae</i>	222	EKITSKQLWV	LIKYMSNTWI	KEIHKKGRHY	RR---LQDWL	FYILVHTPER	VTAEYTSILR	278
<i>C. glabrata</i>	237	NMIDSSNLWT	LVMYMTQIWL	KEIYTFGKNL	ERKKMLSQWL	LYILHLIPTR	LTAEQMSNIR	296
<i>K. lactis</i>	209	LRLEFDDLK	ILGFMIQ-WI	NSITKNKPS	KQ---LQQWL	LYIWFMPNE	LLSPQISQLR	264
<i>A. gossypii</i>	211	-RMNSTQLFD	LLRYLTDNIV	E--HYQTDSA	TD---YGQWL	VYLLHLPRQ	LTANEISEVR	264
<i>P. pastoris</i>	168	VAIPFDVKFK	MIYFTR-WL	N----KTLN	AN---LIKWI	EITLESPEL	LEGTEISLLR	218
hGemin2	184	SRMNAQTVTS	VLEYLSN-WF	GE----RDF	PE---LGRWL	YALLACLEKP	LLPEAHSILR	235
<i>S. cerevisiae</i>	279	DLGKKCLELI	QKKPVEA--H	ENKITLPKEM	AELNVEIPAA	VENMTITELT	VSVIAVNYGQ	336
<i>C. glabrata</i>	297	SLAKQAREIL	NRRVNSNIFG	TTNIVIPDEL	HEHNC--PPC	PPNLDIASLI	LAVVTRKYGQ	354
<i>K. lactis</i>	265	DLGRKC-QLS	LIAASNS--K	ITSLTMPTEI	RD--IPFPNQ	RDQLNAIEIT	LAVIAHRFGQ	319
<i>A. gossypii</i>	265	GLSKKVRALI	IDH--EI--L	KLPMLLPSEI	EDVS-PIPRG	VNP---LHLA	LAVVAVIYGQ	316
<i>P. pastoris</i>	219	NLAKKAIKLR	GNDLDST--S	-----	-----	---LSVMDEI	ISIVGDVYHQ	253
hGemin2	236	QLARRCSEVR	L-----	-----LVDSK	DDERVE-----	-----ALNLI	ICLVSRFYDQ	272
<i>S. cerevisiae</i>	337	KDLIE	341					
<i>C. glabrata</i>	355	HDILE	359					
<i>K. lactis</i>	320	RDLL	323					
<i>A. gossypii</i>	317	RDIL	320					
<i>P. pastoris</i>	254	RDLE	258					
hGemin2	273	RDLEAD	277					

Figure 3.10 Alignment of Brr1 orthologues with human Gemin2. Gregory Van Duyne, Ph.D., performed the sequence alignment, obtained from four iterations of psi-Blast (Altschul *et al.*, 1997) searching with *S. cerevisiae* Brr1 as query sequence. Locations of helices are shown for Gemin2 and the regions in Gemin2 that are close to bound SMN are shaded yellow.

The same careful consideration of the arrangement of the seven α -helices of Gemin2 that suggested the possibility of instability in the absence of the SMN peptide also provides a lens through which to consider the unusual situation of Brr1. Although the residues that are closely involved in binding SMN are not strictly conserved in Brr1, they are similar in type, suggesting that they would also form a hydrophobic binding surface in Brr1 with a character similar to the SMN binding cleft that could similarly accommodate an amphipathic helix. A heretofore-unidentified SMN or SMN-like binding partner may fill that role. It is also possible that Brr1 may fill it itself. In this alternative model, the Brr1 α 1 helix fills the binding pocket itself rather than flanking a binding helix from another protein; it is spatially positioned to do so, and shows the least sequence conservation in this region, perhaps consistent with an alternative role in *S. cerevisiae*.

Zhang *et al.* recently presented the x-ray crystallographic structure of full-length Gemin2 bound to an SMN peptide as well as to the Sm D1/D2/E/F/G pentamer. This structure established, for the first time, a functional role for Gemin2 in coordinating five Sm proteins as a pentameric intermediate until the binding of the snRNA component of spliceosomal U-snRNPs and addition of the Sm D3/B dimer to complete the canonical Sm protein heptameric ring that characterizes of those particles. Structurally, two separate domains of Gemin2 interact with the Sm pentamer; Sm D1 and D2 bind the globular C-terminal SMN-binding domain, on the face opposite the SMN peptide, while Sm E, F and G, though contiguous with D1 and D2, appear to interact with an extended

N-terminal domain of Gemin2 comprising approximately residues 12-100 that is ill-defined in the crystal structure but which appears to evince some α -helical character (Zhang *et al.*, 2011).

Gemin2 receives its Sm protein pentamer substrate from the chaperone pICln, which dissociates from the SMN-Gemin2 complex after delivery of its cargo (Chari *et al.*, 2008). Before this interaction, however, the conformation occupied by Gemin2 and by its N-terminal Sm protein-binding arm remains unexplored. The comparatively poor definition of that region in the crystal structure and its relative paucity of apparent secondary structure make a prediction of its structure in the absence of Sm proteins difficult.

In low-resolution shape reconstructions of Gemin2¹²⁻²⁸⁰-SMN²⁶⁻⁵¹ based on small-angle x-ray scattering data, the N-terminal Sm protein-binding region forms a tubular armlike protrusion that extends away from the SMN-binding domain and which can be reproduced in each shape reconstruction and in their filtered average structure (Figure 3.8A,B). Docking the Gemin2⁹⁵⁻²⁸⁰-SMN²⁶⁻⁵¹ NMR structure by rigid body modeling into the globular domain of the Gemin2¹²⁻²⁸⁰-SMN²⁶⁻⁵¹ molecular envelope positions the α 1 helix to extend the region of the envelope likely representing the N-terminal Sm protein-binding arm (Figure 3.8C). Although the lack of electron density in regions of the Gemin2 Sm protein binding arm in the crystal structure suggested conformational flexibility, a state expected to persist in the absence of Sm protein binding, that region

appears to occupy a fixed extended conformation in the molecular envelopes generated from SAXS data. Gemin2 may create a pre-formed binding surface for its Sm substrates rather than adopting that structure upon binding, a structure that would theoretically be available for interactions with other SMN complex components as well.

The solution studies described here propose a clear role for SMN binding in stabilization of the tertiary fold of Gemin2, while suggesting that, contrary to previous reports, Gemin2 does not detectably self-interact either alone or bound to SMN. The low-resolution solution structure of full-length Gemin2 bound to SMN²⁶⁻⁵¹ revealed a defined extended conformation of the Gemin2 Sm protein-binding arm, broadening structural understanding of the role of Gemin2 in snRNP assembly and contributing to the body of knowledge that will permit analysis of its roles in other biological systems.

Materials and Methods

DNA constructs

The construction of all molecular clones used in this chapter was detailed in the Materials and Methods section of Chapter II and is summarized in Table 2.2.

Expression and purification of human Gemin2 and SMN protein constructs

Gemin2⁹⁵⁻²⁸⁰, Gemin2⁹⁵⁻²⁸⁰-SMN²⁶⁻⁵¹ and Gemin2¹²⁻²⁸⁰-SMN²⁶⁻⁵¹ were expressed and purified as described in the Materials and Methods section of Chapter II.

Size-exclusion chromatography in-line with multi-angle light scattering

The absolute molecular weights of Gemin2⁹⁵⁻²⁸⁰ and the SMN²⁶⁻⁵¹-Gemin2⁹⁵⁻²⁸⁰ and SMN²⁶⁻⁵¹-Gemin2¹²⁻²⁸⁰ complexes were determined using multi-angle light scattering (MALS) in-line with a Superdex 75 10/300 column (GE Healthcare). The column was calibrated using the following proteins (Bio-Rad): thyroglobulin (670,000 Da), bovine gamma globulin (158,000 Da), chicken ovalbumin (44,000 Da), equine myoglobin (17,000 Da) and vitamin B-12 (1350 Da). Blue dextran (Sigma) was used to define the void volume of the column.

Purified proteins, 20 μ l at 1-10mg/ml, were injected onto the column at 0.5 ml/min in buffer containing PBS (10 mM Na₂HPO₄, 2 mM KH₂PO₄, 137 mM NaCl, 2.7 mM KCl, pH 7.4) plus 2mM dithiothreitol (DTT) at room temperature. The scattered light

intensity of the column eluant was recorded at 16 different angles using a DAWN-HELEOS MALS detector (Wyatt Technology Corp.) operating at 658 nm after calibration with 20 μ l of 20mg/ml lysozyme (Sigma). Protein concentration of the eluant was determined using an in-line Optilab DSP interferometric refractometer (Wyatt Technology Corp.). The weight-averaged molecular weight of species within defined chromatographic peaks was calculated using the ASTRA software version 5.2 (Wyatt Technology Corp.), by construction of Debye plots ($KC/R \Theta$ versus $\sin^2[\Theta/2]$) at one-second data intervals. The weight-averaged molecular weight was then calculated at each point of the chromatographic trace from the Debye plot intercept, and an overall average molecular weight was calculated by averaging across the peak.

NMR Spectroscopy and Analysis

NMR samples of ^{15}N -labeled SMN²⁶⁻⁵¹-Gemin2⁹⁵⁻²⁸⁰ and Gemin2⁹⁵⁻²⁸⁰ were prepared in Shigemi NMR tubes in buffer containing 50mM Na/K phosphate, pH 6.5, 50 mM NaCl, 50 mM DTT, 50 μ M EDTA, 0.2mM sodium azide and 95% H₂O/5% D₂O. Two-dimensional $^1\text{H}/^{15}\text{N}$ heteronuclear single quantum correlation (HSQC) spectra were collected at 25°C at 750MHz (^1H) on a Bruker AVANCE III NMR spectrometer equipped with a cryo-probe. Proton chemical shifts were referenced to DSS in the buffer, while ^{15}N chemical shifts were indirectly referenced. Data were processed using FELIX (Molecular Simulations, San Diego, CA, USA) and analyzed in SPARKY (Goddard & Kneller, 2008).

Sedimentation Velocity

Sedimentation velocity ultracentrifugation experiments were performed at 20 °C with an XL-A analytical ultracentrifuge (Beckman Coulter) and a TiAn60 rotor with two-channel charcoal-filled Epon centerpieces and quartz windows. Complete sedimentation velocity profiles of Gemin2⁹⁵⁻²⁸⁰-SMN²⁶⁻⁵¹ and Gemin2⁹⁵⁻²⁸⁰ (18.3 μM and 8.2 μM, optical density of 0.8 and 0.3 at A₂₈₀, respectively) in 1x PBS pH 7.4 were collected every 60 seconds at 42,000 rpm for 200 scans, followed by data analysis using the continuous size-distribution (c(s)) analysis of the Lamm equation in SEDFIT (Schuck & Rossmanith, 2000). After optimizing meniscus position and fitting limits, the sedimentation coefficient (s) and best-fit frictional ratio (f/f_0) was determined by iterative least squares analysis.

Small-angle x-ray scattering

Small-angle x-ray scattering data for Gemin2⁹⁵⁻²⁸⁰ and Gemin2⁹⁵⁻²⁸⁰-SMN²⁶⁻⁵¹ were collected at the Advanced Photon Source beam line 18-ID (BIOCAT) by Kushol Gupta, Ph.D., who also provided assistance with subsequent data processing and analysis. Samples were dialyzed against 100% D₂O buffer (20mM Na/K PO₄, 50 mM NaCl, 2mM DTT) and were centrifuged at 10,000 x g for ten minutes at 4°C immediately before data collection. X-ray radiation at 12 keV was used to collect 10-15 individual one second exposures while the sample was oscillated in a quartz capillary to minimize radiation damage. Data were corrected for the intensity of the incident radiation and reduced to provide one-dimensional intensity profiles as a function of Q (which is equal

to $4\pi\sin\theta/\lambda$, where 2θ is the scattering angle) using the data software Igor Pro.

Accessible scattering was recorded in the range of $0.006 < Q < 0.35 \text{ \AA}^{-1}$.

Small-angle x-ray scattering data for the Gemin2¹²⁻²⁸⁰-SMN²⁶⁻⁵¹ complex were collected at the Advanced Light Source Beamline 12.3.1 (SIBYLS), also by Kushol Gupta, Ph.D. Samples were centrifuged at 3,000 rpm for 10 min at 4°C prior to data collection. Data were collected using a 96-well plate handling sample robot, as previously described (Hura *et al.*, 2009). All samples were characterized with 0.5, 1, and 6 second exposures at 20°C, at a wavelength of 1 Å. Data were automatically reduced using custom software to provide one-dimensional intensity profiles as a function of Q. Accessible scattering was recorded in the range of $0.010 < Q < 0.35 \text{ \AA}^{-1}$.

In all cases, the forward scattering from the samples studied was recorded on a CCD detector and circularly averaged to yield one-dimensional intensity profiles as a function of Q. Scattering from a matching buffer solution was subtracted from the data, and corrected for the incident intensity of x-rays. Replicate exposures were examined carefully for evidence of radiation damage by Guinier analysis and Kratky plot analysis. Silver behenate powder was used to locate the beam center and to calibrate the sample-to-detector distance.

Evidence of the monodispersity of the preparation was gained by analysis of linearity in the Guinier region of the scattering data and agreement of the $I(0)$ and R_g values

determined with inverse Fourier transform analysis by the program GNOM (Semenyuk & Svergun D, 1991). When fitting manually, the maximum diameter of the particle (D_{\max}) was adjusted in 10-Å increments in GNOM to maximize the goodness-of-fit parameter. This analysis also yielded determinations of R_g and $I(0)$.

Low-resolution shapes were determined from solution scattering data using the program GASBOR. The number of dummy residues used in shape reconstruction was prescribed prior to calculation as 189 for Gemin2⁹⁵⁻²⁸⁰, 214 for Gemin2⁹⁵⁻²⁸⁰-SMN²⁶⁻⁵¹ and 294 for Gemin2¹²⁻²⁸⁰-SMN²⁶⁻⁵¹ based on knowledge of the amino acid composition of the proteins and the 1:1 stoichiometry of the Gemin2-SMN complexes. Ten independent calculations were performed for each data set using default parameters. No symmetry constraints were applied. The ten independent reconstructions were then averaged and filtered to a final consensus model using the DAMAVER suite of programs (Volkov & Svergun, 2003). Bead models were visualized in PyMOL (Delano, 2002).

Chapter IV: Oligomerization properties of the *Schizosaccharomyces pombe* SMN-Gemin2 complex

Introduction

The SMN protein is known to self-associate, a capacity that correlates convincingly with the ability of the SMN complex to catalyze the snRNP biogenesis (Lorson *et al.*, 1998; Pellizzoni *et al.*, 1999). Despite its obvious importance, however, neither the oligomerization state of the SMN protein nor the molecular role played by the SMN oligomer in snRNP assembly has been established. Certain experimental indicators point to an SMN multimer containing several subunits: the human SMN complex, purified from HeLa cells, sediments on sucrose gradients as a ribosome-sized 30S-70S species (Gabanella *et al.*, 2005; Paushkin *et al.*, 2002), and recombinant full-length SMN-Gemin2 complex elutes in a broad peak in the void volume in size exclusion chromatography experiments. Speculation has favored the hypothesis that the complex must be sizeable, is likely heterodisperse, and contains a large and possibly non-discrete number of each component (Gubitz *et al.*, 2004).

The search for a model system in which to study SMN oligomerization suggests *Schizosaccharomyces pombe*, the most primitive organism to possess an identifiable SMN orthologue. Unlike many higher organisms, which evince orthologues to several Gemins in addition to SMN, the rudimentary *S. pombe* SMN complex contains only SMN and Gemin2 (Campion *et al.*, 2010). Proving unexpectedly tractable in solution,

the *S. pombe* SMN-Gemin2 complex provides an excellent model system for the examination of the stoichiometry and oligomerization properties of SMN in the SMN complex.

Here, a battery of biophysical techniques is employed in the analysis of the purified spSMN-Gemin2 complex and allows the determination of its concentration-dependent oligomeric state and a description of its hydrodynamic properties.

Results

The spSMN-Gemin2 heterodimer provides a model system for studying the oligomerization of full-length SMN

Despite the evidently critical role that SMN self-association plays in SMN complex-mediated snRNP assembly and SMA pathogenesis, the exact oligomerization state of the self-interacting SMN protein has never been rigorously defined. Results from early size exclusion chromatography and sucrose gradient centrifugation experiments on both the native human SMN complex and the purified human SMN-Gemin2 heterodimer showed a very large apparent molecular mass relative to globular molecular weight standards and were interpreted to indicate a complex of substantial size comprising many copies of SMN and Gemin2 (Liu *et al.*, 1997; Pellizzoni *et al.*, 1999).

The complex formed by full-length *S. pombe* SMN and Gemin2, which forms the most rudimentary functional SMN complex and proved conveniently tractable to bacterial expression and purification, served as a model minimal SMN complex for analysis of its oligomerization state. The spSMN-Gemin2 complex was first examined by analytical size exclusion chromatography, yielding a single elution peak with an apparent molecular weight of ~600 kDa with respect to globular molecular weight standards. That predicted molecular mass, like many size predictions for the human SMN complex and SMN-Gemin2 heterodimer, corresponds to a very large oligomer, here approximately 13 copies of the 44.3 kDa spSMN-Gemin2 heterodimer (Figure 4.1). The Stokes radius (R_s ; the radius of a hard sphere that diffuses at the same rate as the particle in question) for the complex was calculated, based on the recorded Stokes radii of molecular weight standards, to 78.5 Å, a sizeable value consistent with the notion of a large particle.

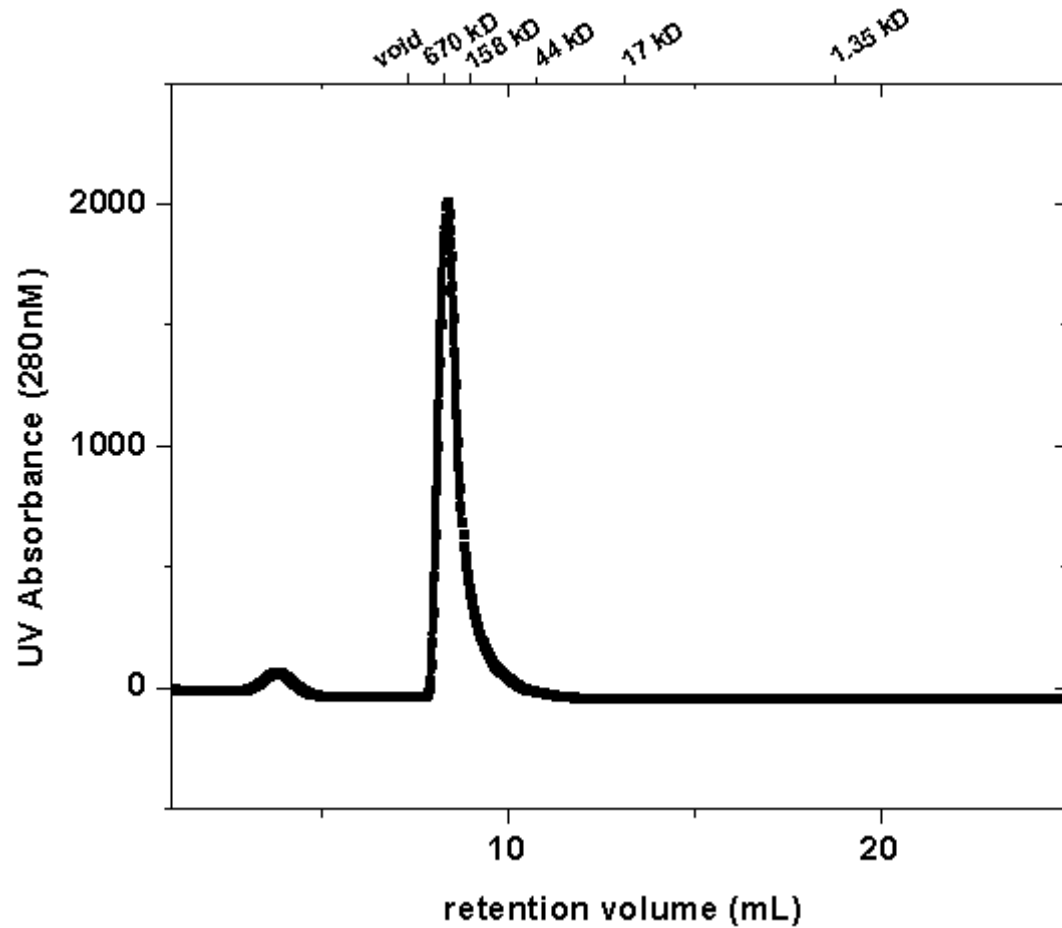


Figure 4.1 Analytical size exclusion chromatography profile of spSMN-Gemin2 on a Superdex 75 10/300 column. The elution volumes of globular protein standards are shown above the panel.

The spSMN-Gemin2 heterodimer occupies small, discrete oligomers that self-associate to form larger assemblies

To establish the absolute molecular weight, and thereby deduce the molecular inventory, of spSMN-Gemin2, the complex was examined by size-exclusion chromatography in-line with multi-angle light scattering (SEC-MALS) over a range of protein concentrations (Figure 4.2). At 10 mg/ml (226 μ M), spSMN-Gemin2 eluted as a single peak with an apparent molecular weight of 310 kDa. Its mass profile across the peak

that varied from 210 kDa to 122 kDa, indicating a surprisingly smaller particle than recourse to molecular weight standards had suggested, as well as suggesting some heterodispersity in the masses of the molecules comprising the peak. Decreasing protein concentration to 5 mg/ml (113 μ M) yielded a peak shift to an apparent molecular weight of 270 kDa and a mass profile spanning 187 to 87 kDa; another decrease to 2 mg/ml (46 μ M) followed the same trend, with a peak shift to an apparent molecular weight of 190 kDa. At two mg/ml, however, the mass profile held a steady value of approximately 80 kDa, indicating the more uniform presence of a species possessing that molecular weight, intriguingly consistent with an 88 kDa spSMN-Gemin2 dimer. A further concentration decrease to 1 mg/ml (23 μ M), the lowest concentration at which it was possible to extract meaningful light scattering data, demonstrated no change in the characteristics of the eluted peak, with the same retention time and mass profile indicative of a dimer of spSMN-Gemin2 heterodimers. The most fundamental oligomer of the spSMN-Gemin2 complex, then, far from the predicted enormous assembly, appears to be a dimer capable of forming higher-order oligomers in a concentration-dependent fashion. In an interesting instance of corroboration, dimerizations of an MBP fusion to the YG oligomerization domain of both human and *S. pombe* SMN were crystallized by Renee Martin, a graduate student in the Van Duyne laboratory at the University of Pennsylvania. (Martin, 2011)

Most trenchantly, no aspect of the SEC-MALS analysis of spSMN-Gemin2 substantiates the existence of any species possessing the large apparent molecular

weight with which the complex eluted in the original analytical size-exclusion chromatography experiment. Rather than comprising a large globular protein containing numerous copies of its component proteins, spSMN-Gemin2 appears to form a much smaller discrete oligomer or oligomers with large hydrodynamic radii, possibly due to an extended shape or to some intrinsic disorder.

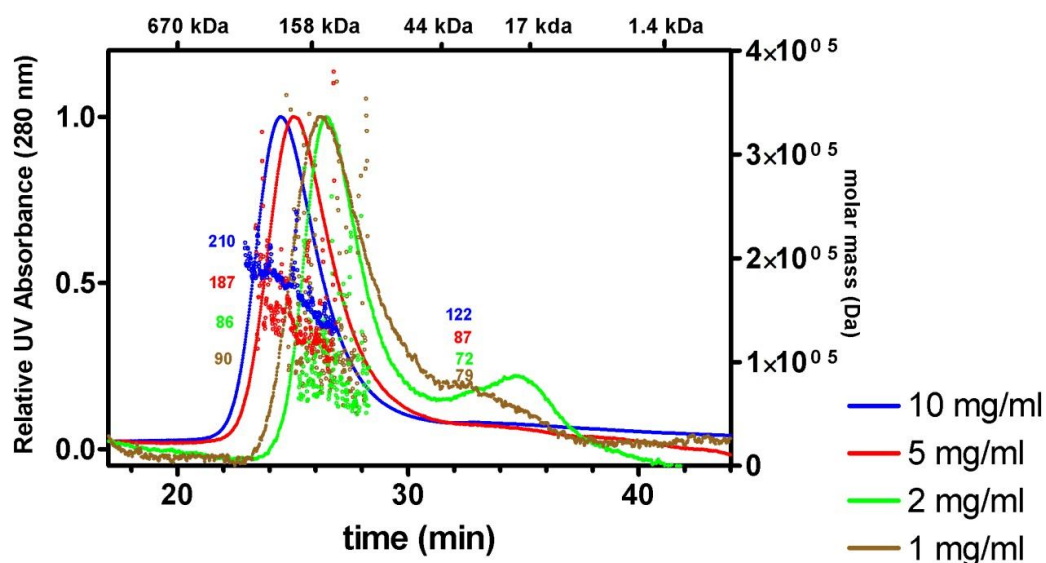


Figure 4.2 Representative SEC-MALS analyses of spSMN-Gemin2 injected at 10 mg/ml (blue), 5 mg/ml (red), 2 mg/ml (green) and 1 mg/ml (brown) on a Superdex 200 10/300 column. The highest and lowest molecular weights sampled in each mass profile are labeled in the same color as the chromatogram for that protein concentration. The elution volumes of globular protein standards are shown above the panel.

A number of self-association models might explain a decreasing trend in the weight-averaged molecular weight of a species over a decreasing range of protein concentrations. Sedimentation equilibrium analytical ultracentrifugation was employed to identify models of self-interaction of the spSMN-Gemin2 heterodimer consistent with observed data for spSMN-Gemin2 and to eliminate incompatible models (Figure 4.3).

The variety of fitting models tested, with goodness-of-fit calculated here by reduced chi-squared values near one and small root-mean-square deviations, is summarized in Table 4.1. With data collected at three speeds and three concentrations (14.0 μ M, 8.8 μ M, 3.5 μ M), spSMN-Gemin2 was best fit by modeling the data as a dimer-tetramer equilibrium, an interchange of two and four spSMN-Gemin2 heterodimers with a dissociation constant (K_D) around 1.8 μ M. The addition of higher order species to the dimer-tetramer model (dimer-tetramer-hexamer or dimer-tetramer-octamer equilibria) perturbed the fit very little, but yielded calculated K_D values in the molar range for the secondary association, so high that no measurable higher order oligomers can be considered to be present. The addition of a monomer to the model (monomer-dimer-tetramer equilibrium) yielded a substantially worse fit to the data, as did the application of monomer-trimer, monomer-trimer-hexamer and monomer-tetramer models; all models assuming monomers were considered inappropriate descriptions of the spSMN-Gemin2 data.

Table 4.1 Fit statistics for *S. pombe* SMN-Gemin2 sedimentation equilibrium analytical ultracentrifugation data to a variety of models. Goodness-of-fit is indicated by the reduced chi squared value (χ_r^2).

Model	KD_1	KD_2	Fit (χ_r^2)	RMSD
2 – 4	1.8 μ M	-	1.3	0.004
2 – 4 – 8	2.6 μ M	152 mM	1.4	0.004
2 – 4 – 6	2.6 μ M	> 1M	1.4	0.004
1 – 3	5.2 μ M	-	6.4	0.008
1 – 3 – 6	1.1 μ M	> 1 M	21	0.014
1 – 2 – 4	1 μ -14	> 1 M	21	0.014
1 – 4	1.8 μ M	-	10	0.009

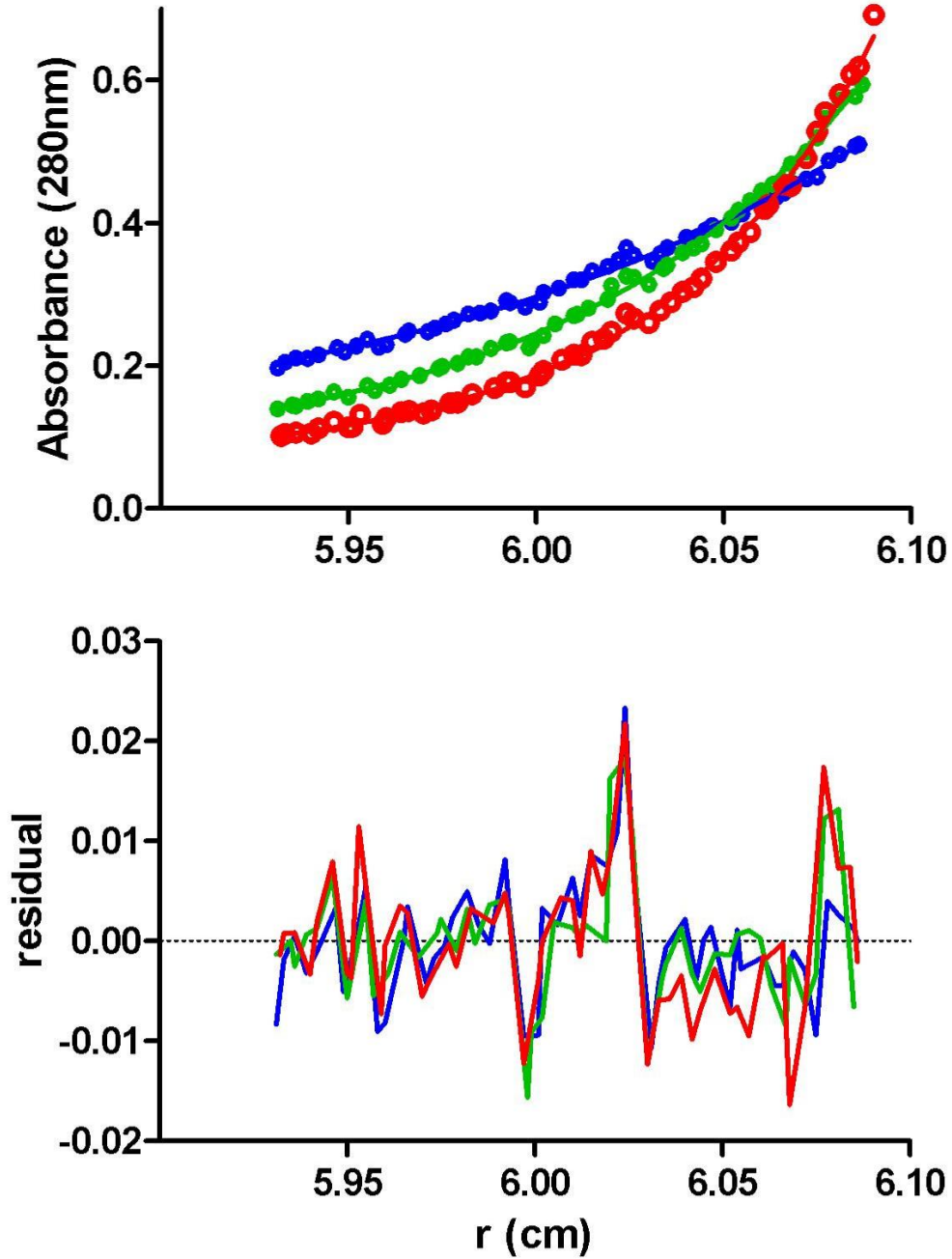


Figure 4.3 Representative sedimentation equilibrium analytical ultracentrifugation experiment on the *S. pombe* SMN-Gemin2 complex Experiments conducted at 4°C at 14 μ M, 8.8 μ M and 3.5 μ M. Here the curves are fit to a dimer-tetramer $(\text{spSMN-Gemin2})_2 \leftrightarrow (\text{spSMN-Gemin2})_4$ equilibrium with residuals of the experimental fits depicted in the bottom panel.

The spSMN-Gemin2 complex possesses a partially disordered character

Given that the largest oligomer sampled by the spSMN-Gemin2 heterodimer at the concentrations used for analytical size exclusion chromatography is a 176 kDa tetramer, one explanation for spSMN-Gemin2's atypical elution profile is that the protein complex possesses either a structured but elongated shape or some regions of intrinsic disorder, granting it a large hydrodynamic radius.

Shape parameters derived from sedimentation velocity analytical ultracentrifugation and small-angle x-ray scattering confirm that spSMN-Gemin2 does not occupy a compact shape. Sedimentation velocity data for spSMN at 10 μM was collected at 20°C and fit well to a continuous $c(s)$ distribution yielding a single species with a sedimentation coefficient of 6.5S. From the sedimentation coefficient, it becomes possible to calculate the frictional ratio f/f_0 of a particle, as discussed mathematically in Chapter II.

The frictional ratio reflects the degree of elongation of a particle and carries a value of ~ 1.2 for a globular protein, increasing with the degree of elongation displayed by the particle. The weight-averaged frictional ratio for the 6.5S complex was calculated to be 1.67, indicating that spSMN-Gemin2 indeed possesses an extended conformation (Figure 4.4).

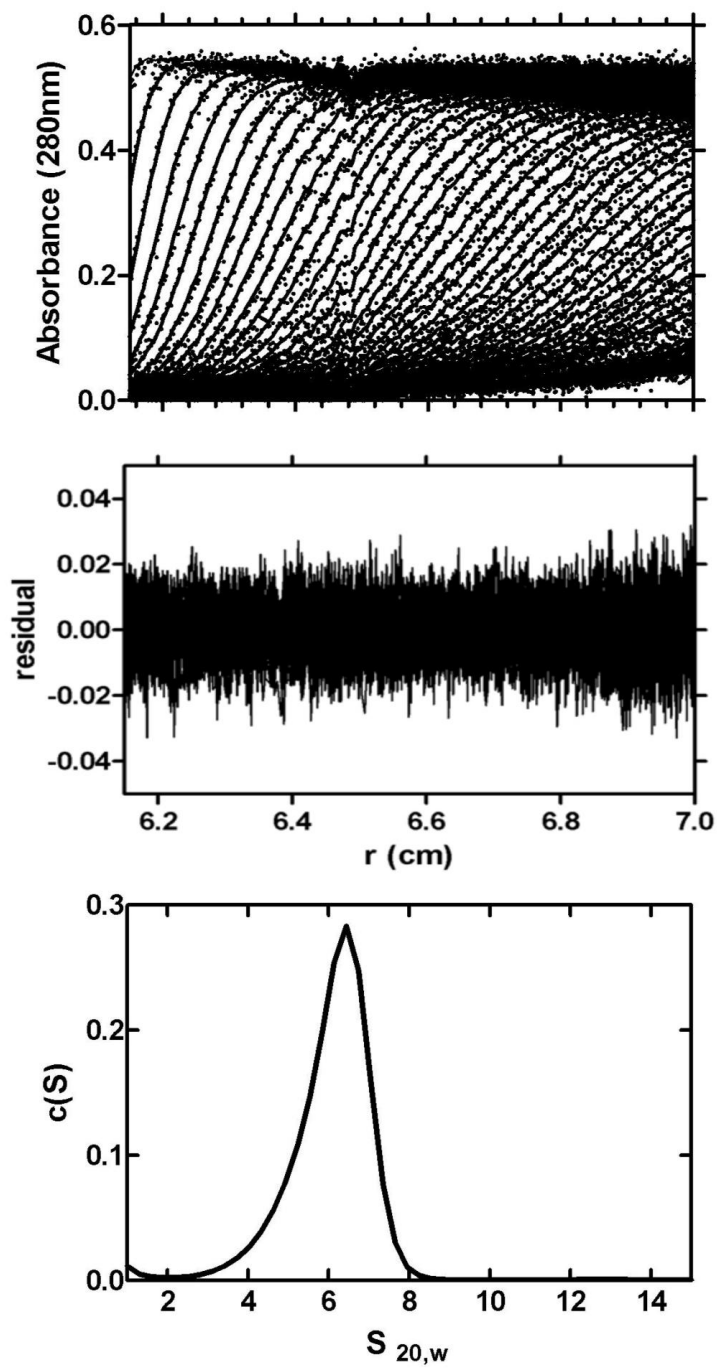


Figure 4.4 Sedimentation velocity analytical ultracentrifugation experiment on the *S. pombe* SMN-Gemin2 complex at 20°C. Sedimentation velocity absorbance traces of spSMN-Gemin2 at 280 nm occupy the top panel, with residuals of the experimental fits in the middle panel and a continuous sedimentation coefficient distribution ($c(S)$) of the protein in the bottom panel.

Small-angle x-ray scattering analysis was also employed to calculate parameters relevant to a consideration of the relative elongation of the spSMN-Gemin2 complex at 10 mg/ml (226 μ M), a concentration at which the protein is predicted to form predominantly tetramers of the heterodimer. Based on Guinier analysis of the scattering curve at very low scattering angles, the spSMN-Gemin2 complex demonstrated a radius of gyration of 85.9 \AA ; a $P(r)$ distance distribution function generated from the collected intensity using an inverse Fourier transform yielded a measure of the particle's maximum dimension of 260 \AA (Figure 4.5). It must be recalled that for the case of a system in equilibrium, these values will represent averaged values over the ensemble. Even as ensemble averages, however, the calculated values are revealing. For a perfect sphere with a partial specific density ν of 0.73 g/cm^3 , the calculated D_{max} ranges from 93.4 \AA for an 88.6 kDa dimer to 118.0 \AA for a 177.2 kDa tetramer, significantly smaller values than the D_{max} calculated for the spSMN-Gemin2 protein complex.

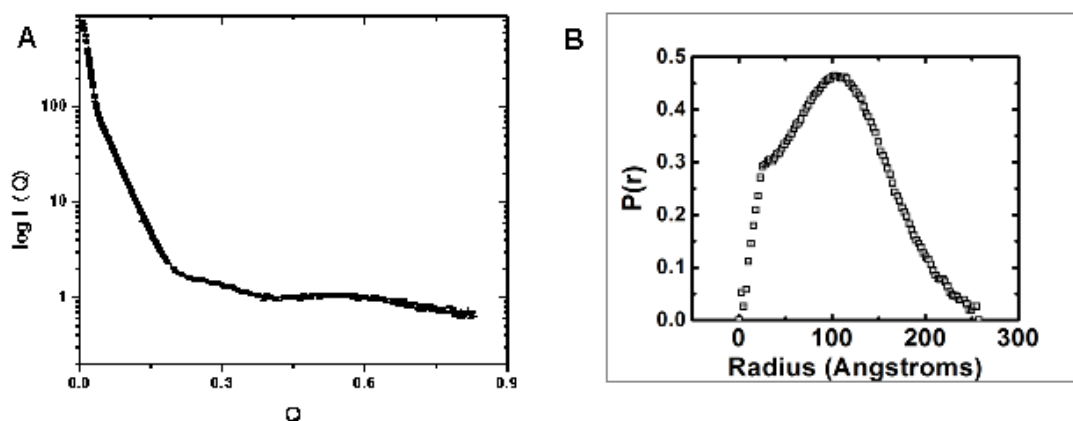


Figure 4.5 SAXS analysis of *S. pombe* SMN-Gemin2.

A) Small-angle scattering data from spSMN-Gemin2. Shown in black squares is the recorded intensity as a function of Q . B) $P(r)$ shape functions for spSMN-Gemin2.

Both sedimentation velocity and SAXS shape parameters demonstrate clearly that spSMN-Gemin2 is an elongated species without indicating whether it possesses a disordered character. A simple examination of the primary sequence of spSMN, however, suggests that properties of that protein favor the latter interpretation. While a disorder prediction for spGemin2 by the DISOPRED2 server shows few unstructured regions, the same analysis performed on spSMN indicates an enormous region of predicted disorder (where the prediction of disorder is greater than 0.5) spanning the length of the protein from its conserved N-terminal region of Gemin2-binding to its C-terminal YG box oligomerization domain (Figure 4.6A, B) (Ward *et al.*, 2004).

A two-dimensional charge-hydrophathy plot provides another means of identifying ordered and disordered proteins. Based on the observation that intrinsically disordered proteins often possess a combination of many charged residues and few hydrophobic ones, a charge-hydrophathy plot graphs the mean net Kyte-Doolittle hydrophathy (calculated here by the Davidson College GCAT server) of the protein against its mean net charge. Proteins with more disordered character and those that are more ordered are cluster in different segments of the plot and are largely segregated by a linear boundary. SMN falls (mean net hydrophathy = 0.402; mean net charged calculated at neutral pH = 0.09) within the disordered region of the plot (Figure 4.6C) (Kyte & Doolittle, 1982; Uversky *et al.*, 2000).

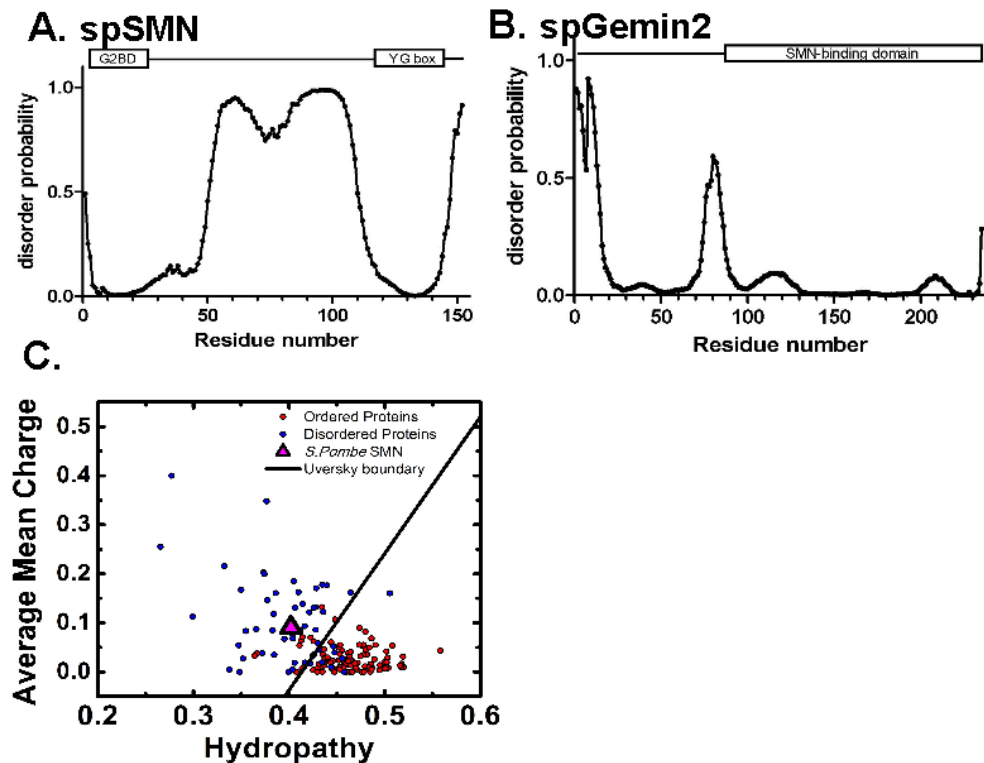


Figure 4.6 Disorder predictions for spSMN and spGemin2.

A) DISOPRED prediction of disorder for spSMN. A residue with a disorder probability > 0.5 is considered disordered. Known structural domains are depicted above the curve and correspond to the residues. B) DISOPRED disorder prediction for spGemin2. C) Charge-hydropathy plot for spSMN.

The disorder predicted for spSMN might be alleviated upon Gemin2 binding or self-association, a Kratky analysis was employed as an experimental diagnostic measure of protein disorder. Based on small angle scattering data, a Kratky plot depicts the intensity of the signal times the square of the scattering vector Q versus Q (where $Q = \frac{4\pi \sin \theta}{\lambda}$; 2θ is the scattering angle and λ is the wavelength) and displays, for globular proteins, a narrow symmetric peak at low Q and approaching zero as Q increases, but a curve that increases linearly with Q in the case of a fully disordered polypeptide (Doniach, 2001).

Broadening of the low Q peak is often observed for multi-domain proteins exhibiting some flexibility. The Kratky analysis of the spSMN-Gemin2 data at 10 mg/ml demonstrates characteristics of both theoretical curves, a peak at low Q that then climbs in value as Q increases (Figure 4.7). Some ordered structure is anticipated for the spSMN-Gemin2 complex, given that work presented earlier in this thesis supports a structured conformation for Gemin2 when bound to SMN; the characteristic increasing Kratky curve, however, indicates that the spSMN-Gemin2 complex is at least partially disordered, while the broad peak may prove an indicator that even the structured regions of the complex display some flexibility.

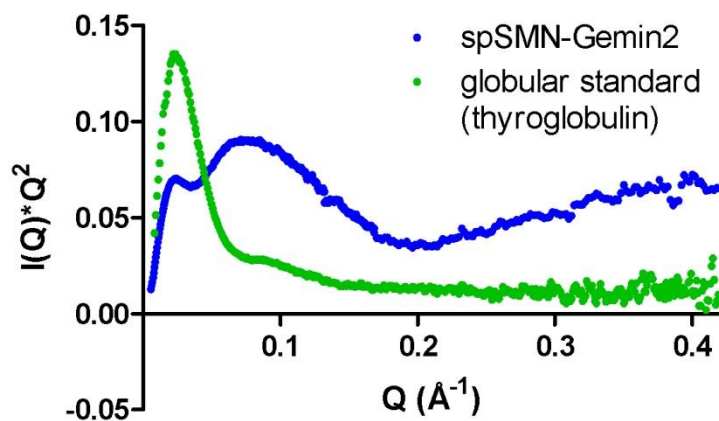


Figure 4.7 Kratky transformation of SAXS data from *S. pombe* SMN-Gemin2
S. pombe SMN-Gemin2 is depicted in blue and a globular thyroglobulin standard green.

Discussion

The self-association of SMN to form a higher-order oligomer is required for its activity in snRNP assembly. It is typically attributed to its tyrosine-glycine-rich exon6/exon7 “YG box” domain, although a region of N-terminal interaction has also been reported (Liu *et al.*, 1997; Lorson *et al.*, 1998; Ogawa *et al.*, 2007; Pellizzoni *et al.*, 1999; Young *et al.*, 2000). Certain missense mutations in the SMN YG box, identified as SMA disease mutations, demonstrably abolish SMN self-interaction *in vitro* and highlight the importance of correct oligomer formation for SMN function (Lorson *et al.*, 1998; Pellizzoni *et al.*, 1999). The precise stoichiometry assumed by SMN in the context of the SMN complex, however, remains unknown (Lorson *et al.*, 1998; Ogawa *et al.*, 2007; Otter *et al.*, 2007; Young *et al.*, 2000).

In early reports, fractionation of HeLa extracts over a size exclusion chromatography column suggested an overall molecular mass for the SMN complex greater than 300 kDa, while sucrose gradient centrifugation of the same complex from either HeLa or murine neural extracts indicated the presence of SMN in particles ranging from 30S-70S (Gabanella *et al.*, 2005; Liu *et al.*, 1997; Paushkin *et al.*, 2002). One study further observed coexpressed SMN and Gemin2, in the absence of other Gemins, forming a 40S particle (Paushkin *et al.*, 2002). The SMN complex has, as a result, been commonly (and perhaps fatalistically) concluded to possess an intractably large number of copies of both proteins, and few attempts have been made to better define its molecular

inventory. Still, given the critical importance of SMN oligomerization in the catalysis of snRNP assembly and in SMN pathogenesis, a more exact description of SMN stoichiometry offers a compelling goal.

Schizosaccharomyces pombe, the most primitive organism in which an orthologue to the human SMN protein can be found, provides an excellent model system for an inquiry into the oligomerization state of the SMN complex. It presents the most rudimentary SMN complex identifiable by sequence, consisting only of SMN and Gemin2, and has been shown functional for snRNP assembly (Campion *et al.*, 2010). Also favoring its choice as an experimental system, the bacterially expressed heterodimer, unlike that of its orthologues in higher organisms, is both stable and soluble in solution. It mirrors the behavior of its human counterpart in size exclusion chromatography experiments, eluting in or near the column void volume and again giving a first impression of a species with a very large molecular weight and a number of both protein components (Figure 4.1 shows a representative size exclusion profile for *S. pombe* SMN-Gemin2).

Multi-angle light scattering and analytical ultracentrifugation sedimentation equilibrium techniques were applied to the determination of the absolute molecular weight of the *S. pombe* SMN complex, from which its molecular inventory might be deduced.

Unexpectedly, despite its short retention time and apparently large molecular weight by size exclusion chromatography, the model best fitting the available data for spSMN-

Gemin2 suggests that it occupies a dimer-tetramer equilibrium of the spSMN-Gemin2 heterodimer.

The behavior of spSMN-Gemin2 during a SEC-MALS experiment over a decreasing range of protein concentrations provide the first intimation both that the protein's molecular mass was much more limited than size exclusion chromatography alone had predicted, and that it appeared to reversibly associate in a concentration-dependent manner. spSMN-Gemin2 at concentrations ranging from 10 mg/ml to 1 mg/ml showed a concomitant increase in size exclusion retention time and a decrease in the molar masses sampled across each peak until a concentration of 2 mg/ml (46 μ M), after which the peaks evinced the same elution profile and yielded mass calculations near 80 kDa, consistent with a dimer of spSMN-Gemin2 heterodimers as the basic operative unit of SMN oligomerization. The behavior of the protein over a 226 μ M – 23 μ M range of concentrations suggests a dissociation constant in the low micromolar range.

As a admonitory aside to the interested practitioner of SEC-MALS, the reported weight-averaged molecular weight across a peak may be misleading if the mass profile is not flat; spSMN-Gemin2 injected at 5 mg/ml is easily misinterpreted to comprise a trimer of heterodimers based on such a faulty analysis, and sooner consideration of the behavior of a concentration series of the protein might have spared some confusion.

A comparison of several models by which to fit spSMN-Gemin2 sedimentation equilibrium data allowed a numerical comparison of the goodness-of-fit of various models of self-interaction and helped eliminate or support models best describing the observed behavior of spSMN-Gemin2. Table 4.1 provides a summary of this analysis. The data were best fit under the assumption of a dimer-tetramer equilibrium. No addition of higher order oligomers (hexamers or octamers) improved the fit; the dissociation constants for the added hexamers and octamers fell in the high millimolar and molar range, respectively, suggesting them irrelevant. A clear deterioration in goodness-of-fit was observed upon the inclusion of monomers or trimers. A dimer-tetramer equilibrium correlates well with data observed in SEC-MALS experiments, where the mass profiles of the high concentration protein samples are easily interpreted as ranging from tetrameric to dimeric species. It is easy to imagine an extension of this dimer-tetramer paradigm to the SMN complex in higher organisms, and that possibility provides an exciting direction in which to take this research. In a promising bit of corroboration, Renee Martin, a previous graduate student in the Van Duyne laboratory at the University of Pennsylvania, solved the crystal structures of human and *S. pombe* YG box constructs fused to maltose binding protein for solubility that show clear dimerization (Martin, 2011).

Given the unquestionable result that spSMN-Gemin2 forms small, discrete oligomers, with data best explained by a dimer-tetramer equilibrium, its deceptive behavior in size exclusion chromatography experiments must originate instead in unusual hydrodynamic

properties. Several measures give credence to the notion of an extended shape, including SAXS measurements of a radius of gyration and maximum dimension greater than expected for a compact particle and a large frictional ratio by sedimentation velocity. A Kratky transformation of the SAXS scattering data, typically employed as a diagnostic for protein unfolding, shows evidence of a flexible, multi-domain molecule with partially disordered character. Particle elongation and flexibility, rather than a substantial molecular mass, account for the abbreviated retention time observed for spSMN-Gemin2 off of size exclusion chromatography columns; the long-held mistaken assumption of a substantial molecular mass for the SMN complex might serve as a cautionary tale for experimenters tempted to attribute size discrimination to molecular weight in experiments where it is correctly based on hydrodynamic volume.

Both experimental evidence from the SAXS Kratky plot and a consideration of the disorder predictions spSMN lend support to the notion that the protein exhibits some intrinsic disorder, even when bound to Gemin2 and in its preferred oligomerization state. The disorder prediction for the protein is striking, proposing that only its very N- and C-terminal binding domains have a strong predisposition to assume a structured fold. A number of functional implications are typically imputed to regions of disorder, including service as interfaces for intermolecular interactions due to their large available surface area. This could have fascinating implications for the involvement of SMN with its snRNP assembly substrates during biogenesis, as well as in its reported roles in other cellular housekeeping processes. These speculations may prove equally germane to the

discussion of human SMN; apart the addition of a Tudor domain lacking in the *S. pombe* orthologue, a disorder prediction for that protein bears a striking resemblance to that of spSMN and suggests that the regions of intrinsic disorder might serve an important function that has been retained evolutionarily. (Figure 4.8)

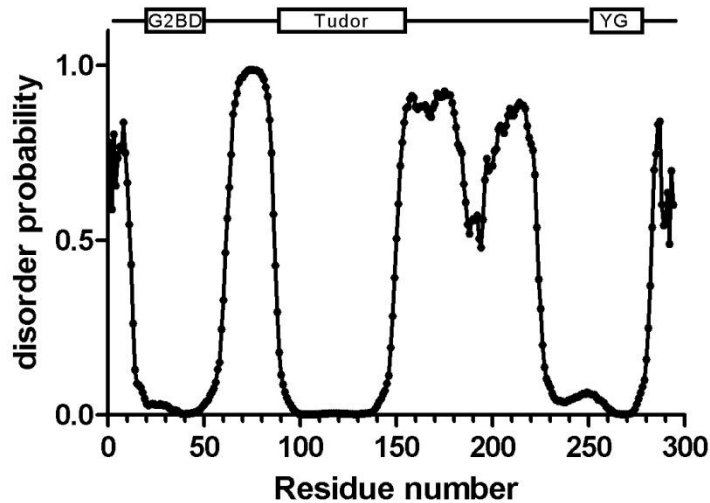


Figure 4.8 Disorder prediction for human SMN. DISOPRED prediction of disorder for spSMN. A residue with a disorder probability > 0.5 is considered disordered. Known structural domains are depicted above the curve and correspond to the residues.

The existing corpus of knowledge relating to SMN oligomerization bears consideration in light of the unexpected structural model of SMN association presented in this chapter. SMN possesses two identified regions of self-interaction, at its exon6/7 encoded tyrosine-glycine-rich “YG box” and an N-terminal region mapped to exons 1-2b (Ogawa *et al.*, 2007; Talbot *et al.*, 1998). The former, identified first and more extensively studied, is a stronger interaction requiring urea to disrupt; the latter is reported to be weaker, sufficiently prone to exchange to require no intervention to

separate units for surface plasmon resonance studies (Young *et al.*, 2000). Young *et al.* emphasize that any molecule with two self-association sites is theoretically capable of forming interactions of a higher order than dimers, and propose a model in which YG-mediated SMN dimers form tetramers or other oligomers through their second N-terminal self-interaction domain (Young *et al.*, 2000). Their prescient prediction of a role for the YG box in mediating the formation of core SMN dimers might be interpreted as consistent with the observation that deletion or disruption of YG box self-interaction abrogates the ability of SMN to assemble snRNPs and underscores severe disease phenotypes in many SMA patients, although the sole study to demonstrate this result biochemically showed only that YG box missense mutations disrupt SMN oligomerization, without conclusively demonstrating that SMN monomers result (Lorson *et al.*, 1998; Pellizzoni *et al.*, 1999).

The function of the N-terminal SMN oligomerization domain in formation of dimers of higher-order species is less clear. In human SMN, the SMA patient mutation of conserved Asp 44 to valine occurs within the SMN Gemin2 binding domain without affecting that interaction; instead its pathogenic influence is proposed to stem from a destabilization of the N-terminal SMN self-interaction (Ogawa *et al.*, 2007; Sun *et al.*, 2005). Conserved in all organisms including *S. pombe*, where a glutamic acid occupies that same amino acid position, Asp44 clearly plays an important role in some aspect of SMN complex function, although its D44V mutation results only in the mild, late-onset Type III form of SMA. It is tempting to speculate from the mild effect of the D44V

mutation on SMA pathogenesis that its predicted effect on N-terminal SMN self-interaction is a disruptive effect on the interaction of core SMN dimers forming a tetramer, although simple loss of an additional factor stabilizing the dimer is also possible. It should be straightforward to test that hypothesis in the context of the same SEC-MALS and sedimentation equilibrium experiments described, mutating the corresponding *S. pombe* glutamic acid, as well as other strictly conserved residues of unknown function in the same region.

Unexpectedly, in full contradiction to most stated opinions in the literature and to conclusions drawn from analytical size exclusion chromatography and sucrose gradient centrifugation, the oligomer formed by the self-association of the *S. pombe* SMN protein is shown here to consist not of an intractably large number of SMN units, but of discrete dimers of the spSMN-Gemin2 heterodimer that self-associate to form larger assemblies. This unanticipated, welcome insight into the higher order structure of SMN in its most rudimentary guise offers a model of SMN oligomerization applicable to higher organisms, and furnishes an additional perspective from which the structural role of oligomerization in snRNP biogenesis and the effects of SMA disease mutations in SMN may be probed.

Materials and Methods

DNA constructs

Full-length *Saccharomyces pombe* Gemin2 (Yip1p) (M1-T235) was amplified by PCR as an NdeI/XhoI fragment and cloned into the MCS II of Twin1B (New England Biosystems); it was later subcloned as an NdeI/XhoI fragment into the MCS II of a petDuet (Novagen) expression vector modified to contain an in-frame C-terminal Mxe intein domain (New England Biosystems), chitin binding domain and hexahistidine tag. Full-length *S. pombe* SMN (Yab8p) (M1-D152) was PCR amplified as an NcoI/BamHI fragment and cloned into the MCS of pET24dHT, and later subcloned into pGBKT7b. From this construct, it was then PCR amplified as an NcoI/NotI fragment and cloned into MCS I of pCDFDuet (Novagen).

Protein expression and purification

The two constructs were co-transformed into *E. coli* BL21(DE3) cells; a culture grown from one positive transformant, identified by growth on media containing ampicillin and streptomycin, was used to create a 10% glycerol stock stored at -80°C. spSMN and spGemin2 were co-expressed in Luria-Bertani (LB) cell cultures grown at 15°C for 20 hours after the addition of IPTG (isopropyl- β -D-thio-galactoside) to a final concentration of 0.5M.

Cells were harvested by centrifugation at 4000 x g for 30 minutes at 4°C. Each liter of cells was resuspended in approximately 20ml of 50mM Na/K phosphate, pH 8.0, 300mM NaCl, 10mM imidazole, 0.5mM ethylenediaminetetraacetic acid (EDTA), 0.5mM 4-(2-Aminoethyl) benzenesulfonyl fluoride hydrochloride (AEBSF; Fisher Scientific), 10µM proteinase inhibitor E-64 (Sigma) and 2mM benzamidine (Fisher Scientific). Cells were lysed in two sequential passes through an Avestin Emulsiflex C-3 homogenizer at approximately 18,000 psi, and the crude lysate thereby obtained was cleared by centrifugation at 16,000 rpm at 4°C for 30 minutes.

Cleared lysate was filtered through grade 802 fluted filter paper (Whatman) and loaded onto 4ml (per 6 liters of cell culture) nickel nitriloacetic acid (Ni-NTA; Qiagen) resin in a 5.3 cm x 10cm Kontes column equilibrated with 50mM Na/K phosphate pH 8.0, 300mM NaCl, 10mM imidazole. The preparation was nutated at room temperature for 60 minutes; the resin and bound protein were then washed with ten column volumes of buffer containing 50mM Na/K phosphate, 300mM NaCl, 20mM imidazole and eluted in 50mM Na/K phosphate, 300mM NaCl, 250mM imidazole. The Ni-NTA eluant was then loaded onto 8ml chitin resin equilibrated in a 2.5 cm x 10 cm Kontes column with 50mM Na/K phosphate, 300mM NaCl, 250mM imidazole and nutated for 90 minutes at room temperature. The resin and bound protein were washed with ten column volumes of 20mM Hepes pH 8.0, 300mM NaCl, 0.1mM EDTA.

spGemin2 bound to spSMN was cleaved from the C-terminal Mxe intein-chitin binding domain-hexahistidine tag by addition of 20mM Hepes pH 8.0, 300mM NaCl, 0.1mM EDTA, plus 50mM 2-mercaptoethanol acting as the cleavage-inducing thiol reagent, to the protein-bound chitin resin followed by overnight (~16 hours) incubation at room temperature. The cleaved preparation was then added to 4ml of fresh chitin resin equilibrated with 20mM Hepes pH 8.0, 300mM NaCl, 0.1mM EDTA, and the cleaved spSMN-Gemin2 complex was eluted in the same buffer.

Purified spGemin2-spSMN was concentrated at 5000 x g at 4°C in 15ml Amicon Ultra 10,000 MWCO Centrifugal Filters (Millipore) and further purified by size exclusion chromatography at room temperature on a Superdex 75 HiLoad 16/60 column (Pharmacia) in 10mM Tris pH 8.0, 50mM NaCl, 2mM dithiothreitol (DTT). When necessary, homogeneous purified protein was stored in that buffer plus 10% glycerol at -80°C. Final protein concentration was assessed using the absorbance at 280 nm (A_{280}), assuming an extinction coefficient of $56965 \text{ M}^{-1} \text{ cm}^{-1}$ based on amino acid compositional analysis by the ProtParam software tool on the ExPASy Proteomics Server (Swiss Institute of Bioinformatics). spSMN-Gemin2 proved moderately soluble and was typically concentrated to between 200 μM and 500 μM . A preparation in LB media yielded approximately 2 mg L⁻¹.

Analytical size exclusion chromatography

Purified *S. pombe* SMN-Gemin2 was concentrated as above to 1ml (~4 mg/ml; ~90 μ M) and injected onto an analytical Superdex 75 10/300 column (GE Healthcare) equilibrated in 10mM Tris pH 8.0, 50mM NaCl, 2mM DTT and run at room temperature at 0.4ml/min. The protein elution profile was monitored by absorbance at 280nm. Column calibration employed gel filtration standards (BioRad) containing thyroglobulin (670,000 Da), bovine gamma globulin (158,000 Da), chicken ovalbumin (44,000 Da), equine myoglobin (17,000 Da) and vitamin B-12 (1350 Da).

Sedimentation velocity

Sedimentation velocity ultracentrifugation experiments were performed at 20 °C with an XL-A analytical ultracentrifuge (Beckman Coulter) and a TiAn60 rotor with two-channel charcoal-filled Epon centerpieces and quartz windows. Complete sedimentation velocity profiles of *S. pombe* SMN-Gemin2 (10.5 μ M, optical density of 0.6 at A_{280}) in 1x PBS pH 7.4 were collected every 60 seconds at 30,000 rpm for 500 scans, followed by data analysis using the continuous size-distribution (c(s)) analysis of the Lamm equation in SEDFIT (Schuck & Rossmanith, 2000). After optimizing meniscus position and fitting limits, the sedimentation coefficient (s) and best-fit frictional ratio (f/f_0) were determined by iterative least squares analysis.

Sedimentation equilibrium

Sedimentation equilibrium ultracentrifugation (SE) experiments were performed at 4°C with an XL-A analytical ultracentrifuge (Beckman Coulter) and a TiAn60 rotor with six-channel charcoal-filled Epon centerpieces and quartz windows. Radial absorption scan data at 280 nm for three protein concentrations were measured (14.0µM, 8.8µM, 3.5µM; 0.8OD, 0.5OD, 0.2OD) at 20 and 22 h for each of four different rotor speeds (12,000, 15,000, 18,000 and 21,000 rpm). Comparison of radial absorption scans verified that equilibrium had been reached. Data were analyzed using the programs SEDFIT and SEDPHAT and fit variously to a single species model and to several models of self-association, with the best solutions exhibiting small goodness of fit and low and randomly distributed residual errors (Schuck & Rossmanith, 2000; Vistica *et al.*, 2004).

Size exclusion chromatography in-line with multi-angle light scattering

The absolute molecular weight of the *S. pombe* SMN-Gemin2 oligomer was determined using multi-angle light scattering (MALS) in-line with a Superdex 200 10/300 column (GE Healthcare). The column was calibrated using the following proteins (Bio-Rad): thyroglobulin (670,000 Da), bovine gamma globulin (158,000 Da), chicken ovalbumin (44,000 Da), equine myoglobin (17,000 Da) and vitamin B-12 (1350 Da). Blue dextran (Sigma) was used to define the void volume of the column.

spSMN-Gemin2, 20 μ l at 1-10 mg/ml (23 μ M – 226 μ M), was injected onto the column at 0.5 ml/min in buffer containing 1x PBS, pH 7.0 and 2mM dithiothreitol at room temperature. The scattered light intensity of the column eluant was recorded at 16 different angles using a DAWN-HELEOS MALS detector (Wyatt Technology Corp.) operating at 658 nm after calibration with 20 μ l of 20mg/ml lysozyme (Sigma). Protein concentration of the eluant was determined using an in-line Optilab DSP interferometric refractometer (Wyatt Technology Corp.). The weight-averaged molecular weight of species within defined chromatographic peaks was calculated using the ASTRA software version 5.2 (Wyatt Technology Corp.), by construction of Debye plots ($KC/R \Theta$ versus $\sin^2[\Theta/2]$) at one-second data intervals. The weight-averaged molecular weight was then calculated at each point of the chromatographic trace from the Debye plot intercept, and an overall average molecular weight was calculated by averaging across the peak.

Small-angle x-ray scattering

Small-angle x-ray scattering (SAXS) data were measured at beam line X9 at the National Synchrotron Light Source (Upton, NY). Sample scattering profiles were collected on two detectors with overlapping geometry: a Mar 165 CCD SAXS detector (Mar USA, Inc., Evanston, IL) 3.4 m from the sample, and a custom built Photonic Science CCD WAXS detector. Two-dimensional images were integrated using software developed at the beam line into one-dimensional intensity profiles as a function of momentum transfer Q (where $Q=4\pi\sin(\theta)/\lambda$, with 2θ the scattering angle and λ the

wavelength). Measurements were taken at 10°C with an X-ray wavelength of 0.855 Å; scattering profiles covered a Q range from 0.006 to 0.22 Å⁻¹. The sample holder was a 1-mm quartz capillary (Hampton Research, Aliso Viejo, CA) that was sealed across the evacuated beam path. Both ends of the capillary were open to allow the sample to flow continuously through to minimize radiation damage to the sample. The sample was centrifuged at 10,000 x g for 10 min at 4°C before measurements; each measurement required 30 µl of sample for three 10 µl, 60 second exposures. After each measurement, the capillary was washed repeatedly with buffer solution and purged with compressed nitrogen.

Averaged scattering curves from the SAXS and WAXS detectors were scaled and merged in PRIMUS; scattering from a matching buffer solution was subtracted from the data and corrected for the incident intensity of x-rays. Replicate exposures were examined carefully for evidence of radiation damage by Guinier analysis and Kratky plot analysis. Silver behenate powder was used to locate the beam center and to calibrate the sample-to-detector distance (Konarev *et al.*, 2003).

Evidence of the monodispersity of the preparation was gained by analysis of linearity in the Guinier region of the scattering data and agreement of the $I(0)$ and R_g values determined with inverse Fourier transform analysis by the programs GNOM and AUTOGNOM. When fitting manually, the maximum diameter of the particle (D_{\max})

was adjusted in 10-Å increments in GNOM to maximize the goodness-of-fit parameter.

This analysis also yielded determinations of R_g (Semenyuk & Svergun D, 1991).

Chapter V: Conclusions and Future Perspectives

Despite a vital interest in achieving a molecular understanding of the structure and function of the SMN complex, an interest founded upon both the biochemist's interest in RNP biogenesis and the clinician's goal of treating SMA, descriptions of its stoichiometry and atomic structures of its components eluded research efforts for many years. This dissertation fills a crucial void in the available knowledge of the SMN complex, offering a detailed depiction of the binding domains of core components SMN and Gemin2, a description of their solution properties and the elucidation of the unanticipated oligomerization state of SMN.

The atomic structure of the complex formed by the minimal binding domains of human SMN and Gemin2 was solved by triple-resonance multidimensional NMR spectroscopy; it was shown to form an all α -helical fold bearing no significant structural homology to known proteins and characterized by a highly conserved hydrophobic SMN-Gemin2 interface. From this structural springboard, it becomes possible to plan and interpret the next generation of studies probing the role of Gemin2 in several cellular processes, many of them related to human health.

Gemin2 interactions are reported for several components of the SMN complex and its snRNP assembly substrates. The minimal SMN-Gemin2 complex demonstrates a number of conserved surface residues bearing no obvious role in SMN binding or the

stabilization of the Gemin2 fold; their judicious mutation provides an opportunity to probe the sites of binding for interacting proteins and to interpret them structurally, either in the context of the minimal SMN-Gemin2 complex or that of full-length Gemin2 binding minimal SMN. One recent structural study implicates full-length Gemin2 in Sm protein binding, positing that Sm D1 and D2 interact, in the context of the NMR structure described, with the face of Gemin2 opposite SMN binding (Zhang *et al.*, 2011). The Gemin2 residues mediating those interactions remain untested biochemically and bear consideration by mutational analysis, both to validate the structural model proposed and to provide some structural insight into Gemin2's function coordinating intermediates along the snRNP assembly pathway.

Gemin2 binding to Gemin7 has also been established, and may represent an interaction with the Gemin6-7 heterodimer though to mimic the Sm D3/B dimer and substitute for it, together with the Sm D1/D1/E/F/G pentamer, in a temporary assembly intermediate of the Sm heptamer. The known interaction of Sm B with Sm D1 in the final assembled snRNP suggests a region of the face of Gemin2, positioned to interact with the free face of Sm D1, where a Gemin7 interaction might occur (Krummel *et al.*, 2010). Pinpointing the binding site of Gemin7 relative to other Sm protein substrates would offer a more detailed glimpse of its role in Sm protein assembly. Gemin5, the snRNA chaperone, also makes its SMN complex contact through Gemin2; determining its binding site through mutational analysis might permit the development of a model for the transfer of snRNA to the SMN complex and into coordination with the Sm proteins. In the case of a

sufficiently stable Gemin2-Gemin7 or Gemin2-Gemin5 interaction, small-angle scattering could also be usefully employed; the difference between shape reconstructions with and without the Gemin6-7 heterodimer or Gemin5 would substantiate its suggested point of interact with the complex. If tractable, a complex containing Gemin5 and snRNA could also be probed by small-angle neutron scattering, which carries the advantage of scattering protein and DNA components differently and allowing for their relative localization within the scattering particle.

As an aside, certain aspects of the minimal SMN-Gemin2 heterodimer suggest future avenues for the interested protein x-ray crystallographer, which might in turn prove a useful tool for rapid consideration of the structural effects of mutations. While protein crystallization for x-ray experiments always relies to some extent on a researcher's luck, certain protein structural features can be predicted to introduce a bias against crystal formation. Large disordered regions of a protein are well established to inhibit crystal packing and the formation of crystal contacts (Canaves *et al.*, 2004), and may have spelled the demise of this project as a crystallography candidate. The minimal SMN-Gemin2 construct contains both a 25-residue unstructured loop between α -helices $\alpha 2$ and $\alpha 3$ in Gemin2 and, in SMN, 10 disordered residues N-terminal to the α -helix binding Gemin2; the strategic trimming of the latter and replacement of the former with a shorter connector, such as the four-residue sequence that bridges the same interhelical gap in *Drosophila*, provide clear possibilities for initial attempts to design a crystallizable minimal SMN-Gemin2.

Despite reports to the contrary, neither full-length Gemin2 nor its minimal SMN binding domain, either bound to SMN or unbound, demonstrated the ability to dimerize (Ogawa *et al.*, 2007), but unbound Gemin2 was shown to undergo a substantial conformational change upon SMN binding, becoming more compact. In good agreement with a recent crystal structure, low resolution shape reconstructions of full-length Gemin2 bound to the minimal binding domain of SMN demonstrate that Gemin2's N-terminal region forms a rigid arm extended away from its globular SMN-binding domain and positioned to bind its Sm protein substrates (Zhang *et al.*, 2011).

The functional relevance of unbound Gemin2 is uncertain. The work presented here demonstrates a patent disordering of Gemin2 when unbound to SMN; it is also well-established, and perhaps a logical conclusion, that cellular knockdown of SMN yields a concomitant decrease in Gemin2 (Jablonka *et al.*, 2002; Shpargel & Matera, 2005). In Gemin2's roles outside of SMN complex-mediated snRNP assembly, however, the presence of SMN remains uncertain or dubiously confirmed. Gemin2 makes a documented interaction with Rad51, a protein that assists in the repair of double-stranded DNA breaks through homologous recombination. The presence of SMN was assessed using an SMN-Gemin2 chimera in which the C-terminus of the latter was fused to the N-terminus of the former; the sheer structural improbability of that molecule calls into question the conclusion offered that SMN is, in fact, necessary. A probe for that direct interaction using more logical Gemin2 and Gemin2-SMN constructs would

provide a more satisfying answer and lay the groundwork for further studies of Gemin2's enhancement of Rad51-mediated DNA repair, a process disrupted in some forms of human cancer.

Importantly, another non-RNP assembly role for Gemin2 involves a direct interaction with HIV-1 integrase (IN) during viral infection, in which it enhances the assembly of reverse transcriptase onto viral RNA and contributes to viral infectivity (Hamamoto *et al.*, 2006; Nishitsuji *et al.*, 2009). Despite its importance, few requirements for the interaction have been established. The presence of SMN during Gemin2-IN binding has yet to be confirmed or excluded, and it will be an important factor in establishing whether Gemin2 interacts with IN in its unbound conformation, bound to SMN or bound to another partner protein. Equally, the IN requirements for Gemin2 binding, given the IN inclination both to oligomerize and to interact tightly with host proteins (LEDGF), remain to be determined (Cherepanov *et al.*, 2003). A binding region of Gemin2 for IN, falling within its SMN-binding domain, has been identified; provided that Gemin2 assumes its SMN-bound fold in the context of IN interaction, it defines a binding surface on Gemin2 that might be probed mutationally. A clear understanding of the part played by Gemin2 in HIV pathogenesis bolsters the mechanistic understanding of integrase and reverse transcriptase function, and may open profitable avenues for the design of future therapeutics.

The intriguing molecular shape reconstructions of full-length Gemin2 bound to the minimal SMN binding domain suggest further SAXS experiments. Those two proteins, bound to the Sm pentamer, were observed in both a recent crystal structure and in electron microscopy shape reconstructions; small-angle x-ray scattering of that particle, containing the Sm pentamer, would give a solution envelope that could be compared both to the reported x-ray and EM structures and to the structure of SMN-bound Gemin2 alone and suggest, in the first case, any differences that might be relevant in solution, and in the second, changes to Gemin2 upon Sm binding. Another exciting target might comprise the SMN-bound Gemin2-Sm pentamer complex just described using an SMN construct extended to include the Tudor domain. That domain, absent only in *S. pombe*, has been implicated in interacting with the R-G rich tails of Sm D3, D1 and B when symmetrically dimethylated (Bühler *et al.*, 1999; Selenko *et al.*, 2001). It would be illustrative to visualize its position relative to the Sm pentamer, particularly Sm D1 and G to which B and D3 respectively bind, as well as to the binding site of Gemin7 if determined (Krummel *et al.*, 2010); it might become possible to visualize the mechanism by which Sm D3 and B are recruited to and incorporated into the pentameric Sm ring to close it as a heptamer.

The ability of SMN to oligomerize is a requirement for the ability of the SMN complex to catalyze snRNP assembly; disruption of oligomerization by SMN transcripts lacking exon 7 or carrying certain missense mutations is also linked convincingly to SMA pathogenesis. While plainly indispensable, however, the actual oligomerization state or

states occupied by SMN has never been revealed. The complex formed by the full-length *Schizosaccharomyces pombe* SMN and Gemin2 orthologues was shown to occupy a dimer-tetramer equilibrium, with a dimer the smallest discrete oligomer of the complex sampled at low concentrations. The protein appears partially disordered, however, contributing to its unusual hydrodynamic properties and large Stokes radius. The discovery that SMN is able to form small, discrete oligomers overturns a long-held assumption, based on sucrose gradient centrifugation and size exclusion chromatography behavior, that SMN forms a very large and possibly heterodisperse oligomer containing multiple copies of the protein.

Although multiple reports have identified two self-interaction sites for SMN, both of which contain known SMA disease mutations, their relative contribution to the formation of SMN dimers and higher order oligomers has yet to be probed. The *S. pombe* SMN-Gemin2 complex can serve as a tractable model system for examining the role that conserved residues and identified SMA disease mutations play in shifting or disrupting the dimer-tetramer equilibrium observed for wildtype protein. These observations could be usefully coupled to functional assessment of the SMN complex's continued capacity to assemble snRNPs; an *in vitro* gel shift snRNP assembly assay has been available for the study of the human SMN complex for over a decade, and the development of an analogous *in vitro* assembly assay using *S. pombe* Sm proteins and the recombinant SMN complex described here would enable complementary functional analysis of any oligomerization mutants tested.

Indeed, the N-terminal region of SMN provides several excellent targets for mutational analysis. A number of residues uninvolved in Gemin2 binding are highly conserved in *S. pombe*, included the invariant W9, D10, D11 triplet and, at the position of the D44V SMA patient mutation in humans, E19. The latter has featured in the literature due to the pathogenesis it introduces, and is specifically suggested to destabilize the N-terminal SMN interaction when mutated. A similar role can be hypothesized for the neighboring W9, D10 and D11. The significance of the N-terminal SMN interaction in stabilizing SMN dimers or tetramers, in contrast to that brokered by the YG box, is uncertain, but might be probed in the context of perturbation of SMN's oligomerization behavior and provide some structural insight into the function of SMN self-association in snRNP assembly and the deficiency in that ability that causes SMA.

Another matter of some importance addresses the applicability of the dimer-tetramer paradigm observed for *S. pombe* SMN-Gemin2 orthologues to higher organisms. Felicitously, early unpublished in-house data show that a construct comprising the human SMN YG box oligomerization domain fused to MBP for solubilization also inhabits a dimer-tetramer equilibrium; this construct was also crystallized as a dimer, suggesting at least some correspondence between the two orthologues. The construct's ability to access a tetramer without the putative N-terminal self-interaction domain casts some doubt on the notion that the YG box mediates dimerization and the N-terminal domain higher order oligomer formation, but may be fruitfully addressed in by the

development of a full-length or near full-length SMN construct exhibiting tractable solution behavior in complex with Gemin2 and naturally possessing both domains.

Finally, the global structure of and orientation of dimeric subunits within each SMN tetramer offers a fascinating question. One can easily imagine the interaction of four similarly-oriented subunits, interacting in parallel and able to exchange with each other when reforming dimers; one can as readily imagine the interaction of two indivisible dimers in an orientation that never allows the exchange of subunits. Two experiments might be instructive. A simple exchange experiment differently tags separate pools of SMN-Gemin2 complexes before combining them; the evolution of mixed oligomers after some equilibration indicates the ability of the subunits to exchange. Low-resolution SAXS envelopes might also assist in supporting or eliminating potential models, particularly in the context of the MBP-YG box human chimeras mentioned above at concentrations favoring tetramer; the comparatively large MBP moieties might be identifiable obviously on a shared side or on opposite sides of the oligomerization domain, giving some indication of dimer-dimer polarity.

The biophysical studies of human SMN and Gemin2 described here mark a noteworthy advance in the structural understanding of the atomic foundations of their interaction, their solution behavior and the discrete oligomerization states occupied by SMN. The structural frameworks they provide will motivate the next generation of structure-function studies on the role of both proteins in many aspects of cellular housekeeping,

and represent a valuable tool for the continued study of U-snRNP biogenesis and SMA pathogenesis.

Appendix A. Backbone and sidechain resonance assignments for SMN²⁶⁻⁵¹ and Gemin2⁹⁵⁻²⁸⁰.

Table A1. Resonance assignments for SMN²⁶⁻⁵¹. Standard deviation to the mean is indicated except in cases where indicated chemical shift is based on a single assignment.

Column 1: atom number

Column 2: residue name

Column 3: atom name

Column 4: chemical shift

Column 5: ambiguity code

The ambiguity code for assignments follows the nomenclature of the Biological Magnetic Resonance Bank as follows:

1: unique

2: ambiguity of geminal atoms or geminal methyl proton groups

3: aromatic atoms on opposite sides of a symmetric ring

1	GLN27	C	176.3182 ± 0.053	1	54	ILE33	CA	61.2072 ± 0.136	1
2	GLN27	CA	56.4212 ± 0.078	1	55	ILE33	CB	38.5862 ± 0.077	1
3	GLN27	CB	29.5252 ± 0.079	1	56	ILE33	CD1	12.8622 ± 0.059	1
4	GLN27	CG	33.7362 ± 0.106	1	57	ILE33	CG1	27.0312 ± 0.076	1
5	GLN27	HA	4.3762 ± 0.007	1	58	ILE33	CG2	17.1432 ± 0.054	1
6	GLN27	HB2	2.0682 ± 0.037	2	59	ILE33	HA	3.9562 ± 0.010	1
7	GLN27	HB3	2.0682 ± 0.037	2	60	ILE33	HB	1.6242 ± 0.008	1
8	GLN27	HE21	7.6222	2	61	ILE33	HD1	0.6782 ± 0.014	1
9	GLN27	HE22	6.8642	2	62	ILE33	HG12	1.1512 ± 0.005	2
10	GLN27	HG2	2.3852 ± 0.008	2	63	ILE33	HG13	0.9382 ± 0.008	2
11	GLN27	HG3	2.3852 ± 0.008	2	64	ILE33	HG2	0.6232 ± 0.008	1
12	GLN27	NE2	112.6672	1	65	ILE33	H	7.7332 ± 0.006	1
13	SER28	C	174.2782 ± 0.038	1	66	ILE33	N	119.8342 ± 0.056	1
14	SER28	CA	58.4752 ± 0.059	1	67	TRP34	CA	56.3412 ± 0.119	1
15	SER28	CB	63.6532 ± 0.187	1	68	TRP34	CB	29.1072 ± 0.098	1
16	SER28	HA	4.4652 ± 0.009	1	69	TRP34	CD1	126.9502 ± 0.074	1
17	SER28	HB2	3.8702 ± 0.020	2	70	TRP34	CE3	121.0332	1
18	SER28	HB3	3.8702 ± 0.020	2	71	TRP34	CH2	124.5102 ± 0.055	1
19	SER28	H	8.5672 ± 0.008	1	72	TRP34	CZ2	114.3972 ± 0.142	1
20	SER28	N	116.7872 ± 0.056	1	73	TRP34	CZ3	121.1832 ± 0.103	1
21	ASP29	C	176.0802 ± 0.023	1	74	TRP34	HA	4.6562 ± 0.015	1
22	ASP29	CA	54.4522 ± 0.075	1	75	TRP34	HB2	3.1802 ± 0.014	2
23	ASP29	CB	41.1052 ± 0.090	1	76	TRP34	HB3	2.9762 ± 0.017	2
24	ASP29	HA	4.6162 ± 0.010	1	77	TRP34	HD1	7.0362 ± 0.007	1
25	ASP29	HB2	2.6982 ± 0.015	2	78	TRP34	HE1	9.8822 ± 0.011	1
26	ASP29	HB3	2.6982 ± 0.015	2	79	TRP34	HE3	7.2512 ± 0.008	1
27	ASP29	H	8.3132 ± 0.008	1	80	TRP34	HH2	6.9712 ± 0.006	1
28	ASP29	N	122.0502 ± 0.050	1	81	TRP34	H	8.2762 ± 0.012	1
29	ASP30	C	176.5802 ± 0.029	1	82	TRP34	HZ2	7.1742 ± 0.009	1
30	ASP30	CA	545642 ± 0.033	1	83	TRP34	HZ3	6.6452 ± 0.004	1
31	ASP30	CB	40.9832 ± 0.088	1	84	TRP34	N	126.5562 ± 0.094	1
32	ASP30	HA	4.6082 ± 0.002	1	85	TRP34	NE1	128.8832 ± 0.015	1
33	ASP30	HB2	2.6942 ± 0.011	2	86	ASP35	CA	52.6222 ± 0.079	1
34	ASP30	HB3	2.6942 ± 0.011	2	87	ASP35	HA	4.3942	1
35	ASP30	H	8.2792 ± 0.007	1	88	ASP35	H	8.0062 ± 0.002	1
36	ASP30	N	120.9312 ± 0.057	1	89	ASP35	N	123.4902 ± 0.061	1
37	SER31	C	174.4182 ± 0.019	1	90	ASP36	C	178.8332	1
38	SER31	CA	59.1542 ± 0.066	1	91	ASP36	CA	56.0282 ± 0.006	1
39	SER31	CB	63.7802 ± 0.089	1	92	ASP36	CB	41.6252	1
40	SER31	HA	4.3162 ± 0.007	1	93	ASP36	HB2	2.7772	2
41	SER31	HB2	3.8392 ± 0.008	2	94	ASP36	HB3	2.7772	2
42	SER31	HB3	3.8392 ± 0.008	2	95	THR37	C	175.1652	1
43	SER31	H	8.2442 ± 0.008	1	96	THR37	CA	61.0172 ± 0.103	1
44	SER31	N	115.7282 ± 0.030	1	97	THR37	CB	68.7452 ± 0.117	1
45	ASP32	C	175.8962 ± 0.047	1	98	THR37	CG2	22.2062 ± 0.069	1
46	ASP32	CA	54.3932 ± 0.082	1	99	THR37	HA	4.2582 ± 0.009	1
47	ASP32	CB	41.0082 ± 0.091	1	100	THR37	HB	4.5552 ± 0.010	1
48	ASP32	HA	4.5752 ± 0.012	1	101	THR37	HG2	1.0952 ± 0.009	1
49	ASP32	HB2	2.5582 ± 0.014	2	102	THR37	H	8.1502 ± 0.013	1
50	ASP32	HB3	2.5582 ± 0.014	2	103	THR37	N	105.6422 ± 0.074	1
51	ASP32	H	8.2802 ± 0.005	1	104	ALA38	C	180.1702 ± 0.005	1
52	ASP32	N	122.0392 ± 0.118	1	105	ALA38	CA	56.4082 ± 0.090	1
53	ILE33	C	175.7422 ± 0.054	1	106	ALA38	CB	19.1602 ± 0.090	1

107	ALA38	HA	3.7022 ± 0.010	1	160	ALA42	HB	1.7262 ± 0.006	1
108	ALA38	HB	0.9572 ± 0.022	1	161	ALA42	H	7.9652 ± 0.008	1
109	ALA38	H	7.4592 ± 0.008	1	162	ALA42	N	121.9532 ± 0.063	1
110	ALA38	N	122.7182 ± 0.095	1	163	TYR43	C	176.0512 ± 0.022	1
111	LEU39	C	178.8352	1	164	TYR43	CA	61.6942 ± 0.070	1
112	LEU39	CA	57.7352 ± 0.079	1	165	TYR43	CB	37.4292 ± 0.223	1
113	LEU39	CB	41.3182 ± 0.091	1	166	TYR43	CD1	129.3572	3
114	LEU39	CD1	25.9042 ± 0.115	1	167	TYR43	CD2	129.3572	3
115	LEU39	CD2	23.4942 ± 0.130	1	168	TYR43	CE1	118.2222 ± 0.193	3
116	LEU39	CG	26.2562 ± 0.462	1	169	TYR43	CE2	118.2222 ± 0.193	3
117	LEU39	HA	4.2102 ± 0.012	1	170	TYR43	HA	3.1322 ± 0.009	1
118	LEU39	HB2	1.8162 ± 0.003	2	171	TYR43	HB2	2.8382 ± 0.018	2
119	LEU39	HB3	1.3442 ± 0.035	2	172	TYR43	HB3	2.2602 ± 0.018	2
120	LEU39	HD1	0.7652 ± 0.014	1	173	TYR43	HD1	6.9172 ± 0.009	3
121	LEU39	HD2	0.7492 ± 0.007	1	174	TYR43	HD2	6.9172 ± 0.009	3
122	LEU39	HG	1.5232 ± 0.008	1	175	TYR43	HE1	6.5322 ± 0.012	3
123	LEU39	H	8.7672 ± 0.009	1	176	TYR43	HE2	6.5322 ± 0.012	3
124	LEU39	N	115.8382 ± 0.091	1	177	TYR43	HH	9.4152	1
125	ILE40	C	177.2072	1	178	TYR43	H	7.6602 ± 0.007	1
126	ILE40	CA	65.7822 ± 0.099	1	179	TYR43	N	121.9492 ± 0.057	1
127	ILE40	CB	38.7682 ± 0.090	1	180	ASP44	C	179.7612	1
128	ILE40	CD1	15.8972 ± 0.077	1	181	ASP44	CA	57.3412 ± 0.162	1
129	ILE40	CG1	29.8282 ± 0.138	1	182	ASP44	CB	39.6102 ± 0.134	1
130	ILE40	CG2	18.2612 ± 0.061	1	183	ASP44	HA	4.1292 ± 0.009	1
131	ILE40	HA	3.4062 ± 0.009	1	184	ASP44	HB2	2.7062 ± 0.019	2
132	ILE40	HB	1.9022 ± 0.008	1	185	ASP44	HB3	2.5442 ± 0.013	2
133	ILE40	HD1	0.6682 ± 0.008	1	186	ASP44	H	8.4362 ± 0.011	1
134	ILE40	HG12	1.2972 ± 0.010	2	187	ASP44	N	119.0592 ± 0.089	1
135	ILE40	HG13	0.7632 ± 0.011	2	188	LYS45	C	178.7742	1
136	ILE40	HG2	0.8052 ± 0.007	1	189	LYS45	CA	59.0192 ± 0.089	1
137	ILE40	H	6.9472 ± 0.008	1	190	LYS45	CB	32.7652 ± 0.074	1
138	ILE40	N	121.8492 ± 0.080	1	191	LYS45	CD	29.4792 ± 0.109	1
139	LYS41	C	179.5032 ± 0.025	1	192	LYS45	CE	42.0312 ± 0.118	1
140	LYS41	CA	59.1542 ± 0.122	1	193	LYS45	CG	25.0872 ± 0.034	1
141	LYS41	CB	32.7692 ± 0.116	1	194	LYS45	HA	4.0172 ± 0.010	1
142	LYS41	CD	29.4142 ± 0.101	1	195	LYS45	HB2	1.8762 ± 0.014	2
143	LYS41	CE	41.8922 ± 0.182	1	196	LYS45	HB3	1.8762 ± 0.014	2
144	LYS41	CG	25.8412 ± 0.100	1	197	LYS45	HD2	1.6462 ± 0.012	2
145	LYS41	HA	4.0302 ± 0.007	1	198	LYS45	HD3	1.6462 ± 0.012	2
146	LYS41	HB2	1.6982 ± 0.025	2	199	LYS45	HE2	2.9382 ± 0.013	2
147	LYS41	HB3	1.6982 ± 0.025	2	200	LYS45	HE3	2.9382 ± 0.013	2
148	LYS41	HD2	1.5652 ± 0.015	2	201	LYS45	HG2	1.4232 ± 0.035	2
149	LYS41	HD3	1.5652 ± 0.015	2	202	LYS45	HG3	1.4232 ± 0.035	2
150	LYS41	HE2	2.9122 ± 0.007	2	203	LYS45	H	8.2082 ± 0.012	1
151	LYS41	HE3	2.9122 ± 0.007	2	204	LYS45	N	119.9972 ± 0.064	1
152	LYS41	HG2	1.4342 ± 0.025	2	205	ALA46	C	181.1622	1
153	LYS41	HG3	1.4342 ± 0.025	2	206	ALA46	CA	55.4272 ± 0.111	1
154	LYS41	H	7.8332 ± 0.008	1	207	ALA46	CB	19.4412 ± 0.116	1
155	LYS41	N	116.2512 ± 0.108	1	208	ALA46	HA	4.1612 ± 0.011	1
156	ALA42	C	180.1362 ± 0.052	1	209	ALA46	HB	1.4392 ± 0.011	1
157	ALA42	CA	55.3872 ± 0.110	1	210	ALA46	H	7.8482 ± 0.007	1
158	ALA42	CB	18.5062 ± 0.067	1	211	ALA46	N	123.9042 ± 0.136	1
159	ALA42	HA	4.0452 ± 0.008	1	212	VAL47	C	177.5272	1

213	VAL47	CA	65.3162 ± 0.111	1	266	LYS51	HD3	1.6532 ± 0.010	2
214	VAL47	CB	31.6872 ± 0.071	1	267	LYS51	HE2	2.9742 ± 0.015	2
215	VAL47	CG1	21.3262 ± 0.164	1	268	LYS51	HE3	2.9742 ± 0.015	2
216	VAL47	CG2	20.8682 ± 0.140	1	269	LYS51	HG2	1.3382 ± 0.014	2
217	VAL47	HA	3.7202 ± 0.008	1	270	LYS51	HG3	1.3382 ± 0.014	2
218	VAL47	HB	2.0192 ± 0.006	1	271	LYS51	H	7.1822 ± 0.007	1
219	VAL47	HG1	0.6442 ± 0.017	1	272	LYS51	N	127.7332 ± 0.063	1
220	VAL47	HG2	0.5922 ± 0.015	1					
221	VAL47	H	8.1392 ± 0.009	1					
222	VAL47	N	114.4472 ± 0.114	1					
223	ALA48	C	178.3502 ± 0.019	1					
224	ALA48	CA	53.4062 ± 0.076	1					
225	ALA48	CB	18.7752 ± 0.095	1					
226	ALA48	HA	4.3132 ± 0.010	1					
227	ALA48	HB	1.4802 ± 0.016	1					
228	ALA48	H	7.5392 ± 0.007	1					
229	ALA48	N	121.3842 ± 0.044	1					
230	SER49	C	174.2942 ± 0.009	1					
231	SER49	CA	59.5382 ± 0.087	1					
232	SER49	CB	64.0162 ± 0.122	1					
233	SER49	HA	4.4122 ± 0.007	1					
234	SER49	HB2	4.1122 ± 0.009	2					
235	SER49	HB3	4.0072 ± 0.008	2					
236	SER49	H	7.7712 ± 0.006	1					
237	SER49	N	112.8012 ± 0.075	1					
238	PHE50	C	173.8712 ± 0.022	1					
239	PHE50	CA	59.0542 ± 0.092	1					
240	PHE50	CB	39.6632 ± 0.123	1					
241	PHE50	CD1	131.6612 ± 0.251	3					
242	PHE50	CD2	131.6612 ± 0.251	3					
243	PHE50	CE1	131.2702 ± 0.345	3					
244	PHE50	CE2	131.2702 ± 0.345	3					
245	PHE50	CZ	132.3432 ± 0.133	1					
246	PHE50	HA	4.0472 ± 0.013	1					
247	PHE50	HB2	2.9072 ± 0.012	2					
248	PHE50	HB3	3.0252 ± 0.020	2					
249	PHE50	HD1	6.6312 ± 0.019	3					
250	PHE50	HD2	6.6312 ± 0.019	3					
251	PHE50	HE1	6.9842 ± 0.024	3					
252	PHE50	HE2	6.9842 ± 0.024	3					
253	PHE50	H	7.7872 ± 0.006	1					
254	PHE50	HZ	6.6392 ± 0.021	1					
255	PHE50	N	122.7832 ± 0.054	1					
256	LYS51	C	180.4482	1					
257	LYS51	CA	57.6472 ± 0.128	1					
258	LYS51	CB	34.0762 ± 0.074	1					
259	LYS51	CD	29.1962 ± 0.151	1					
260	LYS51	CE	42.0912 ± 0.155	1					
261	LYS51	CG	24.5472 ± 0.047	1					
262	LYS51	HA	3.9482 ± 0.009	1					
263	LYS51	HB2	1.7432 ± 0.013	2					
264	LYS51	HB3	1.6392 ± 0.010	2					
265	LYS51	HD2	1.6532 ± 0.010	2					

Table A2. Resonance assignments for Gemin2⁹⁵⁻²⁸⁰. Standard deviation to the mean is indicated except in cases where indicated chemical shift is based on a single assignment.

Column 1: atom number

Column 2: residue name

Column 3: atom name

Column 4: chemical shift

Column 5: ambiguity code

The ambiguity code for assignments follows the nomenclature of the Biological Magnetic Resonance Bank as follows:

1: unique

2: ambiguity of geminal atoms or geminal methyl proton groups

3: aromatic atoms on opposite sides of a symmetric ring

1	GLY95 CA	44.9772	1	54	LEU100HB2	1.6982 ± 0.008	2
2	GLY95 HA2	3.9192	2	55	LEU100HB3	1.6612 ± 0.005	2
3	GLY95 HA3	3.9192	2	56	LEU100HD1	0.9442 ± 0.013	2
4	TYR96 C	175.1852	1	57	LEU100HD2	0.9442 ± 0.013	2
5	TYR96 CA	57.5772 ± 0.100	1	58	LEU100HG	1.6382 ± 0.006	1
6	TYR96 CB	38.9752 ± 0.092	1	59	LEU100H	9.0262 ± 0.010	1
7	TYR96 CD1	133.0652 ± 0.008	3	60	LEU100N	122.8122 ± 0.122	1
8	TYR96 CD2	133.0652 ± 0.008	3	61	GLN101C	178.2192 ± 0.003	1
9	TYR96 CE1	118.4692 ± 0.030	3	62	GLN101CA	59.8032 ± 0.062	1
10	TYR96 CE2	118.4692 ± 0.030	3	63	GLN101CB	28.1372 ± 0.033	1
11	TYR96 HA	4.5002 ± 0.008	1	64	GLN101CG	34.0682 ± 0.042	1
12	TYR96 HB2	2.9202 ± 0.008	2	65	GLN101HA	4.1262 ± 0.031	1
13	TYR96 HB3	2.7422 ± 0.011	2	66	GLN101HB2	2.1352 ± 0.021	2
14	TYR96 HD1	6.9452 ± 0.003	3	67	GLN101HB3	2.1352 ± 0.021	2
15	TYR96 HD2	6.9452 ± 0.003	3	68	GLN101HG2	2.4642 ± 0.022	2
16	TYR96 HE1	6.7192 ± 0.001	3	69	GLN101HG3	2.4642 ± 0.022	2
17	TYR96 HE2	6.7192 ± 0.001	3	70	GLN101H	8.5802 ± 0.010	1
18	SER97 C	172.7472	1	71	GLN101N	117.9082 ± 0.059	1
19	SER97 CA	56.4282 ± 0.038	1	72	TRP102 C	178.6852 ± 0.033	1
20	SER97 CB	63.5542 ± 0.131	1	73	TRP102 CA	62.5792 ± 0.102	1
21	SER97 HA	4.4452 ± 0.011	1	74	TRP102 CB	29.0292 ± 0.167	1
22	SER97 HB2	3.7182 ± 0.011	2	75	TRP102 CD1	128.4322 ± 0.105	1
23	SER97 HB3	3.6292 ± 0.006	2	76	TRP102 HA	4.1552 ± 0.024	1
24	SER97 H	7.9762 ± 0.009	1	77	TRP102 HB2	3.5092 ± 0.017	2
25	SER97 N	117.1652 ± 0.075	1	78	TRP102 HB3	3.3782 ± 0.029	2
26	PRO98 C	177.2812	1	79	TRP102 HD1	7.3862 ± 0.008	1
27	PRO98 CA	62.2432 ± 0.108	1	80	TRP102 HE1	10.3452	1
28	PRO98 CB	32.6372 ± 0.119	1	81	TRP102 H	8.2122 ± 0.008	1
29	PRO98 CD	50.5782	1	82	TRP102 N	121.7842 ± 0.108	1
30	PRO98 CG	27.7632 ± 0.300	1	83	TRP102 NE1	130.9702	1
31	PRO98 HA	4.6082 ± 0.006	1	84	GLN103C	178.0502	1
32	PRO98 HB2	2.1362 ± 0.005	2	85	GLN103CA	60.0482 ± 0.100	1
33	PRO98 HB3	1.9312 ± 0.008	2	86	GLN103CB	27.8082 ± 0.050	1
34	PRO98 HD2	3.6012	2	87	GLN103CG	34.0942 ± 0.003	1
35	PRO98 HD3	3.6012	2	88	GLN103HA	3.9802 ± 0.020	1
36	PRO98 HG2	2.0392 ± 0.029	2	89	GLN103HB2	2.0882 ± 0.002	2
37	PRO98 HG3	2.0392 ± 0.029	2	90	GLN103HB3	2.0882 ± 0.002	2
38	THR99 C	175.8502 ± 0.035	1	91	GLN103HG2	2.4822 ± 0.015	2
39	THR99 CA	61.8532 ± 0.101	1	92	GLN103HG3	2.4822 ± 0.015	2
40	THR99 CB	70.6512 ± 0.102	1	93	GLN103H	8.3782 ± 0.009	1
41	THR99 CG2	22.0732 ± 0.077	1	94	GLN103N	117.0242 ± 0.100	1
42	THR99 HA	4.2432 ± 0.006	1	95	GLN104C	179.6752 ± 0.031	1
43	THR99 HB	4.7452 ± 0.011	1	96	GLN104CA	59.0032 ± 0.068	1
44	THR99 HG2	1.4182 ± 0.006	1	97	GLN104CB	28.0172 ± 0.074	1
45	THR99 H	8.6342 ± 0.011	1	98	GLN104CG	33.9302 ± 0.098	1
46	THR99 N	113.4402 ± 0.100	1	99	GLN104HA	3.9182 ± 0.018	1
47	LEU100 C	179.1522	1	100	GLN104HB2	2.1172 ± 0.020	2
48	LEU100 CA	58.1272 ± 0.166	1	101	GLN104HB3	2.1172 ± 0.020	2
49	LEU100 CB	41.2702 ± 0.104	1	102	GLN104HE21	7.3432 ± 0.001	2
50	LEU100 CD1	23.9992 ± 0.129	2	103	GLN104HE22	6.8222 ± 0.005	2
51	LEU100 CD2	23.9992 ± 0.129	2	104	GLN104HG2	2.5272 ± 0.007	2
52	LEU100 CG	27.1102 ± 0.067	1	105	GLN104HG3	2.3772 ± 0.006	2
53	LEU100 HA	4.0962 ± 0.007	1	106	GLN104H	8.6912 ± 0.009	1

107	GLN104N	117.4402 ± 0.102	1	160	GLN109HG3	2.5102 ± 0.026	2
108	GLN104NE2	110.5112 ± 0.072	1	161	GLN109H	8.1832 ± 0.010	1
109	GLN105C	178.9732 ± 0.016	1	162	GLN109N	117.3562 ± 0.122	1
110	GLN105CA	58.7562 ± 0.108	1	163	PHE110 C	177.0322	1
111	GLN105CB	27.8812 ± 0.129	1	164	PHE110 CA	60.2962 ± 0.094	1
112	GLN105CG	33.8302 ± 0.074	1	165	PHE110 CB	39.8762 ± 0.149	1
113	GLN105HA	4.0482 ± 0.009	1	166	PHE110 CD1	133.1052	3
114	GLN105HB2	2.1012 ± 0.027	2	167	PHE110 CD2	133.1052	3
115	GLN105HB3	2.1012 ± 0.027	2	168	PHE110 HA	4.4142 ± 0.013	1
116	GLN105HG2	2.4692 ± 0.024	2	169	PHE110 HB2	3.1272 ± 0.016	2
117	GLN105HG3	2.4692 ± 0.024	2	170	PHE110 HB3	2.6602 ± 0.010	2
118	GLN105H	8.1522 ± 0.008	1	171	PHE110 HD1	6.8302	3
119	GLN105N	120.6432 ± 0.097	1	172	PHE110 HD2	6.8302	3
120	GLN106C	180.3832 ± 0.031	1	173	PHE110 H	8.2272 ± 0.010	1
121	GLN106CA	57.2482 ± 0.126	1	174	PHE110 N	121.2282 ± 0.112	1
122	GLN106CB	25.9742 ± 0.070	1	175	SER111 C	177.3822	1
123	GLN106CG	30.8512 ± 0.183	1	176	SER111 CA	62.1412 ± 0.149	1
124	GLN106HA	3.8992 ± 0.020	1	177	SER111 CB	62.8152 ± 0.102	1
125	GLN106HB3	1.6342 ± 0.012	2	178	SER111 HA	3.8312 ± 0.011	1
126	GLN106HB2	1.6342 ± 0.012	2	179	SER111 HB2	4.1832 ± 0.010	2
127	GLN106HE21	6.4742 ± 0.003	2	180	SER111 HB3	4.1832 ± 0.010	2
128	GLN106HE22	6.4742 ± 0.003	2	181	SER111 H	8.2222 ± 0.010	1
129	GLN106HG2	1.2742 ± 0.010	2	182	SER111 N	113.3222 ± 0.089	1
130	GLN106HG3	0.6082 ± 0.009	2	183	THR112C	176.0282	1
131	GLN106H	8.0602 ± 0.011	1	184	THR112CA	66.6682 ± 0.093	1
132	GLN106N	117.5282 ± 0.067	1	185	THR112CB	68.5902 ± 0.104	1
133	GLN106NE2	111.5252 ± 0.119	1	186	THR112CG2	22.2242 ± 0.118	1
134	VAL107C	177.3352 ± 0.024	1	187	THR112HA	3.9192 ± 0.009	1
135	VAL107CA	67.4612 ± 0.077	1	188	THR112HB	4.3062 ± 0.012	1
136	VAL107CB	31.6682 ± 0.109	1	189	THR112HG2	1.2372 ± 0.009	1
137	VAL107CG1	24.5732 ± 0.089	1	190	THR112H	7.5292 ± 0.009	1
138	VAL107CG2	22.0312 ± 0.105	1	191	THR112N	118.3302 ± 0.122	1
139	VAL107HA	3.5102 ± 0.015	1	192	VAL113C	178.4492 ± 0.013	1
140	VAL107HB	2.1942 ± 0.004	1	193	VAL113CA	67.1932 ± 0.116	1
141	VAL107HG1	1.0252 ± 0.008	1	194	VAL113CB	31.8562 ± 0.045	1
142	VAL107HG2	1.1132 ± 0.014	1	195	VAL113CG1	20.9912 ± 0.076	1
143	VAL107H	8.1212 ± 0.012	1	196	VAL113CG2	22.7932 ± 0.082	1
144	VAL107N	122.0912 ± 0.048	1	197	VAL113HA	3.6342 ± 0.011	1
145	ALA108C	181.0952 ± 0.018	1	198	VAL113HB	2.1912 ± 0.006	1
146	ALA108CA	55.3992 ± 0.059	1	199	VAL113HG1	0.9292 ± 0.003	1
147	ALA108CB	17.8942 ± 0.101	1	200	VAL113HG2	1.2582 ± 0.005	1
148	ALA108HA	4.2142 ± 0.010	1	201	VAL113H	7.9672 ± 0.012	1
149	ALA108HB	1.5182 ± 0.009	1	202	VAL113N	124.5372 ± 0.091	1
150	ALA108H	7.8212 ± 0.009	1	203	ARG114C	179.3502 ± 0.014	1
151	ALA108N	123.1582 ± 0.144	1	204	ARG114CA	60.0022 ± 0.150	1
152	GLN109C	178.5272 ± 0.015	1	205	ARG114CB	30.3912 ± 0.108	1
153	GLN109CA	58.5542 ± 0.097	1	206	ARG114CD	41.4922	1
154	GLN109CB	28.2922 ± 0.080	1	207	ARG114CG	27.1032 ± 0.166	1
155	GLN109CG	33.9002 ± 0.099	1	208	ARG114HA	3.5332 ± 0.016	1
156	GLN109HA	4.1302 ± 0.016	1	209	ARG114HB2	1.7802 ± 0.011	2
157	GLN109HB2	2.1232 ± 0.014	2	210	ARG114HB3	1.4682 ± 0.008	2
158	GLN109HB3	2.1232 ± 0.014	2	211	ARG114HD2	2.2952	2
159	GLN109HG2	2.5102 ± 0.026	2	212	ARG114HD3	2.2952	2

213	ARG114HG2	1.6432 ± 0.004	2	266	LYS119 HE2	2.8402 ± 0.020	2
214	ARG114HG3	0.4392 ± 0.012	2	267	LYS119 HE3	2.8402 ± 0.020	2
215	ARG114H	8.2132 ± 0.016	1	268	LYS119 HG2	1.2662 ± 0.013	2
216	ARG114N	118.4812 ± 0.126	1	269	LYS119 HG3	1.0332 ± 0.015	2
217	GLN115C	178.7002 ± 0.035	1	270	LYS119 H	8.2832 ± 0.010	1
218	GLN115CA	58.8282 ± 0.085	1	271	LYS119 N	119.4252 ± 0.109	1
219	GLN115CB	28.2302 ± 0.116	1	272	HIS120 C	175.9552 ± 0.049	1
220	GLN115CG	34.0102 ± 0.128	1	273	HIS120 CA	56.4612 ± 0.059	1
221	GLN115HA	4.0892 ± 0.017	1	274	HIS120 CB	31.1242 ± 0.092	1
222	GLN115HB2	2.1662 ± 0.020	2	275	HIS120 CD2	120.1972 ± 0.041	1
223	GLN115HB3	2.1662 ± 0.020	2	276	HIS120 CE1	138.4402 ± 0.069	1
224	GLN115HG2	2.4652 ± 0.031	2	277	HIS120 HA	5.1222 ± 0.012	1
225	GLN115HG3	2.4652 ± 0.031	2	278	HIS120 HB2	3.6712 ± 0.013	2
226	GLN115H	7.8222 ± 0.010	1	279	HIS120 HB3	3.4502 ± 0.019	2
227	GLN115N	119.1792 ± 0.117	1	280	HIS120 HD2	6.9002 ± 0.008	1
228	ASN116C	178.1002	1	281	HIS120 HE1	7.7572 ± 0.003	1
229	ASN116CA	56.0522 ± 0.113	1	282	HIS120 H	7.6562 ± 0.021	1
230	ASN116CB	37.5262 ± 0.111	1	283	HIS120 N	114.2002 ± 0.148	1
231	ASN116HA	4.3342 ± 0.017	1	284	ARG121 C	177.9342 ± 0.017	1
232	ASN116HB2	2.5832 ± 0.016	2	285	ARG121 CA	61.2632 ± 0.080	1
233	ASN116HB3	2.5832 ± 0.016	2	286	ARG121 CB	30.3982 ± 0.055	1
234	ASN116H	7.9382 ± 0.013	1	287	ARG121 CD	43.5912 ± 0.097	1
235	ASN116N	120.0542 ± 0.058	1	288	ARG121 CG	28.9722 ± 0.115	1
236	VAL117C	178.1032 ± 0.006	1	289	ARG121 HA	4.2622 ± 0.008	1
237	VAL117CA	66.9072 ± 0.168	1	290	ARG121 HB2	2.3332 ± 0.010	2
238	VAL117CB	31.5752 ± 0.070	1	291	ARG121 HB3	1.9762 ± 0.013	2
239	VAL117CG1	21.2182 ± 0.126	1	292	ARG121 HD2	3.4332 ± 0.022	2
240	VAL117CG2	24.0142 ± 0.086	1	293	ARG121 HD3	3.3722 ± 0.026	2
241	VAL117HA	3.6992 ± 0.007	1	294	ARG121 HG2	1.9682	2
242	VAL117HB	2.1982 ± 0.007	1	295	ARG121 HG3	1.7192 ± 0.012	2
243	VAL117HG1	0.9302 ± 0.008	1	296	ARG121 H	7.8262 ± 0.020	1
244	VAL117HG2	1.0442 ± 0.013	1	297	ARG121 N	122.6482 ± 0.073	1
245	VAL117H	8.5252 ± 0.010	1	298	SER122 C	176.5282	1
246	VAL117N	122.2512 ± 0.077	1	299	SER122 CA	61.9742 ± 0.087	1
247	ASN118C	178.0862 ± 0.013	1	300	SER122 CB	62.3892 ± 0.073	1
248	ASN118CA	56.5012 ± 0.157	1	301	SER122 HA	4.1012 ± 0.016	1
249	ASN118CB	38.9542 ± 0.104	1	302	SER122 HB2	3.9692 ± 0.013	2
250	ASN118HA	4.4342 ± 0.015	1	303	SER122 HB3	3.9692 ± 0.013	2
251	ASN118HB2	2.8502 ± 0.008	2	304	SER122 H	8.7932 ± 0.014	1
252	ASN118HB3	2.8502 ± 0.008	2	305	SER122 N	112.2832 ± 0.080	1
253	ASN118H	7.7852 ± 0.008	1	306	HIS123 C	177.8902 ± 0.003	1
254	ASN118N	116.0502 ± 0.077	1	307	HIS123 CA	59.2622 ± 0.092	1
255	LYS119 C	178.5862 ± 0.029	1	308	HIS123 CB	29.2352 ± 0.040	1
256	LYS119 CA	59.1382 ± 0.144	1	309	HIS123 CE1	137.5602 ± 0.063	1
257	LYS119 CB	32.8842 ± 0.100	1	310	HIS123 HA	4.0862 ± 0.029	1
258	LYS119 CD	29.3842 ± 0.087	1	311	HIS123 HB2	2.9462 ± 0.020	2
259	LYS119 CE	41.7572 ± 0.097	1	312	HIS123 HB3	2.9462 ± 0.020	2
260	LYS119 CG	24.7682 ± 0.092	1	313	HIS123 HD2	7.0272	1
261	LYS119 HA	4.0432 ± 0.008	1	314	HIS123 HE1	7.3892 ± 0.005	1
262	LYS119 HB2	1.7792 ± 0.013	2	315	HIS123 H	7.8772 ± 0.008	1
263	LYS119 HB3	1.5112 ± 0.013	2	316	HIS123 N	121.3222 ± 0.151	1
264	LYS119 HD2	1.5392 ± 0.016	2	317	TRP124 C	178.2752 ± 0.010	1
265	LYS119 HD3	1.5392 ± 0.016	2	318	TRP124 CA	60.3682 ± 0.081	1

319	TRP124 CB	29.6882 ± 0.034	1	372	GLN128CG	33.7472 ± 0.106	1
320	TRP124 CD1	128.3502 ± 0.069	1	373	GLN128HA	4.1682 ± 0.011	1
321	TRP124 CH2	122.7542 ± 0.025	1	374	GLN128HB2	2.0222 ± 0.008	2
322	TRP124 CZ2	120.8332 ± 0.094	1	375	GLN128HB3	2.0222 ± 0.008	2
323	TRP124 HA	4.1882 ± 0.023	1	376	GLN128HG2	2.3972 ± 0.010	2
324	TRP124 HB2	3.1032 ± 0.017	2	377	GLN128HG3	2.3972 ± 0.010	2
325	TRP124 HB3	3.1032 ± 0.017	2	378	GLN128H	8.6152 ± 0.007	1
326	TRP124 HD1	7.5542 ± 0.003	1	379	GLN128N	122.7902 ± 0.082	1
327	TRP124 HE1	10.4712 ± 0.008	1	380	LEU129 C	177.3272 ± 0.008	1
328	TRP124 HH2	7.1892 ± 0.001	1	381	LEU129 CA	54.3672 ± 0.052	1
329	TRP124 H	7.8952 ± 0.009	1	382	LEU129 CB	43.2722 ± 0.326	1
330	TRP124 HZ2	7.3332 ± 0.003	1	383	LEU129 CD1	24.1962 ± 0.171	2
331	TRP124 N	120.2172 ± 0.106	1	384	LEU129 CD2	24.1962 ± 0.171	2
332	TRP124 NE1	128.3712 ± 0.024	1	385	LEU129 CG	26.8262 ± 0.090	1
333	LYS125 C	176.3172 ± 0.036	1	386	LEU129 HA	4.3932 ± 0.010	1
334	LYS125 CA	58.5492 ± 0.066	1	387	LEU129 HB2	1.6082	2
335	LYS125 CB	32.2442 ± 0.088	1	388	LEU129 HB3	1.5552 ± 0.012	2
336	LYS125 CD	29.4082 ± 0.201	1	389	LEU129 HD1	0.8512 ± 0.010	2
337	LYS125 CE	42.0512 ± 0.107	1	390	LEU129 HD2	0.8512 ± 0.010	2
338	LYS125 CG	24.9632 ± 0.162	1	391	LEU129 HG	1.6732 ± 0.013	1
339	LYS125 HA	4.0852 ± 0.022	1	392	LEU129 H	8.4782 ± 0.011	1
340	LYS125 HB2	1.8032 ± 0.016	2	393	LEU129 N	125.9012 ± 0.052	1
341	LYS125 HB3	1.8032 ± 0.016	2	394	ASP130 C	177.4252 ± 0.025	1
342	LYS125 HD2	1.6682 ± 0.018	2	395	ASP130 CA	55.0882 ± 0.054	1
343	LYS125 HD3	1.6682 ± 0.018	2	396	ASP130 CB	41.9682 ± 0.109	1
344	LYS125 HE2	2.9532 ± 0.024	2	397	ASP130 HA	4.5272 ± 0.012	1
345	LYS125 HE3	2.9532 ± 0.024	2	398	ASP130 HB2	2.7462 ± 0.014	2
346	LYS125 HG2	1.4162 ± 0.027	2	399	ASP130 HB3	2.7462 ± 0.014	2
347	LYS125 HG3	1.4162 ± 0.027	2	400	ASP130 H	8.5752 ± 0.010	1
348	LYS125 H	8.5192 ± 0.016	1	401	ASP130 N	123.3372 ± 0.058	1
349	LYS125 N	117.7372 ± 0.062	1	402	SER131 C	174.6322	1
350	SER126 C	174.6632 ± 0.023	1	403	SER131 CA	60.4652 ± 0.110	1
351	SER126 CA	58.8162 ± 0.025	1	404	SER131 CB	63.1702 ± 0.100	1
352	SER126 CB	64.0642 ± 0.051	1	405	SER131 HA	4.2022 ± 0.012	1
353	SER126 HA	4.4042 ± 0.004	1	406	SER131 HB2	3.9392 ± 0.008	2
354	SER126 HB2	3.8832 ± 0.005	2	407	SER131 HB3	3.9392 ± 0.008	2
355	SER126 HB3	3.8832 ± 0.005	2	408	SER131 H	8.5572 ± 0.010	1
356	SER126 H	7.2792 ± 0.015	1	409	SER131 N	117.8912 ± 0.050	1
357	SER126 N	111.4372 ± 0.076	1	410	ASN132C	174.7532 ± 0.024	1
358	GLN127C	175.6752 ± 0.029	1	411	ASN132CA	53.6732 ± 0.117	1
359	GLN127CA	54.5982 ± 0.059	1	412	ASN132CB	38.3342 ± 0.114	1
360	GLN127CB	29.0162 ± 0.130	1	413	ASN132HA	4.6722 ± 0.011	1
361	GLN127CG	33.1082 ± 0.066	1	414	ASN132HB2	2.9632 ± 0.015	2
362	GLN127HA	4.1432 ± 0.004	1	415	ASN132HB3	2.8512 ± 0.009	2
363	GLN127HB2	2.1462 ± 0.030	2	416	ASN132H	8.6202 ± 0.008	1
364	GLN127HB3	1.9492 ± 0.015	2	417	ASN132N	118.0462 ± 0.077	1
365	GLN127HG2	2.2122 ± 0.007	2	418	VAL133C	174.8932 ± 0.033	1
366	GLN127HG3	2.0702 ± 0.011	2	419	VAL133CA	62.5492 ± 0.079	1
367	GLN127H	7.2142 ± 0.013	1	420	VAL133CB	31.8792 ± 0.152	1
368	GLN127N	121.0652 ± 0.074	1	421	VAL133CG1	21.2162 ± 0.071	1
369	GLN128C	176.2522 ± 0.009	1	422	VAL133CG2	21.5092 ± 0.076	1
370	GLN128CA	56.2792 ± 0.129	1	423	VAL133HA	3.7872 ± 0.011	1
371	GLN128CB	29.1232 ± 0.073	1	424	VAL133HB	2.1352 ± 0.008	1

425	VAL133HG1	0.8512 ± 0.019	1	478	LYS137 H	8.7352 ± 0.005	1
426	VAL133HG2	0.6652 ± 0.011	1	479	LYS137 N	120.6472 ± 0.086	1
427	VAL133H	7.7982 ± 0.011	1	480	SER138 C	175.1712	1
428	VAL133N	121.4042 ± 0.028	1	481	SER138 CA	63.3242 ± 0.119	1
429	THR134C	173.7982	1	482	SER138 CB	62.8602 ± 0.125	1
430	THR134CA	60.7952 ± 0.082	1	483	SER138 HA	4.1702 ± 0.021	1
431	THR134CB	69.5482 ± 0.109	1	484	SER138 HB2	3.8982 ± 0.022	2
432	THR134CG2	21.4242 ± 0.119	1	485	SER138 HB3	3.8982 ± 0.022	2
433	THR134HA	4.2312 ± 0.008	1	486	SER138 H	9.0942 ± 0.009	1
434	THR134HB	3.8802 ± 0.007	1	487	SER138 N	118.9292 ± 0.076	1
435	THR134HG2	0.9922 ± 0.012	1	488	GLU139C	175.7382 ± 0.018	1
436	THR134H	8.2062 ± 0.010	1	489	GLU139CA	57.5432 ± 0.105	1
437	THR134N	123.7512 ± 0.085	1	490	GLU139CB	28.8012 ± 0.033	1
438	MET135 C	172.9952	1	491	GLU139CG	35.9312 ± 0.169	1
439	MET135 CA	53.7142 ± 0.100	1	492	GLU139HA	4.3722 ± 0.012	1
440	MET135 CB	32.1752 ± 0.041	1	493	GLU139HB2	2.1652 ± 0.004	2
441	MET135 CE	17.1812 ± 0.045	1	494	GLU139HB3	1.7452 ± 0.003	2
442	MET135 CG	32.2362 ± 0.088	1	495	GLU139HG2	2.3322 ± 0.005	2
443	MET135 HA	3.3302 ± 0.007	1	496	GLU139HG3	2.2552 ± 0.002	2
444	MET135 HB2	2.1612 ± 0.088	2	497	GLU139H	9.3032 ± 0.006	1
445	MET135 HB3	2.0222 ± 0.015	2	498	GLU139N	117.1372 ± 0.063	1
446	MET135 HE	2.1482 ± 0.005	1	499	ASP140 C	173.7752	1
447	MET135 HG2	1.6202 ± 0.018	2	500	ASP140 CA	52.4452 ± 0.092	1
448	MET135 HG3	1.6202 ± 0.018	2	501	ASP140 CB	39.8642 ± 0.113	1
449	MET135 H	8.5712 ± 0.009	1	502	ASP140 HA	4.6262 ± 0.019	1
450	MET135 N	126.7302 ± 0.049	1	503	ASP140 HB2	3.2742 ± 0.010	2
451	PRO136C	175.4962 ± 0.018	1	504	ASP140 HB3	2.3712 ± 0.015	2
452	PRO136CA	61.5362 ± 0.082	1	505	ASP140 H	7.8542 ± 0.008	1
453	PRO136CB	30.4772 ± 0.116	1	506	ASP140 N	121.2752 ± 0.084	1
454	PRO136CD	48.8102 ± 0.108	1	507	GLU141C	177.6952 ± 0.035	1
455	PRO136CG	26.5822 ± 0.154	1	508	GLU141CA	59.2412 ± 0.104	1
456	PRO136HA	4.0712 ± 0.009	1	509	GLU141CB	29.7792 ± 0.177	1
457	PRO136HB2	1.7952 ± 0.005	2	510	GLU141CG	35.4032 ± 0.061	1
458	PRO136HB3	0.4422 ± 0.013	2	511	GLU141HA	2.3172 ± 0.013	1
459	PRO136HD2	2.3482 ± 0.010	2	512	GLU141HB2	1.6562 ± 0.010	2
460	PRO136HD3	0.3352 ± 0.089	2	513	GLU141HB3	1.4532 ± 0.023	2
461	PRO136HG2	0.8782 ± 0.012	2	514	GLU141HG2	1.9382 ± 0.018	2
462	PRO136HG3	-0.1008 ± 0.011	2	515	GLU141HG3	1.7362 ± 0.016	2
463	LYS137 C	179.9642 ± 0.001	1	516	GLU141H	7.3992 ± 0.009	1
464	LYS137 CA	56.6512 ± 0.043	1	517	GLU141N	127.7902 ± 0.047	1
465	LYS137 CB	32.2932 ± 0.078	1	518	GLU142C	179.4542 ± 0.011	1
466	LYS137 CD	28.8272 ± 0.063	1	519	GLU142CA	58.8912 ± 0.064	1
467	LYS137 CE	41.9882 ± 0.119	1	520	GLU142CB	29.0182 ± 0.085	1
468	LYS137 CG	25.4372 ± 0.050	1	521	GLU142CG	36.3882 ± 0.106	1
469	LYS137 HA	4.2522 ± 0.006	1	522	GLU142HA	3.9212 ± 0.037	1
470	LYS137 HB2	2.1582 ± 0.010	2	523	GLU142HB2	1.9992 ± 0.012	2
471	LYS137 HB3	1.7112 ± 0.010	2	524	GLU142HB3	1.9992 ± 0.012	2
472	LYS137 HD2	1.7282 ± 0.014	2	525	GLU142HG2	2.3322 ± 0.022	2
473	LYS137 HD3	1.7282 ± 0.014	2	526	GLU142HG3	2.3322 ± 0.022	2
474	LYS137 HE2	3.0262 ± 0.003	2	527	GLU142H	8.5562 ± 0.011	1
475	LYS137 HE3	3.0262 ± 0.003	2	528	GLU142N	116.4052 ± 0.123	1
476	LYS137 HG2	1.6342 ± 0.003	2	529	GLY143C	177.6242 ± 0.008	1
477	LYS137 HG3	1.5692 ± 0.002	2	530	GLY143CA	47.2912 ± 0.099	1

531	GLY143HA2	3.6392 ± 0.014	2	584	PHE147 CD2	133.3442 ± 0.065	3
532	GLY143HA3	3.6392 ± 0.014	2	585	PHE147 CE1	130.8072 ± 0.199	3
533	GLY143H	8.2742 ± 0.007	1	586	PHE147 CE2	130.8072 ± 0.199	3
534	GLY143N	108.7152 ± 0.104	1	587	PHE147 HA	4.1482 ± 0.008	1
535	TRP144 C	178.4112 ± 0.015	1	588	PHE147 HB2	3.0312 ± 0.023	2
536	TRP144 CA	61.9702 ± 0.066	1	589	PHE147 HB3	2.8242 ± 0.013	2
537	TRP144 CB	30.1102 ± 0.135	1	590	PHE147 HD1	7.1412 ± 0.005	3
538	TRP144 CD1	128.2382 ± 0.087	1	591	PHE147 HD2	7.1412 ± 0.005	3
539	TRP144 CH2	123.6472 ± 0.087	1	592	PHE147 HE1	6.8392 ± 0.017	3
540	TRP144 CZ2	115.1562 ± 0.182	1	593	PHE147 HE2	6.8392 ± 0.017	3
541	TRP144 HA	4.1782 ± 0.016	1	594	PHE147 H	8.4332 ± 0.010	1
542	TRP144 HB2	3.3022 ± 0.014	2	595	PHE147 N	122.7912 ± 0.128	1
543	TRP144 HB3	3.0282 ± 0.014	2	596	CYS148 C	175.1462 ± 0.025	1
544	TRP144 HD1	7.2712 ± 0.009	1	597	CYS148 CA	62.2652 ± 0.129	1
545	TRP144 HE1	8.1462 ± 0.006	1	598	CYS148 CB	27.8802 ± 0.142	1
546	TRP144 HH2	6.7262 ± 0.005	1	599	CYS148 HA	4.0212 ± 0.008	1
547	TRP144 H	8.4292 ± 0.007	1	600	CYS148 HB2	2.0102 ± 0.007	2
548	TRP144 HZ2	7.0962 ± 0.004	1	601	CYS148 HB3	1.5732 ± 0.011	2
549	TRP144 HZ3	6.4482 ± 0.002	1	602	CYS148 H	8.1422 ± 0.011	1
550	TRP144 N	123.2572 ± 0.140	1	603	CYS148 N	113.2762 ± 0.120	1
551	TRP144 NE1	127.0622 ± 0.034	1	604	LEU149 C	177.5342 ± 0.007	1
552	LYS145 C	177.6482 ± 0.003	1	605	LEU149 CA	54.2522 ± 0.148	1
553	LYS145 CA	61.3962 ± 0.107	1	606	LEU149 CB	41.9742 ± 0.136	1
554	LYS145 CB	32.3202 ± 0.119	1	607	LEU149 CD1	23.2352 ± 0.084	1
555	LYS145 CG	27.1042 ± 0.146	1	608	LEU149 CD2	20.9562 ± 0.103	1
556	LYS145 HA	3.4672 ± 0.008	1	609	LEU149 CG	26.5072 ± 0.170	1
557	LYS145 HB2	1.8022 ± 0.024	2	610	LEU149 HA	4.2182 ± 0.011	1
558	LYS145 HB3	1.8022 ± 0.024	2	611	LEU149 HB2	1.3232 ± 0.013	2
559	LYS145 HG2	1.6582 ± 0.014	2	612	LEU149 HB3	1.0082 ± 0.016	2
560	LYS145 HG3	1.6582 ± 0.014	2	613	LEU149 HD1	-0.6808 ± 0.011	1
561	LYS145 H	7.9552 ± 0.008	1	614	LEU149 HD2	0.1902 ± 0.007	1
562	LYS145 N	119.4302 ± 0.104	1	615	LEU149 HG	0.9152 ± 0.009	1
563	LYS146 C	179.4912 ± 0.028	1	616	LEU149 H	7.6832 ± 0.012	1
564	LYS146 CA	59.4672 ± 0.085	1	617	LEU149 N	112.7562 ± 0.105	1
565	LYS146 CB	32.5542 ± 0.063	1	618	GLY150 C	173.3752 ± 0.052	1
566	LYS146 CD	29.5262 ± 0.192	1	619	GLY150 CA	44.6662 ± 0.091	1
567	LYS146 CE	42.0682 ± 0.147	1	620	GLY150HA2	3.9432 ± 0.016	2
568	LYS146 CG	26.2222 ± 0.083	1	621	GLY150HA3	3.4892 ± 0.008	2
569	LYS146 HA	3.7532 ± 0.019	1	622	GLY150H	7.6142 ± 0.009	1
570	LYS146 HB2	1.7592 ± 0.005	2	623	GLY150N	107.0922 ± 0.120	1
571	LYS146 HB3	1.7592 ± 0.005	2	624	GLU151 CG	33.7612	1
572	LYS146 HD2	1.6642 ± 0.017	2	625	GLU151 HG2	2.3612	2
573	LYS146 HD3	1.6642 ± 0.017	2	626	GLU151 HG3	2.3612	2
574	LYS146 HE2	2.9182 ± 0.010	2	627	GLU151 H	8.3402 ± 0.006	1
575	LYS146 HE3	2.9182 ± 0.010	2	628	GLU151 N	118.3642 ± 0.144	1
576	LYS146 HG2	1.5252 ± 0.007	2	629	LYS152 C	178.2312	1
577	LYS146 HG3	1.2982 ± 0.005	2	630	LYS152 CA	58.8852 ± 0.070	1
578	LYS146 H	7.6502 ± 0.008	1	631	LYS152 CB	32.2132 ± 0.176	1
579	LYS146 N	116.6852 ± 0.042	1	632	LYS152 CD	29.2412	1
580	PHE147 C	175.4162 ± 0.037	1	633	LYS152 CE	41.8662 ± 0.074	1
581	PHE147 CA	61.7822 ± 0.101	1	634	LYS152 CG	25.0712 ± 0.129	1
582	PHE147 CB	40.3962 ± 0.097	1	635	LYS152 HA	4.1062 ± 0.031	1
583	PHE147 CD1	133.3442 ± 0.065	3	636	LYS152 HB2	1.8262	2

637	LYS152 HB3	1.8262	2	690	ALA158H	8.0802 ± 0.010	1
638	LYS152 HE2	2.9622 ± 0.021	2	691	ALA158N	123.5882 ± 0.064	1
639	LYS152 HE3	2.9622 ± 0.021	2	692	VAL159C	176.3312 ± 0.013	1
640	LYS152 HG2	1.4442 ± 0.014	2	693	VAL159CA	62.0912 ± 0.117	1
641	LYS152 HG3	1.4442 ± 0.014	2	694	VAL159CB	32.9352 ± 0.059	1
642	LEU153 C	178.4632	1	695	VAL159CG1	20.9582 ± 0.173	2
643	LEU153 CA	56.1882 ± 0.075	1	696	VAL159CG2	20.9582 ± 0.173	2
644	LEU153 CB	42.1572 ± 0.108	1	697	VAL159HA	4.1722 ± 0.004	1
645	LEU153 CD1	24.4172 ± 0.256	2	698	VAL159HB	2.1012 ± 0.002	1
646	LEU153 CD2	24.4172 ± 0.256	2	699	VAL159HG1	0.9532 ± 0.005	2
647	LEU153 CG	27.8492 ± 0.087	1	700	VAL159HG2	0.9532 ± 0.005	2
648	LEU153 HA	4.3852 ± 0.007	1	701	VAL159H	8.1182 ± 0.006	1
649	LEU153 HB2	1.6332 ± 0.015	2	702	VAL159N	118.9252 ± 0.050	1
650	LEU153 HB3	1.6332 ± 0.015	2	703	GLY160C	171.6202	1
651	LEU153 HD1	0.9862 ± 0.014	2	704	GLY160CA	44.4732 ± 0.116	1
652	LEU153 HD2	0.9862 ± 0.014	2	705	GLY160HA2	4.1782 ± 0.008	2
653	LEU153 HG	1.7302 ± 0.008	1	706	GLY160HA3	4.0082 ± 0.012	2
654	LEU153 H	8.0752 ± 0.011	1	707	GLY160H	8.3112 ± 0.007	1
655	LEU153 N	119.6572 ± 0.089	1	708	GLY160N	112.6552 ± 0.049	1
656	CYS154 C	174.5262	1	709	PRO161 C	176.8082 ± 0.020	1
657	CYS154 CA	60.4722 ± 0.114	1	710	PRO161 CA	63.1012 ± 0.094	1
658	CYS154 CB	27.9452 ± 0.137	1	711	PRO161 CB	32.2032 ± 0.089	1
659	CYS154 HA	4.5482 ± 0.008	1	712	PRO161 CD	49.8352 ± 0.101	1
660	CYS154 HB2	2.9472 ± 0.007	2	713	PRO161 CG	27.2062 ± 0.128	1
661	CYS154 HB3	2.7162 ± 0.013	2	714	PRO161 HA	4.4222 ± 0.007	1
662	CYS154 H	7.6852 ± 0.011	1	715	PRO161 HB2	2.2592 ± 0.008	2
663	CYS154 N	116.1582 ± 0.070	1	716	PRO161 HB3	1.9322 ± 0.007	2
664	ALA155C	177.3912 ± 0.014	1	717	PRO161 HB3	1.9322 ± 0.007	2
665	ALA155CA	52.7272 ± 0.062	1	718	PRO161 HD2	3.6142 ± 0.003	2
666	ALA155CB	19.3542 ± 0.109	1	719	PRO161 HD3	3.6142 ± 0.003	2
667	ALA155HA	4.3802 ± 0.019	1	720	PRO161 HG2	1.9942 ± 0.011	2
668	ALA155HB	1.4602 ± 0.013	1	721	PRO161 HG3	1.9942 ± 0.011	2
669	ALA155H	7.9282 ± 0.008	1	722	ALA162C	178.0262 ± 0.011	1
670	ALA155N	124.1472 ± 0.089	1	723	ALA162CA	52.4502 ± 0.047	1
671	ASP156 C	176.7962 ± 0.014	1	724	ALA162CB	19.2402 ± 0.105	1
672	ASP156 CA	54.6302 ± 0.073	1	725	ALA162HA	4.3802 ± 0.007	1
673	ASP156 CB	41.1692 ± 0.082	1	726	ALA162HB	1.4002 ± 0.006	1
674	ASP156 HA	4.6082 ± 0.010	1	727	ALA162H	8.4642 ± 0.007	1
675	ASP156 HB2	2.7032 ± 0.011	2	728	ALA162N	124.3482 ± 0.056	1
676	ASP156 HB3	2.7032 ± 0.011	2	729	THR163C	174.3552 ± 0.018	1
677	ASP156 H	8.3162 ± 0.006	1	730	THR163CA	61.6702 ± 0.081	1
678	ASP156 N	119.6032 ± 0.128	1	731	THR163CB	69.9712 ± 0.138	1
679	GLY157C	173.8652 ± 0.018	1	732	THR163CG2	21.5482 ± 0.093	1
680	GLY157CA	45.4142 ± 0.113	1	733	THR163HA	4.3282 ± 0.007	1
681	GLY157HA2	3.9582 ± 0.017	2	734	THR163HB	4.2412 ± 0.006	1
682	GLY157HA3	3.9582 ± 0.017	2	735	THR163HG2	1.1832 ± 0.005	1
683	GLY157H	8.3592 ± 0.005	1	736	THR163H	8.1662 ± 0.009	1
684	GLY157N	109.2052 ± 0.065	1	737	THR163N	113.1282 ± 0.029	1
685	ALA158C	177.6422 ± 0.017	1	738	ASN164C	174.9882 ± 0.016	1
686	ALA158CA	52.4642 ± 0.063	1	739	ASN164CA	53.4272 ± 0.077	1
687	ALA158CB	19.3642 ± 0.086	1	740	ASN164CB	38.9272 ± 0.137	1
688	ALA158HA	4.3712 ± 0.006	1	741	ASN164HA	4.6972 ± 0.006	1
689	ALA158HB	1.3972 ± 0.008	1	742	ASN164HB2	2.8312 ± 0.010	2

743	ASN164HB3	2.7572 ± 0.010	2	796	ILE169 N	119.6912 ± 0.049	1
744	ASN164H	8.4332 ± 0.007	1	797	ASP170 C	176.5152 ± 0.024	1
745	ASN164N	120.3192 ± 0.055	1	798	ASP170 CA	53.2502 ± 0.147	1
746	GLU165C	176.1772 ± 0.018	1	799	ASP170 CB	40.9852 ± 0.106	1
747	GLU165CA	56.5772 ± 0.031	1	800	ASP170 HA	4.5522 ± 0.007	1
748	GLU165CB	30.4172 ± 0.095	1	801	ASP170 HB2	2.6852 ± 0.014	2
749	GLU165CG	36.2452 ± 0.060	1	802	ASP170 HB3	2.4792 ± 0.020	2
750	GLU165HA	4.2892 ± 0.006	1	803	ASP170 H	8.1412 ± 0.005	1
751	GLU165HB2	2.0542 ± 0.009	2	804	ASP170 N	124.5832 ± 0.041	1
752	GLU165HB3	1.9242 ± 0.077	2	805	TYR171C	177.2142 ± 0.018	1
753	GLU165HG2	2.2152 ± 0.011	2	806	TYR171CA	58.5772 ± 0.081	1
754	GLU165HG3	2.2152 ± 0.011	2	807	TYR171CB	36.9112 ± 0.064	1
755	GLU165H	8.3552 ± 0.007	1	808	TYR171CD1	133.0372 ± 0.144	3
756	GLU165N	120.8682 ± 0.041	1	809	TYR171CD2	133.0372 ± 0.144	3
757	SER166 C	172.6942	1	810	TYR171CE1	118.1782 ± 0.222	3
758	SER166 CA	56.1982 ± 0.125	1	811	TYR171CE2	118.1782 ± 0.222	3
759	SER166 CB	63.4072 ± 0.127	1	812	TYR171HA	4.1352 ± 0.014	1
760	SER166 HA	4.7402 ± 0.004	1	813	TYR171HB2	2.0772 ± 0.020	2
761	SER166 HB2	3.8482 ± 0.004	2	814	TYR171HB3	1.9102 ± 0.024	2
762	SER166 HB3	3.8062 ± 0.001	2	815	TYR171HD1	6.9812 ± 0.013	3
763	SER166 H	8.3262 ± 0.008	1	816	TYR171HD2	6.9812 ± 0.013	3
764	SER166 N	117.8332 ± 0.022	1	817	TYR171HE1	6.7482 ± 0.016	3
765	PRO167 C	177.2652 ± 0.023	1	818	TYR171HE2	6.7482 ± 0.016	3
766	PRO167 CA	63.4222 ± 0.121	1	819	TYR171H	8.0562 ± 0.009	1
767	PRO167 CB	32.0822 ± 0.069	1	820	TYR171N	122.4142 ± 0.052	1
768	PRO167 CD	50.6682 ± 0.052	1	821	VAL172CA	64.8612 ± 0.092	1
769	PRO167 CG	27.2242 ± 0.069	1	822	VAL172CB	31.7682 ± 0.053	1
770	PRO167 HA	4.4292 ± 0.010	1	823	VAL172CG1	21.4982 ± 0.042	1
771	PRO167 HB2	2.2532 ± 0.008	2	824	VAL172CG2	22.2262 ± 0.116	1
772	PRO167 HB3	1.9482 ± 0.012	2	825	VAL172HA	3.8292 ± 0.007	1
773	PRO167 HD2	3.7622 ± 0.004	2	826	VAL172HB	2.1322 ± 0.014	1
774	PRO167 HD3	3.7092 ± 0.005	2	827	VAL172HG1	0.9022 ± 0.017	1
775	PRO167 HG2	1.9972 ± 0.004	2	828	VAL172HG2	1.0192 ± 0.011	1
776	PRO167 HG3	1.9972 ± 0.004	2	829	VAL172H	7.8862 ± 0.007	1
777	GLY168C	173.5902 ± 0.027	1	830	VAL172N	120.3352 ± 0.098	1
778	GLY168CA	45.0592 ± 0.082	1	831	GLN173CA	57.9392 ± 0.098	1
779	GLY168HA2	3.8962 ± 0.009	2	832	GLN173CB	29.6892 ± 0.073	1
780	GLY168HA3	3.8962 ± 0.009	2	833	GLN173CG	33.8032 ± 0.073	1
781	GLY168H	8.2582 ± 0.007	1	834	GLN173HA	4.2002 ± 0.013	1
782	GLY168N	108.8372 ± 0.052	1	835	GLN173HB2	2.1012 ± 0.010	2
783	ILE169 C	175.2752 ± 0.016	1	836	GLN173HB3	2.1012 ± 0.010	2
784	ILE169 CA	60.8782 ± 0.103	1	837	GLN173HG2	2.3272 ± 0.021	2
785	ILE169 CB	38.6252 ± 0.071	1	838	GLN173HG3	2.3272 ± 0.021	2
786	ILE169 CD1	13.0192 ± 0.197	1	839	GLN173H	7.6212 ± 0.010	1
787	ILE169 CG1	27.1052 ± 0.090	1	840	GLN173N	118.3042 ± 0.105	1
788	ILE169 CG2	17.5252 ± 0.039	1	841	ILE174 C	175.6882	1
789	ILE169 HA	4.0012 ± 0.011	1	842	ILE174 CA	61.9282 ± 0.111	1
790	ILE169 HB	1.6542 ± 0.008	1	843	ILE174 CB	39.3162 ± 0.066	1
791	ILE169 HD1	0.7832 ± 0.008	1	844	ILE174 CD1	14.1042 ± 0.128	1
792	ILE169 HG12	1.3192 ± 0.010	2	845	ILE174 CG1	26.1752 ± 0.113	1
793	ILE169 HG13	1.0122 ± 0.012	2	846	ILE174 CG2	17.9792 ± 0.075	1
794	ILE169 HG2	0.5832 ± 0.005	1	847	ILE174 HA	4.3942 ± 0.010	1
795	ILE169 H	7.9752 ± 0.008	1	848	ILE174 HB	2.0502 ± 0.014	1

849	ILE174 HD1	0.7892 ± 0.003	1	902	LEU179 HG	1.5352 ± 0.009	1
850	ILE174 HG12	1.5432 ± 0.017	2	903	LEU179 H	8.1232 ± 0.010	1
851	ILE174 HG13	1.0222 ± 0.009	2	904	LEU179 N	123.6092 ± 0.113	1
852	ILE174 HG2	0.8812 ± 0.010	1	905	LEU180 CA	58.8072 ± 0.164	1
853	ILE174 H	7.8822 ± 0.005	1	906	LEU180 CB	40.2762 ± 0.103	1
854	ILE174 N	114.0152 ± 0.123	1	907	LEU180 CD1	25.8702 ± 0.099	1
855	GLY175C	172.6152 ± 0.017	1	908	LEU180 CD2	23.7372 ± 0.108	1
856	GLY175CA	44.2822 ± 0.105	1	909	LEU180 CG	27.3842 ± 0.076	1
857	GLY175HA2	3.6942 ± 0.012	2	910	LEU180 HA	3.8282 ± 0.015	1
858	GLY175HA3	3.2482 ± 0.012	2	911	LEU180 HB2	1.1742 ± 0.011	2
859	GLY175H	7.8182 ± 0.006	1	912	LEU180 HB3	0.3592 ± 0.015	2
860	GLY175N	112.3212 ± 0.061	1	913	LEU180 HD1	0.5382 ± 0.013	1
861	PHE176 C	176.9782	1	914	LEU180 HD2	0.6752 ± 0.014	1
862	PHE176 CB	38.8482 ± 0.057	1	915	LEU180 HG	1.4002 ± 0.008	1
863	PHE176 CD1	132.5932 ± 0.127	3	916	LEU180 H	8.7952 ± 0.010	1
864	PHE176 CD2	132.5932 ± 0.127	3	917	LEU180 N	128.5722 ± 0.119	1
865	PHE176 CE1	131.4192 ± 0.148	3	918	SER181 C	174.6422	1
866	PHE176 CE2	131.4192 ± 0.148	3	919	SER181 CA	60.9872 ± 0.032	1
867	PHE176 HA	4.1882 ± 0.025	1	920	SER181 CB	61.7412	1
868	PHE176 HB2	2.4202 ± 0.019	2	921	SER181 HB2	3.9352	2
869	PHE176 HB3	2.0332 ± 0.008	2	922	SER181 HB3	3.9352	2
870	PHE176 HD1	6.7282 ± 0.009	3	923	ILE182 C	177.8772	1
871	PHE176 HD2	6.7282 ± 0.009	3	924	ILE182 CA	64.3612 ± 0.120	1
872	PHE176 HE1	7.1122 ± 0.011	3	925	ILE182 CB	39.6462 ± 0.086	1
873	PHE176 HE2	7.1122 ± 0.011	3	926	ILE182 CD1	13.8512 ± 0.778	1
874	PHE176 H	8.6472 ± 0.007	1	927	ILE182 CG1	28.8372 ± 0.141	1
875	PHE176 N	122.1882 ± 0.091	1	928	ILE182 CG2	17.2192 ± 0.082	1
876	PRO177 CD	49.4552 ± 0.117	1	929	ILE182 HA	4.1492 ± 0.006	1
877	PRO177 CG	26.1712 ± 0.065	1	930	ILE182 HB	2.1162 ± 0.009	1
878	PRO177 HD2	3.3662 ± 0.005	2	931	ILE182 HD1	1.1822 ± 0.019	1
879	PRO177 HD3	3.1712 ± 0.035	2	932	ILE182 HG12	1.8942 ± 0.012	2
880	PRO177 HG2	1.9182 ± 0.003	2	933	ILE182 HG13	1.0432 ± 0.012	2
881	PRO177 HG3	1.7202 ± 0.002	2	934	ILE182 HG2	1.3432 ± 0.007	1
882	PRO178 C	174.1332	1	935	ILE182 H	6.9842 ± 0.067	1
883	PRO178 CA	61.5752 ± 0.046	1	936	ILE182 N	119.6052 ± 0.041	1
884	PRO178 CB	25.8942	1	937	VAL183C	179.8932 ± 0.028	1
885	PRO178 CD	48.6692 ± 0.096	1	938	VAL183CA	65.0752 ± 0.097	1
886	PRO178 CG	30.9472 ± 0.055	1	939	VAL183CB	30.9862 ± 0.100	1
887	PRO178 HD2	2.7862 ± 0.014	2	940	VAL183CG1	22.2732 ± 0.062	1
888	PRO178 HD3	2.1292 ± 0.016	2	941	VAL183CG2	19.9172 ± 0.063	1
889	PRO178 HG2	2.1422	2	942	VAL183HA	4.2432 ± 0.013	1
890	PRO178 HG3	1.5002 ± 0.001	2	943	VAL183HB	2.5142 ± 0.011	1
891	LEU179 C	178.3672	1	944	VAL183HG1	0.8412 ± 0.007	1
892	LEU179 CA	54.0632 ± 0.102	1	945	VAL183HG2	0.7412 ± 0.007	1
893	LEU179 CB	40.9902 ± 0.026	1	946	VAL183H	8.4972 ± 0.007	1
894	LEU179 CD1	24.5332 ± 0.088	1	947	VAL183N	110.7972 ± 0.059	1
895	LEU179 CD2	21.8992 ± 0.109	1	948	SER184 C	173.9842 ± 0.007	1
896	LEU179 CG	26.7122 ± 0.082	1	949	SER184 CA	62.2532 ± 0.119	1
897	LEU179 HA	3.9502 ± 0.006	1	950	SER184 CB	63.3382 ± 0.043	1
898	LEU179 HB2	1.7652	2	951	SER184 HA	4.1742 ± 0.011	1
899	LEU179 HB3	1.2742	2	952	SER184 HB2	3.8602 ± 0.006	2
900	LEU179 HD1	0.9242 ± 0.006	1	953	SER184 HB3	3.8602 ± 0.006	2
901	LEU179 HD2	0.5602 ± 0.005	1	954	SER184 H	8.5882 ± 0.011	1

955	SER184 N	115.5632 ± 0.079	1	1008	THR190C	174.7502	1
956	ARG185 C	176.0212 ± 0.015	1	1009	THR190CA	67.3932 ± 0.156	1
957	ARG185 CA	56.2032 ± 0.082	1	1010	THR190CB	68.1052 ± 0.115	1
958	ARG185 CB	31.5152 ± 0.030	1	1011	THR190CG2	21.4182 ± 0.155	1
959	ARG185 CG	28.6742	1	1012	THR190HA	3.7102 ± 0.013	1
960	ARG185 HA	4.2432	1	1013	THR190HB	4.1692 ± 0.006	1
961	ARG185 HB2	2.0032 ± 0.017	2	1014	THR190HG2	1.0212 ± 0.012	1
962	ARG185 HB3	2.0032 ± 0.017	2	1015	THR190H	8.2862 ± 0.010	1
963	ARG185 HD2	2.8252 ± 0.018	2	1016	THR190N	117.2792 ± 0.088	1
964	ARG185 HD3	2.8252 ± 0.018	2	1017	VAL191C	176.8822	1
965	ARG185 HG2	1.7672	2	1018	VAL191CA	67.5272 ± 0.134	1
966	ARG185 HG3	1.7672	2	1019	VAL191CB	32.1232 ± 0.089	1
967	ARG185 H	7.2382 ± 0.011	1	1020	VAL191CG1	22.7052 ± 0.075	1
968	ARG185 N	116.2022 ± 0.102	1	1021	VAL191CG2	23.7762 ± 0.122	1
969	MET186 C	175.7342 ± 0.013	1	1022	VAL191HA	3.1862 ± 0.007	1
970	MET186 CA	55.8302 ± 0.107	1	1023	VAL191HB	2.0182 ± 0.009	1
971	MET186 CB	34.7382 ± 0.112	1	1024	VAL191HG1	0.7922 ± 0.007	1
972	MET186 CE	18.3622 ± 0.051	1	1025	VAL191HG2	0.8992 ± 0.008	1
973	MET186 CG	32.2152 ± 0.055	1	1026	VAL191H	8.6412 ± 0.007	1
974	MET186 HA	4.4162 ± 0.007	1	1027	VAL191N	122.2392 ± 0.058	1
975	MET186 HB2	2.1272 ± 0.011	2	1028	THR192C	175.6662	1
976	MET186 HB3	1.8902 ± 0.007	2	1029	THR192CA	67.5332 ± 0.130	1
977	MET186 HE	1.6632 ± 0.007	1	1030	THR192CB	68.2482 ± 0.092	1
978	MET186 HG2	2.3052 ± 0.003	2	1031	THR192CG2	21.5812 ± 0.106	1
979	MET186 HG3	2.3052 ± 0.003	2	1032	THR192HA	3.4592 ± 0.012	1
980	MET186 H	7.3492 ± 0.009	1	1033	THR192HB	4.1162 ± 0.014	1
981	MET186 N	119.4792 ± 0.134	1	1034	THR192HG2	1.0212 ± 0.005	1
982	ASN187 C	175.0222	1	1035	THR192H	7.7452 ± 0.009	1
983	ASN187CA	51.6252 ± 0.080	1	1036	THR192N	111.8942 ± 0.093	1
984	ASN187CB	37.5332 ± 0.191	1	1037	SER193 C	173.2262	1
985	ASN187HA	4.7502 ± 0.011	1	1038	SER193 CA	62.7462 ± 0.137	1
986	ASN187HB2	3.4792 ± 0.017	2	1039	SER193 CB	68.1622 ± 0.166	1
987	ASN187HB3	3.1072 ± 0.012	2	1040	SER193 HA	3.7132 ± 0.024	1
988	ASN187H	8.7782 ± 0.005	1	1041	SER193 HB2	4.1652 ± 0.011	2
989	ASN187N	123.1862 ± 0.073	1	1042	SER193 HB3	4.1652 ± 0.011	2
990	GLN188C	178.7142 ± 0.031	1	1043	SER193 H	7.8642 ± 0.010	1
991	GLN188CA	59.0632 ± 0.098	1	1044	SER193 N	118.6862 ± 0.089	1
992	GLN188CB	28.3472 ± 0.113	1	1045	VAL194C	177.8452 ± 0.006	1
993	GLN188CG	34.7792 ± 0.005	1	1046	VAL194CA	66.9582 ± 0.077	1
994	GLN188HA	3.8932 ± 0.020	1	1047	VAL194CB	30.1142 ± 0.062	1
995	GLN188HB2	2.0772 ± 0.038	2	1048	VAL194CG1	22.8572 ± 0.071	1
996	GLN188HB3	2.0772 ± 0.038	2	1049	VAL194CG2	20.8482 ± 0.085	1
997	GLN188HG2	2.5322 ± 0.008	2	1050	VAL194HA	2.9002 ± 0.005	1
998	GLN188HG3	2.5322 ± 0.008	2	1051	VAL194HB	1.3162 ± 0.010	1
999	GLN188H	8.8202 ± 0.012	1	1052	VAL194HG1	0.3752 ± 0.006	1
1000	GLN188N	117.9292 ± 0.082	1	1053	VAL194HG2	-0.7728 ± 0.004	1
1001	ALA189C	180.1982 ± 0.003	1	1054	VAL194H	8.1852 ± 0.008	1
1002	ALA189CA	55.1112 ± 0.114	1	1055	VAL194N	120.0002 ± 0.122	1
1003	ALA189CB	17.6592 ± 0.103	1	1056	LEU195 C	178.9742	1
1004	ALA189HA	4.0442 ± 0.010	1	1057	LEU195 CA	58.5512 ± 0.157	1
1005	ALA189HB	1.4032 ± 0.009	1	1058	LEU195 CB	41.6362 ± 0.063	1
1006	ALA189H	8.5432 ± 0.013	1	1059	LEU195 CD1	24.5192 ± 0.089	1
1007	ALA189N	123.9622 ± 0.101	1	1060	LEU195 CD2	25.6402 ± 0.101	1

1061	LEU195 CG	27.0242	1	1114	SER199 HA	4.3452 ± 0.041	1
1062	LEU195 HA	3.8212 ± 0.015	1	1115	SER199 HB2	4.0572 ± 0.008	2
1063	LEU195 HB2	1.7282	2	1116	SER199 HB3	4.0572 ± 0.008	2
1064	LEU195 HB3	1.6892 ± 0.019	2	1117	SER199 H	8.6132 ± 0.011	1
1065	LEU195 HD1	0.7832 ± 0.013	1	1118	SER199 N	117.1482 ± 0.113	1
1066	LEU195 HD2	0.7412 ± 0.011	1	1119	ASN200C	178.8042	1
1067	LEU195 HG	1.5272 ± 0.015	1	1120	ASN200CA	55.6382 ± 0.129	1
1068	LEU195 H	7.9602 ± 0.008	1	1121	ASN200CB	36.9522 ± 0.107	1
1069	LEU195 N	120.3292 ± 0.097	1	1122	ASN200HA	4.5332 ± 0.008	1
1070	GLU196C	178.1342 ± 0.029	1	1123	ASN200HB2	3.3232 ± 0.010	2
1071	GLU196CA	59.9922 ± 0.059	1	1124	ASN200HB3	3.0182 ± 0.011	2
1072	GLU196CB	28.1552 ± 0.012	1	1125	ASN200H	8.9372 ± 0.012	1
1073	GLU196CG	35.3792 ± 0.122	1	1126	ASN200N	122.4932 ± 0.120	1
1074	GLU196HA	4.3992	1	1127	TRP201 C	177.9742	1
1075	GLU196HB2	2.2102 ± 0.008	2	1128	TRP201 CA	61.5752 ± 0.105	1
1076	GLU196HB3	1.9322 ± 0.013	2	1129	TRP201 CB	29.5152 ± 0.098	1
1077	GLU196HG2	2.2172 ± 0.014	2	1130	TRP201 HA	4.2822 ± 0.010	1
1078	GLU196HG3	2.2172 ± 0.014	2	1131	TRP201 HB2	3.1922 ± 0.004	2
1079	GLU196H	7.7842 ± 0.008	1	1132	TRP201 HB3	3.1922 ± 0.004	2
1080	GLU196N	122.8062 ± 0.052	1	1133	TRP201 HE1	11.5112	1
1081	TYR197C	179.8722 ± 0.026	1	1134	TRP201 H	8.0972 ± 0.009	1
1082	TYR197CA	57.8212 ± 0.203	1	1135	TRP201 N	122.6142 ± 0.056	1
1083	TYR197CB	36.7862 ± 0.119	1	1136	TRP201 NE1	120.1722	1
1084	TYR197CD1	125.1852	3	1137	PHE202 C	176.9842	1
1085	TYR197CD2	125.1852	3	1138	PHE202 CA	55.4532 ± 0.156	1
1086	TYR197CE1	114.8832 ± 0.095	3	1139	PHE202 CB	34.3682 ± 0.110	1
1087	TYR197CE2	114.8832 ± 0.095	3	1140	PHE202 HA	4.5232 ± 0.018	1
1088	TYR197HA	4.6572 ± 0.015	1	1141	PHE202 HB2	2.4052 ± 0.008	2
1089	TYR197HB2	3.2432 ± 0.019	2	1142	PHE202 HB3	2.0482 ± 0.002	2
1090	TYR197HB3	3.0292 ± 0.030	2	1143	PHE202 H	8.7662 ± 0.014	1
1091	TYR197HD1	7.2382	3	1144	PHE202 N	117.5522 ± 0.096	1
1092	TYR197HD2	7.2382	3	1145	GLY203C	173.5372 ± 0.049	1
1093	TYR197HE1	7.4542 ± 0.015	3	1146	GLY203CA	46.9272 ± 0.066	1
1094	TYR197HE2	7.4542 ± 0.015	3	1147	GLY203HA2	3.9912 ± 0.007	2
1095	TYR197H	8.4362 ± 0.007	1	1148	GLY203HA3	3.5082 ± 0.015	2
1096	TYR197N	120.4102 ± 0.075	1	1149	GLY203H	8.2742 ± 0.005	1
1097	LEU198 C	179.5372	1	1150	GLY203N	105.5652 ± 0.046	1
1098	LEU198 CA	57.6332 ± 0.069	1	1151	GLU204C	175.8192	1
1099	LEU198 CB	40.8662 ± 0.205	1	1152	GLU204CA	55.3432 ± 0.090	1
1100	LEU198 CD1	26.0062 ± 0.130	1	1153	GLU204CB	31.8022 ± 0.068	1
1101	LEU198 CD2	20.5532 ± 0.069	1	1154	GLU204CG	35.9982 ± 0.071	1
1102	LEU198 CG	26.6152 ± 0.197	1	1155	GLU204HA	4.4742 ± 0.015	1
1103	LEU198 HA	4.2262 ± 0.011	1	1156	GLU204HB2	2.0662 ± 0.013	2
1104	LEU198 HB2	1.7892	2	1157	GLU204HB3	1.8002 ± 0.010	2
1105	LEU198 HB3	1.3012 ± 0.004	2	1158	GLU204HG2	2.1442 ± 0.002	2
1106	LEU198 HD1	0.7452 ± 0.007	1	1159	GLU204HG3	2.1442 ± 0.002	2
1107	LEU198 HD2	0.4972 ± 0.037	1	1160	GLU204H	7.0802 ± 0.014	1
1108	LEU198 HG	1.8882 ± 0.014	1	1161	GLU204N	114.6252 ± 0.042	1
1109	LEU198 H	8.9722 ± 0.008	1	1162	ARG205 C	173.8252	1
1110	LEU198 N	117.4342 ± 0.100	1	1163	ARG205 CA	54.2142 ± 0.116	1
1111	SER199 C	177.6632	1	1164	ARG205 CB	32.0102 ± 0.159	1
1112	SER199 CA	62.9392 ± 0.117	1	1165	ARG205 CD	42.0352 ± 0.096	1
1113	SER199 CB	62.7822 ± 0.066	1	1166	ARG205 CG	26.6392 ± 0.139	1

1167	ARG205 HA	4.4742 ± 0.008	1	1220	PRO209 HD3	3.8852	2
1168	ARG205 HB2	1.2722 ± 0.011	2	1221	PRO209 HG2	2.1212 ± 0.021	2
1169	ARG205 HB3	0.5812 ± 0.007	2	1222	PRO209 HG3	2.1212 ± 0.021	2
1170	ARG205 HD2	2.5432 ± 0.005	2	1223	GLU210C	179.2932 ± 0.017	1
1171	ARG205 HD3	2.0112 ± 0.008	2	1224	GLU210CA	61.1742 ± 0.072	1
1172	ARG205 HG2	0.8592 ± 0.006	2	1225	GLU210CB	28.3432 ± 0.196	1
1173	ARG205 HG3	0.2992 ± 0.013	2	1226	GLU210CG	37.5942 ± 0.091	1
1174	ARG205 H	7.3512 ± 0.014	1	1227	GLU210HA	3.8522 ± 0.010	1
1175	ARG205 N	120.6452 ± 0.113	1	1228	GLU210HB2	1.9712 ± 0.010	2
1176	ASP206 C	175.5512 ± 0.009	1	1229	GLU210HB3	1.8512 ± 0.014	2
1177	ASP206 CA	52.8862 ± 0.085	1	1230	GLU210HG2	2.6532 ± 0.011	2
1178	ASP206 CB	42.3472 ± 0.119	1	1231	GLU210HG3	2.2132 ± 0.009	2
1179	ASP206 HA	4.8152 ± 0.010	1	1232	GLU210H	8.9702 ± 0.007	1
1180	ASP206 HB2	2.7212 ± 0.008	2	1233	GLU210N	115.8082 ± 0.077	1
1181	ASP206 HB3	2.6522 ± 0.004	2	1234	LEU211 C	178.1092	1
1182	ASP206 H	7.6352 ± 0.005	1	1235	LEU211 CA	57.5882 ± 0.093	1
1183	ASP206 N	116.7722 ± 0.093	1	1236	LEU211 CB	41.8052 ± 0.085	1
1184	PHE207 C	174.7032	1	1237	LEU211 CD1	23.9462 ± 0.115	1
1185	PHE207 CA	60.1712 ± 0.094	1	1238	LEU211 CD2	26.9192 ± 0.095	1
1186	PHE207 CB	40.8922 ± 0.139	1	1239	LEU211 CG	27.0332 ± 0.079	1
1187	PHE207 CD1	131.1982 ± 0.168	3	1240	LEU211 HA	3.8482 ± 0.002	1
1188	PHE207 CD2	131.1982 ± 0.168	3	1241	LEU211 HB2	1.2682 ± 0.017	2
1189	PHE207 CE1	131.2742 ± 0.085	3	1242	LEU211 HB3	1.2682 ± 0.017	2
1190	PHE207 CE2	131.2742 ± 0.085	3	1243	LEU211 HD1	0.9222 ± 0.009	1
1191	PHE207 CZ	129.1562 ± 0.026	1	1244	LEU211 HD2	0.5992 ± 0.025	1
1192	PHE207 HA	4.0322 ± 0.010	1	1245	LEU211 HG	1.1632 ± 0.018	1
1193	PHE207 HB2	3.2382 ± 0.009	2	1246	LEU211 H	6.9782 ± 0.011	1
1194	PHE207 HB3	2.7742 ± 0.027	2	1247	LEU211 N	117.9462 ± 0.096	1
1195	PHE207 HD1	6.8212 ± 0.013	3	1248	GLY212C	174.5642	1
1196	PHE207 HD2	6.8212 ± 0.013	3	1249	GLY212CA	48.8682 ± 0.119	1
1197	PHE207 HE1	7.5272 ± 0.018	3	1250	GLY212HA2	4.2832 ± 0.009	2
1198	PHE207 HE2	7.5272 ± 0.018	3	1251	GLY212HA3	3.4992 ± 0.011	2
1199	PHE207 H	9.0162 ± 0.017	1	1252	GLY212H	8.0002 ± 0.008	1
1200	PHE207 HZ	7.1722 ± 0.007	1	1253	GLY212N	106.4032 ± 0.063	1
1201	PHE207 N	119.5792 ± 0.106	1	1254	ARG213 C	179.3272 ± 0.004	1
1202	THR208 C	173.4132	1	1255	ARG213 CA	59.7722 ± 0.119	1
1203	THR208 CA	57.9532 ± 0.062	1	1256	ARG213 CB	29.4602 ± 0.217	1
1204	THR208 CB	70.3422 ± 0.152	1	1257	ARG213 CD	44.5022 ± 0.145	1
1205	THR208 CG2	22.3842 ± 0.106	1	1258	ARG213 CG	29.0462 ± 0.223	1
1206	THR208 HA	4.8912 ± 0.013	1	1259	ARG213 HA	2.8902 ± 0.013	1
1207	THR208 HB	4.6042 ± 0.008	1	1260	ARG213 HB2	1.3042 ± 0.012	2
1208	THR208 HG2	1.3632 ± 0.008	1	1261	ARG213 HB3	1.3042 ± 0.012	2
1209	THR208 H	5.7602 ± 0.012	1	1262	ARG213 HD2	2.9952 ± 0.010	2
1210	THR208 N	116.5522 ± 0.105	1	1263	ARG213 HD3	2.7802 ± 0.012	2
1211	PRO209 C	177.2412	1	1264	ARG213 HG2	1.1532 ± 0.008	2
1212	PRO209 CA	65.2672 ± 0.103	1	1265	ARG213 HG3	0.8222 ± 0.017	2
1213	PRO209 CB	32.1542 ± 0.061	1	1266	ARG213 H	8.1652 ± 0.007	1
1214	PRO209 CD	50.8612	1	1267	ARG213 N	118.3092 ± 0.122	1
1215	PRO209 CG	28.1492 ± 0.124	1	1268	TRP214 C	178.2372	1
1216	PRO209 HA	4.2512 ± 0.009	1	1269	TRP214 CA	62.8102 ± 0.095	1
1217	PRO209 HB2	2.5452 ± 0.011	2	1270	TRP214 CB	30.0512 ± 0.086	1
1218	PRO209 HB3	1.8172 ± 0.004	2	1271	TRP214 CD1	126.4712 ± 0.105	1
1219	PRO209 HD2	3.8852	2	1272	TRP214 CE3	120.4782 ± 0.131	1

1273	TRP214 CZ2	116.1242 ± 0.022	1	1326	LEU218 CD2	26.9142 ± 0.062	1
1274	TRP214 CZ3	121.9302 ± 0.162	1	1327	LEU218 CG	25.7592 ± 0.080	1
1275	TRP214 HA	3.9582 ± 0.015	1	1328	LEU218 HA	4.0182 ± 0.011	1
1276	TRP214 HB2	3.0892 ± 0.020	2	1329	LEU218 HB2	2.0612 ± 0.014	2
1277	TRP214 HB3	3.0892 ± 0.020	2	1330	LEU218 HB3	2.0612 ± 0.014	2
1278	TRP214 HD1	7.1492 ± 0.012	1	1331	LEU218 HD1	0.7762 ± 0.010	1
1279	TRP214 HE1	11.0672 ± 0.017	1	1332	LEU218 HD2	0.8492 ± 0.008	1
1280	TRP214 HE3	7.4422 ± 0.010	1	1333	LEU218 HG	1.2622 ± 0.002	1
1281	TRP214 HH2	7.1422	1	1334	LEU218 H	8.6172 ± 0.014	1
1282	TRP214 H	7.1212 ± 0.016	1	1335	LEU218 N	116.5712 ± 0.076	1
1283	TRP214 HZ2	7.4552 ± 0.004	1	1336	LEU219 C	179.9572	1
1284	TRP214 HZ3	6.8222 ± 0.014	1	1337	LEU219 CA	58.2892 ± 0.059	1
1285	TRP214 N	118.7412 ± 0.047	1	1338	LEU219 CB	41.1982 ± 0.164	1
1286	TRP214 NE1	131.5652 ± 0.038	1	1339	LEU219 CD1	25.8022 ± 0.069	1
1287	LEU215 C	178.1462	1	1340	LEU219 CD2	22.7452 ± 0.085	1
1288	LEU215 CA	58.6892 ± 0.122	1	1341	LEU219 CG	26.9192 ± 0.111	1
1289	LEU215 CB	42.0802 ± 0.104	1	1342	LEU219 HA	4.0332 ± 0.011	1
1290	LEU215 CD1	26.5102 ± 0.133	1	1343	LEU219 HB2	2.2272 ± 0.008	2
1291	LEU215 CD2	23.0462 ± 0.142	1	1344	LEU219 HB3	2.2272 ± 0.008	2
1292	LEU215 HA	4.0112 ± 0.007	1	1345	LEU219 HD1	0.7442 ± 0.008	1
1293	LEU215 HB2	2.2062 ± 0.020	2	1346	LEU219 HD2	0.5762 ± 0.006	1
1294	LEU215 HB3	1.2232 ± 0.015	2	1347	LEU219 HG	2.0542 ± 0.006	1
1295	LEU215 HD1	0.7812 ± 0.012	1	1348	LEU219 H	8.3422 ± 0.007	1
1296	LEU215 HD2	0.8632 ± 0.014	1	1349	LEU219 N	117.7672 ± 0.114	1
1297	LEU215 H	8.8332 ± 0.006	1	1350	ALA220C	177.2572 ± 0.028	1
1298	LEU215 N	117.9522 ± 0.090	1	1351	ALA220CA	54.6292 ± 0.084	1
1299	TYR216C	176.1292	1	1352	ALA220CB	17.5262 ± 0.057	1
1300	TYR216CA	62.6162 ± 0.101	1	1353	ALA220HA	3.6342 ± 0.010	1
1301	TYR216CB	40.4572 ± 0.128	1	1354	ALA220HB	1.2822 ± 0.009	1
1302	TYR216CD1	133.1602 ± 0.108	3	1355	ALA220H	8.5482 ± 0.007	1
1303	TYR216CD2	133.1602 ± 0.108	3	1356	ALA220N	120.1572 ± 0.067	1
1304	TYR216CE1	118.2862 ± 0.046	3	1357	CYS221 C	175.4432 ± 0.023	1
1305	TYR216CE2	118.2862 ± 0.046	3	1358	CYS221 CA	60.7302 ± 0.113	1
1306	TYR216HA	3.8022 ± 0.016	1	1359	CYS221 CB	29.1762 ± 0.126	1
1307	TYR216HB2	3.1972 ± 0.013	2	1360	CYS221 HA	4.2152 ± 0.007	1
1308	TYR216HB3	3.0462 ± 0.015	2	1361	CYS221 HB2	3.0102 ± 0.010	2
1309	TYR216HD1	6.8362 ± 0.011	3	1362	CYS221 HB3	3.0102 ± 0.010	2
1310	TYR216HD2	6.8362 ± 0.011	3	1363	CYS221 H	7.3452 ± 0.009	1
1311	TYR216HE1	6.5152 ± 0.017	3	1364	CYS221 N	112.0952 ± 0.085	1
1312	TYR216HE2	6.5152 ± 0.017	3	1365	LEU222 C	176.7002 ± 0.012	1
1313	TYR216H	8.6812 ± 0.009	1	1366	LEU222 CA	55.5412 ± 0.125	1
1314	TYR216N	117.9892 ± 0.083	1	1367	LEU222 CB	43.1272 ± 0.075	1
1315	ALA217C	179.0652 ± 0.051	1	1368	LEU222 CD1	24.2692 ± 0.089	1
1316	ALA217CA	55.2652 ± 0.096	1	1369	LEU222 CD2	25.1292 ± 0.104	1
1317	ALA217CB	20.3032 ± 0.082	1	1370	LEU222 CG	25.9812 ± 0.098	1
1318	ALA217HA	3.9032 ± 0.011	1	1371	LEU222 HA	4.4432 ± 0.008	1
1319	ALA217HB	1.3272 ± 0.009	1	1372	LEU222 HB2	1.7812 ± 0.016	2
1320	ALA217H	8.1832 ± 0.009	1	1373	LEU222 HB3	1.6862 ± 0.006	2
1321	ALA217N	119.7012 ± 0.113	1	1374	LEU222 HD1	0.6792 ± 0.011	1
1322	LEU218 C	179.7272	1	1375	LEU222 HD2	0.5332 ± 0.006	1
1323	LEU218 CA	58.4552 ± 0.162	1	1376	LEU222 HG	1.7032 ± 0.007	1
1324	LEU218 CB	41.0902 ± 0.166	1	1377	LEU222 H	7.3932 ± 0.011	1
1325	LEU218 CD1	25.9982 ± 0.150	1	1378	LEU222 N	123.8372 ± 0.058	1

1379	GLU223C	175.0482 ± 0.016	1	1432	LEU227 CD1	25.1172 ± 0.069	1
1380	GLU223CA	56.5992 ± 0.037	1	1433	LEU227 CD2	22.7062 ± 0.088	1
1381	GLU223CB	30.8682 ± 0.132	1	1434	LEU227 CG	27.6322 ± 0.051	1
1382	GLU223CG	36.5602 ± 0.127	1	1435	LEU227 HA	4.5632 ± 0.012	1
1383	GLU223HA	4.2872 ± 0.018	1	1436	LEU227 HB2	1.8372 ± 0.011	2
1384	GLU223HB2	1.9482 ± 0.027	2	1437	LEU227 HB3	1.6502 ± 0.012	2
1385	GLU223HB3	1.7662 ± 0.005	2	1438	LEU227 HD1	0.9812 ± 0.014	1
1386	GLU223HG2	2.3392 ± 0.016	2	1439	LEU227 HD2	1.0022 ± 0.009	1
1387	GLU223HG3	2.3392 ± 0.016	2	1440	LEU227 HG	1.9372 ± 0.006	1
1388	GLU223H	8.8472 ± 0.008	1	1441	LEU227 H	9.0302 ± 0.013	1
1389	GLU223N	127.1562 ± 0.049	1	1442	LEU227 N	125.5332 ± 0.040	1
1390	LYS224 C	175.1512	1	1443	PRO228 C	179.4492 ± 0.004	1
1391	LYS224 CA	54.2112 ± 0.087	1	1444	PRO228 CA	66.3502 ± 0.141	1
1392	LYS224 CB	33.6332 ± 0.046	1	1445	PRO228 CB	31.9572 ± 0.163	1
1393	LYS224 CG	25.4722 ± 0.361	1	1446	PRO228 CD	50.1962 ± 0.161	1
1394	LYS224 HA	4.4422 ± 0.009	1	1447	PRO228 CG	27.7272	1
1395	LYS224 HB2	1.8532	2	1448	PRO228 HA	4.2952 ± 0.008	1
1396	LYS224 HB3	1.6432	2	1449	PRO228 HB2	2.4012 ± 0.005	2
1397	LYS224 HE2	2.7852	2	1450	PRO228 HB3	1.9342 ± 0.039	2
1398	LYS224 HE3	2.7852	2	1451	PRO228 HD2	3.9012 ± 0.018	2
1399	LYS224 HG2	1.4622 ± 0.009	2	1452	PRO228 HD3	3.8412 ± 0.019	2
1400	LYS224 HG3	1.4622 ± 0.009	2	1453	PRO228 HG2	1.9662 ± 0.011	2
1401	LYS224 H	8.3492 ± 0.016	1	1454	PRO228 HG3	1.9662 ± 0.011	2
1402	LYS224 N	119.2842 ± 0.091	1	1455	GLU229C	178.7712 ± 0.015	1
1403	PRO225 C	175.7132	1	1456	GLU229CA	59.8862 ± 0.099	1
1404	PRO225 CA	61.8202 ± 0.065	1	1457	GLU229CB	28.5162 ± 0.107	1
1405	PRO225 CB	34.3132 ± 0.043	1	1458	GLU229CG	36.5802 ± 0.073	1
1406	PRO225 CD	50.6702	1	1459	GLU229HA	4.1212 ± 0.011	1
1407	PRO225 CG	25.0282 ± 0.060	1	1460	GLU229HB2	2.0042 ± 0.002	2
1408	PRO225 HA	4.5122 ± 0.007	1	1461	GLU229HB3	1.9492 ± 0.008	2
1409	PRO225 HB2	2.4152 ± 0.007	2	1462	GLU229HG2	2.3692 ± 0.005	2
1410	PRO225 HB3	2.0342 ± 0.012	2	1463	GLU229HG3	2.2872 ± 0.014	2
1411	PRO225 HD2	3.5382	2	1464	GLU229H	9.5762 ± 0.009	1
1412	PRO225 HD3	3.5382	2	1465	GLU229N	116.8972 ± 0.047	1
1413	PRO225 HG2	1.9362 ± 0.009	2	1466	ALA230C	178.4642 ± 0.034	1
1414	PRO225 HG3	1.9362 ± 0.009	2	1467	ALA230CA	54.7862 ± 0.114	1
1415	LEU226 C	178.5582 ± 0.020	1	1468	ALA230CB	19.2942 ± 0.090	1
1416	LEU226 CA	55.0792 ± 0.089	1	1469	ALA230HA	4.0632 ± 0.012	1
1417	LEU226 CB	42.5832 ± 0.140	1	1470	ALA230HB	1.5482 ± 0.011	1
1418	LEU226 CD1	26.3292 ± 0.052	1	1471	ALA230H	7.3632 ± 0.007	1
1419	LEU226 CD2	23.9862 ± 0.066	1	1472	ALA230N	121.4902 ± 0.070	1
1420	LEU226 CG	27.7812 ± 0.020	1	1473	HIS231 C	176.5482 ± 0.013	1
1421	LEU226 HA	4.3652 ± 0.013	1	1474	HIS231 CA	60.0352 ± 0.186	1
1422	LEU226 HB2	1.5712 ± 0.025	2	1475	HIS231 CB	30.6362 ± 0.132	1
1423	LEU226 HB3	1.5712 ± 0.025	2	1476	HIS231 CD2	118.4872 ± 0.180	1
1424	LEU226 HD1	0.9062 ± 0.006	1	1477	HIS231 CE1	138.5532 ± 0.039	1
1425	LEU226 HD2	0.8132 ± 0.005	1	1478	HIS231 HA	4.0032 ± 0.016	1
1426	LEU226 HG	1.8622 ± 0.008	1	1479	HIS231 HB2	3.3322 ± 0.013	2
1427	LEU226 H	8.7162 ± 0.006	1	1480	HIS231 HB3	3.0712 ± 0.016	2
1428	LEU226N	122.6472 ± 0.075	1	1481	HIS231 HD2	6.8932 ± 0.010	1
1429	LEU227 C	176.4062	1	1482	HIS231 HE1	7.8752 ± 0.002	1
1430	LEU227 CA	53.8122 ± 0.095	1	1483	HIS231 H	8.1602 ± 0.008	1
1431	LEU227 CB	40.2022 ± 0.121	1	1484	HIS231 N	118.0352 ± 0.071	1

1485	SER232 C	177.6042	1	1538	LEU237 CA	58.0302 ± 0.096	1
1486	SER232 CA	61.5622 ± 0.142	1	1539	LEU237 CB	42.0652 ± 0.098	1
1487	SER232 CB	62.6592 ± 0.096	1	1540	LEU237 CD1	24.8012 ± 0.056	1
1488	SER232 HA	4.0552 ± 0.008	1	1541	LEU237 CD2	25.5162 ± 0.128	1
1489	SER232 HB2	3.9532 ± 0.011	2	1542	LEU237 CG	27.5632 ± 0.071	1
1490	SER232 HB3	3.9532 ± 0.011	2	1543	LEU237 HA	4.3472 ± 0.012	1
1491	SER232 H	7.9522 ± 0.009	1	1544	LEU237 HB2	1.9622 ± 0.012	2
1492	SER232 N	111.4302 ± 0.069	1	1545	LEU237 HB3	1.8412 ± 0.010	2
1493	LEU233 C	179.9542 ± 0.006	1	1546	LEU237 HD1	1.1642 ± 0.005	1
1494	LEU233 CA	57.8822 ± 0.127	1	1547	LEU237 HD2	1.0302 ± 0.008	1
1495	LEU233 CB	42.6902 ± 0.109	1	1548	LEU237 HG	1.7562 ± 0.019	1
1496	LEU233 CD1	25.8572 ± 0.078	1	1549	LEU237 H	8.3682 ± 0.010	1
1497	LEU233 CD2	24.3232 ± 0.081	1	1550	LEU237 N	121.1782 ± 0.093	1
1498	LEU233 CG	26.8522 ± 0.115	1	1551	ALA238C	179.5202 ± 0.023	1
1499	LEU233 HA	4.1242 ± 0.018	1	1552	ALA238CA	55.8942 ± 0.078	1
1500	LEU233 HB2	1.9072 ± 0.015	2	1553	ALA238CB	18.1622 ± 0.108	1
1501	LEU233 HB3	1.3842 ± 0.010	2	1554	ALA238HA	3.9512 ± 0.007	1
1502	LEU233 HD1	0.8182 ± 0.009	1	1555	ALA238HB	1.5582 ± 0.009	1
1503	LEU233 HD2	0.8392 ± 0.015	1	1556	ALA238H	8.1452 ± 0.007	1
1504	LEU233 HG	1.7352 ± 0.009	1	1557	ALA238N	121.7542 ± 0.081	1
1505	LEU233 H	7.6332 ± 0.007	1	1558	ARG239 C	179.0552 ± 0.004	1
1506	LEU233 N	121.4872 ± 0.100	1	1559	ARG239 CA	59.8832 ± 0.137	1
1507	ILE234 C	177.6282	1	1560	ARG239 CB	29.5462 ± 0.081	1
1508	ILE234 CA	65.8372 ± 0.109	1	1561	ARG239 CD	43.1742 ± 0.076	1
1509	ILE234 CB	36.7692 ± 0.162	1	1562	ARG239 CG	27.9202 ± 0.176	1
1510	ILE234 CD1	15.7292 ± 0.090	1	1563	ARG239 HA	4.0102 ± 0.005	1
1511	ILE234 CG1	25.9332 ± 0.344	1	1564	ARG239 HB2	1.9202 ± 0.007	2
1512	ILE234 CG2	17.6712 ± 0.086	1	1565	ARG239 HB3	1.9202 ± 0.007	2
1513	ILE234 HA	4.0222 ± 0.010	1	1566	ARG239 HD2	3.1862 ± 0.006	2
1514	ILE234 HB	1.8812 ± 0.009	1	1567	ARG239 HD3	3.1862 ± 0.006	2
1515	ILE234 HD1	0.6082 ± 0.011	1	1568	ARG239 HG2	1.8372 ± 0.002	2
1516	ILE234 HG12	1.7082 ± 0.010	2	1569	ARG239 HG3	1.5922 ± 0.007	2
1517	ILE234 HG13	1.7082 ± 0.010	2	1570	ARG239 H	8.1372 ± 0.007	1
1518	ILE234 HG2	0.6712 ± 0.006	1	1571	ARG239 N	118.1202 ± 0.086	1
1519	ILE234 H	8.4632 ± 0.013	1	1572	ARG240 C	178.4912 ± 0.025	1
1520	ILE234 N	113.7302 ± 0.082	1	1573	ARG240 CA	57.8082 ± 0.145	1
1521	ARG235 C	178.2362	1	1574	ARG240 H	8.3792 ± 0.009	1
1522	ARG235 CA	60.3582 ± 0.111	1	1575	ARG240 N	121.3722 ± 0.050	1
1523	ARG235 HA	3.8122 ± 0.006	1	1576	CYS241 C	176.5512 ± 0.019	1
1524	ARG235 H	7.3392 ± 0.011	1	1577	CYS241 CA	64.8452 ± 0.117	1
1525	ARG235 N	121.9942 ± 0.145	1	1578	CYS241 CB	27.3642 ± 0.161	1
1526	GLN236 C	178.7592	1	1579	CYS241 HA	4.1782 ± 0.011	1
1527	GLN236CA	58.8022 ± 0.095	1	1580	CYS241 HB2	3.4092 ± 0.014	2
1528	GLN236CB	28.1192 ± 0.108	1	1581	CYS241 HB3	2.5502 ± 0.010	2
1529	GLN236CG	33.6992 ± 0.130	1	1582	CYS241 H	8.5652 ± 0.008	1
1530	GLN236HA	4.0352 ± 0.014	1	1583	CYS241 N	116.1842 ± 0.049	1
1531	GLN236HB2	2.2262 ± 0.010	2	1584	SER242 CA	62.0002 ± 0.159	1
1532	GLN236HB3	2.2262 ± 0.010	2	1585	SER242 CB	62.7692 ± 0.199	1
1533	GLN236HG2	2.4342 ± 0.014	2	1586	SER242 HA	3.9862 ± 0.025	1
1534	GLN236HG3	2.4342 ± 0.014	2	1587	SER242 HB2	4.0172 ± 0.006	2
1535	GLN236H	7.8332 ± 0.008	1	1588	SER242 HB3	4.0172 ± 0.006	2
1536	GLN236N	119.3912 ± 0.069	1	1589	SER242 H	8.1152 ± 0.008	1
1537	LEU237 C	179.0322	1	1590	SER242 N	114.6972 ± 0.089	1

1591	GLU243C	179.4842	1	1644	LEU247 CD1	25.3282 ± 0.043	1
1592	GLU243CA	59.3942 ± 0.112	1	1645	LEU247 CD2	22.4942 ± 0.098	1
1593	GLU243CB	30.0092 ± 0.150	1	1646	LEU247 CG	26.4862 ± 0.088	1
1594	GLU243CG	36.3862 ± 0.096	1	1647	LEU247 HA	4.3392 ± 0.007	1
1595	GLU243HA	4.0232 ± 0.010	1	1648	LEU247 HB2	1.9612 ± 0.009	2
1596	GLU243HB2	2.1422 ± 0.024	2	1649	LEU247 HB3	1.6822 ± 0.018	2
1597	GLU243HB3	2.1422 ± 0.024	2	1650	LEU247 HD1	0.9382 ± 0.008	1
1598	GLU243HG2	2.4042 ± 0.017	2	1651	LEU247 HD2	0.8622 ± 0.017	1
1599	GLU243HG3	2.1952 ± 0.014	2	1652	LEU247 HG	1.8352 ± 0.016	1
1600	GLU243H	8.0432 ± 0.009	1	1653	LEU247 H	7.5482 ± 0.008	1
1601	GLU243N	122.3802 ± 0.054	1	1654	LEU247 N	117.4332 ± 0.065	1
1602	VAL244C	178.3042	1	1655	VAL248C	176.0932 ± 0.001	1
1603	VAL244CA	65.9672 ± 0.126	1	1656	VAL248CA	62.7532 ± 0.076	1
1604	VAL244CB	31.6012 ± 0.110	1	1657	VAL248CB	32.1422 ± 0.077	1
1605	VAL244CG1	22.5052 ± 0.105	2	1658	VAL248CG1	22.0572 ± 0.071	1
1606	VAL244CG2	22.5052 ± 0.105	2	1659	VAL248CG2	20.3912 ± 0.061	1
1607	VAL244HA	3.7232 ± 0.009	1	1660	VAL248HA	4.0072 ± 0.005	1
1608	VAL244HB	2.1842 ± 0.016	1	1661	VAL248HB	2.2242 ± 0.004	1
1609	VAL244HG1	1.1112 ± 0.008	2	1662	VAL248HG1	0.9682 ± 0.014	1
1610	VAL244HG2	1.1112 ± 0.008	2	1663	VAL248HG2	0.9112 ± 0.007	1
1611	VAL244H	8.3132 ± 0.014	1	1664	VAL248H	7.3262 ± 0.009	1
1612	VAL244N	118.3362 ± 0.077	1	1665	VAL248N	118.0092 ± 0.062	1
1613	ARG245 C	177.2552 ± 0.012	1	1666	ASP249 C	176.1712 ± 0.024	1
1614	ARG245 CA	59.5862 ± 0.104	1	1667	ASP249 CA	55.0312 ± 0.123	1
1615	ARG245 CB	30.7942 ± 0.173	1	1668	ASP249 CB	42.0892 ± 0.110	1
1616	ARG245 CD	38.7672 ± 0.346	1	1669	ASP249 HA	4.6392 ± 0.009	1
1617	ARG245 CG	26.5342	1	1670	ASP249 HB2	2.7302 ± 0.015	2
1618	ARG245 HA	3.7282 ± 0.011	1	1671	ASP249 HB3	2.7302 ± 0.015	2
1619	ARG245 HB2	2.1422 ± 0.011	2	1672	ASP249 H	8.6532 ± 0.008	1
1620	ARG245 HB3	1.7402 ± 0.010	2	1673	ASP249 N	123.8892 ± 0.050	1
1621	ARG245 HD2	3.0192 ± 0.116	2	1674	SER250 C	174.6732	1
1622	ARG245 HD3	1.7142	2	1675	SER250 CA	57.6262 ± 0.094	1
1623	ARG245 HG2	1.5472	2	1676	SER250 CB	64.5362 ± 0.138	1
1624	ARG245 HG3	1.5472	2	1677	SER250 HA	4.5922 ± 0.005	1
1625	ARG245 H	8.1152 ± 0.007	1	1678	SER250 HB2	3.9642 ± 0.005	2
1626	ARG245 N	120.2122 ± 0.041	1	1679	SER250 HB3	3.8042 ± 0.007	2
1627	LEU246 C	178.2792 ± 0.017	1	1680	SER250 H	7.7592 ± 0.010	1
1628	LEU246 CA	56.7642 ± 0.112	1	1681	SER250 N	113.5092 ± 0.100	1
1629	LEU246 CB	42.3302 ± 0.060	1	1682	LYS251 C	175.8372 ± 0.021	1
1630	LEU246 CD1	25.0852 ± 0.084	1	1683	LYS251 CA	57.4902 ± 0.092	1
1631	LEU246 CD2	23.5012 ± 0.136	1	1684	LYS251 CB	32.1002 ± 0.145	1
1632	LEU246 CG	26.7852 ± 0.107	1	1685	LYS251 CD	29.1102 ± 0.062	1
1633	LEU246 HA	4.1892 ± 0.007	1	1686	LYS251 CE	42.0132	1
1634	LEU246 HB2	1.8852 ± 0.008	2	1687	LYS251 CG	24.5872 ± 0.140	1
1635	LEU246 HB3	1.6402 ± 0.009	2	1688	LYS251 HA	4.0652 ± 0.011	1
1636	LEU246 HD1	0.9512 ± 0.009	1	1689	LYS251 HB2	1.8062 ± 0.011	2
1637	LEU246 HD2	0.9192 ± 0.006	1	1690	LYS251 HB3	1.8062 ± 0.011	2
1638	LEU246 HG	1.8802 ± 0.004	1	1691	LYS251 HD2	1.6192 ± 0.010	2
1639	LEU246 H	7.2822 ± 0.010	1	1692	LYS251 HD3	1.6192 ± 0.010	2
1640	LEU246 N	116.3832 ± 0.070	1	1693	LYS251 HE2	2.9702	2
1641	LEU247 C	177.9302 ± 0.011	1	1694	LYS251 HE3	2.9702	2
1642	LEU247 CA	55.0242 ± 0.039	1	1695	LYS251 HG2	1.3952 ± 0.009	2
1643	LEU247 CB	42.2542 ± 0.104	1	1696	LYS251 HG3	1.3952 ± 0.009	2

1697	LYS251 H	8.6422 ± 0.008	1	1750	ALA258CB	21.0152 ± 0.066	1
1698	LYS251 N	123.0892 ± 0.048	1	1751	ALA258HA	3.9502 ± 0.017	1
1699	ASP252 C	175.4682 ± 0.034	1	1752	ALA258HB	1.5802 ± 0.008	1
1700	ASP252 CA	54.1102 ± 0.086	1	1753	ALA258H	6.6312 ± 0.017	1
1701	ASP252 CB	41.0982 ± 0.109	1	1754	ALA258N	117.2522 ± 0.064	1
1702	ASP252 HA	4.6242 ± 0.006	1	1755	LEU259 C	178.6762	1
1703	ASP252 HB2	2.8042 ± 0.008	2	1756	LEU259 CA	58.0272 ± 0.109	1
1704	ASP252 HB3	2.5302 ± 0.008	2	1757	LEU259 CB	41.2562 ± 0.074	1
1705	ASP252 H	7.9762 ± 0.007	1	1758	LEU259 CD1	25.7082 ± 0.138	1
1706	ASP252 N	117.4312 ± 0.066	1	1759	LEU259 CD2	22.3252 ± 0.065	1
1707	ASP253 CA	55.1202 ± 0.136	1	1760	LEU259 CG	26.1092 ± 0.267	1
1708	ASP253 CB	43.6012 ± 0.109	1	1761	LEU259 HA	3.7592 ± 0.019	1
1709	ASP253 HA	4.4522 ± 0.005	1	1762	LEU259 HB2	1.7062 ± 0.010	2
1710	ASP253 HB2	2.7812 ± 0.013	2	1763	LEU259 HB3	1.0682 ± 0.023	2
1711	ASP253 HB3	2.7812 ± 0.013	2	1764	LEU259 HD1	0.6332 ± 0.008	1
1712	ASP253 H	7.4582 ± 0.014	1	1765	LEU259 HD2	0.5812 ± 0.008	1
1713	ASP253 N	122.2472 ± 0.055	1	1766	LEU259 HG	1.4382 ± 0.002	1
1714	GLU254CB	29.6952	1	1767	LEU259 H	7.8172 ± 0.012	1
1715	GLU254CA	58.6282 ± 0.001	1	1768	LEU259 N	117.7412 ± 0.068	1
1716	GLU254CG	36.4722 ± 0.009	1	1769	ASN260 C	178.8722 ± 0.002	1
1717	GLU254HG2	2.4172 ± 0.007	2	1770	ASN260 CA	55.7502 ± 0.076	1
1718	GLU254HG3	2.4172 ± 0.007	2	1771	ASN260 CB	37.6152 ± 0.274	1
1719	GLU254H	7.9012 ± 0.007	1	1772	ASN260 HA	4.1822 ± 0.011	1
1720	GLU254N	126.0312 ± 0.004	1	1773	ASN260 HB2	2.8092 ± 0.019	2
1721	ARG255 C	177.3342	1	1774	ASN260 HB3	2.8092 ± 0.019	2
1722	ARG255 CA	58.5402 ± 0.019	1	1775	ASN260 H	8.4592 ± 0.009	1
1723	ARG255 HA	4.1872 ± 0.009	1	1776	ASN260 N	116.0852 ± 0.113	1
1724	ARG255 H	9.3132 ± 0.012	1	1777	LEU261 C	176.0742	1
1725	ARG255 N	119.1132 ± 0.085	1	1778	LEU261 CA	54.4222 ± 0.031	1
1726	VAL256 CA	69.4972 ± 0.098	1	1779	LEU261 CB	41.0842	1
1727	VAL256CB	29.5012 ± 0.048	1	1780	LEU261 CD1	25.8212	1
1728	VAL256CG1	25.3762 ± 0.080	1	1781	LEU261 CD2	22.2232 ± 0.046	1
1729	VAL256CG2	21.6302 ± 0.052	1	1782	LEU261 HA	4.1632 ± 0.003	1
1730	VAL256HA	3.3252 ± 0.013	1	1783	LEU261 HD1	0.7622	1
1731	VAL256HB	2.3092 ± 0.008	1	1784	LEU261 HD2	0.9902 ± 0.007	1
1732	VAL256HG1	1.0502 ± 0.010	1	1785	LEU261 H	8.4982 ± 0.017	1
1733	VAL256HG2	0.7652 ± 0.004	1	1786	LEU261 N	122.5472 ± 0.149	1
1734	VAL256H	7.7632 ± 0.007	1	1787	LEU262 C	178.9472	1
1735	VAL256N	116.5952 ± 0.096	1	1788	LEU262 CA	58.9942 ± 0.087	1
1736	PRO257 C	177.7042 ± 0.024	1	1789	LEU262 CB	42.0382 ± 0.124	1
1737	PRO257 CA	66.1712 ± 0.135	1	1790	LEU262 CD1	26.9672 ± 0.060	1
1738	PRO257 CB	31.6692 ± 0.133	1	1791	LEU262 CD2	23.2352 ± 0.037	1
1739	PRO257 CD	49.2102 ± 0.215	1	1792	LEU262 CG	27.1322 ± 0.146	1
1740	PRO257 CG	28.4132 ± 0.176	1	1793	LEU262 HA	3.9132 ± 0.007	1
1741	PRO257 HA	3.5782 ± 0.014	1	1794	LEU262 HB2	2.3202 ± 0.018	2
1742	PRO257 HB2	2.2382 ± 0.019	2	1795	LEU262 HB3	1.2722 ± 0.014	2
1743	PRO257 HB3	1.8922 ± 0.014	2	1796	LEU262 HD1	0.8462 ± 0.003	1
1744	PRO257 HD2	3.5602 ± 0.023	2	1797	LEU262 HD2	0.8592 ± 0.005	1
1745	PRO257 HD3	3.5602 ± 0.023	2	1798	LEU262 HG	1.1452 ± 0.014	1
1746	PRO257 HG2	2.0682 ± 0.007	2	1799	LEU262 H	8.2952 ± 0.007	1
1747	PRO257 HG3	1.7362 ± 0.010	2	1800	LEU262 N	118.9242 ± 0.173	1
1748	ALA258C	179.0462 ± 0.022	1	1801	ILE263 C	178.4962	1
1749	ALA258CA	55.1222 ± 0.193	1	1802	ILE263 CA	66.9812 ± 0.112	1

1803	ILE263	CB	39.1302 ± 0.161	1	1856	ARG268	CA	56.4552 ± 0.083	1
1804	ILE263	CD1	13.0342 ± 0.073	1	1857	ARG268	CB	31.0502 ± 0.153	1
1805	ILE263	CG1	30.7262 ± 0.088	1	1858	ARG268	CD	43.0822 ± 0.060	1
1806	ILE263	CG2	17.1952 ± 0.098	1	1859	ARG268	CG	27.8812 ± 0.158	1
1807	ILE263	HA	3.4292 ± 0.010	1	1860	ARG268	HA	4.5802 ± 0.017	1
1808	ILE263	HB	1.7512 ± 0.010	1	1861	ARG268	HB2	1.9812	2
1809	ILE263	HD1	0.7452 ± 0.011	1	1862	ARG268	HB3	1.9812	2
1810	ILE263	HG12	1.8982 ± 0.007	2	1863	ARG268	HD2	3.1252 ± 0.049	2
1811	ILE263	HG13	0.9672 ± 0.014	2	1864	ARG268	HD3	3.1252 ± 0.049	2
1812	ILE263	HG2	0.9492 ± 0.009	1	1865	ARG268	HG2	1.8672 ± 0.006	2
1813	ILE263	H	8.1372 ± 0.008	1	1866	ARG268	HG3	1.8672 ± 0.006	2
1814	ILE263	N	117.7762 ± 0.077	1	1867	ARG268	H	8.7332 ± 0.010	1
1815	CYS264	C	176.1242 ± 0.024	1	1868	ARG268	N	116.8672 ± 0.141	1
1816	CYS264	CA	61.5712 ± 0.079	1	1869	TYR269	C	175.9922 ± 0.029	1
1817	CYS264	CB	25.9552 ± 0.158	1	1870	TYR269	CA	61.9272 ± 0.093	1
1818	CYS264	HA	4.3952 ± 0.013	1	1871	TYR269	CB	39.0072 ± 0.105	1
1819	CYS264	HB2	3.4282 ± 0.013	2	1872	TYR269	CD1	133.1232 ± 0.131	3
1820	CYS264	HB3	3.1932 ± 0.008	2	1873	TYR269	CD2	133.1232 ± 0.131	3
1821	CYS264	H	8.1422 ± 0.010	1	1874	TYR269	CE1	118.0372 ± 0.120	3
1822	CYS264	N	121.2782 ± 0.184	1	1875	TYR269	CE2	118.0372 ± 0.120	3
1823	LEU265	C	180.2742 ± 0.041	1	1876	TYR269	HA	4.2972 ± 0.018	1
1824	LEU265	CA	58.4272 ± 0.078	1	1877	TYR269	HB2	2.7632 ± 0.008	2
1825	LEU265	CB	40.7852 ± 0.112	1	1878	TYR269	HB3	2.7632 ± 0.008	2
1826	LEU265	CD1	24.2232 ± 0.087	1	1879	TYR269	HD1	6.1582 ± 0.009	3
1827	LEU265	CD2	19.9602 ± 0.093	1	1880	TYR269	HD2	6.1582 ± 0.009	3
1828	LEU265	CG	25.1422 ± 0.096	1	1881	TYR269	HE1	6.4032 ± 0.011	3
1829	LEU265	HA	3.9632 ± 0.018	1	1882	TYR269	HE2	6.4032 ± 0.011	3
1830	LEU265	HB2	1.7952 ± 0.015	2	1883	TYR269	H	7.8232 ± 0.012	1
1831	LEU265	HB3	0.8432 ± 0.023	2	1884	TYR269	N	119.1132 ± 0.128	1
1832	LEU265	HD1	0.0272 ± 0.009	1	1885	PHE270	C	175.6422	1
1833	LEU265	HD2	0.2292 ± 0.008	1	1886	PHE270	CA	59.2032 ± 0.100	1
1834	LEU265	HG	1.9662 ± 0.009	1	1887	PHE270	CB	38.3722 ± 0.203	1
1835	LEU265	H	8.8362 ± 0.016	1	1888	PHE270	CD1	132.4402 ± 0.049	3
1836	LEU265	N	118.5062 ± 0.122	1	1889	PHE270	CD2	132.4402 ± 0.049	3
1837	VAL266	CA	68.2052 ± 0.101	1	1890	PHE270	HA	4.4732 ± 0.008	1
1838	VAL266	CB	32.2562 ± 0.101	1	1891	PHE270	HB2	3.6082 ± 0.010	2
1839	VAL266	CG1	20.6462 ± 0.083	1	1892	PHE270	HB3	3.4322 ± 0.021	2
1840	VAL266	CG2	22.5882 ± 0.072	1	1893	PHE270	HD1	7.4142 ± 0.010	3
1841	VAL266	HA	3.8132 ± 0.011	1	1894	PHE270	HD2	7.4142 ± 0.010	3
1842	VAL266	HB	2.1332 ± 0.015	1	1895	PHE270	H	7.8512 ± 0.008	1
1843	VAL266	HG1	0.8272 ± 0.008	1	1896	PHE270	N	113.2532 ± 0.065	1
1844	VAL266	HG2	1.1492 ± 0.013	1	1897	ASP271	C	175.4212 ± 0.110	1
1845	VAL266	H	8.3072 ± 0.011	1	1898	ASP271	CA	56.3292 ± 0.051	1
1846	VAL266	N	118.3512 ± 0.251	1	1899	ASP271	CB	39.4892 ± 0.070	1
1847	SER267	C	175.5892	1	1900	ASP271	HA	4.3462 ± 0.006	1
1848	SER267	CA	60.6182 ± 0.099	1	1901	ASP271	HB2	3.0382 ± 0.005	2
1849	SER267	CB	63.7782 ± 0.158	1	1902	ASP271	HB3	2.6392 ± 0.007	2
1850	SER267	HA	4.0512 ± 0.012	1	1903	ASP271	H	6.9852 ± 0.010	1
1851	SER267	HB2	3.6272 ± 0.023	2	1904	ASP271	N	112.6152 ± 0.114	1
1852	SER267	HB3	3.6272 ± 0.023	2	1905	GLN272	C	176.5802 ± 0.020	1
1853	SER267	H	8.5262 ± 0.011	1	1906	GLN272	CA	52.0562 ± 0.012	1
1854	SER267	N	112.3602 ± 0.097	1	1907	GLN272	CB	26.2242	1
1855	ARG268	C	177.6812 ± 0.021	1	1908	GLN272	HA	4.7562 ± 0.001	1

1909	GLN272HB2	1.8622	2	1962	ASP277 H	8.9062 ± 0.010	1
1910	GLN272HB3	1.8622	2	1963	ASP277 N	120.4812 ± 0.042	1
1911	GLN272H	7.8972 ± 0.011	1	1964	GLU278C	174.4682	1
1912	GLN272N	118.6042 ± 0.107	1	1965	GLU278CA	53.4122 ± 0.046	1
1913	ARG273 C	177.2942 ± 0.022	1	1966	GLU278CB	30.2652 ± 0.201	1
1914	ARG273 CA	59.1502 ± 0.085	1	1967	GLU278CG	35.4312 ± 0.156	1
1915	ARG273 CB	30.2492 ± 0.078	1	1968	GLU278HA	4.7242 ± 0.004	1
1916	ARG273 CD	42.9992 ± 0.089	1	1969	GLU278HB2	2.0252 ± 0.013	2
1917	ARG273 CG	27.4102 ± 0.077	1	1970	GLU278HB3	1.8782 ± 0.019	2
1918	ARG273 HA	3.8772 ± 0.011	1	1971	GLU278HG2	2.2542	2
1919	ARG273 HB2	1.8672 ± 0.010	2	1972	GLU278HG3	2.2032 ± 0.004	2
1920	ARG273 HB3	1.8672 ± 0.010	2	1973	GLU278H	8.5482 ± 0.010	1
1921	ARG273 HD2	3.2152 ± 0.023	2	1974	GLU278N	125.4112 ± 0.108	1
1922	ARG273 HD3	3.2152 ± 0.023	2	1975	PRO279 C	176.7742 ± 0.023	1
1923	ARG273 HG2	1.6802 ± 0.008	2	1976	PRO279 CA	63.2222 ± 0.080	1
1924	ARG273 HG3	1.6802 ± 0.008	2	1977	PRO279 CB	32.2372 ± 0.126	1
1925	ARG273 H	7.8002 ± 0.004	1	1978	PRO279 CD	50.6162 ± 0.044	1
1926	ARG273 N	120.7692 ± 0.056	1	1979	PRO279 CG	27.3532 ± 0.170	1
1927	ASP274 C	176.2872 ± 0.021	1	1980	PRO279 HA	4.4012 ± 0.022	1
1928	ASP274 CA	55.0132 ± 0.043	1	1981	PRO279 HB2	2.2692 ± 0.010	2
1929	ASP274 CB	38.7432 ± 0.080	1	1982	PRO279 HB3	1.9582	2
1930	ASP274 HA	4.3942 ± 0.002	1	1983	PRO279 HD2	3.7632 ± 0.006	2
1931	ASP274 HB2	2.7182 ± 0.011	2	1984	PRO279 HD3	3.7052 ± 0.010	2
1932	ASP274 HB3	2.7182 ± 0.011	2	1985	PRO279 HG2	1.9932 ± 0.025	2
1933	ASP274 H	9.1192 ± 0.010	1	1986	PRO279 HG3	1.2972	2
1934	ASP274 N	116.5312 ± 0.085	1	1987	SER280 C	174.3672 ± 0.018	1
1935	LEU275 C	175.7752	1	1988	SER280 CA	58.3112 ± 0.104	1
1936	LEU275 CA	53.9862 ± 0.162	1	1989	SER280 CB	63.7312 ± 0.113	1
1937	LEU275 CB	41.1892 ± 0.099	1	1990	SER280 HA	4.4002 ± 0.003	1
1938	LEU275 CD1	22.2572 ± 0.036	1	1991	SER280 HB2	3.8492 ± 0.011	2
1939	LEU275 CD2	22.3942 ± 0.073	1	1992	SER280 HB3	3.8492 ± 0.011	2
1940	LEU275 CG	26.8082 ± 0.203	1	1993	SER280 H	8.2812 ± 0.008	1
1941	LEU275 HA	4.4222 ± 0.007	1	1994	SER280 N	115.7672 ± 0.047	1
1942	LEU275 HB2	1.6302 ± 0.021	2	1995	LEU281 C	176.9132 ± 0.010	1
1943	LEU275 HB3	1.6302 ± 0.021	2	1996	LEU281 CA	55.0222 ± 0.086	1
1944	LEU275 HD1	0.7662 ± 0.014	1	1997	LEU281 CB	42.4992 ± 0.067	1
1945	LEU275 HD2	0.7372 ± 0.009	1	1998	LEU281 CD1	24.7422 ± 0.155	1
1946	LEU275 HG	1.5472 ± 0.013	1	1999	LEU281 CD2	23.4912 ± 0.108	1
1947	LEU275 H	7.7482 ± 0.007	1	2000	LEU281 CG	27.0192 ± 0.072	1
1948	LEU275 N	119.4492 ± 0.040	1	2001	LEU281 HA	4.3762 ± 0.005	1
1949	ALA276C	178.1512 ± 0.012	1	2002	LEU281 HB2	1.5662 ± 0.022	2
1950	ALA276CA	52.1932 ± 0.119	1	2003	LEU281 HB3	1.5662 ± 0.022	2
1951	ALA276CB	19.7892 ± 0.070	1	2004	LEU281 HD1	0.9162 ± 0.006	1
1952	ALA276HA	4.1932 ± 0.006	1	2005	LEU281 HD2	0.8592 ± 0.005	1
1953	ALA276HB	1.2942 ± 0.006	1	2006	LEU281 HG	1.6072 ± 0.012	1
1954	ALA276H	7.1832 ± 0.014	1	2007	LEU281 H	8.2412 ± 0.007	1
1955	ALA276N	120.1382 ± 0.097	1	2008	LEU281 N	123.9482 ± 0.027	1
1956	ASP277 C	175.8322 ± 0.027	1	2009	GLU282C	174.9142 ± 0.021	1
1957	ASP277 CA	54.4972 ± 0.133	1	2010	GLU282CA	56.3692 ± 0.079	1
1958	ASP277 CB	41.1282 ± 0.109	1	2011	GLU282CB	30.6572 ± 0.057	1
1959	ASP277 HA	4.6752 ± 0.005	1	2012	GLU282CG	36.2672 ± 0.091	1
1960	ASP277 HB2	2.5662 ± 0.026	2	2013	GLU282HA	4.2472 ± 0.003	1
1961	ASP277 HB3	2.5662 ± 0.026	2	2014	GLU282HB2	1.9752 ± 0.012	2

2015	GLU282HB3	1.8162 ± 0.009	2
2016	GLU282HG2	2.1472 ± 0.013	2
2017	GLU282HG3	2.1472 ± 0.013	2
2018	GLU282H	8.2302 ± 0.005	1
2019	GLU282N	121.5522 ± 0.038	1
2020	TYR283C	180.2402	1
2021	TYR283CA	58.9982 ± 0.040	1
2022	TYR283CB	39.4582 ± 0.102	1
2023	TYR283CD1	133.5212 ± 0.168	3
2024	TYR283CD2	133.5212 ± 0.168	3
2025	TYR283CE1	118.1702 ± 0.119	3
2026	TYR283CE2	118.1702 ± 0.119	3
2027	TYR283HA	4.3662 ± 0.008	1
2028	TYR283HB2	3.0292 ± 0.008	2
2029	TYR283HB3	2.8852 ± 0.007	2
2030	TYR283HD1	7.0672 ± 0.013	3
2031	TYR283HD2	7.0672 ± 0.013	3
2032	TYR283HE1	6.7792 ± 0.013	3
2033	TYR283HE2	6.7792 ± 0.013	3
2034	TYR283H	7.6392 ± 0.007	1
2035	TYR283N	125.7052 ± 0.027	1

Appendix B. Structural restraints

Table B1. Nuclear Overhauser effect (NOE) distance restraints used in the XPLOR-NIH calculation of the SMN²⁶⁻⁵¹-Gemin2⁹⁵⁻²⁸⁰ ensemble. After the two atom selections, the observed distance is indicated in Angstroms, followed by increments defining its upper and lower bound.

From the 3D ¹⁵N NOESY-HSQC:

```
assign (segid B and residue 38 and name HN) (segid B and residue 39 and name HN) 2.35 0.65 0.65
assign (segid B and residue 42 and name HN) (segid B and residue 43 and name HN) 2.35 0.65 0.65
assign (segid B and residue 43 and name HN) (segid B and residue 44 and name HN) 2.35 0.65 0.65
assign (segid B and residue 46 and name HN) (segid B and residue 47 and name HN) 2.35 0.65 0.65
assign (segid A and residue 102 and name HN) (segid A and residue 103 and name HN) 2.35 0.65 0.65
assign (segid A and residue 113 and name HN) (segid A and residue 114 and name HN) 2.35 0.65 0.65
assign (segid A and residue 114 and name HN) (segid A and residue 115 and name HN) 2.35 0.65 0.65
assign (segid A and residue 121 and name HN) (segid A and residue 122 and name HN) 2.35 0.65 0.65
assign (segid A and residue 190 and name HN) (segid A and residue 191 and name HN) 2.35 0.65 0.65
assign (segid A and residue 199 and name HN) (segid A and residue 200 and name HN) 2.35 0.65 0.65
assign (segid A and residue 214 and name HN) (segid A and residue 215 and name HN) 2.35 0.65 0.65
assign (segid A and residue 143 and name HN) (segid A and residue 144 and name HN) 2.35 0.65 0.65
assign (segid A and residue 231 and name HN) (segid A and residue 232 and name HN) 2.35 0.65 0.65
assign (segid A and residue 243 and name HN) (segid A and residue 244 and name HN) 2.35 0.65 0.65

assign (segid B and residue 37 and name HN) (segid B and residue 38 and name HN) 2.35 0.65 0.65
assign (segid B and residue 39 and name HN) (segid B and residue 40 and name HN) 2.35 0.65 0.65
assign (segid B and residue 40 and name HN) (segid B and residue 41 and name HN) 2.35 0.65 0.65
assign (segid B and residue 44 and name HN) (segid B and residue 45 and name HN) 2.35 0.65 0.65
assign (segid B and residue 45 and name HN) (segid B and residue 46 and name HN) 2.35 0.65 0.65
assign (segid B and residue 47 and name HN) (segid B and residue 48 and name HN) 2.35 0.65 0.65
assign (segid B and residue 48 and name HN) (segid B and residue 49 and name HN) 2.35 0.65 0.65
assign (segid A and residue 100 and name HN) (segid A and residue 101 and name HN) 2.35 0.65 0.65
assign (segid A and residue 101 and name HN) (segid A and residue 102 and name HN) 2.35 0.65 0.65
assign (segid A and residue 103 and name HN) (segid A and residue 104 and name HN) 2.35 0.65 0.65
assign (segid A and residue 104 and name HN) (segid A and residue 105 and name HN) 2.35 0.65 0.65
assign (segid A and residue 107 and name HN) (segid A and residue 108 and name HN) 2.35 0.65 0.65
assign (segid A and residue 108 and name HN) (segid A and residue 109 and name HN) 2.35 0.65 0.65
assign (segid A and residue 111 and name HN) (segid A and residue 112 and name HN) 2.35 0.65 0.65
assign (segid A and residue 112 and name HN) (segid A and residue 113 and name HN) 2.35 0.65 0.65
assign (segid A and residue 116 and name HN) (segid A and residue 117 and name HN) 2.35 0.65 0.65
```


assign (segid A and residue 263 and name HA) (segid A and residue 266 and name HB) 3.10 1.40 1.40

From the 4D HCCH NOESY-HMQC

assign (segid A and residue 118 and name HA) (segid A and residue 121 and name HB#) 2.60 0.90 0.90
assign (segid A and residue 118 and name HA) (segid A and residue 121 and name HB#) 2.60 0.90 0.90
assign (segid B and residue 44 and name HA) (segid B and residue 47 and name HB) 2.60 0.90 0.90
assign (segid A and residue 243 and name HA) (segid A and residue 246 and name HB#) 2.60 0.90 0.90
assign (segid A and residue 243 and name HA) (segid A and residue 246 and name HB#) 2.60 0.90 0.90
assign (segid A and residue 262 and name HA) (segid A and residue 265 and name HB#) 2.60 0.90 0.90
assign (segid A and residue 116 and name HA) (segid A and residue 119 and name HB#) 2.60 0.90 0.90
assign (segid A and residue 116 and name HA) (segid A and residue 119 and name HB#) 2.60 0.90 0.90
assign (segid A and residue 116 and name HA) (segid A and residue 119 and name HB#) 2.60 0.90 0.90
assign (segid A and residue 116 and name HA) (segid A and residue 119 and name HB#) 2.60 0.90 0.90
assign (segid A and residue 212 and name HA#) (segid A and residue 215 and name HB#) 2.60 0.90 0.90

From the 3D ¹³C-NOESY HSQC

assign (segid B and residue 28 and name HA) (segid B and residue 29 and name HN) 3.10 1.40 1.40
assign (segid B and residue 28 and name HB#) (segid B and residue 28 and name HN) 3.10 1.40 1.40
assign (segid B and residue 28 and name HB#) (segid B and residue 28 and name HA) 3.10 1.40 1.40
assign (segid B and residue 29 and name HA) (segid B and residue 29 and name HB#) 2.85 1.15 1.15
assign (segid B and residue 29 and name HB#) (segid B and residue 29 and name HA) 2.85 1.15 1.15
assign (segid B and residue 29 and name HB#) (segid B and residue 29 and name HN) 3.10 1.40 1.40
assign (segid B and residue 30 and name HB#) (segid B and residue 30 and name HA) 3.10 1.40 1.40
assign (segid B and residue 30 and name HB#) (segid B and residue 30 and name HN) 3.35 1.65 1.65
assign (segid B and residue 29 and name HN) (segid B and residue 30 and name HA) 2.85 1.15 1.15
assign (segid B and residue 30 and name HA) (segid B and residue 30 and name HN) 3.35 1.65 1.65
assign (segid B and residue 30 and name HA) (segid B and residue 30 and name HB#) 2.85 1.15 1.15
assign (segid B and residue 31 and name HA) (segid B and residue 31 and name HB#) 2.85 1.15 1.15
assign (segid B and residue 31 and name HA) (segid B and residue 31 and name HN) 2.85 1.15 1.15
assign (segid B and residue 31 and name HA) (segid B and residue 32 and name HA) 3.35 1.65 1.65
assign (segid B and residue 31 and name HB#) (segid B and residue 31 and name HN) 3.10 1.40 1.40
assign (segid B and residue 32 and name HA) (segid B and residue 32 and name HB#) 2.85 1.15 1.15
assign (segid B and residue 32 and name HA) (segid B and residue 33 and name HN) 3.10 1.40 1.40
assign (segid B and residue 32 and name HB#) (segid B and residue 32 and name HA) 3.10 1.40 1.40
assign (segid B and residue 32 and name HB#) (segid B and residue 32 and name HN) 3.10 1.40 1.40
assign (segid B and residue 32 and name HB#) (segid B and residue 33 and name HA) 3.35 1.65 1.65
assign (segid B and residue 32 and name HB#) (segid B and residue 33 and name HN) 3.10 1.40 1.40
assign (segid B and residue 33 and name HA) (segid B and residue 33 and name HB) 3.10 1.40 1.40
assign (segid B and residue 33 and name HA) (segid B and residue 33 and name HD1#) 3.35 1.65 1.65
assign (segid B and residue 33 and name HA) (segid B and residue 33 and name HG1#) 3.10 1.40 1.40


```

assign (segid A and residue 281 and name HG) (segid A and residue 281 and name HD2#) 3.10 1.40 1.40
assign (segid A and residue 281 and name HG) (segid A and residue 282 and name HN) 3.35 1.65 1.65
assign (segid A and residue 282 and name HA) (segid A and residue 282 and name HB#) 3.10 1.40 1.40
assign (segid A and residue 282 and name HA) (segid A and residue 282 and name HG#) 3.10 1.40 1.40
assign (segid A and residue 282 and name HA) (segid A and residue 282 and name HN) 3.35 1.65 1.65
assign (segid A and residue 282 and name HA) (segid A and residue 283 and name HN) 2.85 1.15 1.15
assign (segid A and residue 282 and name HB#) (segid A and residue 282 and name HN) 3.10 1.40 1.40
assign (segid A and residue 282 and name HB#) (segid A and residue 283 and name HN) 3.10 1.40 1.40
assign (segid A and residue 282 and name HG#) (segid A and residue 282 and name HA) 3.10 1.40 1.40
assign (segid A and residue 282 and name HG#) (segid A and residue 282 and name HB#) 2.85 1.15 1.15
assign (segid A and residue 282 and name HG#) (segid A and residue 282 and name HN) 3.10 1.40 1.40
assign (segid A and residue 282 and name HG#) (segid A and residue 283 and name HN) 3.10 1.40 1.40
assign (segid A and residue 283 and name HA) (segid A and residue 283 and name HD#) 3.10 1.40 1.40
assign (segid A and residue 283 and name HA) (segid A and residue 283 and name HN) 3.10 1.40 1.40
assign (segid A and residue 283 and name HB#) (segid A and residue 283 and name HA) 2.85 1.15 1.15
assign (segid A and residue 283 and name HB#) (segid A and residue 283 and name HD#) 3.10 1.40 1.40
assign (segid A and residue 283 and name HB#) (segid A and residue 283 and name HN) 3.10 1.40 1.40

```

From the 4D HCCH-NOESY-HMQC

```

assign (segid B and residue 27 and name HA) (segid B and residue 27 and name HB#) 3.350 1.650 1.650
assign (segid B and residue 27 and name HA) (segid B and residue 27 and name HG#) 3.350 1.650 1.650
assign (segid B and residue 27 and name HA) (segid B and residue 28 and name HB#) 3.350 1.650 1.650
assign (segid B and residue 27 and name HG#) (segid B and residue 27 and name HA) 3.350 1.650 1.650
assign (segid B and residue 27 and name HG#) (segid B and residue 27 and name HB#) 2.600 0.900 0.900
assign (segid B and residue 27 and name HG#) (segid B and residue 28 and name HB#) 3.350 1.650 1.650
assign (segid B and residue 28 and name HA) (segid B and residue 28 and name HB#) 2.600 0.900 0.900
assign (segid B and residue 28 and name HA) (segid B and residue 29 and name HA) 3.350 1.650 1.650
assign (segid B and residue 28 and name HA) (segid B and residue 29 and name HB#) 3.350 1.650 1.650
assign (segid B and residue 33 and name HB) (segid B and residue 33 and name HG1#) 2.600 0.900 0.900
assign (segid B and residue 33 and name HB) (segid B and residue 33 and name HG1#) 2.600 0.900 0.900
assign (segid B and residue 33 and name HB) (segid B and residue 33 and name HG2#) 2.900 1.200 1.200
assign (segid B and residue 31 and name HB#) (segid B and residue 33 and name HD1#) 3.350 1.650 1.650
assign (segid B and residue 33 and name HD1#) (segid B and residue 33 and name HG1#) 2.900 1.200 1.200
assign (segid B and residue 33 and name HD1#) (segid B and residue 33 and name HG1#) 2.900 1.200 1.200
assign (segid B and residue 33 and name HD1#) (segid B and residue 33 and name HG2#) 3.850 2.150 2.150
assign (segid B and residue 30 and name HB#) (segid B and residue 33 and name HG2#) 3.350 1.650 1.650
assign (segid B and residue 33 and name HG2#) (segid B and residue 33 and name HD1#) 3.850 2.150 2.150
assign (segid B and residue 34 and name HB#) (segid B and residue 34 and name HA) 3.350 1.650 1.650
assign (segid B and residue 37 and name HA) (segid B and residue 40 and name HG2#) 3.600 1.900 1.900
assign (segid B and residue 37 and name HA) (segid A and residue 179 and name HD2#) 3.600 1.900 1.900
assign (segid B and residue 37 and name HB) (segid A and residue 179 and name HD2#) 3.600 1.900 1.900

```


assign (segid A and residue 262 and name HD1#) (segid A and residue 266 and name HG1#)	3.85	2.15	2.15
assign (segid A and residue 262 and name HD1#) (segid A and residue 262 and name HD2#)	3.85	2.15	2.15
assign (segid A and residue 262 and name HD1#) (segid A and residue 275 and name HD2#)	3.85	2.15	2.15
assign (segid B and residue 46 and name HB#) (segid A and residue 109 and name HG#)	3.60	1.90	1.90
assign (segid B and residue 46 and name HB#) (segid A and residue 106 and name HE2#)	3.60	1.90	1.90
assign (segid A and residue 100 and name HD#) (segid A and residue 104 and name HE2#)	3.60	1.90	1.90
assign (segid A and residue 100 and name HB#) (segid A and residue 104 and name HE2#)	3.35	1.65	1.65
assign (segid A and residue 104 and name HE2#) (segid A and residue 108 and name HB#)	3.60	1.90	1.90
assign (segid A and residue 100 and name HG) (segid A and residue 104 and name HE2#)	3.35	1.65	1.65
assign (segid A and residue 135 and name HE#) (segid A and residue 190 and name HG2#)	3.85	2.15	2.15
assign (segid A and residue 186 and name HA) (segid A and residue 190 and name HG2#)	3.60	1.90	1.90
assign (segid A and residue 186 and name HB#) (segid A and residue 190 and name HG2#)	3.60	1.90	1.90
assign (segid A and residue 149 and name HD2#) (segid A and residue 211 and name HD1#)	3.85	2.15	2.15
assign (segid A and residue 149 and name HG) (segid A and residue 194 and name HG1#)	3.60	1.90	1.90
assign (segid B and residue 34 and name HA) (segid B and residue 35 and name HN)	3.35	1.65	1.65
assign (segid B and residue 35 and name HN) (segid B and residue 38 and name HB#)	3.60	1.90	1.90

From the 4D HNCH NOESY-HSQC

assign (segid B and residue 29 and name HA) (segid B and residue 30 and name HN)	2.350	0.650	0.650
assign (segid B and residue 30 and name HA) (segid B and residue 31 and name HN)	2.350	0.650	0.650
assign (segid B and residue 30 and name HB#) (segid B and residue 31 and name HN)	2.350	0.650	0.650
assign (segid B and residue 31 and name HN) (segid B and residue 31 and name HA)	2.350	0.650	0.650
assign (segid B and residue 31 and name HN) (segid B and residue 31 and name HB#)	2.350	0.650	0.650
assign (segid B and residue 31 and name HB#) (segid B and residue 32 and name HN)	2.350	0.650	0.650
assign (segid B and residue 32 and name HN) (segid B and residue 32 and name HB#)	2.350	0.650	0.650
assign (segid B and residue 32 and name HN) (segid B and residue 33 and name HA)	3.350	1.650	1.650
assign (segid B and residue 32 and name HN) (segid B and residue 33 and name HD1#)	3.600	1.900	1.900
assign (segid B and residue 32 and name HN) (segid B and residue 33 and name HG1#)	3.350	1.650	1.650
assign (segid B and residue 32 and name HN) (segid B and residue 33 and name HG2#)	3.600	1.900	1.900
assign (segid B and residue 31 and name HA) (segid B and residue 33 and name HN)	3.350	1.650	1.650
assign (segid B and residue 31 and name HB#) (segid B and residue 33 and name HN)	3.350	1.650	1.650
assign (segid B and residue 33 and name HN) (segid B and residue 33 and name HA)	2.350	0.650	0.650
assign (segid B and residue 33 and name HN) (segid B and residue 33 and name HD1#)	3.600	1.900	1.900
assign (segid B and residue 33 and name HN) (segid B and residue 33 and name HG2#)	2.600	0.900	0.900
assign (segid B and residue 32 and name HA) (segid B and residue 34 and name HN)	3.350	1.650	1.650
assign (segid B and residue 32 and name HB#) (segid B and residue 34 and name HN)	3.350	1.650	1.650
assign (segid B and residue 34 and name HN) (segid B and residue 34 and name HA)	3.350	1.650	1.650
assign (segid B and residue 34 and name HN) (segid B and residue 34 and name HB#)	3.350	1.650	1.650
assign (segid B and residue 36 and name HB#) (segid B and residue 37 and name HN)	3.350	1.650	1.650
assign (segid B and residue 37 and name HN) (segid B and residue 37 and name HA)	3.350	1.650	1.650


```

assign (segid A and residue 174 and name HA) (segid A and residue 175 and name HN) 3.350 1.650 1.650
assign (segid A and residue 186 and name HA) (segid A and residue 187 and name HN) 3.350 1.650 1.650
assign (segid A and residue 223 and name HN) (segid A and residue 223 and name HB#) 3.350 1.650 1.650
assign (segid A and residue 226 and name HN) (segid A and residue 226 and name HG) 3.350 1.650 1.650
assign (segid A and residue 231 and name HA) (segid A and residue 232 and name HN) 3.350 1.650 1.650
assign (segid A and residue 230 and name HA) (segid A and residue 233 and name HN) 3.350 1.650 1.650
assign (segid A and residue 233 and name HN) (segid A and residue 233 and name HB#) 3.350 1.650 1.650
assign (segid A and residue 242 and name HA) (segid A and residue 243 and name HN) 3.350 1.650 1.650
assign (segid A and residue 246 and name HN) (segid A and residue 246 and name HG) 3.350 1.650 1.650
assign (segid A and residue 248 and name HN) (segid A and residue 248 and name HG1#) 3.600 1.900 1.900
assign (segid A and residue 281 and name HN) (segid A and residue 281 and name HB#) 3.350 1.650 1.650
assign (segid A and residue 282 and name HN) (segid A and residue 282 and name HB#) 3.350 1.650 1.650

```

From the 3D ¹³C aromatic NOESY-HSQC

```

assign (segid B and residue 33 and name HG2#) (segid B and residue 34 and name HD1) 3.60 1.90 1.90
assign (segid B and residue 34 and name HD1) (segid B and residue 34 and name HA) 3.35 1.65 1.65
assign (segid B and residue 34 and name HD1) (segid B and residue 34 and name HB#) 3.35 1.65 1.65
assign (segid B and residue 34 and name HE3) (segid B and residue 34 and name HZ3) 3.35 1.65 1.65
assign (segid B and residue 33 and name HG1#) (segid B and residue 34 and name HH2) 3.35 1.65 1.65
assign (segid B and residue 34 and name HH2) (segid B and residue 34 and name HZ2) 3.35 1.65 1.65
assign (segid B and residue 34 and name HH2) (segid B and residue 34 and name HZ3) 3.35 1.65 1.65
assign (segid B and residue 33 and name HD1#) (segid B and residue 34 and name HZ2) 3.60 1.90 1.90
assign (segid B and residue 33 and name HG1#) (segid B and residue 34 and name HZ2) 3.35 1.65 1.65
assign (segid B and residue 34 and name HZ2) (segid B and residue 34 and name HH2) 3.35 1.65 1.65
assign (segid B and residue 34 and name HZ2) (segid B and residue 34 and name HZ3) 3.35 1.65 1.65
assign (segid B and residue 34 and name HZ3) (segid B and residue 34 and name HE3) 3.35 1.65 1.65
assign (segid B and residue 34 and name HZ3) (segid B and residue 34 and name HH2) 3.35 1.65 1.65
assign (segid B and residue 43 and name HE#) (segid B and residue 43 and name HA) 3.35 1.65 1.65
assign (segid B and residue 43 and name HE#) (segid B and residue 43 and name HB#) 3.35 1.65 1.65
assign (segid B and residue 43 and name HE#) (segid B and residue 43 and name HD#) 3.35 1.65 1.65
assign (segid B and residue 43 and name HE#) (segid A and residue 212 and name HA2) 3.35 1.65 1.65
assign (segid B and residue 50 and name HD#) (segid B and residue 50 and name HA) 3.35 1.65 1.65
assign (segid B and residue 50 and name HD#) (segid B and residue 50 and name HB#) 3.35 1.65 1.65
assign (segid B and residue 50 and name HD#) (segid B and residue 50 and name HE#) 3.35 1.65 1.65
assign (segid B and residue 50 and name HE#) (segid B and residue 50 and name HB#) 3.35 1.65 1.65
assign (segid B and residue 50 and name HE#) (segid B and residue 50 and name HD#) 3.35 1.65 1.65
assign (segid B and residue 50 and name HZ) (segid B and residue 50 and name HE#) 3.35 1.65 1.65
assign (segid A and residue 96 and name HD#) (segid A and residue 96 and name HA) 3.35 1.65 1.65
assign (segid A and residue 96 and name HD#) (segid A and residue 96 and name HB#) 3.35 1.65 1.65
assign (segid A and residue 96 and name HD#) (segid A and residue 96 and name HE#) 3.35 1.65 1.65
assign (segid A and residue 96 and name HE#) (segid A and residue 96 and name HA) 3.35 1.65 1.65

```


Table B2. Backbone ϕ and ψ angles calculated from chemical shifts using the TALOS+ software program and used in the XPLOR-NIH calculation of the SMN²⁶⁻⁵¹-Gemin2⁹⁵⁻²⁸⁰ ensemble. The value of each dihedral angle is measured in degrees.

φ dihedral angles

<u>residue</u>	<u>angle (°)</u>	<u>error (°)</u>	<u>residue</u>	<u>angle (°)</u>	<u>error (°)</u>
D32	-89	20.2	S131	-65.8	11.6
D36	-63.2	10.9	T134	-102.3	7.9
T37	-97.5	18.4	S138	-60	4.5
A38	-57.3	8.7	E139	-77.8	9.3
L39	-64	5.7	E141	-54.4	7.6
I40	-66.2	5.2	E142	-57.6	6.5
K41	-62	7.1	G143	-65.7	5.5
A42	-64.9	4.1	W144	-63.1	5.2
Y43	-67	9	K145	-63.5	4.2
D44	-64.4	3.2	K146	-66.4	4.5
K45	-67.5	3.2	F147	-66.3	8.3
A46	-65.2	4.2	C148	-67	11.7
V47	-66.4	5.8	L149	-91.1	7.7
A48	-68.2	9.3	G150	-60.5	3.5
L100	-60.8	2.9	L153	-65.2	9.9
Q101	-66.3	10	Y171	-59	7.4
W102	-65.7	5.3	V172	-67.5	10.1
Q103	-62.3	4.4	I174	-100.4	16.1
Q104	-63.1	5	F176	-88.3	17.4
Q105	-65.5	4.2	P177	-69.4	9.5
Q106	-62.4	3.7	P178	-72.2	6.7
Q109	-63.9	6.1	L180	-57.1	6.4
F110	-63.4	4.8	S181	-60.2	6.2
S111	-64.2	4.5	I182	-65.3	11.3
T112	-66.7	4.2	V183	-63.1	3.9
V113	-65.5	7.1	S184	-67.1	10.4
R114	-63.8	6.4	R185	-99	10.2
Q115	-65.3	3.3	N187	-80.6	13.3
N116	-64.7	2.3	Q188	-59.6	3.9
V117	-67.5	11.8	A189	-65	4.8
N118	-65.6	6	T190	-64.5	3
K119	-66.6	7.3	T192	-66.8	6.3
H120	-89.5	19.6	S193	-68.9	20.8
R121	-57.7	8.1	V194	-60.4	7.8
S122	-63.9	5.2	L195	-62.3	3.3
H123	-65.8	3.1	E196	-65.4	3.9
W124	-63.9	4.9	Y197	-63.2	5.1
K125	-67.7	9.3	L198	-61.9	7.7
S126	-93	14.5	S199	-66.7	6.8

<u>residue</u>	<u>angle (°)</u>	<u>error (°)</u>	<u>residue</u>	<u>angle (°)</u>	<u>error (°)</u>
N200	-67.4	5.5	V248	-74.8	17.1
W201	-62.6	8.9	D249	-66.3	12.2
F202	68.3	13.5	S250	-94.7	15.4
D206	-100.3	21.7	V256	-53	7.6
E210	-63	5.5	P257	-58.5	3.7
L211	-64.2	4.9	A258	-73.2	16.4
G212	-64.2	4.9	L259	-63.6	3.6
R213	-61	3.8	N260	-62.5	4.2
W214	-67.4	9.1	L261	-65.2	4.7
L215	-58	7.3	L262	-60.7	5
Y216	-63.2	5.9	I263	-63.7	5.2
A217	-59	2.7	C264	-60.7	5.4
L218	-62.4	3.6	L265	-62.7	3.3
L219	-65.2	9.7	V266	-66.7	4.5
A220	-65.2	6.7	S267	-69.7	13.1
C221	-99.3	14.4	R268	-75.4	14.2
L222	-82.2	18.8	Y269	-65.8	8.3
E223	-73.5	8.2	F270	-76.9	18.6
L226	-100.1	22.9	R273	-66.1	12
L227	-84.8	24.9	D274	-74.2	15.4
P228	-51.7	5.6	L275	-102	11.6
E229	-63.5	5.6	R278	-83.9	18.6
A230	-65.1	5.5			
H231	-60.4	9.3			
S232	-57.7	7.1			
L233	-64.1	3.7			
I234	-63	4.2			
R235	-64.9	6			
Q236	-64.4	3.4			
L237	-62.8	5.6			
A238	-62.4	4.4			
R239	-64.5	7.8			
R240	-66.1	2.7			
C241	-60.2	4.3			
S242	-65.8	5.6			
E243	-66.4	2.7			
V244	-63.4	5.4			
R245	-64.1	6.8			
L246	-67.2	9.9			
L247	-91.5	15.2			

ψ dihedral angles

<u>residue</u>	<u>angle (°)</u>	<u>error (°)</u>	<u>residue</u>	<u>angle (°)</u>	<u>error (°)</u>
D32	-11	21.9	S131	-32.4	11.5
D36	-29.7	13	T134	122.2	10.1
T37	-11.1	19.5	S138	-33.4	7.2
A38	-46.4	7.9	E139	-2.5	10
L39	-38.9	8.7	E141	-38.3	18
I40	-41.9	7.7	G143	-41.5	5.9
K41	-38.2	8.5	W144	-42.4	3.8
A42	-37.4	6.5	K145	-44.3	5.1
Y43	-44.1	7.1	K146	-35.4	9
D44	-40.9	5.5	F147	-44.1	6.9
K45	-39.2	4.6	C148	-32	11.7
A46	-44.5	6	K152	-39.4	10.4
V47	-32.5	9.7	L153	-42.6	8.3
A48	-29.4	19.8	Y171	-32.2	12.2
L100	-37.8	6.1	I174	-0.2	22.7
W102	-43.8	4	F176	122.7	20.4
Q103	-43.7	5	P177	150.5	10.9
Q104	-42.5	6.7	P178	148.4	8.7
Q105	-44.9	4.7	L180	-32.6	15.4
V107	-45.3	4.5	S181	-37	6.2
A108	-46	6.3	I182	-48	11.3
Q109	-41.5	3.6	V183	-35.4	3.9
F110	-43.1	4.2	S184	-30.3	12.4
S111	-39.1	2.8	R185	-4.8	15.8
T112	-42.6	7.2	N187	159.9	20.4
V113	-41.9	5.1	Q188	-34.7	6.7
R114	-43.1	6.3	A189	-37.2	4.8
Q115	-41.9	5.1	T192	-34.7	10.5
N116	-42.5	5.5	S193	-40.4	6.2
V117	-39.5	11.2	L195	-37.4	9.2
N118	-41.3	8.2	E196	-42.5	4
K119	-39	6.1	Y197	-39.3	10
H120	-10	22.1	L198	-40	7.6
R121	-46.5	9.3	S199	-39	8.5
S122	-37.2	7	N200	-41.4	6
H123	-43.6	5.6	W201	-41.4	5.5
W124	-35.4	11.6	G203	24.1	14.7
K125	-28.2	10.2	D206	156.9	10.5
S126	-0.5	20.3	E210	-35.3	5.5

<u>residue</u>	<u>angle (°)</u>	<u>error (°)</u>	<u>residue</u>	<u>angle (°)</u>	<u>error (°)</u>
L211	-40.9	12.3	A258	-29.2	18.8
G212	-42	6.7	L259	-41.9	5.9
R213	-44.5	6.7	N260	-38	6.7
W214	-45.5	6.2	L261	-38.2	13.9
L215	-40.9	12.3	I263	-42.5	6.3
Y216	-43.7	4.1	C264	-42	8
A217	-41.2	7.6	L265	-39.5	5.7
L218	-43.1	4	V266	-41	4.9
L219	-39.6	8.7	S267	-35.5	14.8
A220	-27	16.6	R268	-29.4	15.8
C221	-7.1	9.2	Y269	-37.8	7.4
L222	131	8.4	F270	-26.3	18.3
P225	151.6	9.2	R273	-28	18.1
L226	131.4	16.3	D274	-18	13.1
L227	145.7	23.6	L275	5.5	16.6
P228	-38.2	5.8	R278	133.7	19.9
A230	-40.7	7.3			
H231	-47.4	6.8			
S232	-46.1	5.8			
L233	-41	9.2			
I234	-36.7	5.2			
R235	-40.7	3.4			
Q236	-42.6	4.6			
L237	-39.4	4.7			
A238	-39.2	4.4			
R239	-39.8	8.4			
R240	-43	4.2			
C241	-45.8	7.1			
S242	-39.6	5.4			
E243	-44.1	4.4			
V244	-39.4	7.4			
R245	-39	7.7			
L246	-34.8	9.5			
D249	-27	15.8			
K251	-26.1	10.7			
D252	-7.8	17.1			
E254	-35.3	7.9			
R255	-40.5	8			
V256	-51.8	5.7			
P257	-34	9.2			

Table B3. Hydrogen bonding distance restraints from regions of helical secondary structure used in the XPLOR-NIH calculation of the SMN²⁶⁻⁵¹-Gemin2⁹⁵⁻²⁸⁰ ensemble.

After the two atom selections, the distance is indicated in Angstroms, followed by increments defining its upper and lower bound.

```
assign (residue 38 and name O) (residue 42 and name HN) 3.0 0.5 0.5
assign (residue 39 and name O) (residue 43 and name HN) 3.0 0.5 0.5
assign (residue 40 and name O) (residue 44 and name HN) 3.0 0.5 0.5
assign (residue 41 and name O) (residue 45 and name HN) 3.0 0.5 0.5
assign (residue 42 and name O) (residue 46 and name HN) 3.0 0.5 0.5
assign (residue 43 and name O) (residue 47 and name HN) 3.0 0.5 0.5

assign (residue 101 and name O) (residue 105 and name HN) 3.0 0.5 0.5
assign (residue 102 and name O) (residue 106 and name HN) 3.0 0.5 0.5
assign (residue 103 and name O) (residue 107 and name HN) 3.0 0.5 0.5
assign (residue 105 and name O) (residue 109 and name HN) 3.0 0.5 0.5
assign (residue 106 and name O) (residue 110 and name HN) 3.0 0.5 0.5
assign (residue 108 and name O) (residue 112 and name HN) 3.0 0.5 0.5
assign (residue 110 and name O) (residue 114 and name HN) 3.0 0.5 0.5
assign (residue 111 and name O) (residue 115 and name HN) 3.0 0.5 0.5
assign (residue 112 and name O) (residue 116 and name HN) 3.0 0.5 0.5
assign (residue 113 and name O) (residue 117 and name HN) 3.0 0.5 0.5
assign (residue 114 and name O) (residue 118 and name HN) 3.0 0.5 0.5
assign (residue 115 and name O) (residue 119 and name HN) 3.0 0.5 0.5
assign (residue 116 and name O) (residue 120 and name HN) 3.0 0.5 0.5
assign (residue 117 and name O) (residue 121 and name HN) 3.0 0.5 0.5
assign (residue 118 and name O) (residue 122 and name HN) 3.0 0.5 0.5
assign (residue 119 and name O) (residue 123 and name HN) 3.0 0.5 0.5

assign (residue 189 and name O) (residue 193 and name HN) 3.0 0.5 0.5
assign (residue 190 and name O) (residue 194 and name HN) 3.0 0.5 0.5
assign (residue 191 and name O) (residue 195 and name HN) 3.0 0.5 0.5
assign (residue 192 and name O) (residue 196 and name HN) 3.0 0.5 0.5
assign (residue 193 and name O) (residue 197 and name HN) 3.0 0.5 0.5
assign (residue 194 and name O) (residue 198 and name HN) 3.0 0.5 0.5
assign (residue 195 and name O) (residue 199 and name HN) 3.0 0.5 0.5
assign (residue 196 and name O) (residue 200 and name HN) 3.0 0.5 0.5
assign (residue 197 and name O) (residue 201 and name HN) 3.0 0.5 0.5

assign (residue 212 and name O) (residue 216 and name HN) 3.0 0.5 0.5
assign (residue 213 and name O) (residue 217 and name HN) 3.0 0.5 0.5
assign (residue 214 and name O) (residue 218 and name HN) 3.0 0.5 0.5
assign (residue 215 and name O) (residue 219 and name HN) 3.0 0.5 0.5
assign (residue 216 and name O) (residue 220 and name HN) 3.0 0.5 0.5

assign (residue 230 and name O) (residue 234 and name HN) 3.0 0.5 0.5
assign (residue 231 and name O) (residue 235 and name HN) 3.0 0.5 0.5
assign (residue 232 and name O) (residue 236 and name HN) 3.0 0.5 0.5
assign (residue 233 and name O) (residue 237 and name HN) 3.0 0.5 0.5
assign (residue 234 and name O) (residue 238 and name HN) 3.0 0.5 0.5
assign (residue 235 and name O) (residue 239 and name HN) 3.0 0.5 0.5
```

```
assign (residue 236 and name O) (residue 240 and name HN) 3.0 0.5 0.5
assign (residue 237 and name O) (residue 241 and name HN) 3.0 0.5 0.5
assign (residue 238 and name O) (residue 242 and name HN) 3.0 0.5 0.5
assign (residue 239 and name O) (residue 243 and name HN) 3.0 0.5 0.5
assign (residue 240 and name O) (residue 244 and name HN) 3.0 0.5 0.5
assign (residue 241 and name O) (residue 245 and name HN) 3.0 0.5 0.5
assign (residue 242 and name O) (residue 246 and name HN) 3.0 0.5 0.5

assign (residue 259 and name O) (residue 263 and name HN) 3.0 0.5 0.5
assign (residue 260 and name O) (residue 264 and name HN) 3.0 0.5 0.5
assign (residue 261 and name O) (residue 265 and name HN) 3.0 0.5 0.5
assign (residue 262 and name O) (residue 266 and name HN) 3.0 0.5 0.5
assign (residue 263 and name O) (residue 267 and name HN) 3.0 0.5 0.5
assign (residue 264 and name O) (residue 268 and name HN) 3.0 0.5 0.5
```

Table B4a. The small-angle scattering curve input as an XPLOR-NIH restraint.
The scattering angle q and associated intensity $I(q)$ are indicated; error ($\sigma(q)$) represents the standard deviation to the mean.

q (\AA^{-1})	$I(q)$	$\sigma(q)$	q (\AA^{-1})	$I(q)$	$\sigma(q)$
6.850E-03	7.531E+01	2.739E+01	2.378E-02	5.593E+01	9.051E-01
7.084E-03	6.770E+01	2.112E+01	2.460E-02	5.604E+01	8.575E-01
7.326E-03	6.316E+01	1.903E+01	2.544E-02	5.554E+01	8.080E-01
7.577E-03	6.117E+01	1.435E+01	2.631E-02	5.568E+01	7.715E-01
7.836E-03	5.929E+01	1.536E+01	2.721E-02	5.505E+01	7.396E-01
8.104E-03	5.855E+01	9.980E+00	2.814E-02	5.454E+01	7.145E-01
8.382E-03	5.980E+01	1.010E+01	2.910E-02	5.400E+01	6.835E-01
8.668E-03	5.891E+01	8.473E+00	3.010E-02	5.357E+01	6.538E-01
8.965E-03	6.117E+01	8.519E+00	3.113E-02	5.286E+01	6.465E-01
9.272E-03	5.969E+01	6.667E+00	3.219E-02	5.228E+01	6.243E-01
9.589E-03	6.046E+01	6.369E+00	3.329E-02	5.191E+01	6.198E-01
9.917E-03	5.754E+01	6.459E+00	3.443E-02	5.136E+01	6.291E-01
1.026E-02	5.691E+01	5.517E+00	3.561E-02	5.050E+01	6.104E-01
1.061E-02	5.690E+01	4.815E+00	3.683E-02	5.003E+01	5.996E-01
1.097E-02	5.747E+01	4.678E+00	3.809E-02	4.939E+01	5.825E-01
1.135E-02	5.718E+01	4.409E+00	3.939E-02	4.886E+01	5.722E-01
1.173E-02	5.705E+01	3.967E+00	4.074E-02	4.802E+01	5.554E-01
1.214E-02	5.816E+01	3.638E+00	4.214E-02	4.694E+01	5.440E-01
1.255E-02	5.803E+01	3.244E+00	4.358E-02	4.650E+01	5.274E-01
1.298E-02	5.691E+01	3.164E+00	4.507E-02	4.564E+01	5.150E-01
1.342E-02	5.681E+01	2.784E+00	4.661E-02	4.456E+01	4.996E-01
1.388E-02	5.797E+01	2.689E+00	4.820E-02	4.382E+01	4.871E-01
1.436E-02	5.891E+01	2.366E+00	4.985E-02	4.256E+01	4.736E-01
1.485E-02	5.791E+01	2.231E+00	5.156E-02	4.149E+01	4.605E-01
1.536E-02	5.782E+01	2.069E+00	5.332E-02	4.040E+01	4.470E-01
1.588E-02	5.800E+01	1.880E+00	5.515E-02	3.925E+01	4.339E-01
1.643E-02	5.876E+01	1.833E+00	5.703E-02	3.826E+01	4.228E-01
1.699E-02	5.823E+01	1.629E+00	5.899E-02	3.703E+01	4.094E-01
1.757E-02	5.833E+01	1.539E+00	6.100E-02	3.599E+01	3.989E-01
1.817E-02	5.764E+01	1.459E+00	6.309E-02	3.480E+01	3.864E-01
1.879E-02	5.736E+01	1.343E+00	6.525E-02	3.332E+01	3.761E-01
1.944E-02	5.828E+01	1.267E+00	6.748E-02	3.215E+01	3.630E-01
2.010E-02	5.755E+01	1.179E+00	6.979E-02	3.072E+01	3.549E-01
2.079E-02	5.732E+01	1.104E+00	7.218E-02	2.933E+01	3.420E-01
2.150E-02	5.712E+01	1.082E+00	7.465E-02	2.797E+01	3.322E-01
2.224E-02	5.693E+01	9.762E-01	7.720E-02	2.654E+01	3.229E-01
2.300E-02	5.653E+01	9.591E-01			

q (\AA^{-1})	$I(q)$	$\sigma(q)$	q (\AA^{-1})	$I(q)$	$\sigma(q)$
7.984E-02	2.488E+01	3.124E-01	1.195E-01	8.322E+00	2.156E-01
8.257E-02	2.348E+01	3.030E-01	1.236E-01	7.378E+00	2.088E-01
8.540E-02	2.202E+01	2.942E-01	1.279E-01	6.246E+00	2.144E-01
8.832E-02	2.052E+01	2.842E-01	1.322E-01	5.383E+00	2.249E-01
9.134E-02	1.922E+01	2.757E-01	1.368E-01	4.313E+00	2.294E-01
9.447E-02	1.758E+01	2.671E-01	1.414E-01	3.672E+00	2.332E-01
9.770E-02	1.635E+01	2.600E-01	1.463E-01	2.930E+00	2.368E-01
1.010E-01	1.474E+01	2.513E-01	1.513E-01	2.342E+00	2.413E-01
1.045E-01	1.329E+01	2.437E-01	1.565E-01	1.626E+00	2.434E-01
1.081E-01	1.219E+01	2.363E-01	1.618E-01	1.622E+00	2.401E-01
1.118E-01	1.072E+01	2.293E-01	1.673E-01	1.198E+00	2.370E-01
1.156E-01	9.493E+00	2.219E-01	1.731E-01	8.607E-01	2.309E-01

Table B4b. The sparsened (50 points) small-angle scattering curve data set calculated by XPLOR-NIH and used in calculations. The scattering angle q and associated intensity $I(q)$ are indicated; error ($\sigma(q)$) represents the standard deviation to the mean.

q (\AA^{-1})	$I(q)$	$\sigma(q)$	q (\AA^{-1})	$I(q)$	$\sigma(q)$
6.800E-03	7.531E+01	2.739E+01	1.438E-01	3.302E+00	2.350E-01
1.040E-02	5.690E+01	5.274E+00	1.474E-01	2.802E+00	2.378E-01
1.390E-02	5.794E+01	2.691E+00	1.509E-01	2.390E+00	2.409E-01
1.740E-02	5.830E+01	1.566E+00	1.544E-01	1.912E+00	2.426E-01
2.090E-02	5.729E+01	1.100E+00	1.579E-01	1.625E+00	2.425E-01
2.440E-02	5.601E+01	8.676E-01	1.614E-01	1.623E+00	2.404E-01
2.790E-02	5.466E+01	7.201E-01	1.649E-01	1.383E+00	2.384E-01
3.140E-02	5.269E+01	6.398E-01	1.684E-01	1.133E+00	2.358E-01
3.500E-02	5.098E+01	6.207E-01	1.719E-01	9.260E-01	2.321E-01
3.850E-02	4.924E+01	5.795E-01	1.755E-01	6.810E-01	2.265E-01
4.200E-02	4.706E+01	5.452E-01	1.790E-01	4.180E-01	2.205E-01
4.550E-02	4.534E+01	5.107E-01			
4.900E-02	4.321E+01	4.804E-01			
5.250E-02	4.090E+01	4.531E-01			
5.600E-02	3.879E+01	4.286E-01			
5.950E-02	3.674E+01	4.064E-01			
6.310E-02	3.482E+01	3.866E-01			
6.660E-02	3.263E+01	3.682E-01			
7.010E-02	3.055E+01	3.533E-01			
7.360E-02	2.855E+01	3.363E-01			
7.710E-02	2.660E+01	3.232E-01			
8.060E-02	2.448E+01	3.097E-01			
8.410E-02	2.268E+01	2.981E-01			
8.760E-02	2.087E+01	2.864E-01			
9.120E-02	1.930E+01	2.762E-01			
9.470E-02	1.750E+01	2.667E-01			
9.820E-02	1.611E+01	2.587E-01			
1.017E-01	1.447E+01	2.499E-01			
1.052E-01	1.307E+01	2.422E-01			
1.087E-01	1.193E+01	2.350E-01			
1.122E-01	1.057E+01	2.284E-01			
1.157E-01	9.448E+00	2.216E-01			
1.193E-01	8.408E+00	2.160E-01			
1.228E-01	7.578E+00	2.102E-01			
1.263E-01	6.669E+00	2.123E-01			
1.298E-01	5.865E+00	2.189E-01			
1.333E-01	5.130E+00	2.260E-01			
1.368E-01	4.305E+00	2.294E-01			
1.403E-01	3.824E+00	2.323E-01			

Table B5. Observed $^1D_{NH}$ backbone amide and tryptophan $\epsilon 1$ residual dipolar couplings used in the XPLOR-NIH calculation of the SMN²⁶⁻⁵¹-Gemin2⁹⁵⁻²⁸⁰ ensemble. The value of each observed RDC is measured in Hz; the experimental values were twice those listed here and were uniformly halved for convenience. The error was approximated from visual inspection of point-to-point resolution of the 1H - ^{15}N HSQC IPAP spectra.

Backbone amide RDCs

<u>Residue</u>	<u>RDC (Hz)</u>	<u>Error (Hz)</u>	<u>Residue</u>	<u>RDC (Hz)</u>	<u>Error (Hz)</u>
W34	4.75	2.5	T190	-4.3	2.5
D35	5.36	2.5	T192	-6.18	2.5
T37	10.85	3.5	S193	1.5	2.5
A38	5.47	2.5	L198	-8.66	2.5
I40	12.46	3.5	N200	-0.84	2.5
D44	13.22	2.5	G203	2.56	2.5
V47	13.16	2.5	R205	-7.81	2.5
A48	4.07	2.5	D206	5.85	2.5
S49	7.35	2.5	F207	8.46	2.5
F50	10.32	2.5	E210	-9.59	2.5
T99	11.03	2.5	L211	-5.77	2.5
Q105	2.82	3.5	G212	-6.91	3.5
A108	8.86	3.5	W214	-9.62	2.5
Q109	3.82	3.5	A220	-5.95	2.5
T112	5.75	2.5	L227	11.65	3.5
V113	9.32	2.5	E229	4.69	2.5
V117	11.38	3.5	A230	-2.35	3.5
Q127	15.08	2.5	S232	4.1	2.5
Q128	9.79	3.5	I234	-7.01	2.5
L129	7.04	2.5	R235	3.32	5
N132	8.17	2.5	L247	0.24	2.5
V133	1	2.5	V248	-4.41	2.5
M135	-1.37	2.5	D249	11.87	2.5
K137	-1.22	2.5	S250	6.82	2.5
S138	-2.46	2.5	D252	-1.52	3.5
E139	8.64	2.5	D252	12.96	2.5
E141	10.3	2.5	R255	-4.82	2.5
W144	10.79	3.5	V256	-3.36	3.5
G150	-1.43	2.5	A258	-9.34	2.5
L153	2.85	2.5	L259	-4.29	3.5
D170	4.04	2.5	N260	-0.37	3.5
V172	13.04	2.5	L265	-3.12	3.5
Q173	12.99	2.5	S267	-2.54	3.5
F176	-2.4	3.5	R268	2.03	3.5
L180	12.34	2.5	R273	-7.07	3.5
I182	8.9	2.5	D274	8.13	2.5
S184	15.89	2.5	A276	1.03	2.5
M186	10.45	2.5	D277	12.44	2.5
Q188	-8.02	2.5	E278	0.03	2.5

Tryptophan sidechain $\epsilon 1$ RDCs

<u>Residue</u>	<u>RDC (Hz)</u>	<u>Error (Hz)</u>
W44	6.13	3.5
W102	13.79	3.5
W124	10.75	3.5
W144	4.55	3.5
W201	6.53	3.5
W214	10.62	3.5

Table B6. Distance restraints, based upon observed paramagnetic relaxation enhancement due to an MTSSL moiety covalently coupled to Cys241, used in the XPLOR-NIH calculation of the SMN²⁶⁻⁵¹-Gemin2⁹⁵⁻²⁸⁰ ensemble.

Shown here in XPLOR format. After the two atom selections, the distance is indicated in Angstroms, followed by increments defining its upper and lower bound.

```
assign ( resid 241 and segid A and name OS1 ) ( resid 38 and segid B
and name HN ) 20.5 3.0 3.0
assign ( resid 241 and segid A and name OS1 ) ( resid 39 and segid B
and name HN ) 20.4 3.0 3.0
assign ( resid 241 and segid A and name OS1 ) ( resid 40 and segid B
and name HN ) 22.8 3.0 3.0
assign ( resid 241 and segid A and name OS1 ) ( resid 46 and segid B
and name HN ) 21.5 3.0 3.0
assign ( resid 241 and segid A and name OS1 ) ( resid 50 and segid B
and name HN ) 20.1 3.0 3.0
assign ( resid 241 and segid A and name OS1 ) ( resid 108 and segid A
and name HN ) 20.2 3.0 3.0
assign ( resid 241 and segid A and name OS1 ) ( resid 112 and segid A
and name HN ) 22.1 3.0 3.0
assign ( resid 241 and segid A and name OS1 ) ( resid 113 and segid A
and name HN ) 20.4 3.0 3.0
assign ( resid 241 and segid A and name OS1 ) ( resid 135 and segid A
and name HN ) 22.1 3.0 3.0
assign ( resid 241 and segid A and name OS1 ) ( resid 138 and segid A
and name HN ) 23.6 3.0 3.0
assign ( resid 241 and segid A and name OS1 ) ( resid 139 and segid A
and name HN ) 22.1 3.0 3.0
assign ( resid 241 and segid A and name OS1 ) ( resid 141 and segid A
and name HN ) 21.0 3.0 3.0
assign ( resid 241 and segid A and name OS1 ) ( resid 144 and segid A
and name HN ) 20.0 3.0 3.0
assign ( resid 241 and segid A and name OS1 ) ( resid 150 and segid A
and name HN ) 17.6 3.0 3.0
assign ( resid 241 and segid A and name OS1 ) ( resid 182 and segid A
and name HN ) 22.1 3.0 3.0
assign ( resid 241 and segid A and name OS1 ) ( resid 183 and segid A
and name HN ) 18.4 3.0 3.0
assign ( resid 241 and segid A and name OS1 ) ( resid 184 and segid A
and name HN ) 19.7 3.0 3.0
assign ( resid 241 and segid A and name OS1 ) ( resid 185 and segid A
and name HN ) 23.6 3.0 3.0
assign ( resid 241 and segid A and name OS1 ) ( resid 186 and segid A
and name HN ) 22.8 3.0 3.0
assign ( resid 241 and segid A and name OS1 ) ( resid 200 and segid A
and name HN ) 15.0 15.0 3.0
assign ( resid 241 and segid A and name OS1 ) ( resid 203 and segid A
and name HN ) 15.0 15.0 3.0
assign ( resid 241 and segid A and name OS1 ) ( resid 205 and segid A
and name HN ) 15.0 15.0 3.0
assign ( resid 241 and segid A and name OS1 ) ( resid 223 and segid A
and name HN ) 20.0 3.0 3.0
```



```
assign ( resid 241 and segid A and name OS1 ) ( resid 226 and segid A
and name HN ) 20.6 3.0 3.0
assign ( resid 241 and segid A and name OS1 ) ( resid 229 and segid A
and name HN ) 22.1 3.0 3.0
assign ( resid 241 and segid A and name OS1 ) ( resid 232 and segid A
and name HN ) 18.7 3.0 3.0
assign ( resid 241 and segid A and name OS1 ) ( resid 246 and segid A
and name HN ) 18.9 3.0 3.0
assign ( resid 241 and segid A and name OS1 ) ( resid 249 and segid A
and name HN ) 20.3 3.0 3.0
assign ( resid 241 and segid A and name OS1 ) ( resid 251 and segid A
and name HN ) 21.5 3.0 3.0
assign ( resid 241 and segid A and name OS1 ) ( resid 256 and segid A
and name HN ) 15.8 3.0 3.0
assign ( resid 241 and segid A and name OS1 ) ( resid 258 and segid A
and name HN ) 21.0 3.0 3.0
```

Appendix C. Sample python XPLOR-NIH refinement script. Run under XPLOR-NIH 2.26.

```
xplor.requireVersion("2.18")

#
#After high-temp dynamics, performs slow cooling protocol in
#torsion angle space, then in Cartesian space for Gemin2(95-
#280)/SMN(26-51). Uses NOE, TALOS backbone dihedral, hbond,
#small-angle x-ray scattering, RDC and PRE restraints.
#
#Each restraint type was added iteratively, in the order listed
#above.
#This is the script for the final refinement, including all
#restraints and starting from the lowest-energy structure in the
#previous iteration.

#Gemin2 in this step only (anneal_rdc_mtsl.pdb) is the
#C154S/C221S/C264S mutant to accommodate the MTSSL moiety bound
#to C241.

# KLS 2011/10/20
#

(opts,args) = xplor.parseArguments(["quick"]) # check for
command-line typos

quick=False
for opt in opts:
    if opt[0]=="quick": #specify -quick to just test that the
script runs
        quick=True
        pass
    pass

outFilename = "SCRIPT_STRUCTURE.pdb"
numberOfStructures=92

if quick:
    numberOfStructures=3
    pass

# protocol module has many high-level helper functions.
#
import protocol
protocol.initRandomSeed(326) #explicitly set random seed
```

```

#
# annealing settings
#

command = xplor.command

protocol.initTopology(('protein'))
protocol.initParams("protein")

# read an existing model
#
protocol.initStruct("gemin2smn_mtsl.psf")
protocol.initCoords("anneal_rdc_mtsl.pdb")
xplor.simulation.deleteAtoms("not known")

protocol.fixupCovalentGeom(maxIters=100,useVDW=1)

# a PotList contains a list of potential terms. This is used to
# specify which terms are active during refinement.

from potList import PotList
potList = PotList()

# parameters to ramp up during the simulated annealing protocol

from simulationTools import MultRamp, StaticRamp, InitialParams

rampedParams=[]
highTempParams=[]

# set up RDC potential

from varTensorTools import create_VarTensor
media={}
#           medium Da   rhombicity
# you could have a whole list here
for (medium, Da, Rh) in [ ('t', -10.56, 0.35)]:
    oTensor = create_VarTensor(medium)
    oTensor.setDa(Da)
    oTensor.setRh(Rh)
    media[medium] = oTensor
    pass

from rdcPotTools import create_RDCPot, scale_toNH
rdcs = PotList('rdc')
for (medium, expt, file, scale) in \
    [ ('t', 'NH', 'gemin2smn_rdc.tbl', 1),

```

```

    ]:
    rdc =
create_RDCPot("%s_%s"%(medium,expt),file,media[medium])
    rdc.setScale(scale)
    rdc.setShowAllRestrains(1) #all restraints are printed
during analysis
    rdc.setThreshold(0.5)      # in Hz
    rdc.setPotType("square")
    rdcs.append(rdc)
    pass
potList.append(rdcs)
rampedParams.append(MultRamp(0.03,3.0,"rdcs.setScale(VALUE)") )

from varTensorTools import calcTensorOrientation
for medium in media.values():
    calcTensorOrientation(medium)
    pass

# set up NOE potential
noe=PotList('noe')
potList.append(noe)
from noePotTools import create_NOEPot
for (name,scale,file) in [('all',1,"gemin2smn_noe_clean.tbl"),
                          ('hbond',1,"gemin2smn_hbond.tbl")
                          #add entries for additional tables
                          ]:
    pot = create_NOEPot(name,file)
    # pot.setPotType("soft") - if you think there may be bad
    # NOEs
    pot.setScale(scale)
    noe.append(pot)
rampedParams.append( MultRamp(2,50, "noe.setScale( VALUE )" ) )

# set up PRE potential
pre=PotList('pre')
potList.append(pre)
from noePotTools import create_NOEPot
for (name,scale,file) in [('c241s',1,"c241stest.tbl"),
                          #add entries for additional tables
                          ]:
    pot = create_NOEPot(name,file)
    pot.setScale(scale)
    pot.setThreshold(0)
    pre.append(pot)
rampedParams.append( MultRamp(2,50, "pre.setScale( VALUE )" ) )

# set up dihedral angles
from xplorPot import XplorPot

```

```

protocol.initDihedrals("gemin2smn_dihed.tbl",
                      #useDefaults=False
                      # by default, symmetric sidechain
                      # restraints are included
                      )
potList.append( XplorPot('CDIH') )
highTempParams.append(
StaticRamp("potList['CDIH'].setScale(10)") )
rampedParams.append(StaticRamp("potList['CDIH'].setScale(200)")
)
#set custom values of threshold values for violation calculation
#
potList['CDIH'].setThreshold( 5 ) #5 degrees is the default
#value, though

#Rama torsion angle database
#
protocol.initRamaDatabase()
potList.append( XplorPot('RAMA') )
rampedParams.append(
MultRamp(.002,1,"potList['RAMA'].setScale(VALUE)") )

#
# setup parameters for atom-atom repulsive term. (van der Waals-
# like term)
#
potList.append( XplorPot('VDW') )
rampedParams.append( StaticRamp("protocol.initNBond()") )
rampedParams.append( MultRamp(0.9,0.8,
                              "command('param nbonds repel VALUE
end end')") )
rampedParams.append( MultRamp(.004,8,
                              "command('param nbonds rcon VALUE
end end')") )
# nonbonded interaction only between CA atoms
highTempParams.append(
StaticRamp("""protocol.initNBond(cutnb=100,
tolerance=45,
repel=0.5,
onlyCA=0)""") )

potList.append( XplorPot("BOND") )
potList.append( XplorPot("ANGL") )
potList['ANGL'].setThreshold( 5 )

```

```

rampedParams.append(
MultRamp(0.4,1,"potList['ANGL'].setScale(VALUE)") )
potList.append( XplorPot("IMPR") )
potList['IMPR'].setThreshold( 5 )
rampedParams.append(
MultRamp(0.1,1,"potList['IMPR'].setScale(VALUE)") )

#set up SAXS term
from solnXRayPotTools import create_solnXRayPot
import solnXRayPotTools

xray=create_solnXRayPot('xray',experiment='G2SMN_D2O_Hi_t.dat',
                        numPoints=50,
                        normalizeIndex=-3,preweighted=False)

solnXRayPotTools.useGlobs(xray)

xray.setNumAngles(50)
xray.setScale(40)
xray.setCmpType("plain")
potList.append(xray)

print xray.calcEnergy()
from solnScatPotTools import fitParams

# Give atoms uniform weights, except for the anisotropy axis
#
from atomAction import SetProperty
import varTensorTools
AtomSel("not rename ANI").apply( SetProperty("mass",100.) )
varTensorTools.massSetup(media.values(),300)
AtomSel("all          ").apply( SetProperty("fric",10.) )

# IVM setup
# the IVM is used for performing dynamics and minimization in
# torsion-angle and in Cartesian space.
#
from ivm import IVM
dyn = IVM()
for m in media.values():
    m.setFreedom("fixDa, fixRh")          #fix tensor Rh, Da, vary
# orientation
protocol.torsionTopology(dyn,oTensors=media.values())

# minc used for final cartesian minimization

```

```

#
minc = IVM()
protocol.initMinimize(minc)
for m in media.values():
    m.setFreedom("fixDa, fixRh")    #allow all tensor parameters
# float here
    pass
protocol.cartesianTopology(minc,oTensors=media.values())

# object which performs simulated annealing
#
from simulationTools import AnnealIVM
init_t = 3000.    # Need high temp and slow annealing to
converge
cool = AnnealIVM(initTemp =init_t,
                 finalTemp=0,
                 tempStep =10,
                 ivm=dyn,
                 rampedParams = rampedParams)
# a round of Cartesian space cooling always following torsion-
# angle space cooling. Not standard, but truly necessary for
# this unwieldy system.
cart_cool = AnnealIVM(initTemp =init_t,
                     finalTemp=0,
                     tempStep =10,
                     ivm=minc,
                     rampedParams = rampedParams)

def accept(potList):
    """
    return True if current structure meets acceptance criteria
    """
    if potList['noe'].violations()>5:
        return False
    if potList['CDIH'].violations()>5:
        return False
    if potList['BOND'].rms()>0.1:
        return False
    if potList['ANGL'].rms()>2:
        return False
    if potList['IMPR'].rms()>4:
        return False

    return True

def calcOneStructure(loopInfo):
    """ this function calculates a single structure, performs
analysis on the

```

```

structure, and then writes out a pdb file, with remarks.
"""

# initialize parameters for high temp dynamics.
InitialParams( rampedParams )
# high-temp dynamics setup - only need to specify parameters
# which
# differ from initial values in rampedParams
InitialParams( highTempParams )

# high temp dynamics
#
protocol.initDynamics(dyn,
    potList=potList, # potential terms to
                    # use
    bathTemp=init_t,
    initVelocities=1,
    finalTime=25,   # stops at 10ps or
                    #5000 steps
    numSteps=20000, # whichever comes
                    # first
    printInterval=100)

dyn.setETolerance( init_t/100 ) #used to det. stepsize.
                                # default: t/1000
dyn.run()

# initialize parameters for cooling loop
InitialParams( rampedParams )

# initialize integrator for simulated annealing
#
protocol.initDynamics(dyn,
    potList=potList,
    numSteps=1000,   #at each temp:
                    # 100 steps or
    finalTime=2 ,    # .2ps, whichever
                    #is less
    printInterval=100)

# perform simulated annealing
#
cool.run()

# final torsion angle minimization
#
protocol.initMinimize(dyn,

```



```

                                printInterval=50)
dyn.run()
protocol.initDynamics(minc,
                      potList=potList,
                      numSteps=1000,      #at each temp:
                                           #100 steps or
                      finalTime=2 ,      # .2ps, whichever
                                           #is less
                                printInterval=100)
cart_cool.run()

# final all- atom minimization
#
protocol.initMinimize(minc,
                     potList=potList,
                     dEPred=10)
minc.run()

#do analysis and write structure
loopInfo.writeStructure(potList)
pass

from simulationTools import StructureLoop, FinalParams
StructureLoop(numStructures=numberOfStructures,
              pdbTemplate=outFilename,
              structLoopAction=calcOneStructure,
              genViolationStats=1,
              averagePotList=potList,

averageSortPots=[potList['BOND'],potList['ANGL'],potList['IMPR']
,
noe,xray,rdcs,pre,potList['CDIH']],
              averageTopFraction=1, #report only on best 50% of
                                   #structs
              averageAccept=accept, #only use structures which
                                   #pass accept()
              averageContext=FinalParams(rampedParams),
              averageFilename="SCRIPT_ave.pdb", #generate
                                   # regularized ave structure
              averageFitSel="name CA",
              averageCompSel="not hydro"      ).run()

```

References

- Altschul SF, Madden TL, Schäffer AA, Zhang J, Zhang Z et al. (1997) Gapped BLAST and PSI-BLAST: a new generation of protein database search programs. *Nucleic Acids Res* 25: 3389-3402.
- Alfás L, Bernal S, Fuentes-Prior P, Barceló MJ, Also E et al. (2009) Mutation update of spinal muscular atrophy in Spain: molecular characterization of 745 unrelated patients and identification of four novel mutations in the SMN1 gene. *Hum Genet* 125: 29-39.
- Ast G (2004) How did alternative splicing evolve?. *Nat Rev Genet* 5: 773-782.
- Baccon J, Pellizzoni L, Rappsilber J, Mann M, Dreyfuss G (2002) Identification and characterization of Gemin7, a novel component of the survival of motor neuron complex. *J Biol Chem* 277: 31957-31962.
- Battiste JL, Wagner G (2000) Utilization of site-directed spin labeling and high-resolution heteronuclear nuclear magnetic resonance for global fold determination of large proteins with limited nuclear overhauser effect data. *Biochemistry* 39: 5355-5365.
- Battle DJ, Kasim M, Wang J, Dreyfuss G (2007) SMN-independent subunits of the SMN complex. Identification of a small nuclear ribonucleoprotein assembly intermediate. *J Biol Chem* 282: 27953-27959.
- Battle DJ, Lau C, Wan L, Deng H, Lotti F et al. (2006) The Gemin5 protein of the SMN complex identifies snRNAs. *Mol Cell* 23: 273-279.
- Beadle GW, Tatum EL (1941) Genetic Control of Biochemical Reactions in *Neurospora*. *Proc Natl Acad Sci U S A* 27: 499-506.
- Berget SM (1995) Exon recognition in vertebrate splicing. *J Biol Chem* 270: 2411-2414.
- Berget SM, Moore C, Sharp PA (1977) Spliced segments at the 5' terminus of adenovirus 2 late mRNA. *Proc Natl Acad Sci U S A* 74: 3171-3175.
- Bouveret E, Rigaut G, Shevchenko A, Wilm M, Séraphin B (2000) A Sm-like protein complex that participates in mRNA degradation. *EMBO J* 19: 1661-1671.
- Brahms H, Meheus L, de Brabandere V, Fischer U, Lührmann R (2001) Symmetrical dimethylation of arginine residues in spliceosomal Sm protein B/B' and the Sm-like protein LSm4, and their interaction with the SMN protein. *RNA* 7: 1531-1542.

Briese M, Esmaili B, Fraboulet S, Burt EC, Christodoulou S et al. (2009) Deletion of *smn-1*, the *Caenorhabditis elegans* ortholog of the spinal muscular atrophy gene, results in locomotor dysfunction and reduced lifespan. *Hum Mol Genet* 18: 97-104.

Briese M, Esmaili B, Sattelle DB (2005) Is spinal muscular atrophy the result of defects in motor neuron processes?. *Bioessays* 27: 946-957.

Brzustowicz LM, Kleyn PW, Boyce FM, Lien LL, Monaco AP et al. (1992) Fine-mapping of the spinal muscular atrophy locus to a region flanked by *MAP1B* and *D5S6*. *Genomics* 13: 991-998.

Brzustowicz LM, Lehner T, Castilla LH, Penchaszadeh GK, Wilhelmsen KC et al. (1990) Genetic mapping of chronic childhood-onset spinal muscular atrophy to chromosome 5q11.2-13.3. *Nature* 344: 540-541.

Brünger AT, Adams PD, Clore GM, DeLano WL, Gros P et al. (1998) Crystallography & NMR system: A new software suite for macromolecular structure determination. *Acta Crystallogr D Biol Crystallogr* 54: 905-921.

Burge CB, Tuschli T, Sharp PA (1999) Splicing of precursors to mRNAs by the spliceosomes. In: Gesteland RF, Cech TR, Atkins J F, editors. *The rna world*, 2nd edn.. Cold Spring Harbor Laboratory Press. pp. 525-560.

Burghes AHM, Beattie CE (2009) Spinal muscular atrophy: why do low levels of survival motor neuron protein make motor neurons sick?. *Nat Rev Neurosci* 10: 597-609.

Béchéde C, Rostaing P, Cisterni C, Kalisch R, La Bella V et al. (1999) Subcellular distribution of survival motor neuron (SMN) protein: possible involvement in nucleocytoplasmic and dendritic transport. *Eur J Neurosci* 11: 293-304.

Bühler D, Raker V, Lührmann R, Fischer U (1999) Essential role for the tudor domain of SMN in spliceosomal U snRNP assembly: implications for spinal muscular atrophy. *Hum Mol Genet* 8: 2351-2357.

Camasses A, Bragado-Nilsson E, Martin R, Séraphin B, Bordonné R (1998) Interactions within the yeast Sm core complex: from proteins to amino acids. *Mol Cell Biol* 18: 1956-1966.

Campion Y, Neel H, Gostan T, Soret J, Bordonné R (2010) Specific splicing defects in *S. pombe* carrying a degtron allele of the Survival of Motor Neuron gene. *EMBO J* 29: 1817-1829.

Canaves JM, Page R, Wilson IA, Stevens RC (2004) Protein biophysical properties that correlate with crystallization success in *Thermotoga maritima*: maximum clustering strategy for structural genomics. *J Mol Biol* 344: 977-991.

Carissimi C, Baccon J, Straccia M, Chiarella P, Maiolica A et al. (2005) Unrip is a component of SMN complexes active in snRNP assembly. *FEBS Lett* 579: 2348-2354.

Carissimi C, Saieva L, Baccon J, Chiarella P, Maiolica A et al. (2006a) Gemin8 is a novel component of the survival motor neuron complex and functions in small nuclear ribonucleoprotein assembly. *J Biol Chem* 281: 8126-8134.

Carissimi C, Saieva L, Gabanella F, Pellizzoni L (2006b) Gemin8 is required for the architecture and function of the survival motor neuron complex. *J Biol Chem* 281: 37009-37016.

Carrel TL, McWhorter ML, Workman E, Zhang H, Wolstencroft EC et al. (2006) Survival motor neuron function in motor axons is independent of functions required for small nuclear ribonucleoprotein biogenesis. *J Neurosci* 26: 11014-11022.

Cartegni L, Krainer AR (2002) Disruption of an SF2/ASF-dependent exonic splicing enhancer in SMN2 causes spinal muscular atrophy in the absence of SMN1. *Nat Genet* 30: 377-384.

Chan YB, Miguel-Aliaga I, Franks C, Thomas N, Trülzsch B et al. (2003) Neuromuscular defects in a *Drosophila* survival motor neuron gene mutant. *Hum Mol Genet* 12: 1367-1376.

Chang HC, Dimlich DN, Yokokura T, Mukherjee A, Kankel MW et al. (2008) Modeling spinal muscular atrophy in *Drosophila*. *PLoS One* 3: e3209.

Chari A, Golas MM, Klingenhäger M, Neuenkirchen N, Sander B et al. (2008) An assembly chaperone collaborates with the SMN complex to generate spliceosomal SnRNPs. *Cell* 135: 497-509.

Charroux B, Pellizzoni L, Perkinson RA, Shevchenko A, Mann M et al. (1999) Gemin3: A novel DEAD box protein that interacts with SMN, the spinal muscular atrophy gene product, and is a component of gems. *J Cell Biol* 147: 1181-1194.

Charroux B, Pellizzoni L, Perkinson RA, Yong J, Shevchenko A et al. (2000) Gemin4. A novel component of the SMN complex that is found in both gems and nucleoli. *J Cell Biol* 148: 1177-1186.

- Cherepanov P, Maertens G, Proost P, Devreese B, Van Beeumen J et al. (2003) HIV-1 integrase forms stable tetramers and associates with LEDGF/p75 protein in human cells. *J Biol Chem* 278: 372-381.
- Cho S, Dreyfuss G (2010) A degron created by SMN2 exon 7 skipping is a principal contributor to spinal muscular atrophy severity. *Genes Dev* 24: 438-442.
- Chow LT, Gelinas RE, Broker TR, Roberts RJ (1977) An amazing sequence arrangement at the 5' ends of adenovirus 2 messenger RNA. *Cell* 12: 1-8.
- Clore GM, Gronenborn AM, Bax A (1998) A robust method for determining the magnitude of the fully asymmetric alignment tensor of oriented macromolecules in the absence of structural information. *J Magn Reson* 133: 216-221.
- Clore GM, Gronenborn AM, Nilges M, Ryan CA (1987) Three-dimensional structure of potato carboxypeptidase inhibitor in solution. A study using nuclear magnetic resonance, distance geometry, and restrained molecular dynamics. *Biochemistry* 26: 8012-8023.
- Covert DD, Le TT, McAndrew PE, Strasswimmer J, Crawford TO et al. (1997) The survival motor neuron protein in spinal muscular atrophy. *Hum Mol Genet* 6: 1205-1214.
- Crick FH (1958) On protein synthesis. *Symp Soc Exp Biol* 12: 138-163.
- Cuscó I, Barceló MJ, del Río E, Baiget M, Tizzano EF (2004) Detection of novel mutations in the SMN Tudor domain in type I SMA patients. *Neurology* 63: 146-149.
- D'Amico A, Mercuri E, Tiziano FD, Bertini E (2011) Spinal muscular atrophy. *Orphanet J Rare Dis* 6: 71.
- Delano W (2002) The pymol molecular graphics system. . p.
- Deutsch M, Long M (1999) Intron-exon structures of eukaryotic model organisms. *Nucleic Acids Res* 27: 3219-3228.
- Diercks T, Coles M, Kessler H (1999) An efficient strategy for assignment of cross-peaks in 3D heteronuclear NOESY experiments. *J. Biomol. NMR* 15: 177-180.
- Dmitrova M, Younès-Cauet G, Oertel-Buchheit P, Porte D, Schnarr M et al. (1998) A new LexA-based genetic system for monitoring and analyzing protein heterodimerization in *Escherichia coli*. *Mol Gen Genet* 257: 205-212.

Doniach S (2001) Changes in biomolecular conformation seen by small angle X-ray scattering. *Chem Rev* 101: 1763-1778.

Early P, Rogers J, Davis M, Calame K, Bond M et al. (1980) Two mRNAs can be produced from a single immunoglobulin mu gene by alternative RNA processing pathways. *Cell* 20: 313-319.

Eggert C, Chari A, Laggerbauer B, Fischer U (2006) Spinal muscular atrophy: the RNP connection. *Trends Mol Med* 12: 113-121.

Erickson HP (2009) Size and shape of protein molecules at the nanometer level determined by sedimentation, gel filtration, and electron microscopy. *Biol Proced Online* 11: 32-51.

Fan L, Simard LR (2002) Survival motor neuron (SMN) protein: role in neurite outgrowth and neuromuscular maturation during neuronal differentiation and development. *Hum Mol Genet* 11: 1605-1614.

Farrow NA, Muhandiram R, Singer AU, Pascal SM, Kay CM et al. (1994) Backbone dynamics of a free and phosphopeptide-complexed Src homology 2 domain studied by ¹⁵N NMR relaxation. *Biochemistry* 33: 5984-6003.

Feng W, Gubitza AK, Wan L, Battle DJ, Dostie J et al. (2005) Gemins modulate the expression and activity of the SMN complex. *Hum Mol Genet* 14: 1605-1611.

Fernandez CF, Pannone BK, Chen X, Fuchs G, Wolin SL (2004) An Lsm2-Lsm7 complex in *Saccharomyces cerevisiae* associates with the small nucleolar RNA snR5. *Mol Biol Cell* 15: 2842-2852.

Fischer U, Liu Q, Dreyfuss G (1997) The SMN-SIP1 complex has an essential role in spliceosomal snRNP biogenesis. *Cell* 90: 1023-1029.

Fox-Walsh KL, Dou Y, Lam BJ, Hung S, Baldi PF et al. (2005) The architecture of pre-mRNAs affects mechanisms of splice-site pairing. *Proc Natl Acad Sci U S A* 102: 16176-16181.

Friesen WJ, Massenet S, Paushkin S, Wyce A, Dreyfuss G (2001a) SMN, the product of the spinal muscular atrophy gene, binds preferentially to dimethylarginine-containing protein targets. *Mol Cell* 7: 1111-1117.

Friesen WJ, Paushkin S, Wyce A, Massenet S, Pesiridis GS et al. (2001b) The methylosome, a 20S complex containing JBP1 and pICln, produces dimethylarginine-modified Sm proteins. *Mol Cell Biol* 21: 8289-8300.

- Gabanella F, Butchbach MER, Saieva L, Carissimi C, Burghes AHM et al. (2007) Ribonucleoprotein assembly defects correlate with spinal muscular atrophy severity and preferentially affect a subset of spliceosomal snRNPs. *PLoS One* 2: e921.
- Gabanella F, Carissimi C, Usiello A, Pellizzoni L (2005) The activity of the spinal muscular atrophy protein is regulated during development and cellular differentiation. *Hum Mol Genet* 14: 3629-3642.
- Gasteiger E, Gattiker A, Hoogland C, Ivanyi I, Appel RD et al. (2003) ExPASy: The proteomics server for in-depth protein knowledge and analysis. *Nucleic Acids Res* 31: 3784-3788.
- Gavrilina TO, McGovern VL, Workman E, Crawford TO, Gogliotti RG et al. (2008) Neuronal SMN expression corrects spinal muscular atrophy in severe SMA mice while muscle-specific SMN expression has no phenotypic effect. *Hum Mol Genet* 17: 1063-1075.
- Goddard T, Kneller D (2008) Sparky 3. : .
- Grimmler M, Bauer L, Nousiainen M, Körner R, Meister G et al. (2005b) Phosphorylation regulates the activity of the SMN complex during assembly of spliceosomal U snRNPs. *EMBO Rep* 6: 70-76.
- Grimmler M, Otter S, Peter C, Müller F, Chari A et al. (2005a) Unrip, a factor implicated in cap-independent translation, associates with the cytosolic SMN complex and influences its intracellular localization. *Hum Mol Genet* 14: 3099-3111.
- Gubitz AK, Feng W, Dreyfuss G (2004) The SMN complex. *Exp Cell Res* 296: 51-56.
- Gubitz AK, Mourelatos Z, Abel L, Rappsilber J, Mann M et al. (2002) Gemin5, a novel WD repeat protein component of the SMN complex that binds Sm proteins. *J Biol Chem* 277: 5631-5636.
- Hamamoto S, Nishitsuji H, Amagasa T, Kannagi M, Masuda T (2006) Identification of a novel human immunodeficiency virus type 1 integrase interactor, Gemin2, that facilitates efficient viral cDNA synthesis in vivo. *J Virol* 80: 5670-5677.
- Hannus S, Bühler D, Romano M, Seraphin B, Fischer U (2000) The *Schizosaccharomyces pombe* protein Yab8p and a novel factor, Yip1p, share structural and functional similarity with the spinal muscular atrophy-associated proteins SMN and SIP1. *Hum Mol Genet* 9: 663-674.

Hao LT, Fuller HR, Lam LT, Le TT, Burghes AHM et al. (2007) Absence of gemin5 from SMN complexes in nuclear Cajal bodies. *BMC Cell Biol* 8: 28.

Henry SA, Patton-Vogt JL (1998) *Progress in nucleic acid research and molecular biology*. Academic Press. p.

Hirokawa N (1998) Kinesin and dynein superfamily proteins and the mechanism of organelle transport. *Science* 279: 519-526.

Hochleitner EO, Sondermann P, Lottspeich F (2004) Determination of the stoichiometry of protein complexes using liquid chromatography with fluorescence and mass spectrometric detection of fluorescently labeled proteolytic peptides. *Proteomics* 4: 669-676.

Holm L, Sander C (1995) Dali: a network tool for protein structure comparison. *Trends Biochem Sci* 20: 478-480.

Hsieh-Li HM, Chang JG, Jong YJ, Wu MH, Wang NM et al. (2000) A mouse model for spinal muscular atrophy. *Nat Genet* 24: 66-70.

Hura GL, Menon AL, Hammel M, Rambo RP, Poole FL2 et al. (2009) Robust, high-throughput solution structural analyses by small angle X-ray scattering (SAXS). *Nat Methods* 6: 606-612.

Jablonka S, Beck M, Lechner BD, Mayer C, Sendtner M (2007) Defective Ca²⁺ channel clustering in axon terminals disturbs excitability in motoneurons in spinal muscular atrophy. *J Cell Biol* 179: 139-149.

Jablonka S, Holtmann B, Meister G, Bandilla M, Rossoll W et al. (2002) Gene targeting of Gemin2 in mice reveals a correlation between defects in the biogenesis of U snRNPs and motoneuron cell death. *Proc Natl Acad Sci U S A* 99: 10126-10131.

Janson J (2011) *Protein purification: principles, high resolution methods, and applications*. John Wiley & Sons. 61 p.

Kambach C, Walke S, Young R, Avis JM, de la Fortelle E et al. (1999) Crystal structures of two Sm protein complexes and their implications for the assembly of the spliceosomal snRNPs. *Cell* 96: 375-387.

Kashima T, Manley JL (2003) A negative element in SMN2 exon 7 inhibits splicing in spinal muscular atrophy. *Nat Genet* 34: 460-463.

- Kenakin TP (1993) Pharmacologic analysis of drug-receptor interaction. Raven Press. 483 p.
- Konarev PV, Volkov VV, Sokolova AV, Koch MHJ, Svergun DI (2003) PRIMUS - a Windows-PC based system for small-angle scattering data analysis. *J Appl Cryst* 36: 1277-1282.
- Kroiss M, Schultz J, Wiesner J, Chari A, Sickmann A et al. (2008) Evolution of an RNP assembly system: a minimal SMN complex facilitates formation of UsnRNPs in *Drosophila melanogaster*. *Proc Natl Acad Sci U S A* 105: 10045-10050.
- Krummel DAP, Nagai K, Oubridge C (2010) Structure of spliceosomal ribonucleoproteins. *F1000 Biol Rep* 2: .
- Kyte J, Doolittle RF (1982) A simple method for displaying the hydropathic character of a protein. *J Mol Biol* 157: 105-132.
- Lau C, Bachorik JL, Dreyfuss G (2009) Gemin5-snRNA interaction reveals an RNA binding function for WD repeat domains. *Nat Struct Mol Biol* 16: 486-491.
- Lebowitz J, Lewis MS, Schuck P (2002) Modern analytical ultracentrifugation in protein science: a tutorial review. *Protein Sci* 11: 2067-2079.
- Lefebvre S, Burlet P, Liu Q, Bertrand S, Clermont O et al. (1997) Correlation between severity and SMN protein level in spinal muscular atrophy. *Nat Genet* 16: 265-269.
- Lefebvre S, Bürglen L, Reboullet S, Clermont O, Burlet P et al. (1995) Identification and characterization of a spinal muscular atrophy-determining gene. *Cell* 80: 155-165.
- Lehmeier T, Raker V, Hermann H, Lührmann R (1994) cDNA cloning of the Sm proteins D2 and D3 from human small nuclear ribonucleoproteins: evidence for a direct D1-D2 interaction. *Proc Natl Acad Sci U S A* 91: 12317-12321.
- Lipari G, Szabo A (1982) Model-free approach to the interpretation of nuclear magnetic resonance relaxation in macromolecules. 1. Theory and range of validity.. *J. Am. Chem. Soc.* 104: 4546-4559.
- Liu Q, Dreyfuss G (1996) A novel nuclear structure containing the survival of motor neurons protein. *EMBO J* 15: 3555-3565.
- Liu Q, Fischer U, Wang F, Dreyfuss G (1997) The spinal muscular atrophy disease gene product, SMN, and its associated protein SIP1 are in a complex with spliceosomal snRNP proteins. *Cell* 90: 1013-1021.

- Lorson CL, Androphy EJ (1998) The domain encoded by exon 2 of the survival motor neuron protein mediates nucleic acid binding. *Hum Mol Genet* 7: 1269-1275.
- Lorson CL, Androphy EJ (2000) An exonic enhancer is required for inclusion of an essential exon in the SMA-determining gene SMN. *Hum Mol Genet* 9: 259-265.
- Lorson CL, Strasswimmer J, Yao JM, Baleja JD, Hahnen E et al. (1998) SMN oligomerization defect correlates with spinal muscular atrophy severity. *Nat Genet* 19: 63-66.
- Ma Y, Dostie J, Dreyfuss G, Van Duyne GD (2005) The Gemin6-Gemin7 heterodimer from the survival of motor neurons complex has an Sm protein-like structure. *Structure* 13: 883-892.
- Martin R (2011) Structural and biochemical studies of the SMN oligomerization domain: a novel glycine zipper. : .
- Matera AG, Terns RM, Terns MP (2007) Non-coding RNAs: lessons from the small nuclear and small nucleolar RNAs. *Nat Rev Mol Cell Biol* 8: 209-220.
- McWhorter ML, Boon K, Horan ES, Burghes AHM, Beattie CE (2008) The SMN binding protein Gemin2 is not involved in motor axon outgrowth. *Dev Neurobiol* 68: 182-194.
- Meister G, Bühler D, Pillai R, Lottspeich F, Fischer U (2001a) A multiprotein complex mediates the ATP-dependent assembly of spliceosomal U snRNPs. *Nat Cell Biol* 3: 945-949.
- Meister G, Eggert C, Bühler D, Brahms H, Kambach C et al. (2001b) Methylation of Sm proteins by a complex containing PRMT5 and the putative U snRNP assembly factor pICln. *Curr Biol* 11: 1990-1994.
- Neidhardt FC, Bloch PL, Smith DF (1974) Culture medium for enterobacteria. *J Bacteriol* 119: 736-747.
- Neri D, Szyperski T, Otting G, Senn H, Wüthrich K (1989) Stereospecific nuclear magnetic resonance assignments of the methyl groups of valine and leucine in the DNA-binding domain of the 434 repressor by biosynthetically directed fractional ¹³C labeling. *Biochemistry* 28: 7510-7516.
- Nilsen TW, Graveley BR (2010) Expansion of the eukaryotic proteome by alternative splicing. *Nature* 463: 457-463.

- Nishitsuji H, Hayashi T, Takahashi T, Miyano M, Kannagi M et al. (2009) Augmentation of reverse transcription by integrase through an interaction with host factor, SIP1/Gemin2 Is critical for HIV-1 infection. *PLoS One* 4: e7825.
- Nizami ZF, Deryusheva S, Gall JG (2010) Cajal bodies and histone locus bodies in *Drosophila* and *Xenopus*. *Cold Spring Harb Symp Quant Biol* 75: 313-320.
- Noble SM, Guthrie C (1996a) Identification of novel genes required for yeast pre-mRNA splicing by means of cold-sensitive mutations. *Genetics* 143: 67-80.
- Noble SM, Guthrie C (1996b) Transcriptional pulse-chase analysis reveals a role for a novel snRNP-associated protein in the manufacture of spliceosomal snRNPs. *EMBO J* 15: 4368-4379.
- Ogawa C, Usui K, Aoki M, Ito F, Itoh M et al. (2007) Gemin2 plays an important role in stabilizing the survival of motor neuron complex. *J Biol Chem* 282: 11122-11134.
- Ogawa C, Usui K, Ito F, Itoh M, Hayashizaki Y et al. (2009) Role of survival motor neuron complex components in small nuclear ribonucleoprotein assembly. *J Biol Chem* 284: 14609-14617.
- Oprea GE, Kröber S, McWhorter ML, Rossoll W, Müller S et al. (2008) Plastin 3 is a protective modifier of autosomal recessive spinal muscular atrophy. *Science* 320: 524-527.
- Otter S, Grimm M, Neuenkirchen N, Chari A, Sickmann A et al. (2007) A comprehensive interaction map of the human survival of motor neuron (SMN) complex. *J Biol Chem* 282: 5825-5833.
- Ottiger M, Delaglio F, Bax A (1998) Measurement of J and dipolar couplings from simplified two-dimensional NMR spectra. *J Magn Reson* 131: 373-378.
- Owen N, Doe CL, Mellor J, Davies KE (2000) Characterization of the *Schizosaccharomyces pombe* orthologue of the human survival motor neuron (SMN) protein. *Hum Mol Genet* 9: 675-684.
- Pagliardini S, Giavazzi A, Setola V, Lizier C, Di Luca M et al. (2000) Subcellular localization and axonal transport of the survival motor neuron (SMN) protein in the developing rat spinal cord. *Hum Mol Genet* 9: 47-56.
- Palfi Z, Jaé N, Preusser C, Kaminska KH, Bujnicki JM et al. (2009) SMN-assisted assembly of snRNP-specific Sm cores in trypanosomes. *Genes Dev* 23: 1650-1664.

Pan Q, Shai O, Lee LJ, Frey BJ, Blencowe BJ (2008) Deep surveying of alternative splicing complexity in the human transcriptome by high-throughput sequencing. *Nat Genet* 40: 1413-1415.

Patel AA, Steitz JA (2003) Splicing double: insights from the second spliceosome. *Nat Rev Mol Cell Biol* 4: 960-970.

Paushkin S, Charroux B, Abel L, Perkinson RA, Pellizzoni L et al. (2000) The survival motor neuron protein of *Schizosaccharomyces pombe*. Conservation of survival motor neuron interaction domains in divergent organisms. *J Biol Chem* 275: 23841-23846.

Paushkin S, Gubitz AK, Massenet S, Dreyfuss G (2002) The SMN complex, an assembly of ribonucleoproteins. *Curr Opin Cell Biol* 14: 305-312.

Pellizzoni L (2007) Chaperoning ribonucleoprotein biogenesis in health and disease. *EMBO Rep* 8: 340-345.

Pellizzoni L, Baccon J, Rappsilber J, Mann M, Dreyfuss G (2002a) Purification of native survival of motor neurons complexes and identification of Gemin6 as a novel component. *J Biol Chem* 277: 7540-7545.

Pellizzoni L, Charroux B, Dreyfuss G (1999) SMN mutants of spinal muscular atrophy patients are defective in binding to snRNP proteins. *Proc Natl Acad Sci U S A* 96: 11167-11172.

Pellizzoni L, Yong J, Dreyfuss G (2002b) Essential role for the SMN complex in the specificity of snRNP assembly. *Science* 298: 1775-1779.

Pesiridis GS, Diamond E, Van Duyne GD (2009) Role of pICln in methylation of Sm proteins by PRMT5. *J Biol Chem* 284: 21347-21359.

Pu WT, Krapivinsky GB, Krapivinsky L, Clapham DE (1999) pICln inhibits snRNP biogenesis by binding core spliceosomal proteins. *Mol Cell Biol* 19: 4113-4120.

Rajendra TK, Gonsalvez GB, Walker MP, Shpargel KB, Salz HK et al. (2007) A *Drosophila melanogaster* model of spinal muscular atrophy reveals a function for SMN in striated muscle. *J Cell Biol* 176: 831-841.

Raker VA, Plessel G, Lührmann R (1996) The snRNP core assembly pathway: identification of stable core protein heteromeric complexes and an snRNP subcore particle in vitro. *EMBO J* 15: 2256-2269.

- Reed R (2000) Mechanisms of fidelity in pre-mRNA splicing. *Curr Opin Cell Biol* 12: 340-345.
- Ritchie DB, Schellenberg MJ, MacMillan AM (2009) Spliceosome structure: piece by piece. *Biochim Biophys Acta* 1789: 624-633.
- Ross A, Czisch M, Cieslar C, Holak T (1993) Efficient methods for obtaining phase-sensitive, gradient-enhanced HMQC data. *J. Biol. NMR* 3: 215-224.
- Rossoll W, Jablonka S, Andreassi C, Kröning A, Karle K et al. (2003) Smn, the spinal muscular atrophy-determining gene product, modulates axon growth and localization of beta-actin mRNA in growth cones of motoneurons. *J Cell Biol* 163: 801-812.
- Rossoll W, Kröning A, Ohndorf U, Steegborn C, Jablonka S et al. (2002) Specific interaction of Smn, the spinal muscular atrophy determining gene product, with hnRNP-R and gry-rbp/hnRNP-Q: a role for Smn in RNA processing in motor axons?. *Hum Mol Genet* 11: 93-105.
- Sattler M, Schleucher J, Griesinger C (1999) Heteronuclear multidimensional NMR experiments for the structure determination of proteins in solution employing pulsed field gradients. *Prog. Nuc. Mag. Res. Spectroscopy* 34: 93-158.
- Schrank B, Götz R, Gunnensen JM, Ure JM, Toyka KV et al. (1997) Inactivation of the survival motor neuron gene, a candidate gene for human spinal muscular atrophy, leads to massive cell death in early mouse embryos. *Proc Natl Acad Sci U S A* 94: 9920-9925.
- Schuck P, Rossmanith P (2000) Determination of the sedimentation coefficient distribution by least-squares boundary modeling. *Biopolymers* 54: 328-341.
- Schwieters CD, Kuszewski JJ, Clore GM (2006) Using Xplor-NIH for NMR molecular structure determination. *Progress in Nuclear Magnetic Resonance Spectroscopy* 48: 47-62.
- Schwieters CD, Kuszewski JJ, Tjandra N, Clore GM (2003) The Xplor-NIH NMR molecular structure determination package. *J Magn Reson* 160: 65-73.
- Selenko P, Sprangers R, Stier G, Bühler D, Fischer U et al. (2001) SMN tudor domain structure and its interaction with the Sm proteins. *Nat Struct Biol* 8: 27-31.
- Semenyuk A, Svergun D (1991) GNOM - A program package for small-angle scattering data processing. *J. Appl. Cryst.* 24: 537-540.

- Seyfang A, Jin JH (2004) Multiple site-directed mutagenesis of more than 10 sites simultaneously and in a single round. *Anal Biochem* 324: 285-291.
- Sharma A, Lambrechts A, Hao LT, Le TT, Sewry CA et al. (2005) A role for complexes of survival of motor neurons (SMN) protein with gemins and profilin in neurite-like cytoplasmic extensions of cultured nerve cells. *Exp Cell Res* 309: 185-197.
- Shen Y, Delaglio F, Cornilescu G, Bax A (2009) TALOS+: a hybrid method for predicting protein backbone torsion angles from NMR chemical shifts. *J Biomol NMR* 44: 213-223.
- Shpargel KB, Matera AG (2005) Gemin proteins are required for efficient assembly of Sm-class ribonucleoproteins. *Proc Natl Acad Sci U S A* 102: 17372-17377.
- Spiller MP, Reijns MAM, Beggs JD (2007) Requirements for nuclear localization of the Lsm2-8p complex and competition between nuclear and cytoplasmic Lsm complexes. *J Cell Sci* 120: 4310-4320.
- Sprangers R, Groves MR, Sinning I, Sattler M (2003) High-resolution X-ray and NMR structures of the SMN Tudor domain: conformational variation in the binding site for symmetrically dimethylated arginine residues. *J Mol Biol* 327: 507-520.
- Staley JP, Guthrie C (1998) Mechanical devices of the spliceosome: motors, clocks, springs, and things. *Cell* 92: 315-326.
- Staley JP, Woolford JLJ (2009) Assembly of ribosomes and spliceosomes: complex ribonucleoprotein machines. *Curr Opin Cell Biol* 21: 109-118.
- Stark H, Dube P, Lührmann R, Kastner B (2001) Arrangement of RNA and proteins in the spliceosomal U1 small nuclear ribonucleoprotein particle. *Nature* 409: 539-542.
- Stern DA, Carlo T, Berget SM (1996) Architectural limits on split genes. *Proc Natl Acad Sci U S A* 93: 15081-15085.
- Sun Y, Grimm M, Schwarzer V, Schoenen F, Fischer U et al. (2005) Molecular and functional analysis of intragenic SMN1 mutations in patients with spinal muscular atrophy. *Hum Mutat* 25: 64-71.
- Svergun DI, Petoukhov MV, Koch MH (2001) Determination of domain structure of proteins from X-ray solution scattering. *Biophys J* 80: 2946-2953.

Takaku M, Tsujita T, Horikoshi N, Takizawa Y, Qing Y et al. (2011) Purification of the human SMN-GEMIN2 complex and assessment of its stimulation of RAD51-mediated DNA recombination reactions. *Biochemistry* 50: 6797-6805.

Takizawa Y, Qing Y, Takaku M, Ishida T, Morozumi Y et al. (2010) GEMIN2 promotes accumulation of RAD51 at double-strand breaks in homologous recombination. *Nucleic Acids Res* 38: 5059-5074.

Talbot K, Miguel-Aliaga I, Mohaghegh P, Ponting CP, Davies KE (1998) Characterization of a gene encoding survival motor neuron (SMN)-related protein, a constituent of the spliceosome complex. *Hum Mol Genet* 7: 2149-2156.

Tharun S, He W, Mayes AE, Lennertz P, Beggs JD et al. (2000) Yeast Sm-like proteins function in mRNA decapping and decay. *Nature* 404: 515-518.

Uversky VN, Gillespie JR, Fink AL (2000) Why are "natively unfolded" proteins unstructured under physiologic conditions?. *Proteins* 41: 415-427.

Vistica J, Dam J, Balbo A, Yikilmaz E, Mariuzza RA et al. (2004) Sedimentation equilibrium analysis of protein interactions with global implicit mass conservation constraints and systematic noise decomposition. *Anal Biochem* 326: 234-256.

Volkov VV, Svergun DI (2003) Uniqueness of ab initio shape determination in small-angle scattering. *J. Appl. Crystallogr.* 36: 860-864.

Vuister G, Clore G, Gronenborn A, Powers R, Garrett D et al. (1993) Increased resolution and improved spectral quality in four-dimensional ¹³C/¹³C separated HMQC-NOESY-HMQC spectra using pulsed field gradients. *J. Mag. Res. B* 101: 210-213.

Walker MP, Rajendra TK, Saieva L, Fuentes JL, Pellizzoni L et al. (2008) SMN complex localizes to the sarcomeric Z-disc and is a proteolytic target of calpain. *Hum Mol Genet* 17: 3399-3410.

Ward JJ, Sodhi JS, McGuffin LJ, Buxton BF, Jones DT (2004) Prediction and functional analysis of native disorder in proteins from the three kingdoms of life. *J Mol Biol* 337: 635-645.

Whipple FW (1998) Genetic analysis of prokaryotic and eukaryotic DNA-binding proteins in *Escherichia coli*. *Nucleic Acids Res* 26: 3700-3706.

Will CL, Lührmann R (2001) Spliceosomal UsnRNP biogenesis, structure and function. *Curr Opin Cell Biol* 13: 290-301.

- Will CL, Lührmann R (2005) Splicing of a rare class of introns by the U12-dependent spliceosome. *Biol Chem* 386: 713-724.
- Will CL, Lührmann R (2011) Spliceosome structure and function. *Cold Spring Harb Perspect Biol* 3: .
- Winkler C, Eggert C, Gradl D, Meister G, Giegerich M et al. (2005) Reduced U snRNP assembly causes motor axon degeneration in an animal model for spinal muscular atrophy. *Genes Dev* 19: 2320-2330.
- Wüthrich K (1986) Nmr of proteins and nucleic acids. Wiley-Interscience. p.
- Yamashita M, Nishio H, Harada Y, Matsuo M, Yamamoto T (2004) Significant increase in the number of the SMN2 gene copies in an adult-onset Type III spinal muscular atrophy patient with homozygous deletion of the NAIP gene. *Eur Neurol* 52: 101-106.
- Yong J, Kasim M, Bachorik JL, Wan L, Dreyfuss G (2010) Gemin5 delivers snRNA precursors to the SMN complex for snRNP biogenesis. *Mol Cell* 38: 551-562.
- Young PJ, Man NT, Lorson CL, Le TT, Androphy EJ et al. (2000) The exon 2b region of the spinal muscular atrophy protein, SMN, is involved in self-association and SIP1 binding. *Hum Mol Genet* 9: 2869-2877.
- Zerres K, Davies KE (1999) 59th ENMC International Workshop: Spinal Muscular Atrophies: recent progress and revised diagnostic criteria 17-19 April 1998, Soestduinen, The Netherlands. *Neuromuscul Disord* 9: 272-278.
- Zhang H, Xing L, Rossoll W, Wichterle H, Singer RH et al. (2006) Multiprotein complexes of the survival of motor neuron protein SMN with Gemin traffic to neuronal processes and growth cones of motor neurons. *J Neurosci* 26: 8622-8632.
- Zhang HL, Pan F, Hong D, Shenoy SM, Singer RH et al. (2003) Active transport of the survival motor neuron protein and the role of exon-7 in cytoplasmic localization. *J Neurosci* 23: 6627-6637.
- Zhang R, So BR, Li P, Yong J, Glisovic T et al. (2011) Structure of a key intermediate of the SMN complex reveals Gemin2's crucial function in snRNP assembly. *Cell* 146: 384-395.
- Zhang Z, Lotti F, Dittmar K, Younis I, Wan L et al. (2008) SMN deficiency causes tissue-specific perturbations in the repertoire of snRNAs and widespread defects in splicing. *Cell* 133: 585-600.